Proceedings of the Mini-Workshop on *Channeling Radiation Phenomena and Positron Production*

17 January, 2003, KEK, Tsukuba

Editors

Tsuyoshi Suwada and Masanori Satoh

KEK, High Energy Accelerator Research Organization,
Oho 1-1, Tsukuba, Ibaraki, 305-0801 Japan

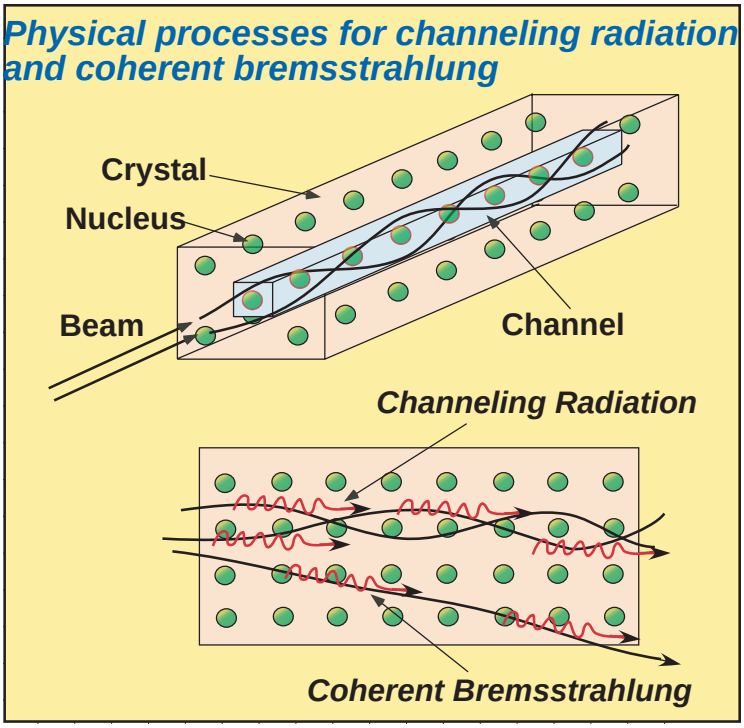

A mini-workshop on "*Channeling Radiation Phenomena and Positron Production*" has been held at KEK on 17 January 2003. Six talks (theory 2, design 2, experiment 2) were presented.

The channeling radiation in crystal material is well known from old days. The application to positron-production source of high-energy electron accelerators was proposed in 1989 by R. Chehab, *et al*. in Orsay. In Japan, Yoshida, *et al.* at INS of Tokyo University (at that time) started to carry out a proof-of-principle experiment on the positron production through the channeling radiation phenomena in a crystal target. Since then, these two groups have been continuing the experimental research in order to investigate the application to the high-intensity positron source for the next generation linear colliders and B factories.

On the other hand, the theoretical unified formulation is now under way on the positron production scheme through electromagnetic-shower development by channeling radiation along with classical bremsstrahlung and coherent bremsstrahlung processes. Thus, it is a very interesting theme to understand theoretically and experimentally the channeling radiation phenomena as an elemental physical process. From the applicative point of view, the channeling radiation phenomena are investigated (or utilized) for cooling of charged particles, bending of a proton beam, and polarization/polarimetry of charged particles, *etc*. and its application extends widely to another area.

This workshop was held to discuss, exchange and summarize present theoretical and experimental ideas on the channeling radiation phenomena and positron production by the experts. We expect that the channeling phenomena in crystal will further be studied and extend its area widely.

These proceedings were compiled by Tsuyoshi Suwada and Masanori Satoh of KEK.

Tsuyoshi Suwada
Accelerator Laboratory, KEK
20 February, 2003

Memorandum on mini-workshop "Positron production in oriented crystals"

V. N. Baier
Budker Institute of Nuclear Physics,
Novosibirsk, 630090, Russia

January 22, 2003

During last two years the results were published for the first time of quantitative study of positron production from high energy electrons in oriented single crystals. The rate of positron yield was measured in tungsten, silicon and diamond axially oriented crystals with accuracy of order $15 \div 20\%$. The obtained data are in quite satisfactory agreement with the theory and based on this theory simulation. This may be considered as a summary of reports presented at mini-workshop.

In my opinion this means that now is just a time to make the next step and start investigation of optimization of the positron source. This includes:

1. Reasonable definition of needed intensity of positron source. What is the optimal energy both for electron and positron? For KEKB factory the current requirements are known.

2. For Japan Linear Collider project one can start from existing project.

3. Transverse size and angular width of beams? For positions these beam characteristics are defined basically by the source matching system.

4. Search of optimal crystal type, its thickness, distance between crystal and amorphous parts (for combined target) taking into account energy losses both in the crystal and target. What are maximal permitted energy losses, their dependence on the beam size?

5. Calculation and measurement of positron yield. One can expect that increase of positron yield in crystal comparing with amorphous target will be of the order $1.3 \div 1.5$ and diminishing of energy losses in crystal comparing with amorphous target will be at least 2 times.

A lot of efforts are needed to solve these problems. It seems promising if this investigation will be done by an international collaboration including KEK, Tokyo MU, BINP(Novosibirsk), ...

Mini-workshop on Channeling Radiation Phenomena and Positron Production

(January 17, 2003 at KEK)

Program

(1) V. N. Baier (BINP)

Comparison of theory with experiment for positron production from high energy electrons moving along crystal axes.

(2) T. Suwada (KEK)

Positron-production experiment using Diamond and Si crystals in the KEKB 8-GeV linac.

(3) R. Hamatsu (Tokyo Metropolitan Univ.)

Review of the positron production experiment using axial channeling at the KEK.

(4) T.Kamitani (KEK)

Positron source design in Japan linear collider.

(5) A. Potylitsyn (Tomsk Univ.)

Comparison of undulator-based and crystal-based positron sources.

(6) H. Nitta (Tokyo Gakugei Univ.)

Semiclassical Theory of Crystal-Assisted Pair Production:

Beyond the Constant Field Approximation.

Presentation paper

phys. stat. sol. (b) 133, 583 (1986)

Subject classification: 61.80 and 78.70; S1.1; S1.2; S5; S5.11; S5.12

Institute of Nuclear Physics, Academy of Sciences of the USSR, Novosibirsk[1])

Radiation Yield of High-Energy Electrons in Thick Crystals

By

V. N. Baier, V. M. Katkov, and V. M. Strakhovenko

1. Description of Radiation in Thick Crystals

According to the performed analysis [1, 2] dealing with the kinetics of the distribution, which is due to multiple scattering, the DF for large depths (l) is of the form

$$\begin{aligned} dF^{pl}(\boldsymbol{v}_\perp, x, l) &= \frac{dx\, d^2v_\perp}{d_{pl}\, \pi g(l)} \exp\left(-\frac{\boldsymbol{v}_\perp^2}{g(l)}\right) \\ dF^{ax}(\boldsymbol{v}_\perp, \boldsymbol{\varrho}, l) &= \frac{d^2\varrho\, d^2v_\perp}{S\, \pi g(l)} \exp\left(-\frac{\boldsymbol{v}_\perp^2}{g(l)}\right) \end{aligned} \tag{1}$$

where x, $y(\boldsymbol{\varrho})$ are the transverse coordinates: $|x| \leqq d_{pl}/2$ for the planar case and $|\boldsymbol{\varrho}| \leqq r_0$ for the axial case; $S = \pi r_0^2$ is the area of a cell in the transverse plane which contains the projection of one atomic chain, and $n_\perp = 1/S$ is the density of the chains of atoms (axes). The quantity $g(l)$ has the form

$$g(l) = \Delta^2 + \int_0^l \dot{\vartheta}_s^2(t)\, dt\,, \tag{2}$$

where $\dot{\vartheta}_s^2$ is the rate of variation of the squared angle of multiple scattering in an appropriate amorphous medium. The time (depth) dependence of $\dot{\vartheta}_s^2$ is connected with the variation of the particle energy because of radiation losses. The first term in $g(l)$ reflects the character of the angular (velocity) distribution established at the initial stage of electron motion in a crystal which depends on the angular (over ϑ_0) distribution in an incident beam. Even with the angle of incidence $\vartheta_0 = 0$, the angular spread of particles in the crystal proves to be roughly equal to the Lindhard angle: $\vartheta_c = \sqrt{2U_0/\varepsilon}$ (U_0 is the depth of the potential well and ε is the energy of a particle); therefore, assuming the incident beam to be rather narrow, $\vartheta_0 \leqq \vartheta_c$, we can put $\Delta^2 = c_1 \vartheta_c^2$, where c_1 is a coefficient of the order of unity. The magnitude of c_1 can be influenced also by the imperfectness

and modifications of incoherent contributions are small, distinctions in the soft cascade development in crystal and amorphous media are mainly due to the coherent contribution to the radiation. This contribution changes the shape of photon spectra, enriching their soft part and noticeably diminishing the effective radiation length L_{ef} determined by the relation

$$L_{ef}^{-1} = \tilde{L}_{rad}^{-1} + L_{ch}^{-1} .$$

So, for the $< 111 >$ axis of tungsten, we find $L_{ef} \simeq 0.13\,cm$ at $\varepsilon = 2GeV$ and $L_{ef} \simeq 0.08\,cm$ at $\varepsilon = 5GeV$, which are several times less than the amorphous value $L_{rad} \simeq 0.35\,cm$. Thus in a crystal the initial electron is converted into photons along appreciably shorter length than in a corresponding amorphous medium, while further development of the soft shower in both media is more or less the same. Hence the most pronounced distinctions of shower characteristics in the amorphous and crystal case appear for small thicknesses. It is clear that for the valuable use of crystal properties in the case of suggested target composed of crystal and amorphous layers, the former must be of a few L_{ef} thick.

tained within the approximation mentioned . We have compared the shape of the spectrum (2) with available experimental data, but this procedure is somewhat indirect for several reasons. Sometimes very thin samples were used where the distribution of electrons over transverse coordinates was far from being uniform, sometimes energy loss spectra were measured which are noticeably different from true intensity spectra, sometimes emitted photons were collimated that also results in a change of the observed shape of spectra. Nevertheless, a qualitative agreement of the spectrum (2) with known experimental data holds for all energies beginning with $900\,MeV$.

The contribution to any process going on in a crystal is a sum $Y = Y_{coh} + Y_{inc}$ where, generally speaking, the incoherent contribution Y_{inc} differs from the amorphous value Y_{am}. The scale of this modification depends on the process under consideration. For the total intensity of the incoherent radiation and the quantity $\tilde{L}_{rad} = \varepsilon / I_{br}$ connected to it, the typical scale of diminishing of I_{br} as compared to I_{am} at room temperature is depending on media 9 to 13 per cent. The diminishing of the total probability of pair-production is of the same order of magnitude. In particular, we obtain for tungsten in the case of a full screening $\tilde{L}_{rad} = 1.1\, L_{rad}$. As far as the coherent contribution to the pair-production probability is negligible in the considered energy region

given by eq.(2) with a corresponding expression obtained in CFA BKS(1987) for the uniform distribution over transverse coordinates. So eq.(2) reproduces the energy dependence of coherent contribution to the radiation length $L_{ch} = \varepsilon/I_{ch}(\varepsilon)$ inherent to CFA which as mentioned above is valid in a wide energy range. For the sake of possible use, we have fitted our results for the function $r(\varepsilon)$ in the energy interval $\varepsilon < 5GeV$ by a polynomial

$$r(\varepsilon) = \sum_{n=0}^{9} a_n \varepsilon^n ,$$

where ε is measured in GeV and coefficients a_n for $<110>$-axis of Si and Ge crystals and for $<111>$-axis of W crystal are calculated. The fitting provides the accuracy better than 1 percent for Si and Ge and better than 3 percent for W.

The position of a maximum in the spectrum given by eq.(2) is always consistent with the estimate (1). For relatively small energies when $\rho_c \ll 1$ and correspondingly $u_0 \ll 1$, we can neglect the first term in the right-hand side of eq.(3) since $\rho_c/\chi_s = 2ma_s \gg 1$. In this case the spectrum (2) has a maximum at $\omega = \omega_{max} \simeq 0.05\varepsilon u_0 \simeq 2\varepsilon\sqrt{\rho_c}/(ma_s)$ which evidently coincides in this (dipole) approximation with eq.(1). When $\rho_c \gg 1$ and CFA is valid the spectrum (2) reproduces not only the position of a maximum but also the shape of spectral distributions like those shown in Fig.2 of BKS(1987) ob-

where a_s is the screening radius of a corresponding potential and

$$\rho \simeq (2V_0/m\theta_0)^2 \; for \; \theta_0 > \theta_c$$

and

$$\rho \simeq \rho_c = 2V_0\varepsilon/m^2 \; for \; \theta_0 < \theta_c .$$

The estimate BKS(1987) for the characteristic frequency of emitted photons ω at given frequency of motion ω_0 reads

$$u \equiv \frac{\omega}{\varepsilon - \omega} \simeq \frac{2N\omega_0\varepsilon}{m^2\,(1 + \rho/2)}, \qquad (1)$$

where N is the characteristic number of emitted harmonics. Note that N = 1 for $\rho \leq 1$ and N $\propto \rho^{3/2}$ for $\rho \gg 1$. Using also that $\omega_0 \sim \theta_0/a_s$, we suggest to describe the radiation from channeled and moving not very high above the potential barrier particles the following heuristic intensity spectrum:

$$\frac{dI_{ch}}{d\omega} = \frac{r(\varepsilon)\varepsilon}{u_0(\varepsilon)}\left[1 + \frac{1}{(1+u)^2}\right]\left(\frac{u}{u_0}\right)^{1/3} \ln\left(\frac{u_0}{u}\right)\vartheta(u_0 - u), \qquad (2)$$

where $\vartheta(z) = 1$ for $z > 0$ and $\vartheta(z) = 0$ for $z < 0$,

$$u_0 = \frac{25}{6}\chi_s + 80\,\frac{1}{ma_s}\,\frac{\sqrt{\rho_c}}{(2 + \rho_c)}. \qquad (3)$$

The function $r(\varepsilon)$ in eq.(2) is determined by the condition of the coincidence of the total intensity

$$I_{ch}(\varepsilon) = \int_0^{\varepsilon} d\omega \left(\frac{dI_{ch}}{d\omega}\right)$$

BKS NIM B 103 (1995) 147

Here we consider axial alignment when θ_0 with respect to the chosen axis is not too large as compared to the critical (Lindhard) angle $\theta_c = (2V_0/\varepsilon)^{1/2}$,where V_0 is a typical scale of the corresponding potential and ε is the particle energy, since in this case the most pronounced effects take place.

Let us start with the coherent contribution to the radiation. As already mentioned, at sufficiently high energies corresponding expressions valid at any angle of incidence θ_0 were obtained in BKS(1987). For $\theta_0 \ll V_0/m$ they reproduce CFA-limit. But even if the initial electron energy is high enough to apply mentioned description, charged particles arising in the course of a shower development may not satisfy this condition. In the case of a soft cascade we have to describe the radiation from these "soft" particles as well. Let us remind that within semiclassical theory of the QED- processes in any external field there are only two parameters: ρ and χ. The parameter ρ is a measure of the particle velocity deviation from a straight line in units of the natural emission angle $\gamma^{-1} = m/\varepsilon$, while the parameter χ being the ratio of the external field strength in the particle rest system to the critical QED-value $E_c = 1.32 \cdot 10^{16}\, eV/cm$ is responsible for the magnitude of quantum recoil effects. In crystals

$$\chi \sim \chi_s = V_0\varepsilon/m^3 a_s ,$$

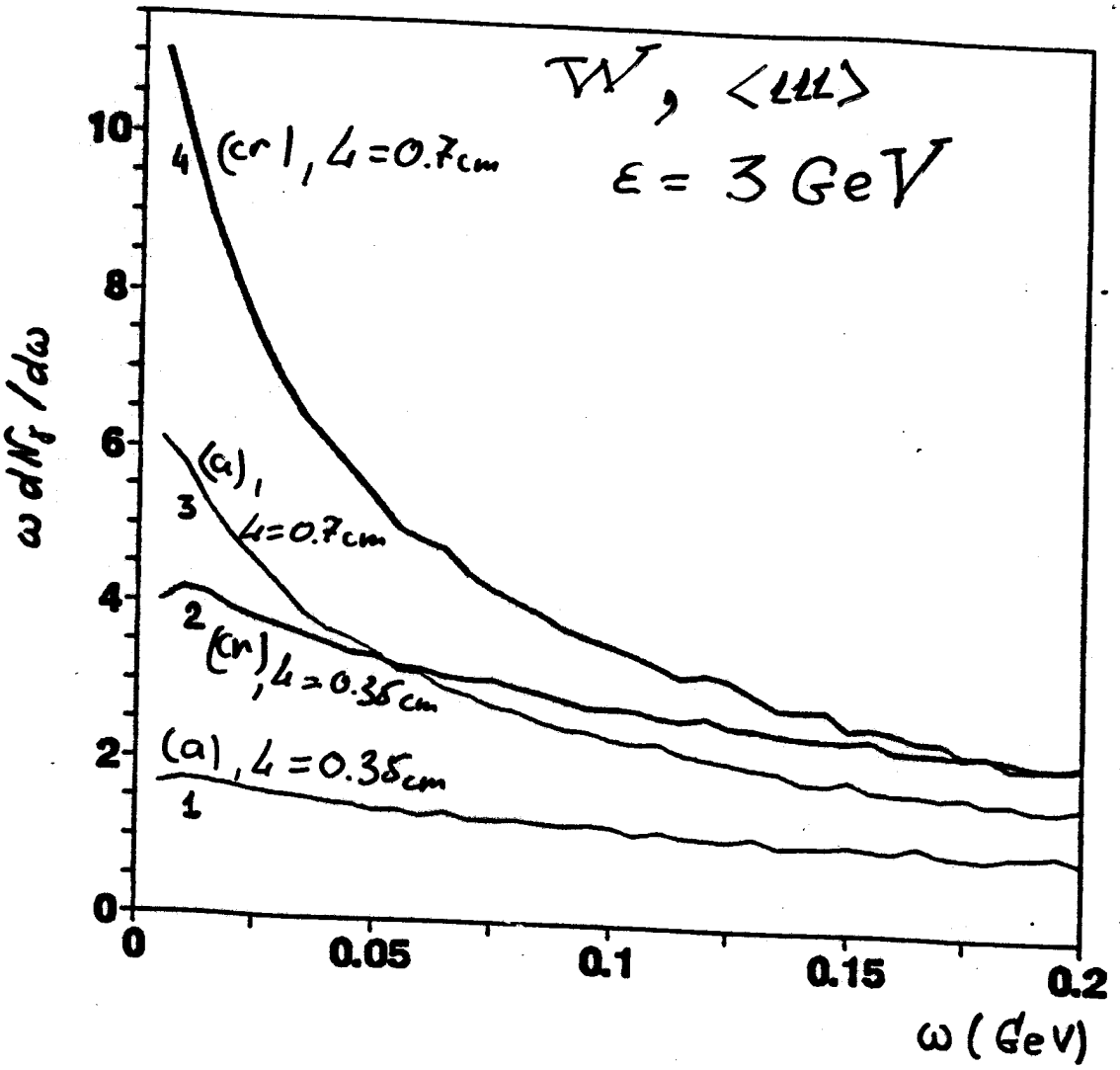
W, <111>
ε = 3 GeV
4 (cr), L = 0.7cm
3 (a), L = 0.7cm
2 (cr), L = 0.35cm
1 (a), L = 0.35cm
ω dN_γ / dω
ω (GeV)
0
2
4
6
8
10
0
0.05
0.1
0.15
0.2

Fig. 1(a)

esides the radiation under study, the bremsstrahlung (below with the subscript ') also contributes to the intensity. Generally speaking, the bremsstrahlung can ige in comparison with an amorphous medium, under channeling conditions. No oretical analysis of this problem is available. Nevertheless, to give an idea of the

Table 1

Parameters of the potential for the ⟨111⟩ axis and some characteristics of the radiation

al	u_1 (10^{-10} m) $T = 293$ K	V_0 (eV)	U_0 (eV)	β	a_s (10^{-10} m)	$c = \frac{L_{rad}}{L_{ph}}$	R	ω_{ch} (MeV)	L_0 (mm)
(d)	0.040	29	103	0.025	0.326	0.61	1.87	21.1	15.6
i	0.075	54	106	0.150	0.30	0.57	0.80	23.3	15.3
/	0.082	135	280	0.135	0.306	0.49	1.16	37.0	4.8
r	0.061	165	358	0.122	0.272	0.48	1.64	47.0	3.6
e	0.068	180	363	0.145	0.276	0.48	1.46	46.6	3.15
e	0.085	91	191	0.13	0.30	0.51	0.53	31.1	4.3
93 K)	0.050	417	937	0.115	0.215	0.50	1.48	96.2	0.65
K)	0.030	348	1255	0.027	0.228	0.50	2.38	105.0	0.61

plitude of thermal vibrations, V_0, β, a_s parameters of the potential (6), U_0 depth of the potential, c ratio of the radiation length to the effective length of photon absorption, $R = I_{as}/I_{br}$ ratio = 1 GeV, ω_{ch} frequency calculated by means of (16) at $\varepsilon_0 = 1$ GeV, L_0 optimal thickness of rystal at $\varepsilon_0 = 1$ GeV.

nitude of the effect, we shall make use of the model of a corresponding amorphous ium for a description of the bremsstrahlung. Assuming the condition (4) to be fied, for the bremsstrahlung intensity at depth l we find

$$\frac{dI_{br}}{d\Omega} = \frac{I_{br}}{\pi g(l)} \equiv \frac{1}{\pi g(l)} \frac{\varepsilon}{L_{rad}}. \tag{9}$$

[1, 2] the energy variation will be taken into account in an adiabatic approximawith due regard for both mechanisms of radiation losses. Hence, for the energy epth l we have

$$\frac{\varepsilon(s)}{\varepsilon_0} = \frac{e^{-s}}{1 + R(\varepsilon_0)(1 - e^{-s})} = G(s), \tag{10}$$

ere $s = l/L_{rad}$, ε_0 is the initial energy and $R(\varepsilon) = I_{as}/I_{br}$. Substituting $\varepsilon(s)$ into nd (9), we find

$$\frac{dI_{ch}}{d\Omega} = \frac{\alpha}{(2\pi)^2} \frac{\varepsilon_0^3 R(\varepsilon_0)}{m^2 L_{rad}} G^2(s) f(s),$$

$$\frac{dI_{br}}{d\Omega} = \frac{\alpha}{(2\pi)^2} \frac{\varepsilon_0^3}{m^2 L_{rad}} G(s) f(s), \tag{11}$$

re

$$f(s) = \left[\frac{1}{2}(1+R)^2(e^{2s}-1) - 2R(1+R)(e^s-1) + R^2 + \frac{l_a}{L_{rad}}\right]^{-1}, \tag{12}$$

$R \equiv R(\varepsilon_0)$, l_a is defined in (3), and $G(s)$ is given by (10).

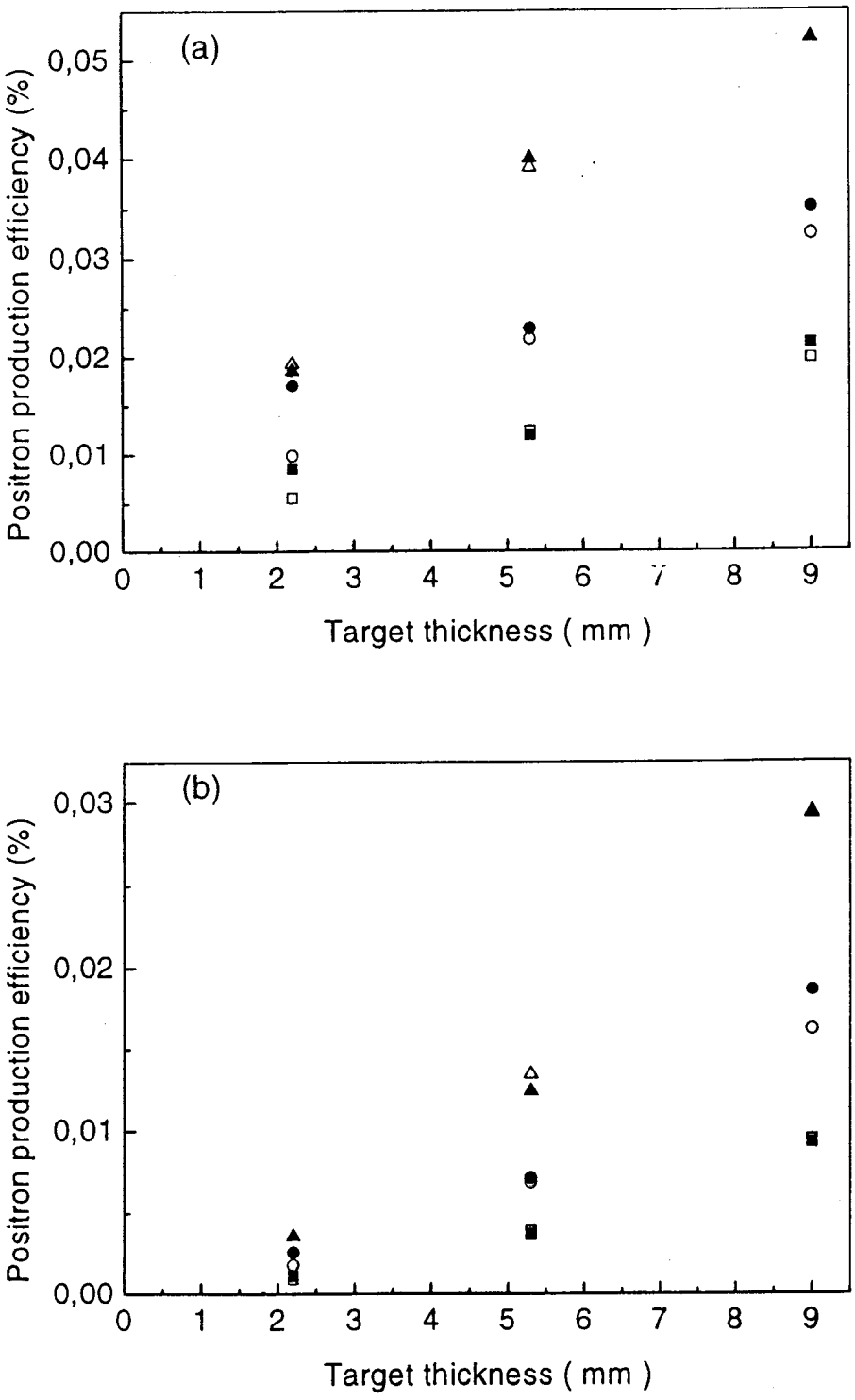

FIG. 6: Positron production efficiency from crystal (a) and amorphous (b) targets depending on thickness. Open symbols - our calculation, filled symbols - results from Fig.5 of [15]; $\triangle$ are for $p = 20$ Mev/c, $\bigcirc$ are for $p = 15$ Mev/c, and $\square$ are for $p = 10$ Mev/c.

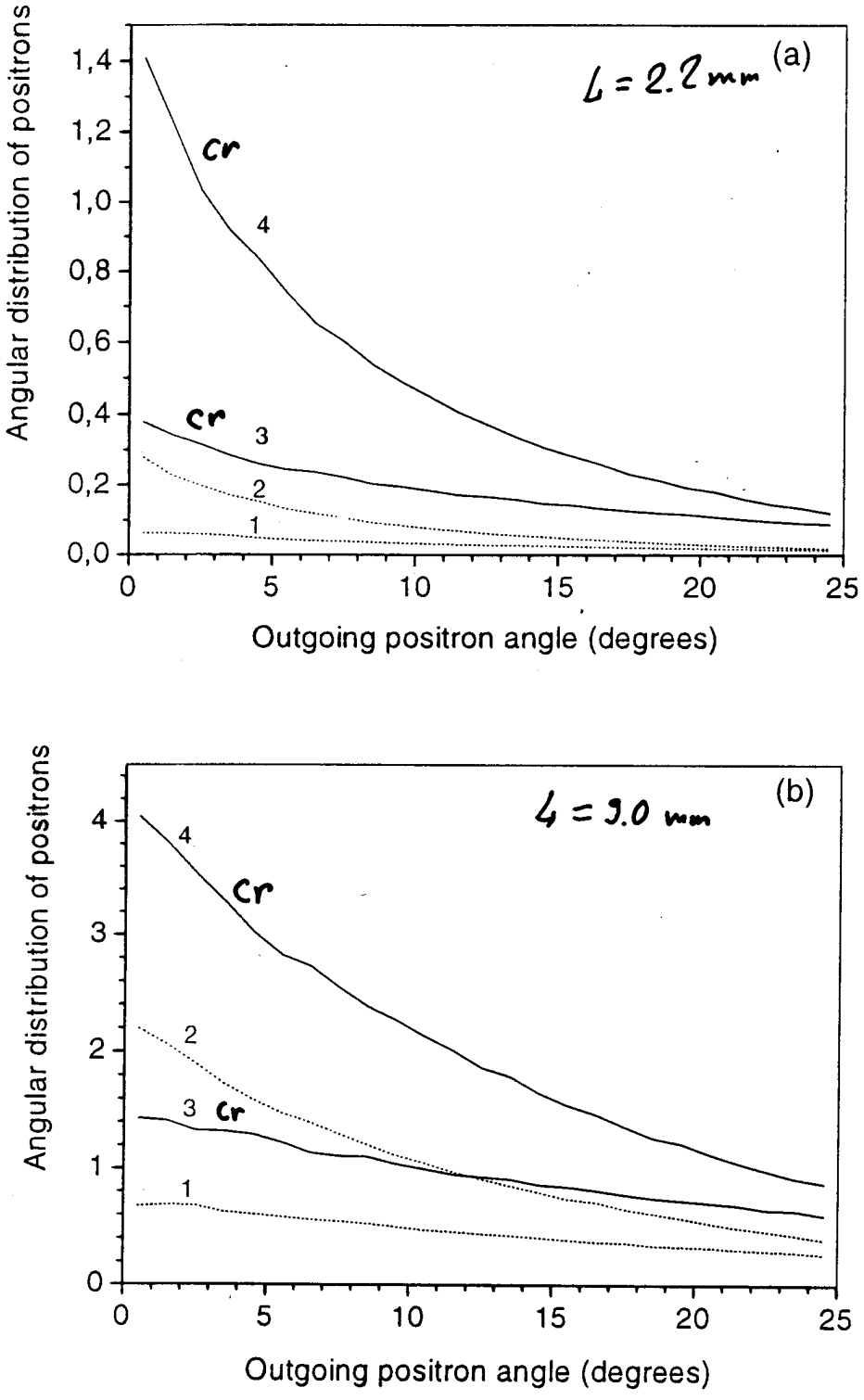

FIG. 5: Angular distribution $dN^{(+)}/d\Omega$ depending on outgoing positron angle at $L = 2.2$ mm (a) and at $L = 9.0$ mm (b) for $p_\perp \in (8.5 \div 11.5)$ Mev/c (curves 1 and 3) and for $p_\perp \in (17 \div 23)$ Mev/c (curves 2 and 4). Solid curves represent the yield from crystal and dotted from amorphous targets.

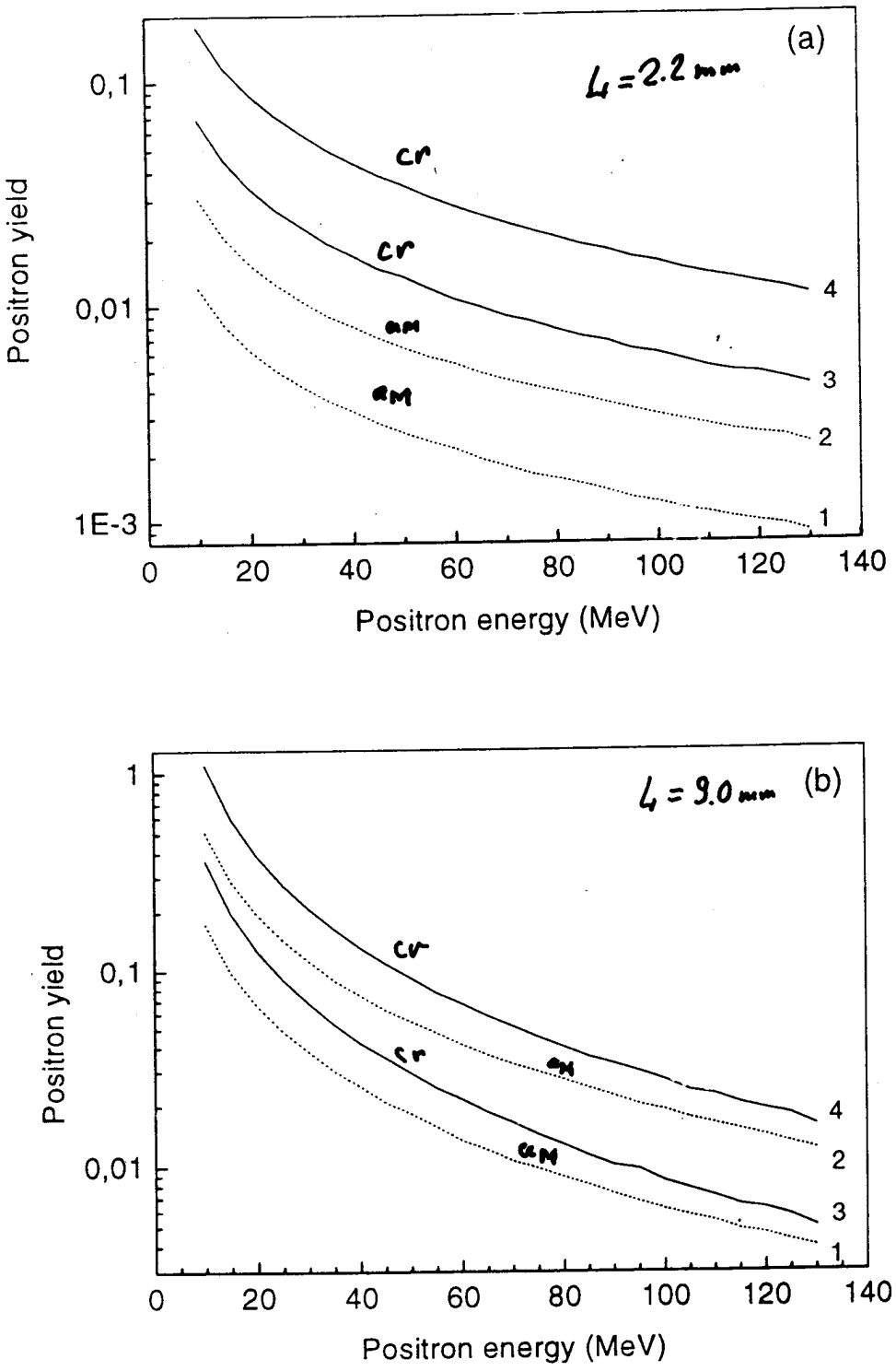

FIG. 4: Positron yield depending on energy at $L = 2.2$ mm (a) and $L = 9.0$ mm (b) for $p_{\perp}^{max} =$ 2.5 MeV/c (curves 1 and 3) and for $p_{\perp}^{max} = 5$ MeV/c (curves 2 and 4). Solid curves represent the yield from crystal and dotted from amorphous targets.

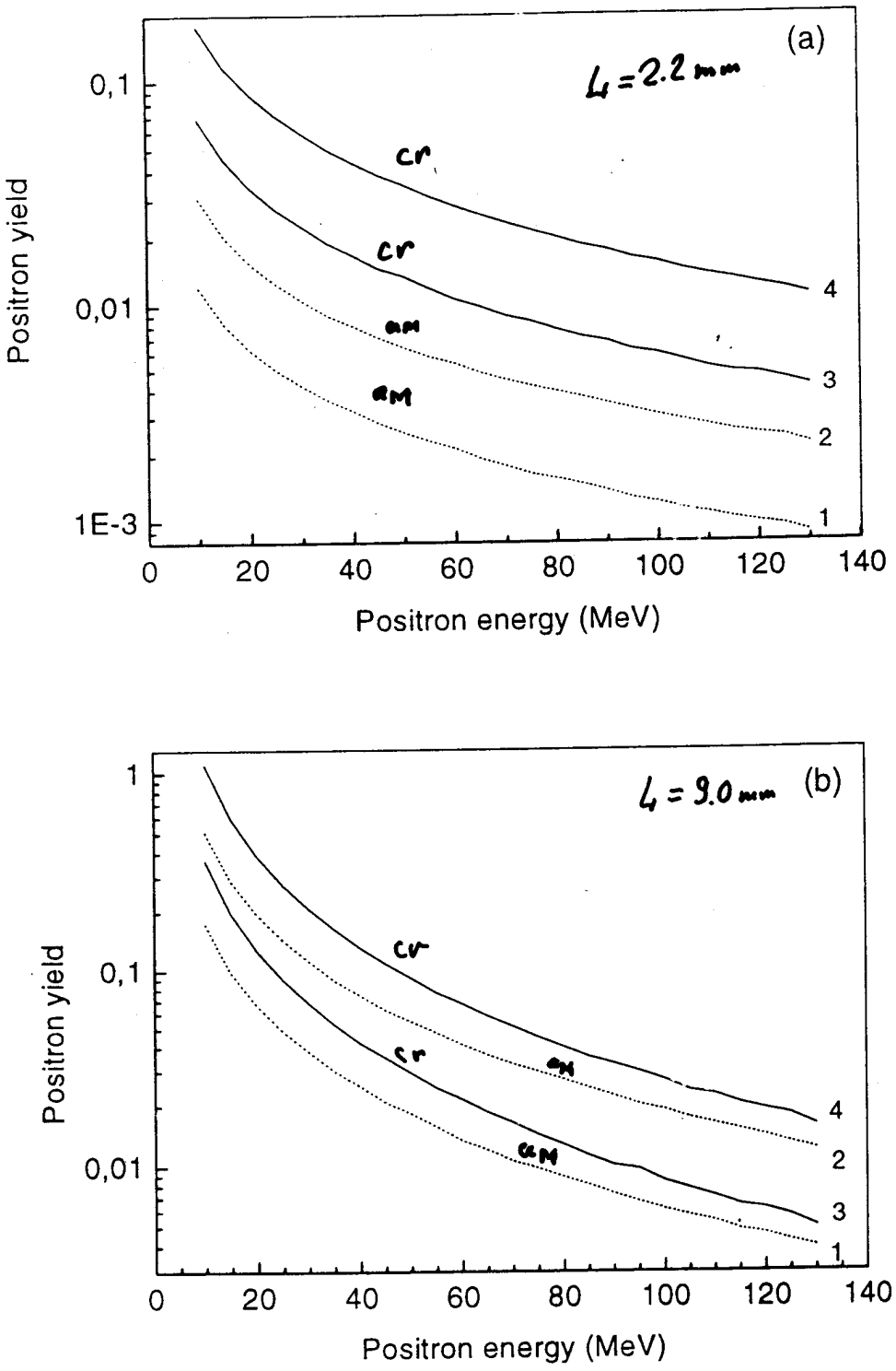

FIG. 4: Positron yield depending on energy at $L = 2.2$ mm (a) and $L = 9.0$ mm (b) for $p_{\perp}^{max} =$ 2.5 MeV/c (curves 1 and 3) and for $p_{\perp}^{max} = 5$ MeV/c (curves 2 and 4). Solid curves represent the yield from crystal and dotted from amorphous targets.

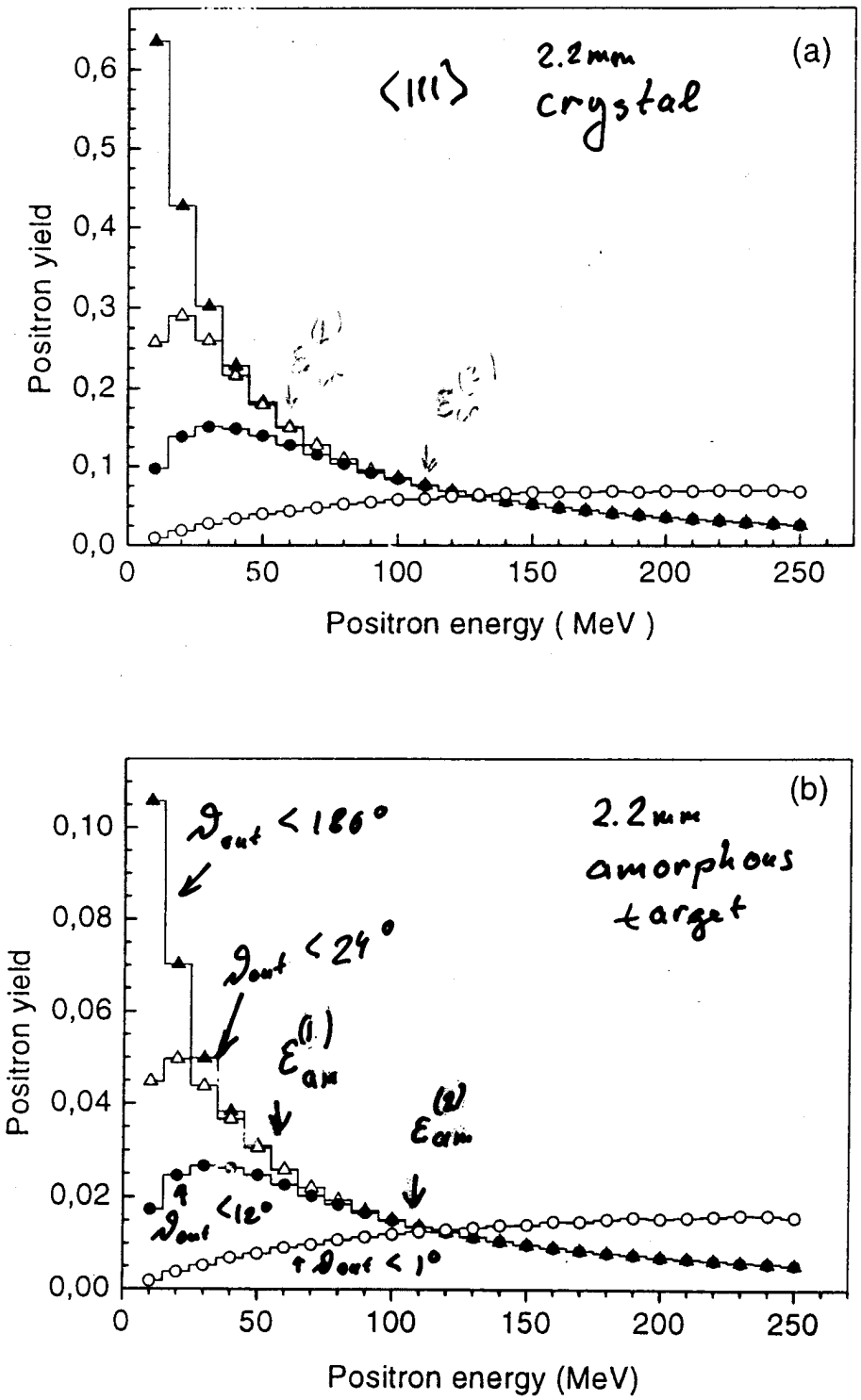

FIG. 2: Positron yield depending on energy from 2.2 - mm - thick crystal (a) and amorphous (b) targets at different collimation . Filled triangles - no collimation ($\vartheta_{out} \leq 180°$), open triangles - $\vartheta_{out} \leq 24°$, filled circles - $\vartheta_{out} \leq 12°$, and open circles - $\vartheta_{out} \leq 1°$ (multiplied by 10).

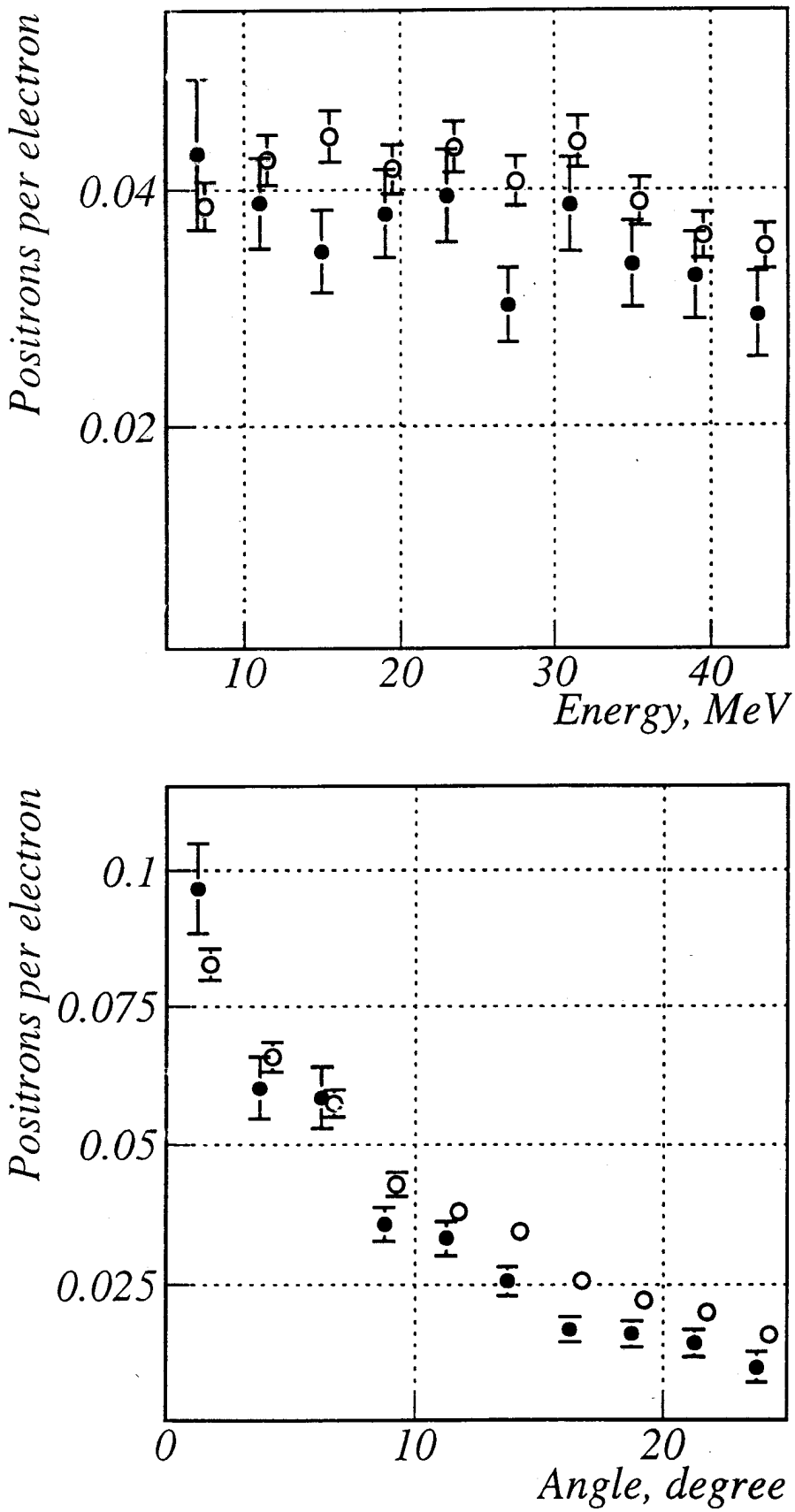

FIG. 1: Spectral (left) and angular (right) distributions of positrons from 10 GeV electrons traversing 8 - mm - thick crystal tungsten target along the < 111 >- axis. Open circles - simulation, filled circles - experiment.

In contrast to the magnitude of the positron yield, the enhancement is not very sensitive to the acceptance conditions. The calculated values of the enhancement(theory) are presented in Table 1 along with those taken from Table 1 of [15] (experiment). Purely statistical errors are figured in Table 1 as theoretical ones. The relative error in PPE was estimated as $N_{ef}^{-1/2}$, where N_{ef} is the mean number of events in the phase space corresponding to the acceptance conditions used in calculations. The total statistics was chosen so that approximately to equalize values of N_{ef} for amorphous and crystal targets of the same thickness. At given total statistics, the quantity N_{ef} increases with growing positron momentum in accord with a shape of the positron spectra at hard collimation shown in Figs. 2,3. This fact leads to a better statistical accuracy for larger momentum. We emphasize that the differences of the estimated and experimental enhancement values are smaller than corresponding experimental errors for all momenta and samples figured in Table 1.

3 Conclusion

Using the simple computer code suggested in [11] and [10], we have compared the theoretical predictions for some characteristics of the electromagnetic shower developing in axially aligned crystals with experimental results reported in [12],[13] and [14],[15]. On the whole, theory and experiment are consistent within the experimental accuracy. From this comparison we also conclude that the accuracy provided by the existing simplified code is at least better than 20%. This accuracy may be slightly improved if we include into consideration some processes like annihilation of positrons or Compton scattering of photons which were ignored as corresponding cross sections are small in the energy region of inter-

lation of the magnitudes of positron production efficiency (PPE), we simply put ϑ_{out}^{max} to 20 mrad. The value of $\Delta p/p$ was chosen to reproduce at applied collimation the experimental magnitude of PPE for the 9.0 - mm - thick amorphous target. Acting in this way, we have got $\Delta p/p = 3.2$ %. We realize that our regard for the acceptance conditions is rather rough. An additional inaccuracy was introduced when we determined the PPE numbers from Fig.5 of [15]. Note that the experimental numbers obtained in a such way, which are presented by filled symbols in Fig.6, do not reproduce exactly the whole set of mean experimental values for the enhancement given in Table 1 of [15]. Moreover, in Fig.5 of [15] there are no experimental points for 2.2 and 5.3 - mm - thick amorphous targets. For these two cases, we present in Fig.6 the values of PPE given by smooth - curve fits corresponding to simulation fitting in Fig.5 of [15]. Bearing all this in mind, we, nevertheless, can assert that a rather good agreement is seen in Fig.6 of the experimental results and our estimations. Relative difference of them is better than 13 % everywhere except the values of PPE at $p = 10$ and 15 Mev/c from both thinnest ($L = 2.2$ mm) targets, where the experimental yield is underestimated by 19 % to 42 %. Note that just for this thickness the largest inaccuracy was introduced while determining the PPE numbers from Fig.5 of [15] at $p = 10$ and 15 Mev/c, as the magnitude of the yield is especially small in this case.

Table 1: Enhancement of the positron yield from crystal targets

Momentum (MeV/c)	Enhancement (2.2-mm-thick)		Enhancement (5.3-mm-thick)		Enhancement (9.0-mm-thick)	
	theory	experiment	theory	experiment	theory	experiment
10	6.0 ± 0.5	6.5 ± 0.6	3.2 ± 0.3	3.4 ± 0.7	2.1 ± 0.2	2.3 ± 0.4
15	5.5 ± 0.3	6.2 ± 0.8	3.2 ± 0.2	3.2 ± 0.5	2.0 ± 0.1	2.0 ± 0.2
20	5.4 ± 0.2	5.1 ± 0.5	2.9 ± 0.1	3.0 ± 0.5	1.8 ± 0.1	1.8 ± 0.2

at $L = 9.0$ mm. These factors turn out to be practically (within an accuracy of a few percent) independent of the total positron momentum p. This fact can be easily understood if we assume that the width of the angular distribution of positrons is completely due to multiple scattering being, thereby, proportional to p^{-1}. Such assumption is confirmed by results of the calculation shown in Fig.5 for two groups of positrons. One of them contains positrons having momentum in the interval $p \in (8.5 \div 11.5)$ Mev/c , for another group $p \in (17 \div 23)$ Mev/c.

For the given target, the width of the angular distribution of positrons with $p \approx 10$ Mev/c is approximately twice as much that for $p \approx 20$ Mev/c as expected. The width of every distribution evidently increases when we go on to the thicker target of the same kind. Comparing angular distributions from crystal and amorphous targets of the same thickness, we find that at $L = 9.0$ mm the distributions are somewhat (about 1.5°) wider in the crystal case for both groups. In units of FWHM of the distribution from the crystal target these differences are about 6.5 % at $p \approx 10$ Mev/c and 14 % at $p \approx 20$ Mev/c. At $L = 2.2$ mm the distribution from the crystal target is wider by 15.5 % at $p \approx 20$ Mev/c whereas this is narrower by 10 % at $p \approx 10$ Mev/c.

Going on to the comparison of our results with those obtained in [15], let us remind that to perform an accurate comparison of such kind, exact information is needed concerning the acceptance conditions and registration efficiency of detectors in the experiment. As noted in [15], at $p = 20$ Mev/c, the momentum acceptance $(\Delta p/p)$ was 3 % (FWHM) and the polar angle acceptance was less than 20 mrad (FWHM). Since the shape of the acceptance curves was unavailable to us, we have tried to simulate experimental conditions using the same angular collimation $\vartheta_{out} \leq \vartheta_{out}^{max}$ and the same value of $\Delta p/p$ for all momenta and targets. So, at the calcu-

the yield is increased by $6 \div 7$ times for a crystal and by $17 \div 20$ times for amorphous samples. As a result, the enhancement at $L = 9.0$ mm is almost 3 times less than at $L = 2.2$ mm in this energy range. At $L = 9.0$ mm the enhancement is peaked in the first bin ($\varepsilon \in (5 \div 15)$ MeV) for every collimation. Its maximum values are $\mu_{max}(\vartheta_{out} \leq 180°) \simeq 2.25$, $\mu_{max}(\vartheta_{out} \leq 24°) \simeq 2.15$, $\mu_{max}(\vartheta_{out} \leq 12°) \simeq 2.08$, and $\mu_{max}(\vartheta_{out} \leq 1°) \simeq 2.06$. The enhancement monotonically decreases with growing positron energy and approximately halves at $\varepsilon \approx 250$ MeV. Thus, positron spectra from the crystal target are softer at $L = 9.0$ mm as well, and this property is much more pronounced in comparison with $L = 2.2$ mm.

Matching systems can be characterized also by the maximum transverse momentum $p_{\perp}^{max}$ of accepted positrons. In this connection, spectra of positrons having $p_{\perp} < p_{\perp}^{max}$ are of undoubted interest. Such spectra at $L = 2.2$ mm (a) and at $L = 9.0$ mm (b) from crystal and amorphous targets are shown in Fig.4. In contrast to the case of the pure angular selection (cf. Figs.2,3 the position of spectral maxima at limited $p_{\perp}$ values is always in the first bin ($\varepsilon \in (7.5 \div 12.5)$ MeV). Corresponding maximum values are $\mu_{max}(5\ MeV/c) \simeq 5.82$, $\mu_{max}(2.5\ MeV/c) \simeq 5.62$ at $L = 2.2$ mm and $\mu_{max}(5\ MeV/c) \simeq 2.17$, $\mu_{max}(2.5\ MeV/c) \simeq 2.11$ at $L = 9.0$ mm. The enhancement monotonically decreases with growing positron energy. Its variation over the whole energy interval presented in Fig.4 is about 15 % at $L = 2.2$ mm and 40 % at $L = 9.0$ mm. So, for this selection too, positron spectra from crystal targets are softer than those from amorphous targets of the same thickness. The interesting feature of spectral curves in Fig.4 is the similarity of those obtained for two different values of $p_{\perp}^{max}$ from the same target. The scaling factors η are $\eta_{cr} \simeq 2.6$, $\eta_{am} \simeq 2.5$ at $L = 2.2$ mm and $\eta_{cr} \simeq 3.1$, $\eta_{am} \simeq 3.0$

The specific features of the radiation under consideration, which occurs for electrons moving in a continuous potential of the axes (planes), are dictated by the particles which are in the channel and are not too high above the barrier. The contribution of these particles can be enhanced by a photon collimator. For this purpose, the collimation angle ϑ_{col} (we count it from the axis oriented to the centre of the collimator) should be chosen approximately equal to the Lindhard angle $\vartheta_{col} \approx \vartheta_c$. On the other hand, if $\vartheta_{col} < m/\varepsilon \equiv 1/\gamma$, we shall omit a fraction of the radiation of interest. For energies from several hundreds of MeV to several GeV considered, we have $\vartheta_s \gg 1/\gamma$ and $\vartheta_s \gg \vartheta_c$ at a crystal thickness $L \approx L_0$. Thus, the condition

$$\max\left(\frac{1}{\gamma}, \vartheta_c\right) \lesssim \vartheta_{col} \ll \vartheta_s \tag{4}$$

assumed to be satisfied and then the factor $\exp\left(-r_\perp^2/g(l)\right)$ can be substituted for unity[3]) for particles whose radiation reaches the collimator, and the distribution proves to be uniform in a transverse phase space. As a consequence, for the intensity of the radiation under consideration (labelled by "ch") at the depth l we have

$$\frac{dI_{ch}}{d\Omega} = \frac{\bar{I}}{\pi g(l)}, \tag{5}$$

where $\bar{I} = \int I(x)\,dx/d_{pl}$ for the plane and $\bar{I} = \int I(\varrho)\,d^2\varrho/S$ for the axis. It is worth noting that $\bar{I}$ coincides with I_{as}, the asymptotic value achieved by the intensity at the incident angles $\vartheta_0 \geqq \vartheta_c$ and $\vartheta_0 \gg \vartheta_c$ for the axial and planar cases, respectively. Emphasize that (5) incorporates the radiation from all the particles rather than from the above-barrier ones only. The appearance of I_{as} in (5) is due to the uniformity of the distribution in transverse phase space under the indicated assumptions, see (4), while the uniformity of the distribution with respect to $v_\perp$ resulted, in (5), in a uniform distribution with respect to the solid angle of emitted photons for the angles $\vartheta_{ph} \lesssim \vartheta_s$.

The values of $\bar{I} = I_{as}$ are readily calculated for any potential of the axes, or planes. For the potentials used, an explicit expression for I_{as} is given by formulae (29) in [1, 2]. Thus, the axial potential has been taken in the form (see [5, 6])

$$U(x) = V_0\left[\ln\left(1 + \frac{1}{x + \beta}\right) - \ln\left(1 + \frac{1}{x_0 + \beta}\right)\right]. \tag{6}$$

For it,

$$\bar{I} = I_{as} = I_0 \varphi(\beta), \tag{7}$$

where

$$I_0 = \frac{8\pi e^2 V_0^2 \varepsilon^2}{3m^4} n_\perp, \qquad \varphi(\beta) = (1 + 2\beta)\ln\left(1 + \frac{1}{\beta}\right) - 2. \tag{8}$$

In (6), $x = \varrho^2/a_s^2$ where a_s is the screening radius and the parameter β is proportional to the squared amplitude of thermal vibrations. In [6, 1] we took $V_0 = Ze^2/d$ where d is the average distance between the atoms in the chain, and the parameters β and a_s were determined by means of the fitting procedure described in [6]. Their values for the $\langle 100\rangle$ axis of some substances are listed in the tables of [6, 1]. For the $\langle 111\rangle$ axis, we have made a three-parametric fitting: the quantity V_0 is regarded to be a fitting parameter as well. The results of this procedure are illustrated in Table 1.

$\vartheta_{out} \leq 24°$ are overlapping within precision better than 1 % starting from $\varepsilon_{cr}^{(1)} \simeq 55$ MeV. In turn, from $\varepsilon_{cr}^{(2)} \simeq 110$ MeV, the same happens with curves corresponding to $\vartheta_{out} \leq 24°$ and $\vartheta_{out} \leq 12°$. Such behavior is also seen in Fig.2 (b) for the amorphous target where $\varepsilon_{am}^{(1)} \simeq 50$ MeV and $\varepsilon_{am}^{(2)} \simeq 105$ MeV. In other words, positrons with energies $\varepsilon > \varepsilon^{(1)}$ are practically concentrated within the cone $\vartheta_{out} \leq 24°$ and those with $\varepsilon > \varepsilon^{(2)}$ have $\vartheta_{out} \leq 12°$. In accordance with this picture, the spectral maximum is shifted to the right while the width of the distribution increases when the collimation angle decreases. The enhancement μ, being bin-by-bin ratio of the positron yield from the crystal target to that from the amorphous one at the same collimation, is almost constant for $\varepsilon <$ 45 MeV and monotonically decreases with growing positron energy. This means that positron spectra from the crystal target are softer. Somewhat lower values of $\varepsilon^{(1)}, \varepsilon^{(2)}$ in the amorphous case point at the same feature. For given collimation, the variation of the enhancement is about 20 % over the whole energy interval presented in Fig.2. The maximum values of the enhancement at different collimation are $\mu_{max}(\vartheta_{out} \leq 180°) \simeq 6.09$, $\mu_{max}(\vartheta_{out} \leq 24°) \simeq 5.92$, $\mu_{max}(\vartheta_{out} \leq 12°) \simeq 5.67$, and $\mu_{max}(\vartheta_{out} \leq 1°) \simeq 5.29$. Apparently, they diminish as the collimation angle does so. Shown in Fig.3 is the same as in Fig.2 but for the target thickness $L =$ 9.0 mm. The yield at $\vartheta_{out} \leq 1°$ (open circles) is multiplied now by 30. The qualitative behavior of spectra depending on the collimation angle at $L = 9.0$ mm is the same as at $L = 2.2$ mm. However, all the spectra become softer for the larger target thickness. This is indicated already by the increase in $\varepsilon^{(1)}$, $\varepsilon^{(2)}$ values which are now $\varepsilon_{cr}^{(1)} \simeq 85$ MeV, $\varepsilon_{cr}^{(2)} \simeq 185$ MeV, $\varepsilon_{am}^{(1)} \simeq 75$ MeV, $\varepsilon_{am}^{(2)} \simeq 165$ MeV. It is clear that the magnitude of the yield from the thicker target is essentially larger but this increase is different in the crystal and amorphous cases. For example, in the energy range $\varepsilon < 45$ MeV

(ε_{dep}^{am}) in the amorphous one. Such interrelation of ε_{dep}^{cr} and ε_{dep}^{am} should take place in the case of [14], where the crystal thickness is about 1.8 L_{ef} (see discussion in the Introduction). This is confirmed by our calculations which give $\varepsilon_{dep}^{cr} \simeq 11$ MeV and $\varepsilon_{dep}^{am} \simeq 277$ MeV per one incident electron.

2.3 Qualitative features of positron distributions and experiment (KEK) at $\varepsilon_0 = 8$ GeV

In [15] the positron production efficiency from 2.2 - mm, 5.3 - mm and 9.0 - mm - thick tungsten crystals was measured using an 8 - GeV electron beam. Positrons produced in the forward direction with momenta 10, 15 and 20 MeV/c were detected by the magnetic spectrometer. Thus, only several points in the energy distribution were determined under hard collimation conditions. Therefore, before going on to the comparison of the experimental results with our, let us remind some important qualitative features of spectral - angular distributions using 8 GeV electrons and the $< 111 >$ - axis of the tungsten crystals as an example. For the sake of comparison, the corresponding distributions for amorphous tungsten will be presented as well. Below all the quantities characterizing the positron yield are normalized per one incident electron.

The use of matching systems implies some collimation (typically $\vartheta_{out} \leq 25^\circ$) of outgoing positrons. Shown in Fig.2 is the energy dependence (energy step is equal to 10 MeV) of the positron yield from crystal (a) and amorphous (b) targets of the same thickness $L = 2.2$ mm. In the case of the hard collimation, when $\vartheta_{out} \leq 1^\circ$ (open circles), the yield is multiplied by 10 to make it visible. The larger the positron energy, the smaller is the typical value of ϑ_{out} since both production and multiple scattering processes are characterized by smaller angles for higher energies. This is seen in Fig.2 (a) where the spectral curves for $\vartheta_{out} < 180^\circ$ and that for

positrons having energies in the 5÷45 MeV range. We emphasize that the relative difference between measured and simulated results typically does not exceed 20 % in both spectral and angular distributions as seen in Fig.1. We are aware that preliminary results for another settings used in the same experiment do not contradict with the estimated scale of the difference between the data and theoretical predictions. We hope that this interrelation will not become worse after performing the complete analysis of the data which now is underway. This analysis will also give more detailed information concerning spectral - angular distributions of positrons depending on initial electron energies and target thicknesses.

2.2 Experiment (KEK) at $\varepsilon_0 = 3$ GeV

The main goal of the experiment [14] was an attempt to apply the crystal target to the working electron/positron linac, the injector for the electron - positron collider B - Factory at KEK. Thus, the acceptance conditions for created positrons were determined by the momentum acceptance of the positron linac with the matching section which is 8.2 MeV/c $< p <$ 11.6 MeV/c and $p_\perp <$ 2.4 MeV/c. The hybrid target used consists of 1.7 - mm - thick tungsten crystal followed by 7 - mm - thick amorphous tungsten. The observed positron yield was enhanced by the factor 1.40 when the $< 111 >$ crystal axis was aligned with 3 GeV incident electron beam as compared to the case of the disoriented crystal. Our number for this enhancement is 1.47 being only 5 % larger than the experimental one. Note that in the experiment [14] the crystal and amorphous parts of the hybrid target were separated by the distance of 70 mm. This circumstance, which, in principle, may slightly change the enhancement value, was not taken into account in our calculation. Recollect that the amount of the energy deposited in the crystal part (ε^{cr}_{dep}) of the hybrid target may be much smaller than that

simplified description of the shower development takes into account coherent (induced by the regular motion of particles in the field of crystal axes) and incoherent (like that in an amorphous medium) mechanisms of photon emission and pair production processes. The multiple scattering and the ionization energy loss of electrons and positrons are taken into account neglecting crystal effects. The coherent radiation from channelling and moving not very high above the axis potential barrier particles is described using the semi - phenomenological spectrum suggested in [11]. The corresponding computer code was developed. This allows one to calculate energy, angular, and coordinate distributions of positrons emergent from the crystal or hybrid target and to find an amount of the energy deposition. We think that the investigation of such distributions should be the main object of the experiments having the creation of the crystal assisted positron source as their ultimate aim.

2.1 Experiment (CERN) at $\varepsilon_0 = 10$ GeV

Among experiments cited above, spectral - angular distributions of created positrons were measured only in WA103 experiment at CERN (see [12], [13]) where our code was used in simulations as the event generator. This simulation allowed for the acceptance conditions and the efficiency of the detectors used. Shown in Fig.1 taken from [13] is one example of the measured and simulated distributions of positrons from 10 - GeV electrons aligned with the $< 111 >$- axis of the 8 - mm - thick crystal tungsten.

The angular acceptance conditions in WA103 experiment were approximately $|\vartheta_V^{out}| \leq 1.5°$ for the vertical and $0 \leq \vartheta_H^{out} \leq 25°$ for the horizontal angle of outgoing positron with respect to the initial electron beam direction. We shell see below that the shape of the positron spectrum depends on the degree of collimation. The one-dimensional (over ϑ_H^{out}) angular distribution is presented for

present the scale, let us list some values ω_{max} where this spectrum is maximum: $\omega_{max}(1GeV) \simeq 31$ MeV, $\omega_{max}(4GeV) \simeq 170$ MeV, and $\omega_{max}(8GeV) \simeq 490$ MeV. Note that the width of the spectrum is typically several times larger than ω_{max}. The increase in the number of relatively soft photons turns out to be much more pronounced than that in the total radiation intensity. In the end, just this fact leads to the substantial enhancement of the positron yield from crystal targets.

Recently the positron production in axially aligned single crystals was studied in two series of experiments performed at CERN [12], [13] and KEK [14], [15]. The initial energy of electrons was 3 GeV [14], 6 and 10 GeV [13], 8 GeV [15], and 10 GeV [12]. In all cases the initial electron beam was aligned with the $< 111 >$ - axis of the tungsten crystal that sometimes served as the crystal part of the hybrid target which contained an additional amorphous tungsten target. A noticeable enhancement of the low-energy positron yield was observed in all experiments cited above when the yield from the crystal target was compared with that from the amorphous target of the same thickness. The experimental results and our theoretical estimations presented in the next Section display a rather good agreement with each other.

2 Comparison of theory with experiment

Theoretical results for the conditions of the experiments cited above were obtained using the approach developed in [11] and [10] where various positron and photon distributions as well as deposited energies in different crystals were calculated for the energy range of initial electrons from 2 to 300 GeV. In these papers, all the formulas used in Monte-Carlo simulations of the specific $e^-e^+\gamma$ - shower characteristics are given in the explicit form. Remember that our

ergy region. The substantial advance in the description of shower formation at axial alignment was caused by the invention of the semi - phenomenological radiation spectrum [11] . This allows one to consider the relatively low (of a few GeV) energy range of the initial electrons which is presumed for the efficient positron source. The radiation intensity increases with the initial electron energy. As a result, at some energy the effective radiation length L_{ef} in the crystal becomes smaller than the conventional radiation length L_{rad} and continues its decrease at further increase of the energy. All numerical examples will be given below for the electron beam aligned with the $< 111 >$ - axis of the tungsten crystals. Then we have for the quantity L_{ef} defined as in Sec.3 of [11]: $L_{ef}(1\ \mathrm{Gev}) \simeq 0.166$ cm, $L_{ef}(4\ \mathrm{Gev}) \simeq 0.084$ cm, and $L_{ef}(8\ \mathrm{Gev}) \simeq 0.061$ cm. In the hybrid target which consists of the crystal part followed by the amorphous one, the thickness of the crystal constituent of several L_{ef} is obviously quite enough. Indeed, at the depth $L_0 \approx (3 \div 4)L_{ef}$ most of the particles, including the initial electrons, are sufficiently soft to reduce the coherent contribution to the radiation to the level of the incoherent one. Thereby, the further development of the shower proceeds more or less in the same way for the crystal or amorphous type of the remaining part of the target. We emphasize that the crystal part $L \leq L_0$ of the target serves as the radiator, and secondary charged particles are still not so numerous at this stage of the shower development. Therefore only a small portion of the total energy loss is deposited in the crystal part of the target which considerably reduces a danger of its overheating. The softness of photon spectra is another important feature of the crystal radiator giving additional advantages for the positron production in comparison with the entirely amorphous target. To get more definite idea concerning the shape of the power spectrum one can use its explicit form given by Eq.(2) in [11]. To

[1],the radiation intensity in a crystal exceeds that of the conventional bremsstrahlung starting with electron energies $\varepsilon \sim 1$ GeV. Simple estimations of the width of the power spectrum performed indicate a soft character of this spectrum. So '...a source of hard and directed radiation concentrated within a comparatively narrow frequency range...' was proposed in [1]. Basing on these properties of the photon emission process, the use of this phenomenon in positron source for future accelerators was proposed [2]. The pair production rate which is due to the coherent (crystal) effects exceeds that of the standard (Bethe-Heitler) mechanism starting with photon energies $\omega \simeq \omega_{th}$. The value of ω_{th} is about 22 GeV for the $< 111 >$ - axis of tungsten being several times larger for another crystals. (See review [3] and recent book [4] for further details concerning QED - processes in crystals.) For energies well above ω_{th}, the crystal effects become really strong and may be used to create effective and compact electromagnetic calorimeters [5]. For very high energies ($\varepsilon \gg \omega_{th}$) of initial and created particles, kinetic equations describing the shower development were solved analytically [6]. Though the initial electron energies were high enough in the first experimental investigation [7] of shower formation in crystals, energies of detected particles were too low to allow us the direct comparison with [6]. To explain the results of [7], Monte-Carlo simulations were performed in [8]. The probabilities of basic processes used in [8] were obtained within so-called constant field approximation. A good agreement was demonstrated in [8] with the results of [7] for Ge crystals.

When the initial electron energy is below ω_{th}, photons are mainly emitted with energies $\omega \ll \omega_{th}$ and so, up to minor modifications (see [9], [10]), the pair production process proceeds in a crystal as in an amorphous medium. The enhancement of radiation from initial electrons is thereby the main crystal effect in this en-

Comparison of theory with experiment for positron production from high-energy electrons moving along crystal axes

B. S.
Phys. Rev ST Accel. Beams, 5, 121001 (2002)

1 Introduction

An efficient positron source is one of the important components of future electron - positron colliders. Positrons are generated from electrons in the course of the $e^-e^+\gamma$ - shower developing in a medium. In high-energy region, the basic processes involved in the shower development are typically considerably enhanced in oriented crystals as compared with corresponding amorphous media . The most pronounced effects take place at axial alignment when initial electrons are moving along the main axes of a crystal. This alignment alone will be considered below. According to

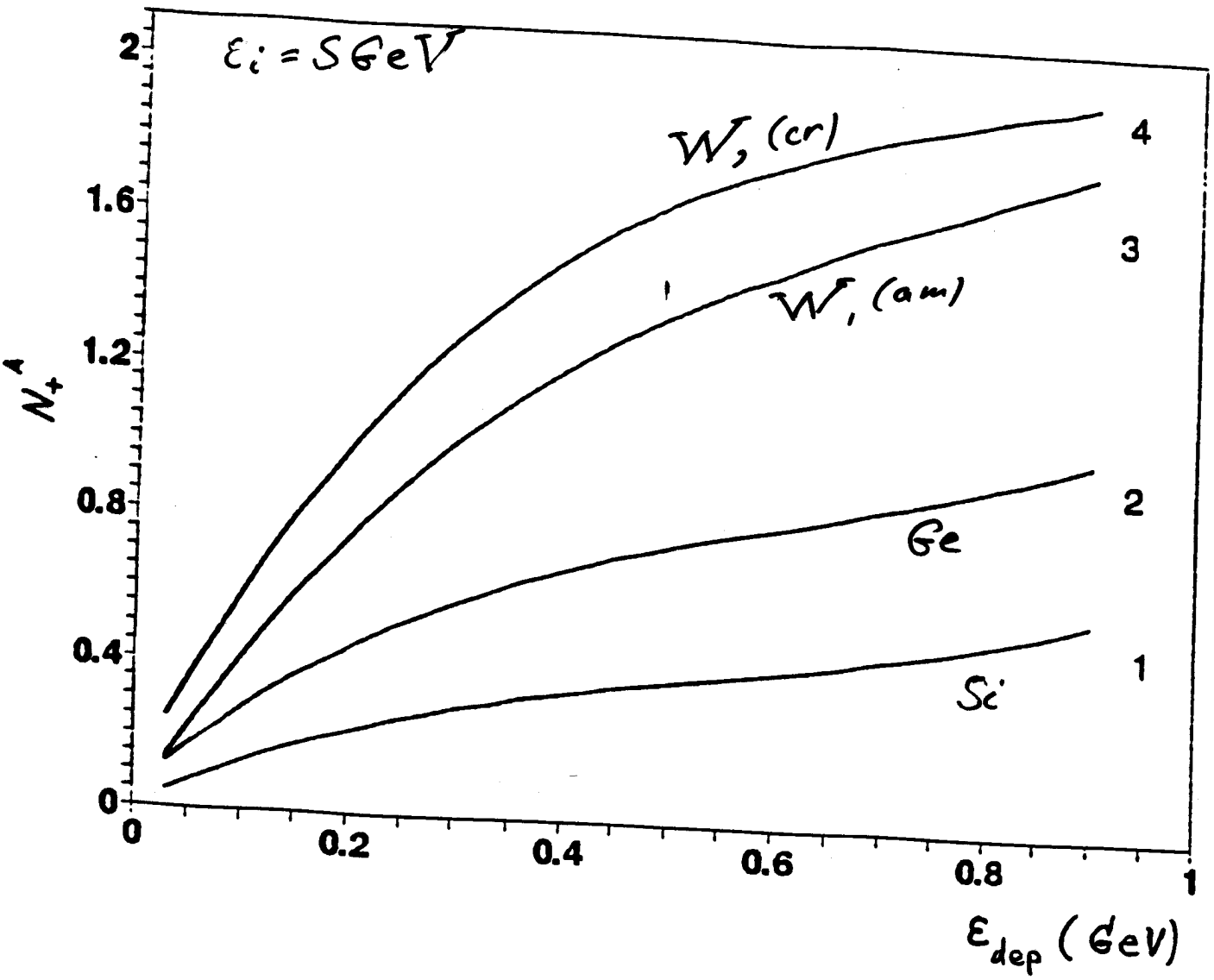
$\varepsilon_i = 5\,GeV$
W, (cr)
W, (am)
Ge
Si
4
3
2
1
N_+^A
0
0.4
0.8
1.2
1.6
2
0.2
0.6
1
ε_{dep} (GeV)

Fig. 9

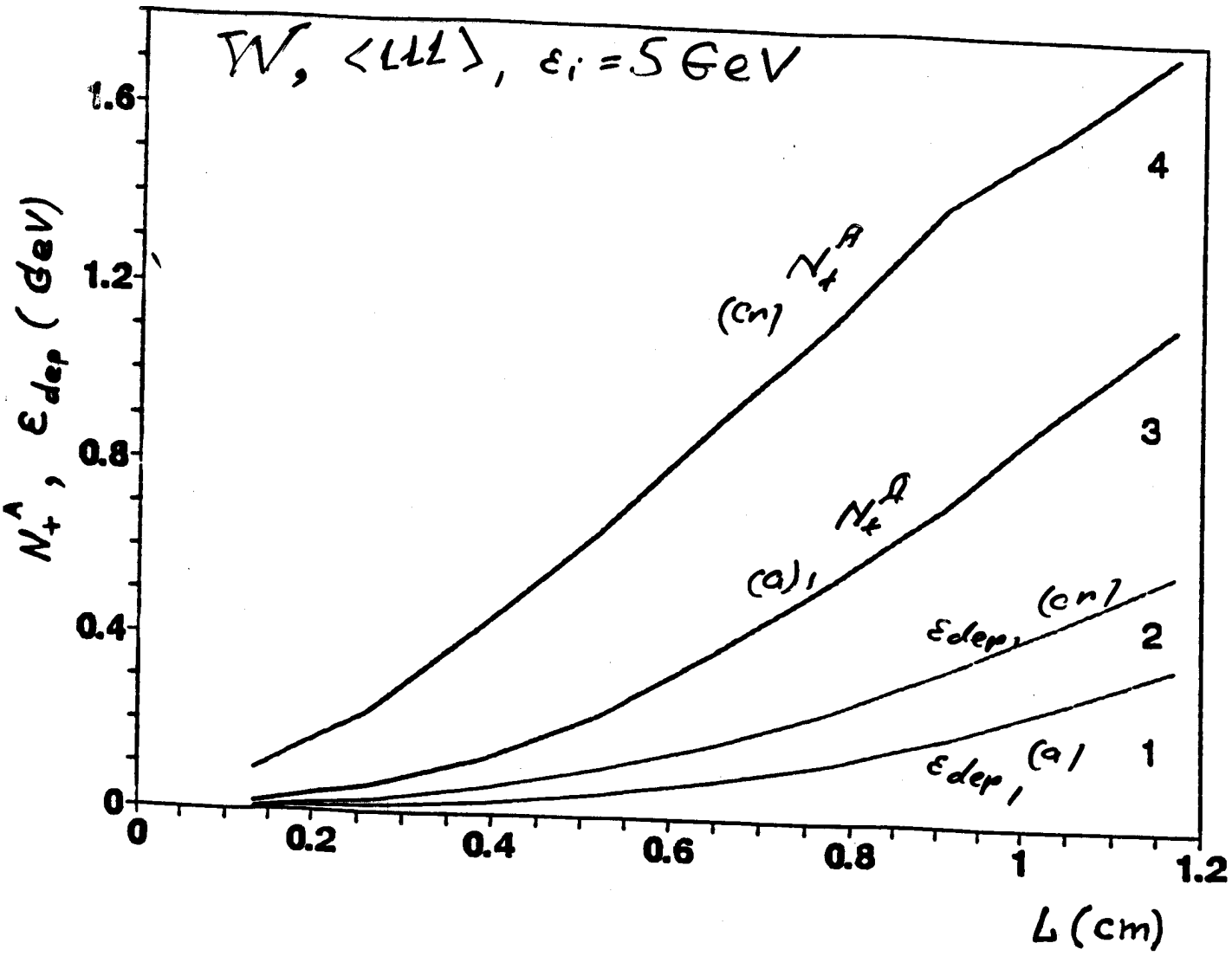
W, <111>, ε_i = 5 GeV
N_+^A , ε_{dep} (GeV)
L (cm)
N_+^A (cm)
N_+^A (a)
ε_{dep} (cm)
ε_{dep} (a)
1
2
3
4
0
0.2
0.4
0.6
0.8
1
1.2
1.6

Fig. 8 (B)

A : accepted $5\,MeV \leq \varepsilon_+ \leq 25\,MeV$

$p_\perp \leq 4\,MeV/c$

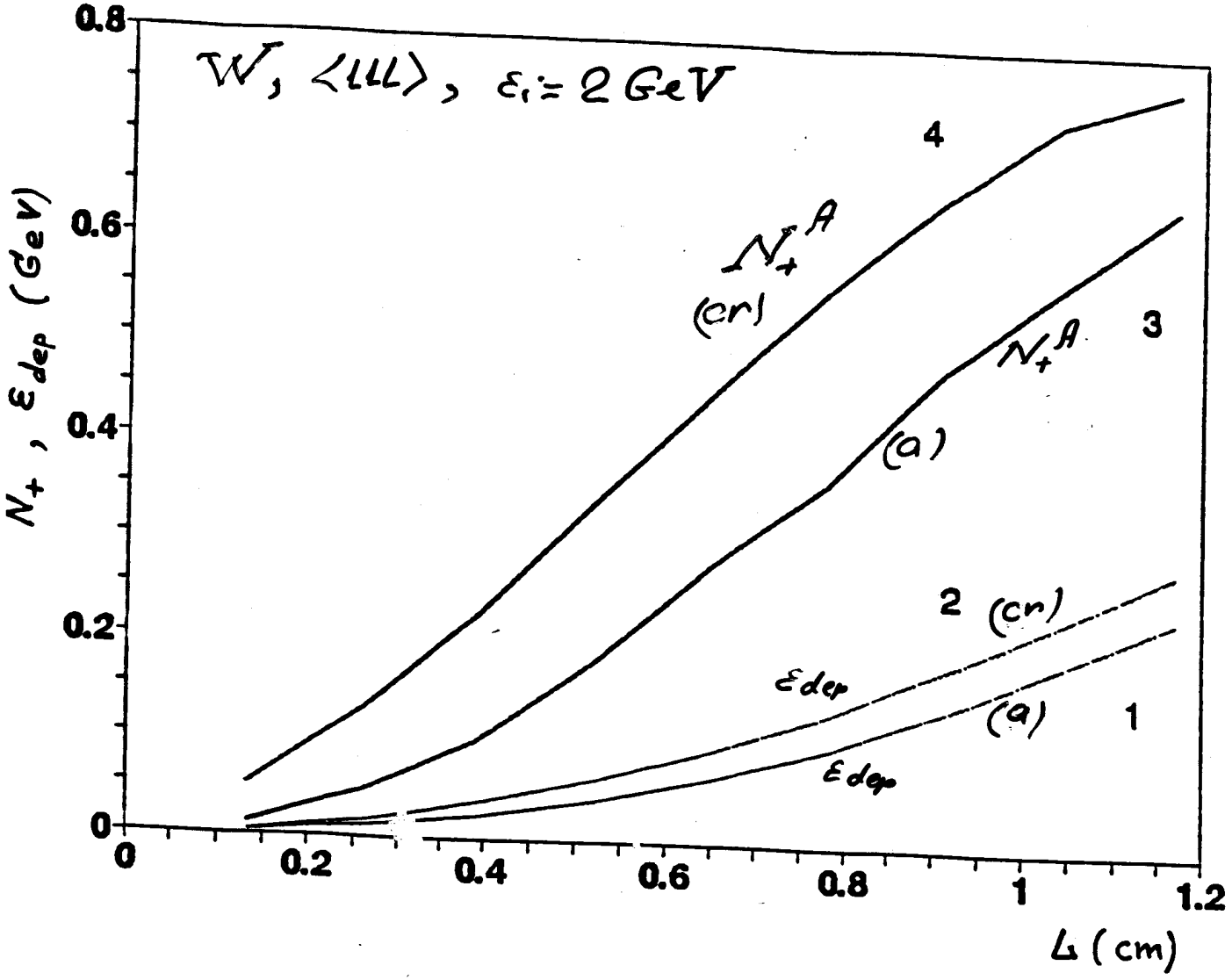

Fig. 8 (a)

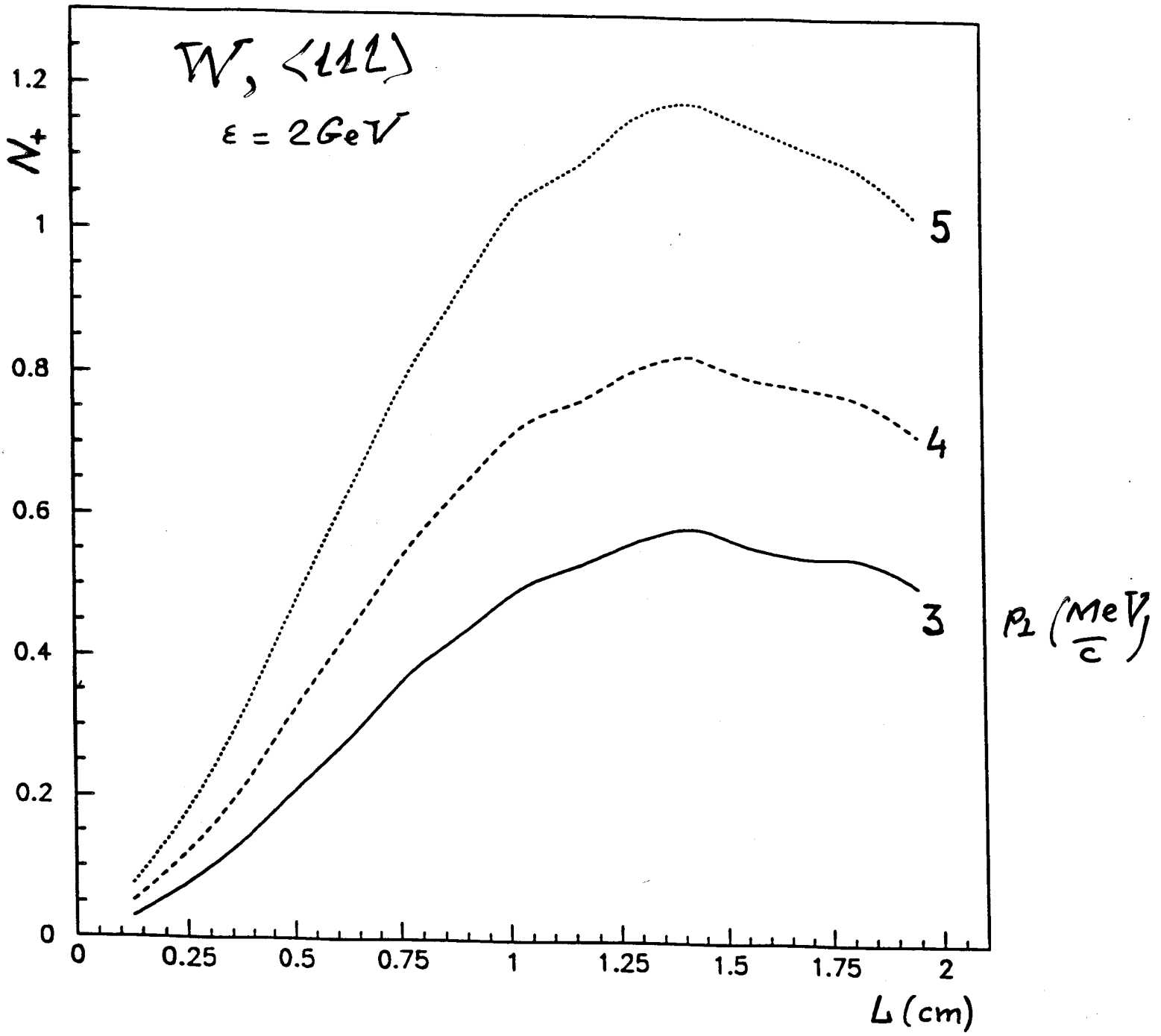
W, <111>
ε = 2GeV
N+
1.2
1
0.8
0.6
0.4
0.2
0
0
0.25
0.5
0.75
1
1.25
1.5
1.75
2
L (cm)
5
4
3
P⊥ (MeV/c)

Fig. 7

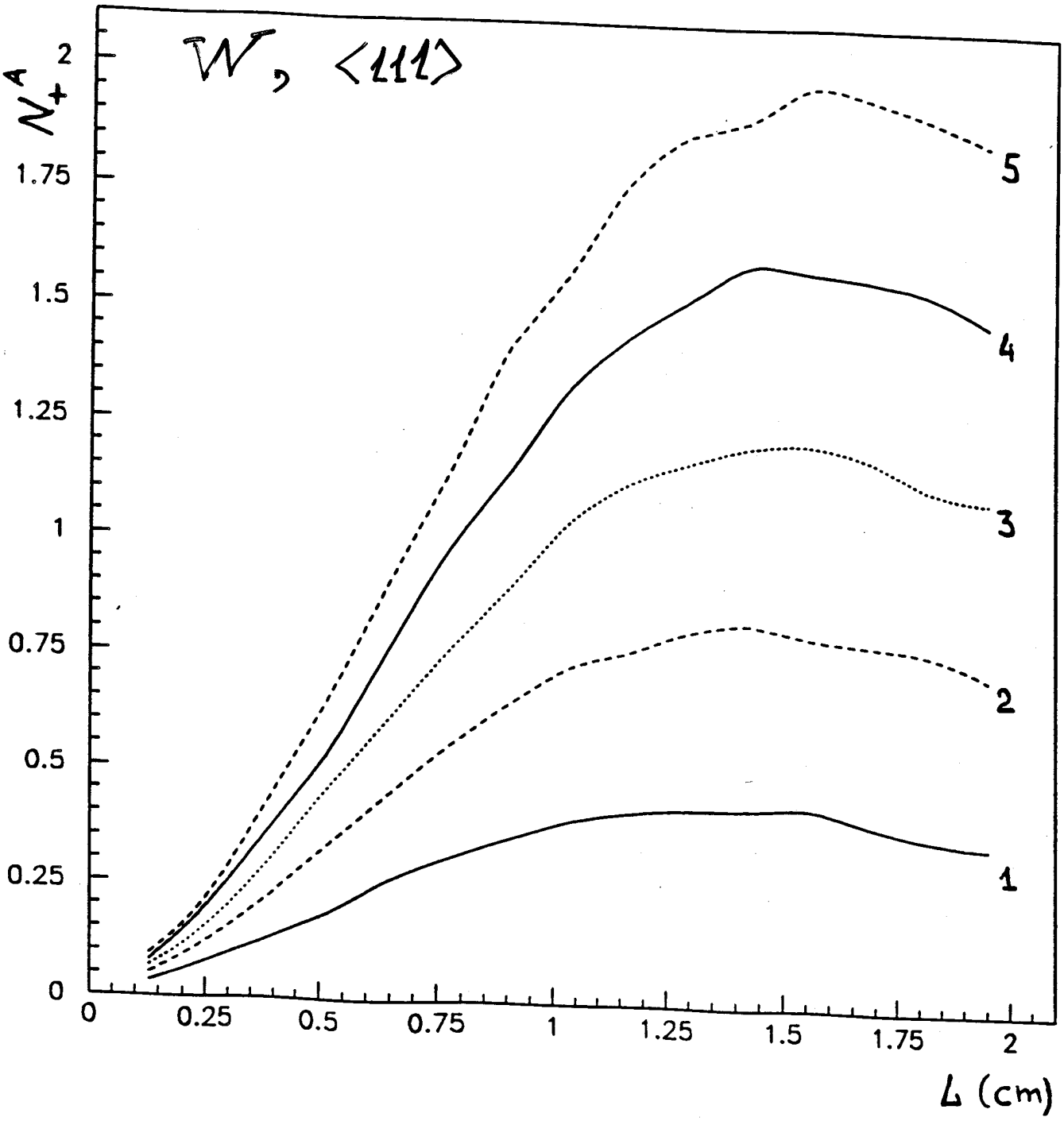
W, <111>
N_+^A
2
1.75
1.5
1.25
1
0.75
0.5
0.25
0
0
0.25
0.5
0.75
1
1.25
1.5
1.75
2
L (cm)
1
2
3
4
5

Fig. 6

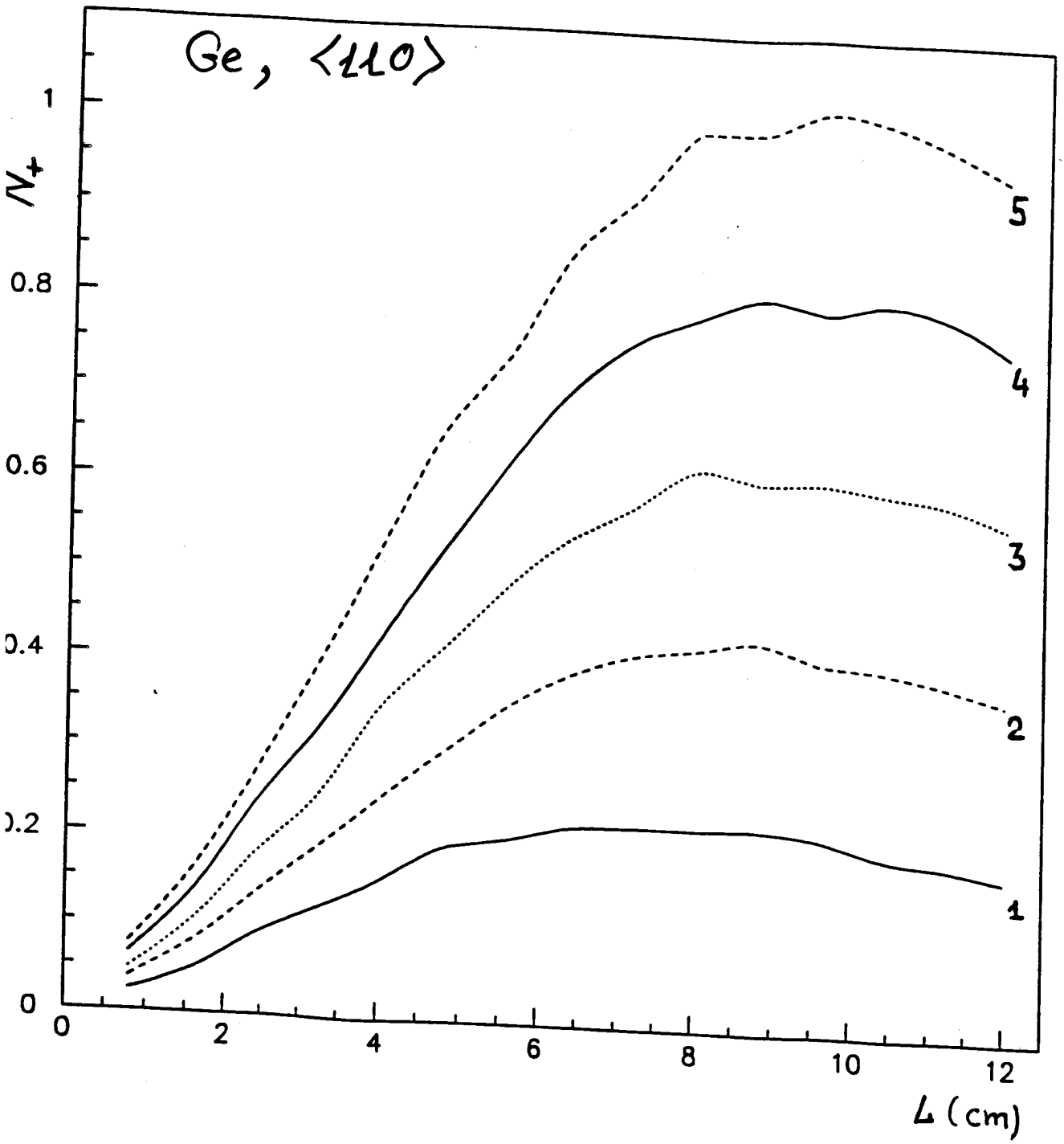

Fig. 5

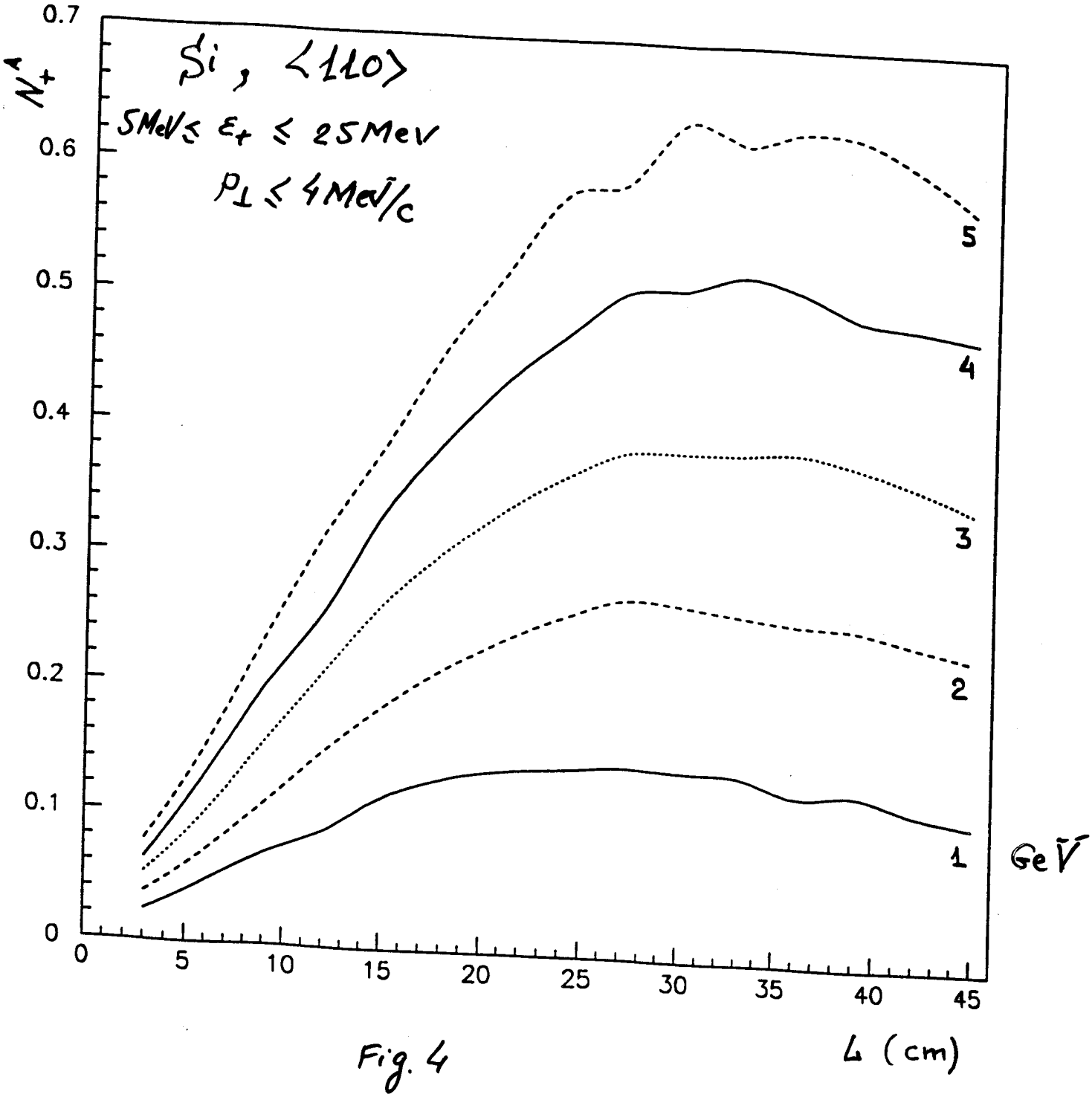
Si , <110>
5MeV ≤ ε+ ≤ 25MeV
p⊥ ≤ 4MeV/c
N+
0.7
0.6
0.5
0.4
0.3
0.2
0.1
0
0
5
10
15
20
25
30
35
40
45
1
2
3
4
5
GeV
L (cm)

Fig. 4

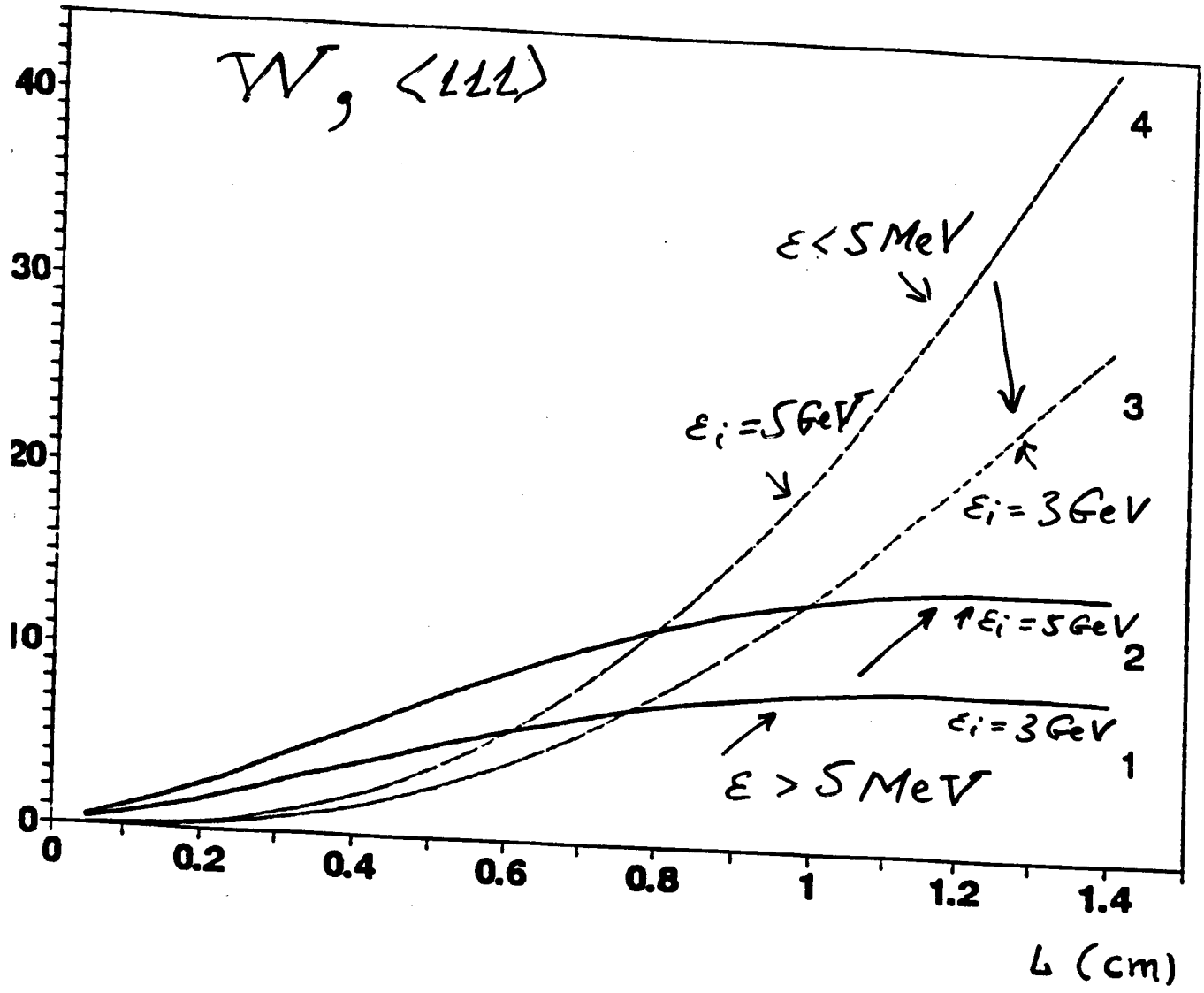
W, <L12>
40
30
20
10
0
0
0.2
0.4
0.6
0.8
1
1.2
1.4
L (cm)
ε<5MeV
4
εi=5GeV
3
εi=3GeV
εi=5GeV
2
εi=3GeV
ε>5MeV
1

Fig. 3

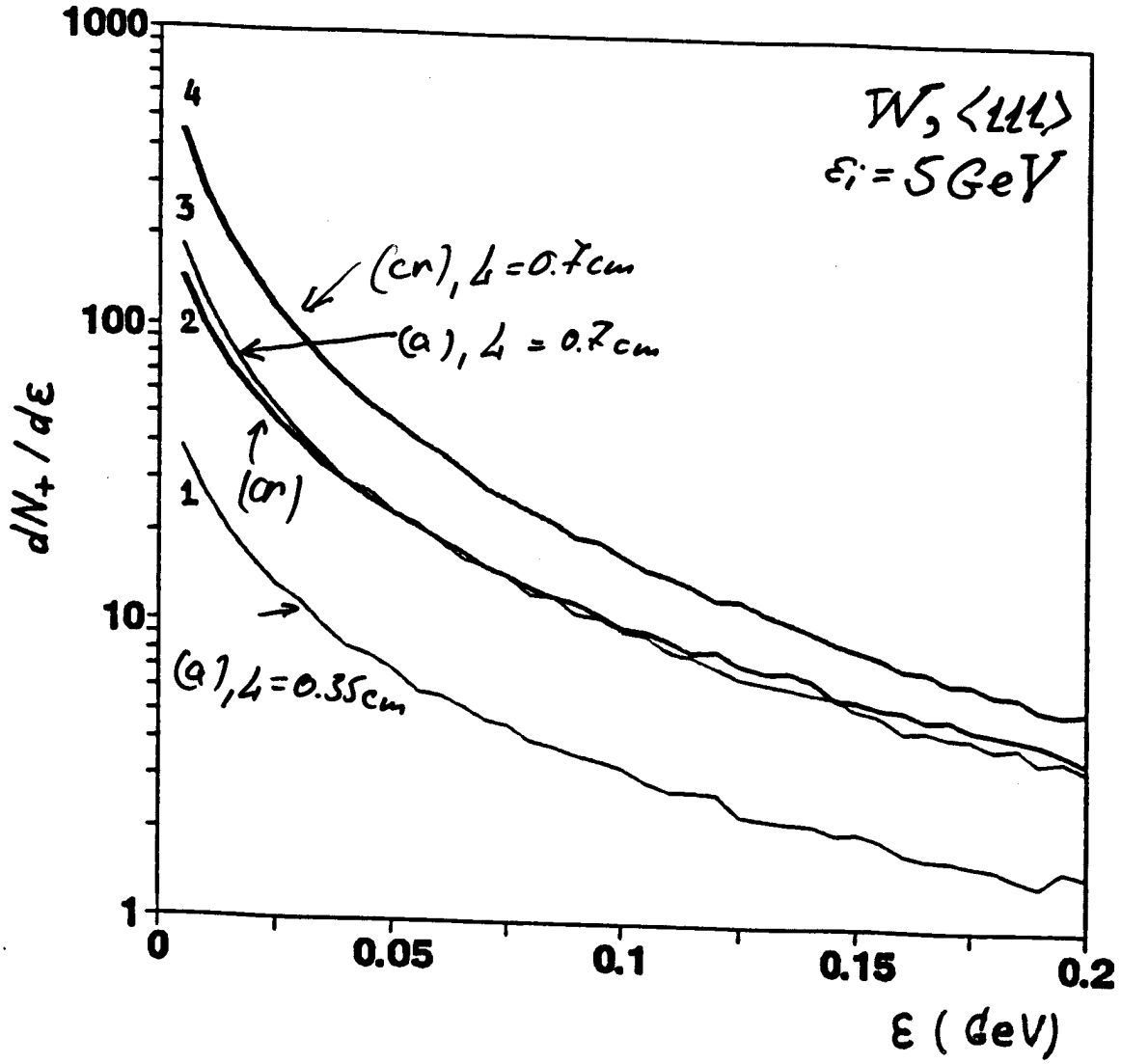
1000
100
10
1
0
0.05
0.1
0.15
0.2
dN+ / dε
ε (keV)
W, <111>
ε_i = 5 keV
(cr), L = 0.7 cm
(a), L = 0.7 cm
(cr)
(a), L = 0.35 cm
1
2
3
4

Fig. 2 (b)

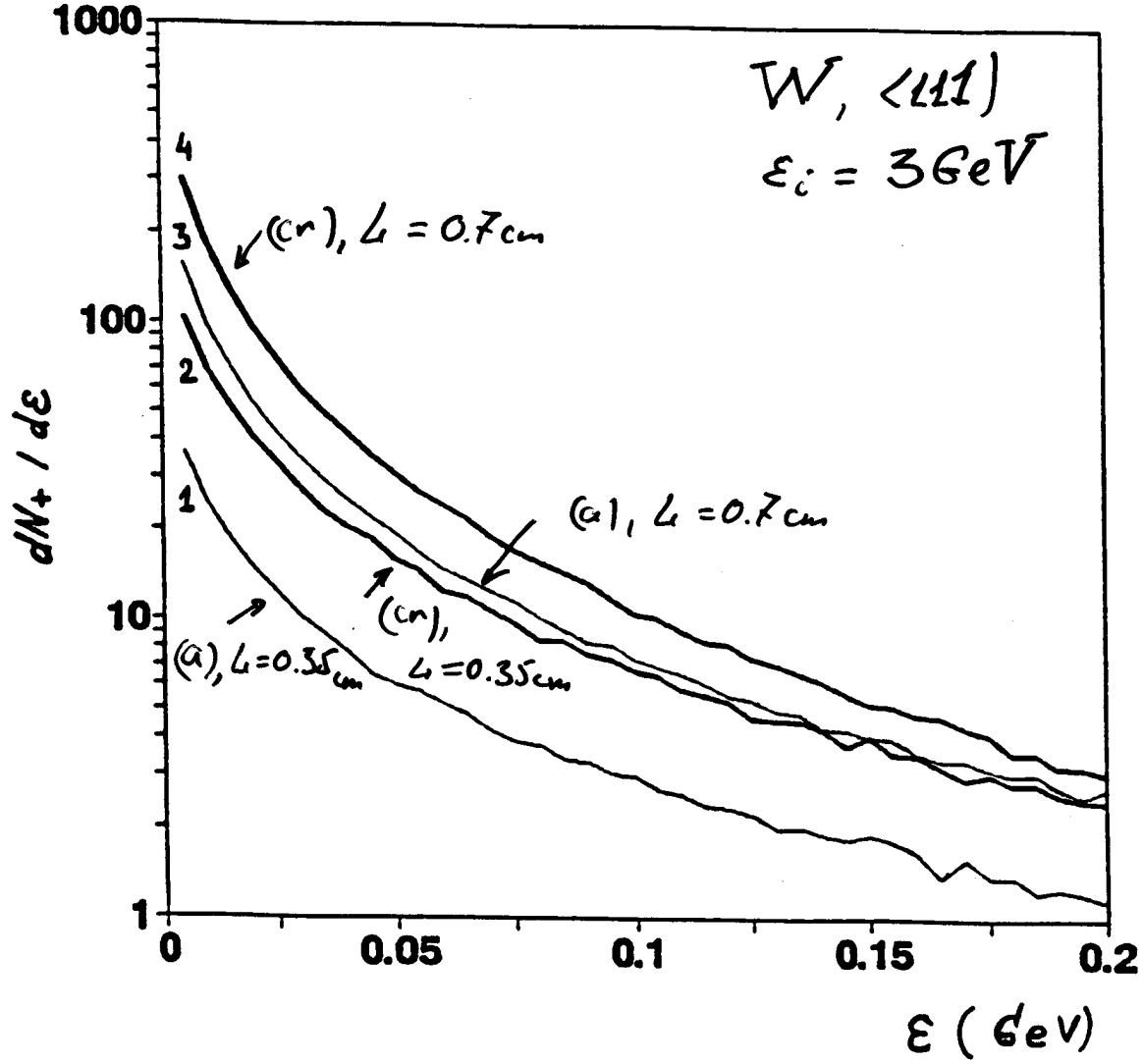
1000
100
10
1
dN+ / dε
W, <111>
εi = 3GeV
4
3
2
1
(cr), L = 0.7cm
(a), L = 0.7cm
(cr), L = 0.35cm
(a), L = 0.35cm
0
0.05
0.1
0.15
0.2
ε (eV)

Fig. 2 (a)

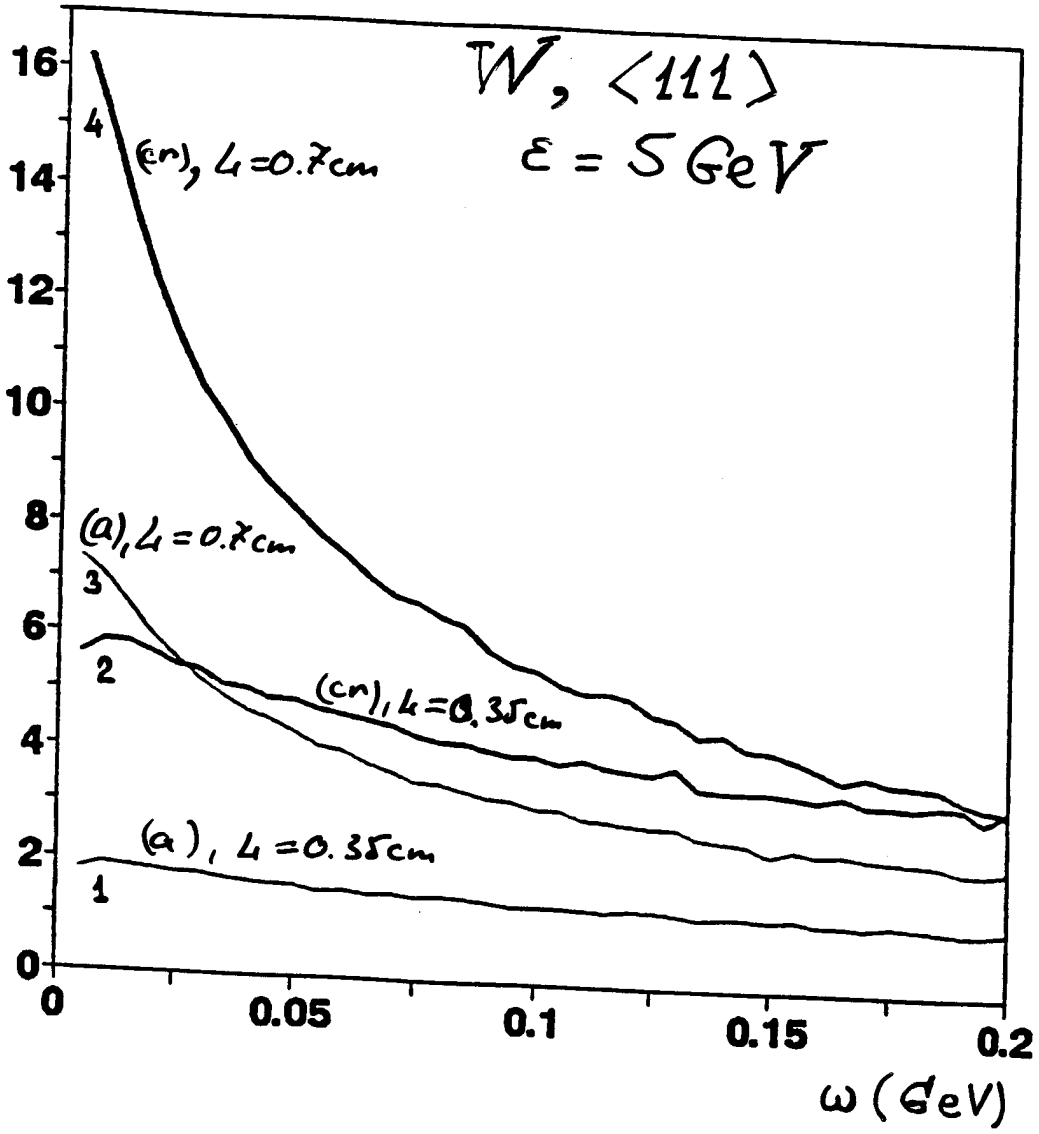
W, <111>
ε = 5 GeV
4
(cr), L=0.7cm
(a), L=0.7cm
3
2
(cr), L=0.35cm
(a), L=0.35cm
1
16
14
12
10
8
6
4
2
0
0
0.05
0.1
0.15
0.2
ω (GeV)

Fig. 1 (B)

1. V.N.Baier, V.M.Katkov,and V.M.Strakhovenko, phys.stat.sol.(b) **133**, 583 (1986). RADIATION YIELD OF HIGH-ENERGY ELECTRONS IN THICK CRYSTAL

2. V.N.Baier, V.M.Katkov,and V.M.Strakhovenko, Sov.Phys.Dokl, **30**, 474 (1986).

3. V.N.Baier, V.M.Katkov,and V.M.Strakhovenko, Nucl. Instr. and Meth. **B 16**, 5 (1986).

4. V.N.Baier, V.M.Katkov,and V.M.Strakhovenko, Nucl. Instr. and Meth. **B 27**, 360 (1987).

5. V.N.Baier, V.M.Katkov,and V.M.Strakhovenko, Sov. Phys.JETP **65**, 686 (1987).

6. V.N.Baier, V.M.Katkov,and V.M.Strakhovenko, phys.stat.sol.(b) **149**, 403 (1988).

7. V.N.Baier, V.M.Katkov,and V.M.Strakhovenko, Sov. Phys.Usp. **32**, 972 (1989).

8. V.N.Baier, V.M.Katkov,and V.M.Strakhovenko, Nucl. Instr. and Meth. **B 103**, 147 (1995). ELECTROMAGNETIC SHOWERS IN CRYSTALS AT GeV ENERGIES

9. V.N.Baier, V.M.Katkov,and V.M.Strakhovenko, Nucl. Instr. and Meth. **B 119**, 131 (1996).

10. V.N.Baier, V.M.Katkov,and V.M.Strakhovenko, *Electromagnetic Processes at High Energies in Oriented Single Crystals*, World Scientific, Sigapore, 1998.

11. V.N.Baier, and V.M.Strakhovenko, Nucl. Instr. and Meth. **B 155**, 403 (1999).

12. V.N.Baier, and V.M.Strakhovenko, Phys.Rev. ST Accel. Beams **5**, 121001 (2002).

Positron-production experiment using Diamond and Si crystals in the KEKB 8-GeV injector linac

T.Suwada (tsuyoshi.suwada@kek.jp)

Accelerator Laboratory, KEK

Collaboration

S.Anami, A.Enomoto, K.Furukawa, K.Kakihara,
T.Kamitani,Y.Ogawa, S.Ohsawa, T.Oogoe, M.Satoh,
T.Sugimura, T.Suwada and K.Yoshida

Accelerator Laboratory, KEK

H.Okuno,

Institute of Particle and Nuclear Studies, KEK

K.Umemori,

Institute of Materials Structure Science, KEK

R.Hamatsu, J.Hara

Physics Department, Tokyo Metropolitan University

V.Ababiy, A.P.Potylitsin, I.E.Vnukov,

NPI, Tomsk Polytechnic University

R.Chehab,

LAL, IN2P3-CNRS, Universite de Paris-Sud

Motivation

- **High-intensity positron sources are required for future linear colliders and B-factories.**
- **Conventional methods using amorphous heavy metals limit to increase the intensity of primary electron beams due to the heat load on the target.**
- **New method using the processes of coherent bremsstrahlung (CB) and channeling radiation (CR) is one of the bright schemes for high-intensity e^+ production.**

Introduction

- **New method utilizing a crystal target was proposed by Chehab, *et al.* In 1989.**

  (R. Chehab, *et al.*, PAC'89, Chicago, IL, USA, Mar. 1989, p.283)

- **Yoshida, *et al.*, demonstrated a clear enhancement of the *e*+ yield in a tungsten crystal target using a 1.2-GeV electron beam.**

  (K. Yoshida, *et al.*, Phys. Rev. Lett. 80, 1437, 1998)

Introduction (cont'd)

- **A series of e+ production experiments based on the new scheme has been continued,**

  ⇒by Yoshida(Hiroshima/KEK), *et al.*,

  using 1.2-GeV *e*- beam of the ES at KEK-Tana branch, 3-GeV *e*- beam at *e*+ station, and *e*- beam(<8GeV) at the end station of the KEKB injector linac.

  ⇒by Chehab(LAL), *et al.*,

  using 5-40 GeV secondary *e*- beam at CERN-SPS.

Introduction (cont'd)

- **Theoretically unified treatment taking into account both processes of CR and CB has not yet been established on the simulation.**
- **More experimental data are expected to clearly understand the elementary physical processes of the CR and CB, and they are also required to develop the design of a real-type positron source.**

Historical View of the KEK Experiments

Month/Year			
May/1997	KEK Tanashi, ES	1.2	Crystal W (W_c) [1.2]
Apr, Jun/1998	KEK Tsukuba, Electron Linac	3	W_c [1.7] + Amor. W (W_a) [7]
Nov/1998	KEK Tanashi, ES	0.6, 0.8, 1	W_c [0.4, 1.2, 2.2], GaAs [0.36], Diamond[1.1]
Sep, Oct/2000	KEK Tsukuba, Electron Linac	8	W_c [2.2], W_c [2.2]+W_a [5, 10, 15]
Apr/2001	KEK Tsukuba, Electron Linac	8	W_c [2.2], W_c [9] W_c [9]+W_a [2, 4]
Sep/2001	KEK Tsukuba, Electron Linac	8	W_c [2.2], W_c [5.3], W_c [9] Combined targets(W_c +W_a)
Jan/2002	KEK Tsukuba, Electron Linac	4	W_c [2.2], W_c [5.3], W_c [9] Combined targets(W_c +W_a)
Aug-Sep/2002	KEK Tsukuba, Electron Linac	8	Si <110> 2.6, 30, 48 Diamond <110> 4.57 Combined (Si/Dia.+W_a)
Dec/2002	KEK Tsukuba, Electron Linac	8	Si <110> 10, 30, 48 Diamond <110> 4.57 Combined (Si/Dia.+W_a)

Channeling Radiation & Coherent Bremsstrahlung Processes

Physical processes for the channeling radiation and coherent bremsstrahlung

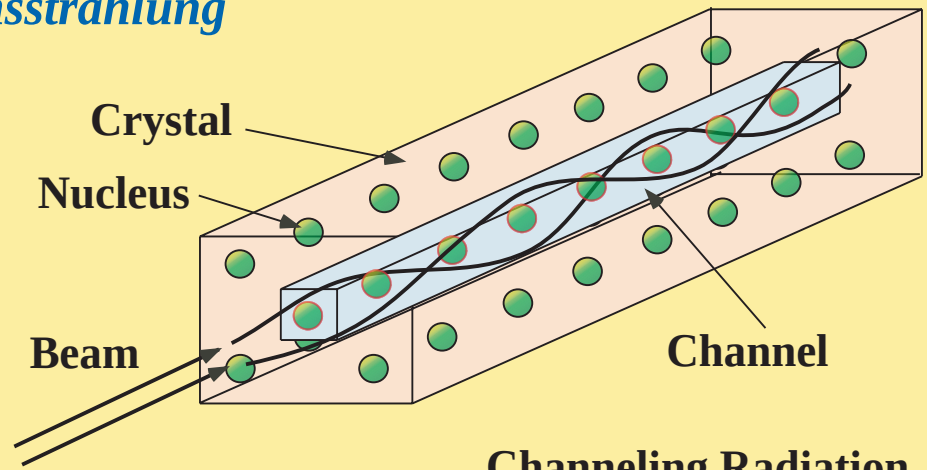

Critical Angle of Channeling Radiation

$F_c=(2U_0/E_b)^{1/2}$

$\sim 0.43\text{mrad}@E_b=8GeV$

U_0:**Potential Energy of a Channel**

E_b:**Beam Energy**

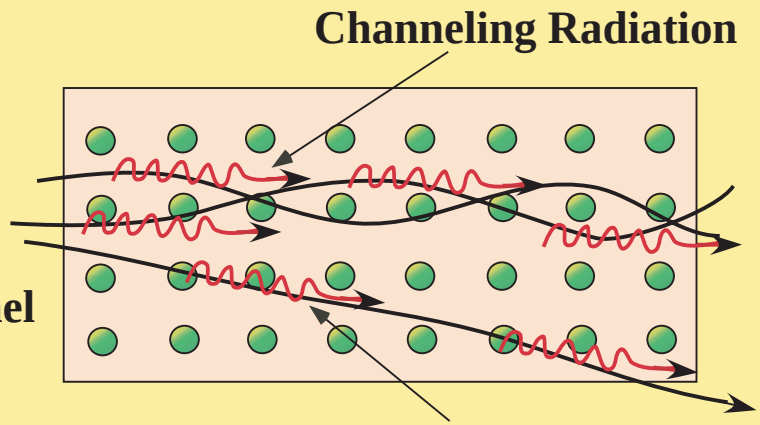

New Positron Production Schemes

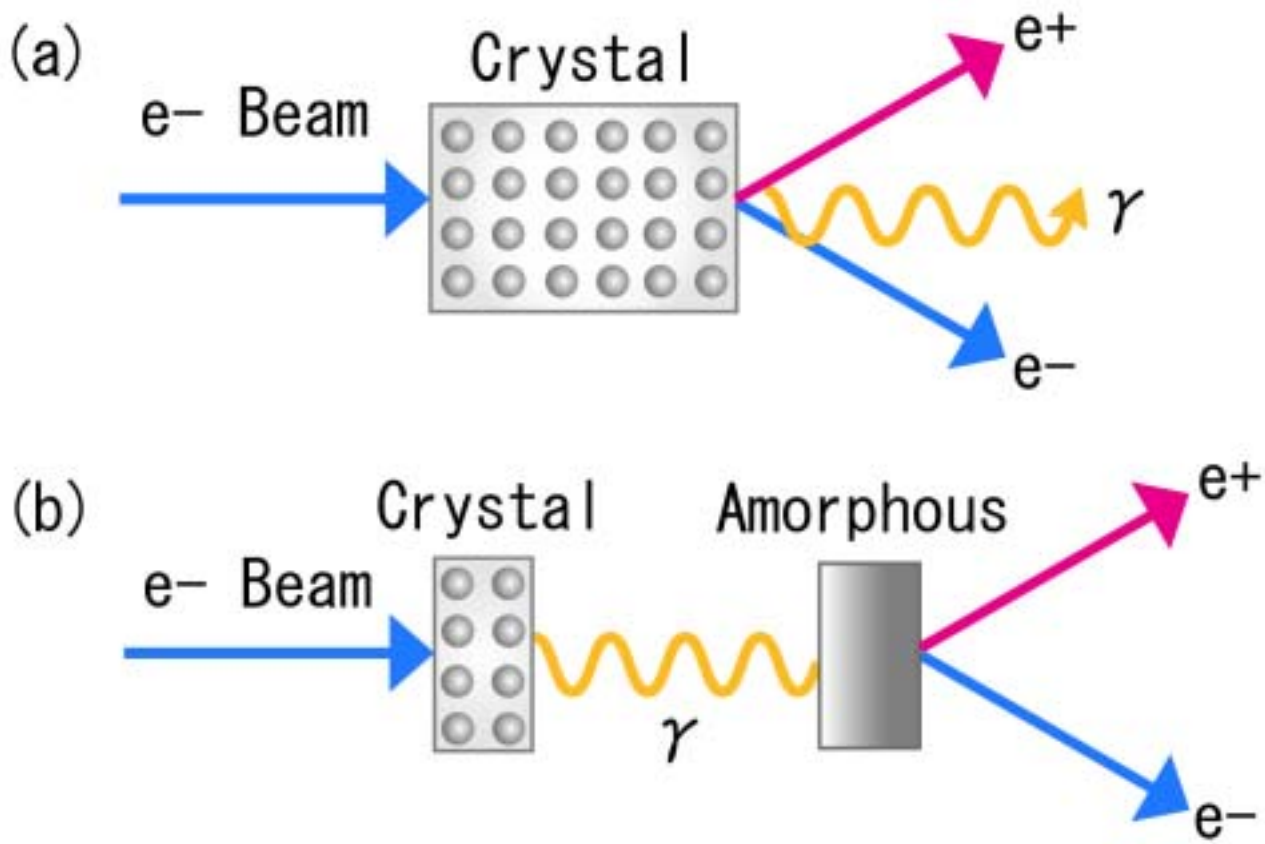

Experimental Setup

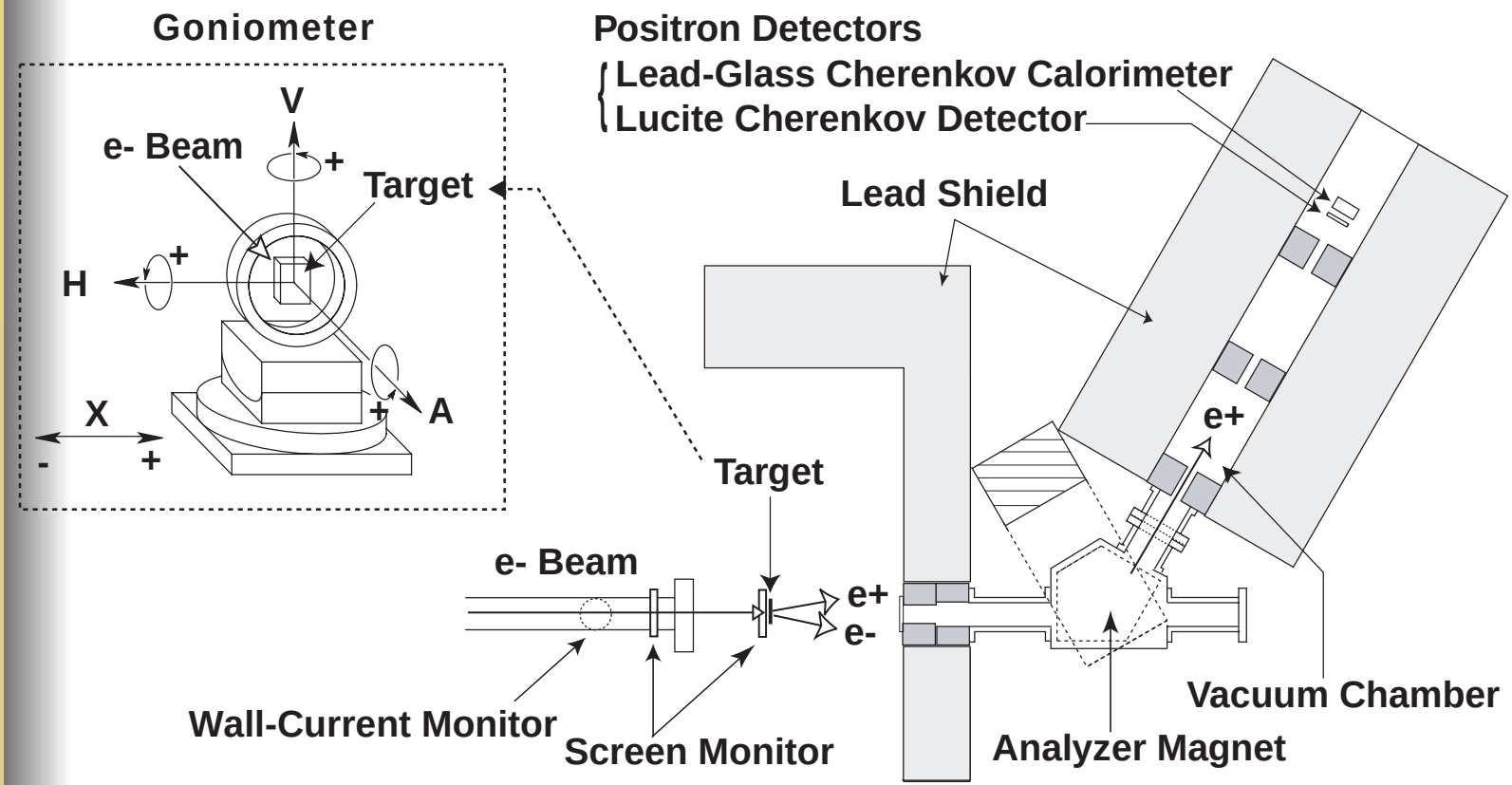

Linac Beam Line at the 3rd switch yard

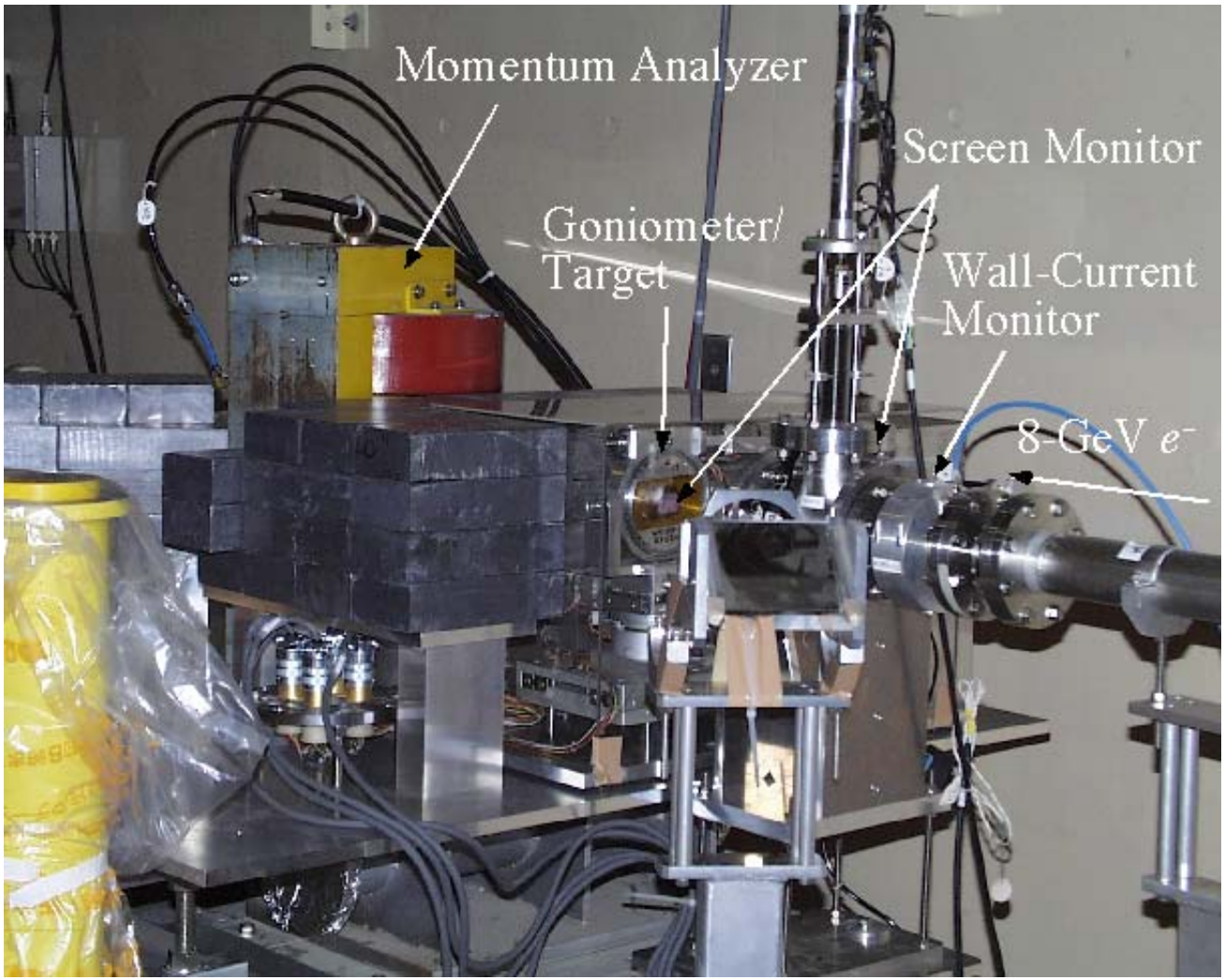

Experimental Setup (cont'd):Photo picture of a crystal target on a goniometer

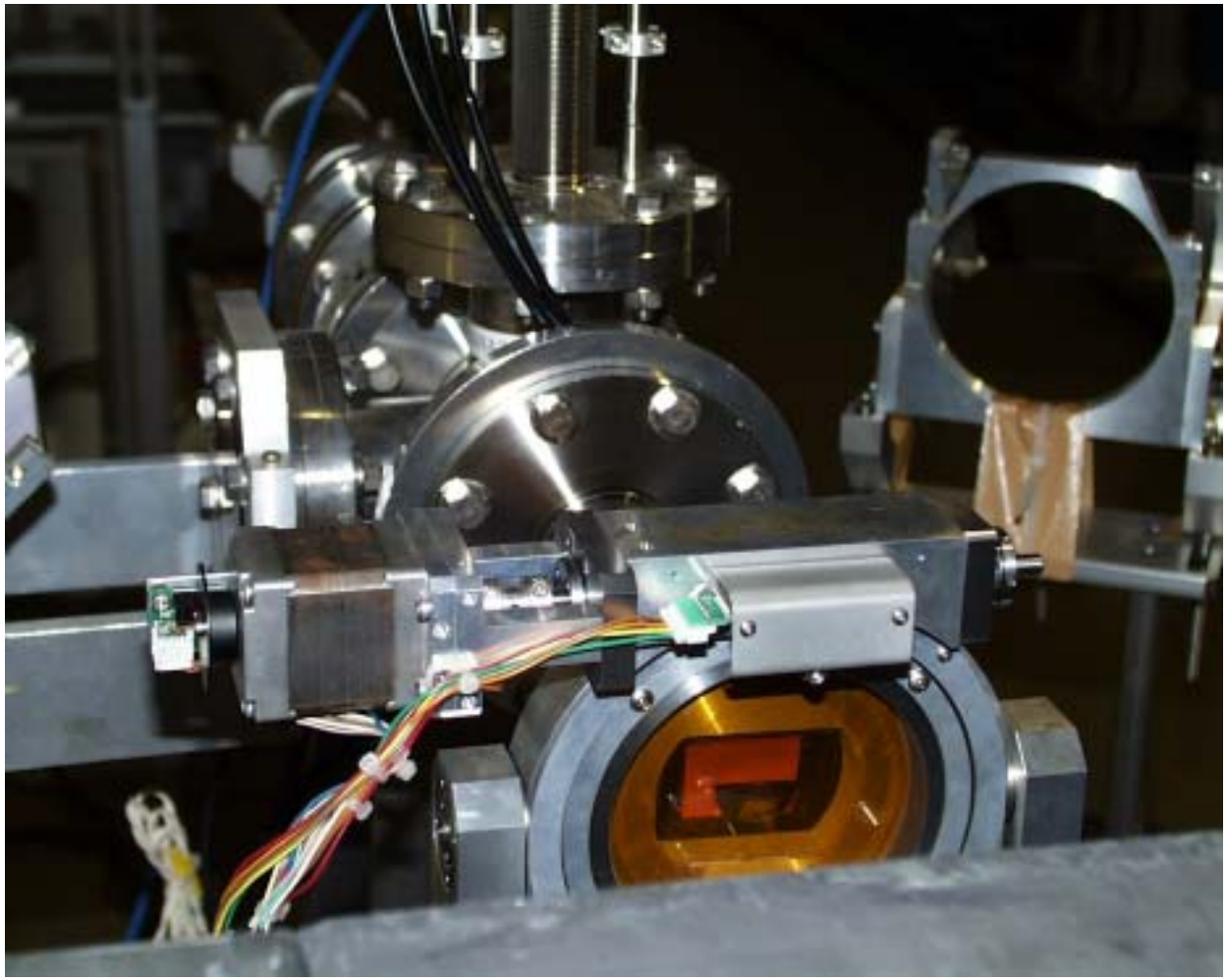

Experimental Setup (cont'd):Photo picture of crystal & amorphous targets

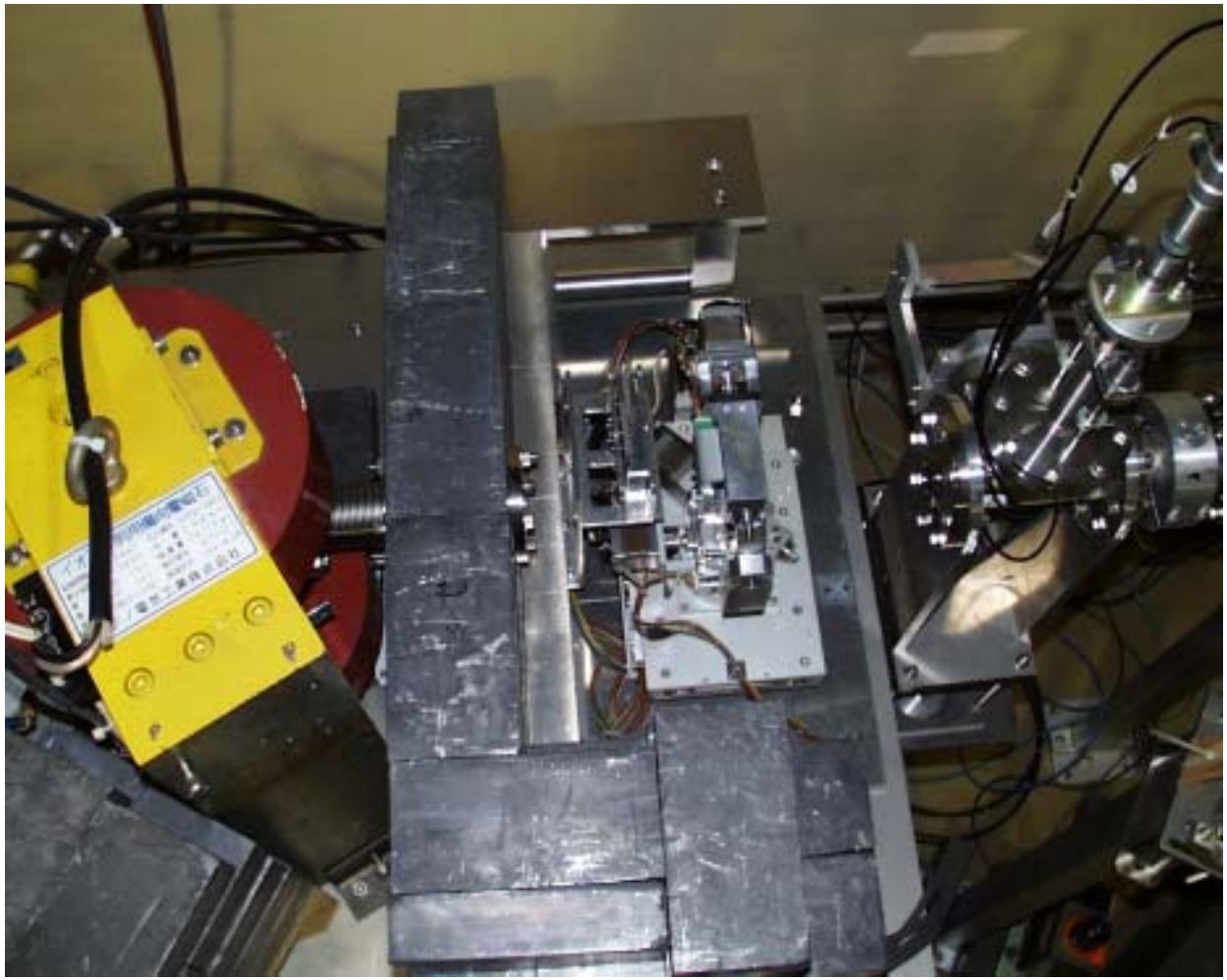

Experimental Setup (cont'd):Positron spectrometer

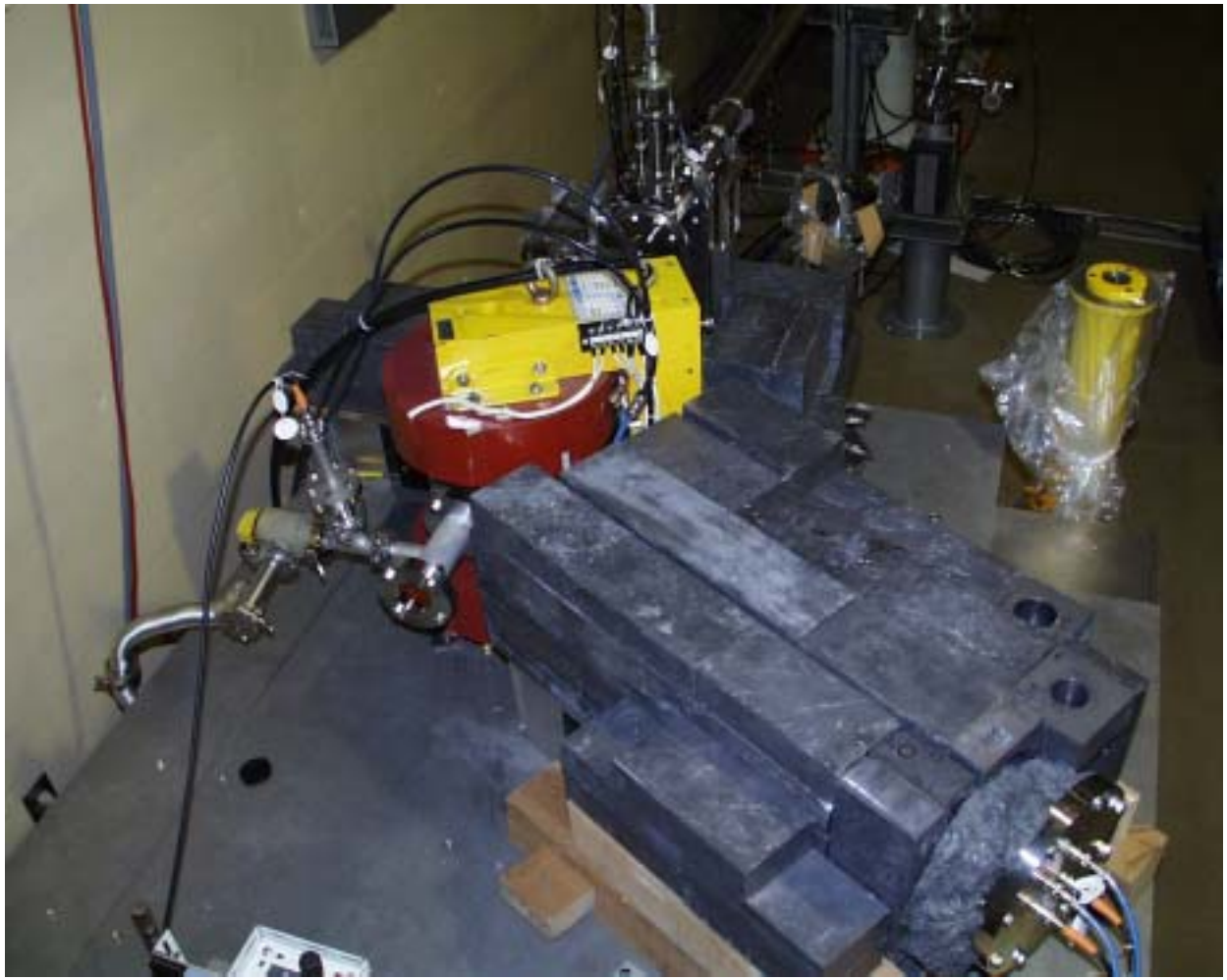

Acceptance of the Positron Spectrometer

Pe+ (MeV/c)	Acceptance ($\Delta P \Delta \Omega$) (10^{-4} x (MeV/c)•sr)
5	1.08 ± 0.03
10	2.47 ± 0.07
15	3.80 ± 0.1
20	4.81 ± 0.12

- **The acceptance ($\Delta P \Delta \Omega$) was obtained by using the simulation code (GEANT3).**
- **Typical acceptance Momentum: $\Delta P/P$=2.4% (FWHM)& Geometrical: $\Delta \Omega$=1msr at Pe+=20MeV/c.**

Experimental Condition

***Electron Beam*:**

- **Beam Energy = 8 GeV**
- **Angular Spread ~22 μrad (H), ~44 μrad (V)**
- **Transverse Beam Size ~0.8mm (FWHM) in diameter**
- **Beam Charge = 0.1 nC/bunch**
- **Bunch Length (Single Bunch) ~9 ps (FWHM)**
- **Beam Repetition = 25Hz**

Angular Spread of the Electron Beam at the Positron Target

- **Φ ~ 55 μrad < Φc (due to multiple scattering by a beam-extraction vacuum window(30μm-thick SUS))**

Critical Angle for the Channeling Condition at the Positron Target

Linhard Crytical Angles

- **Φc ~ 170μrad @8 GeV for Silicon Crystal**
- **Φc ~ 130μrad @8 GeV for Diamond Crystal**

Experimental Condition (cont.)

***Positron-Production Targets*:**

- **Crystal Silicon Target : 2.55, 9.9, 29.9 and 48.15mm thickness**
- **Crystal Diamond Target : 4.57mm thickness**
- **Amorphous Tungsten Target: 3-18mm (3mm step) thickness (for the purpose of hybrid targets and for the e^+ production yield calibration)**

Detected Momentum Range:

- **10 MeV/c $\leq Pe^+ \leq$ 30 MeV/c**

Positron Detectors

- ***Lead-Glass Calorimeter:Measurement of total energy of e+***
- ***Acrylic Cherenkov Counter:Measurement of number of e+***

Beam Monitors

- ***Wall-current monitor* for the electron beam-charge measurement**
- ***Screen monitor* for the beam-profile measurement**

Experimental Results: 2-Dimensional Axis Scan for 5mm-thick Diamond Crystal at Ee-=8 GeV (Pe+=20MeV/c)

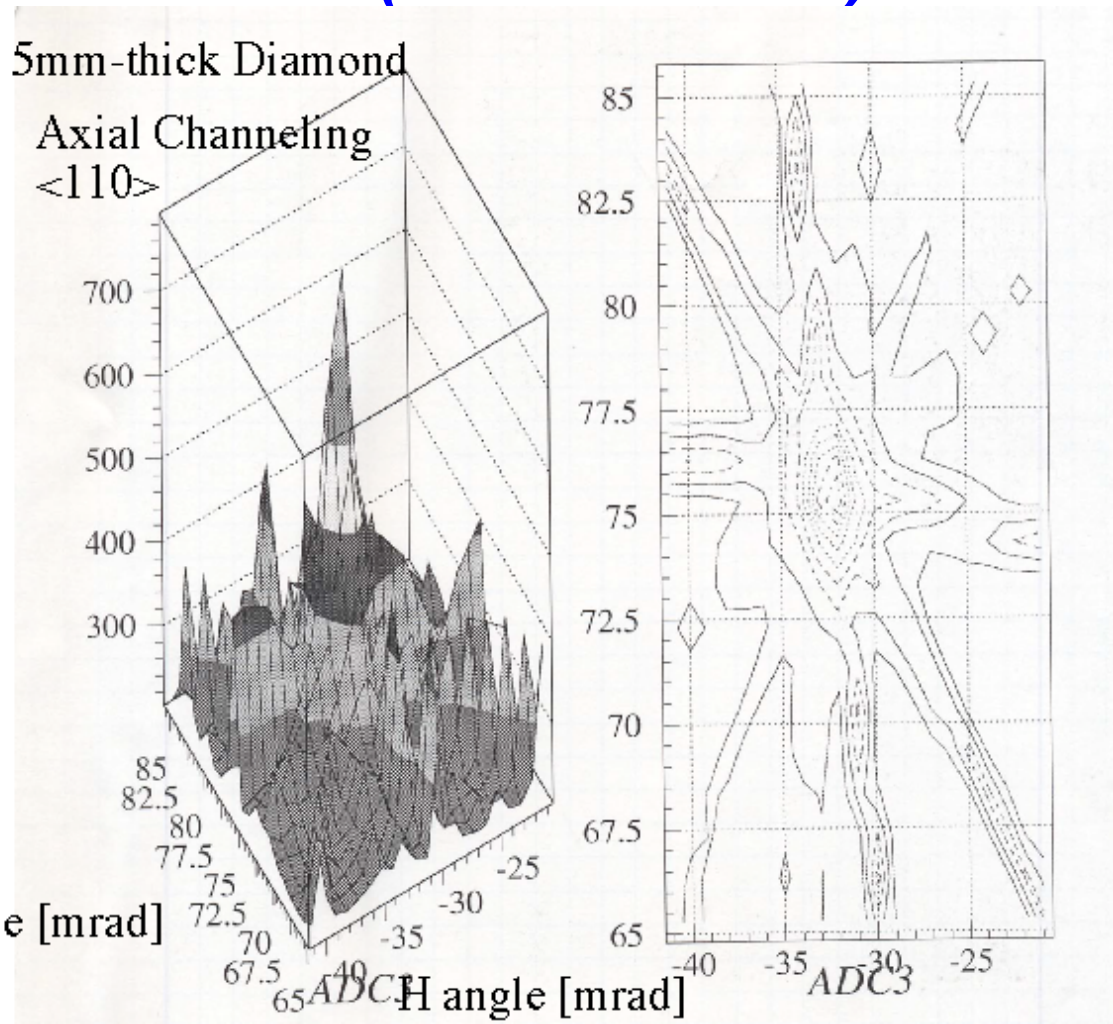

Experimental Results: 2-Dimensional Axis Scan for 30-mm thick Si Crystal at Ee-=8 GeV (Pe+=20MeV/c)

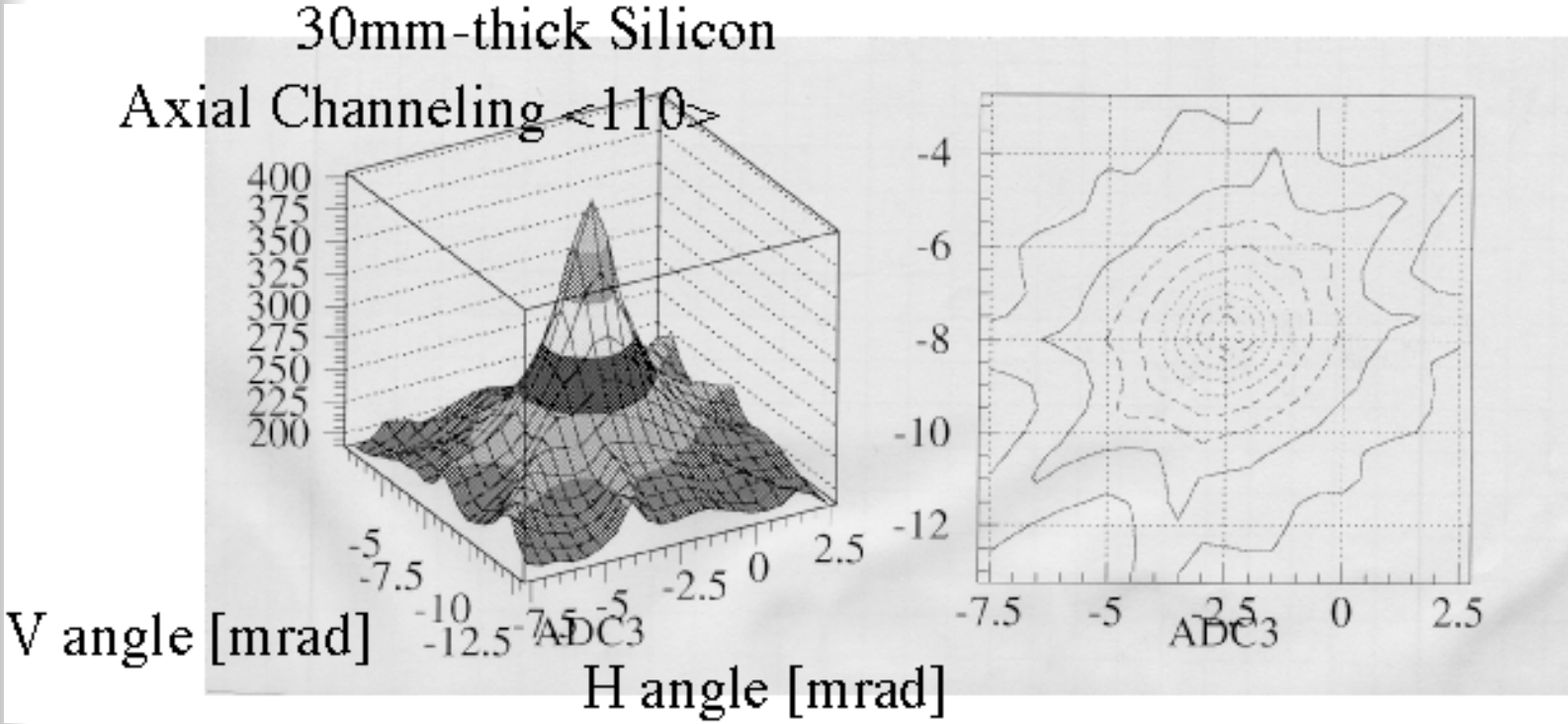

Experimental Results: Rocking Curves (Axis <110>) for 5mm-thick Diamond and 30mm-thick Si Crystals at Ee-=8 GeV (Pe+=20MeV/c)

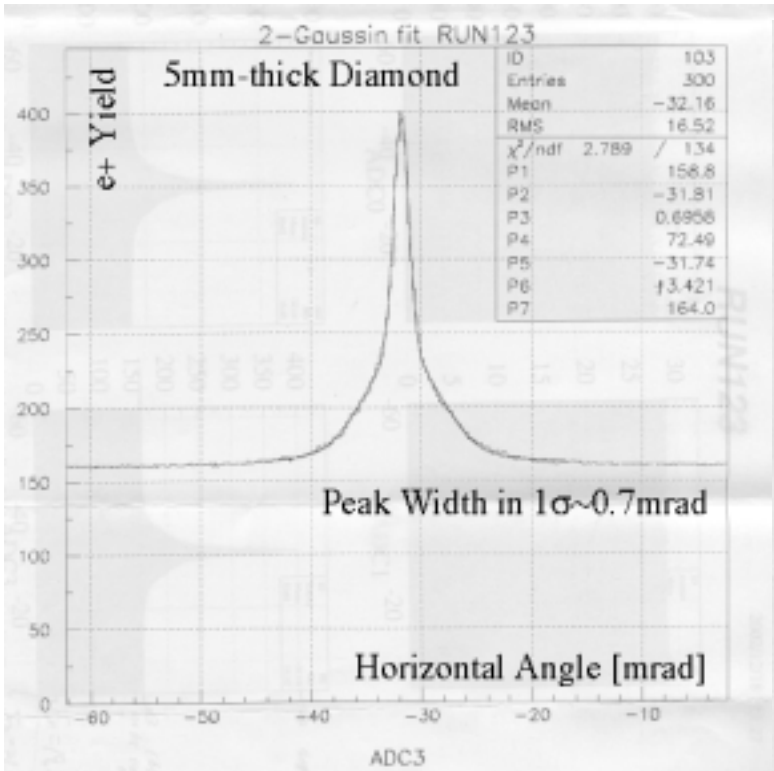

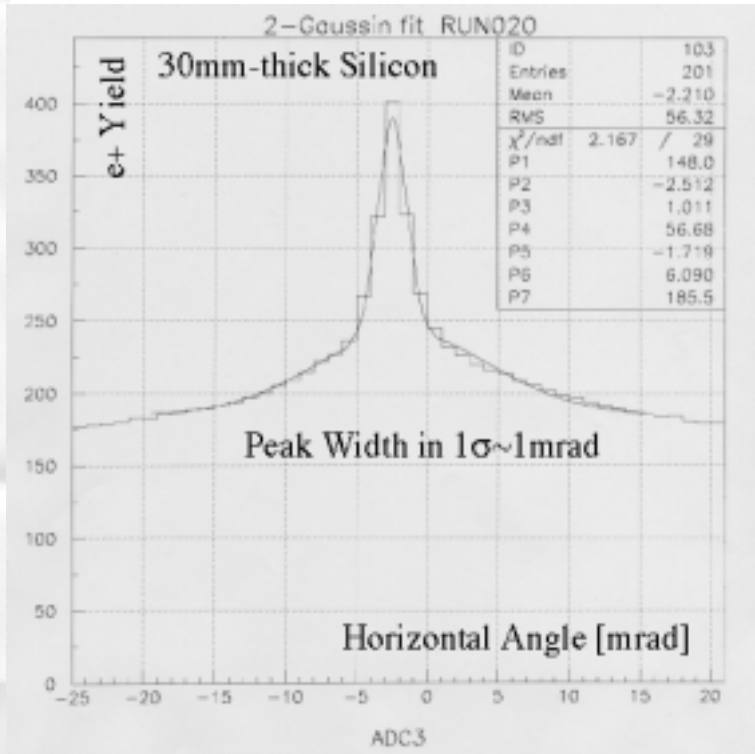

Experimental Results: Variations in the width of the rocking-curve peak for Ee-=8 GeV (Pe+=20MeV/c)

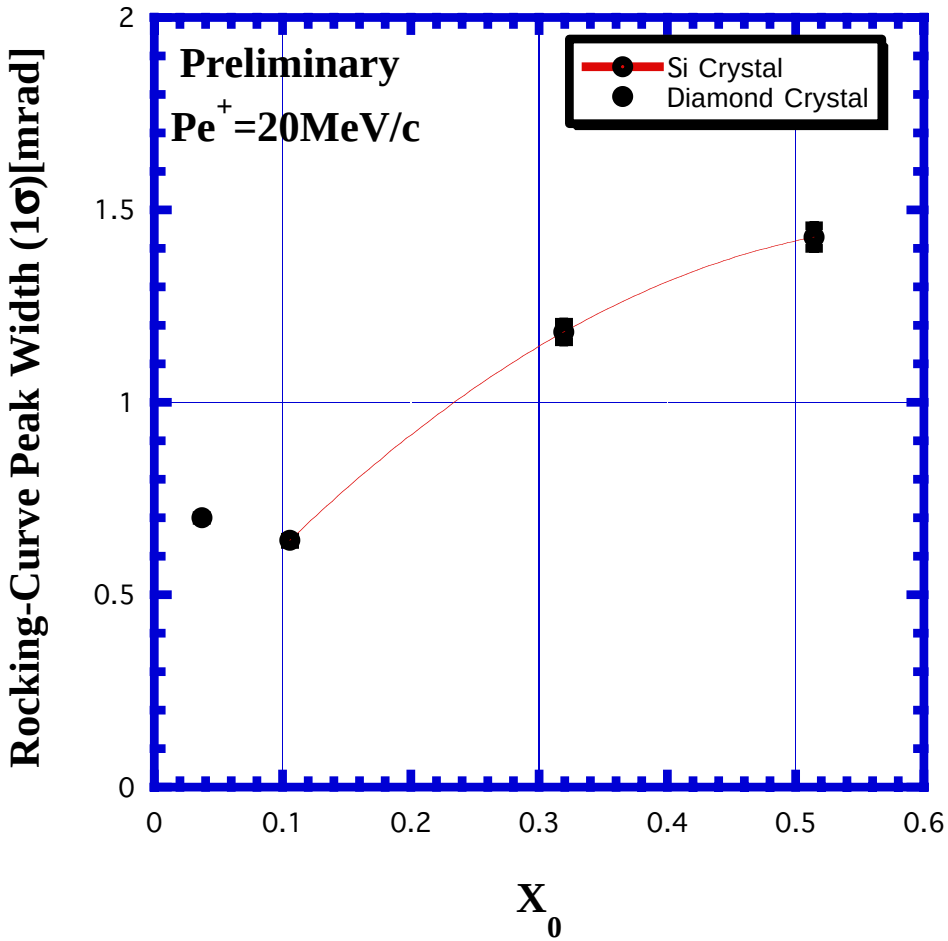

Experimental Results: Variations in the enhancement ($N_{e+@peak}$/ $N_{e+@base}$) of the e+ yield at Ee-=8 GeV (Pe+=20MeV/c)

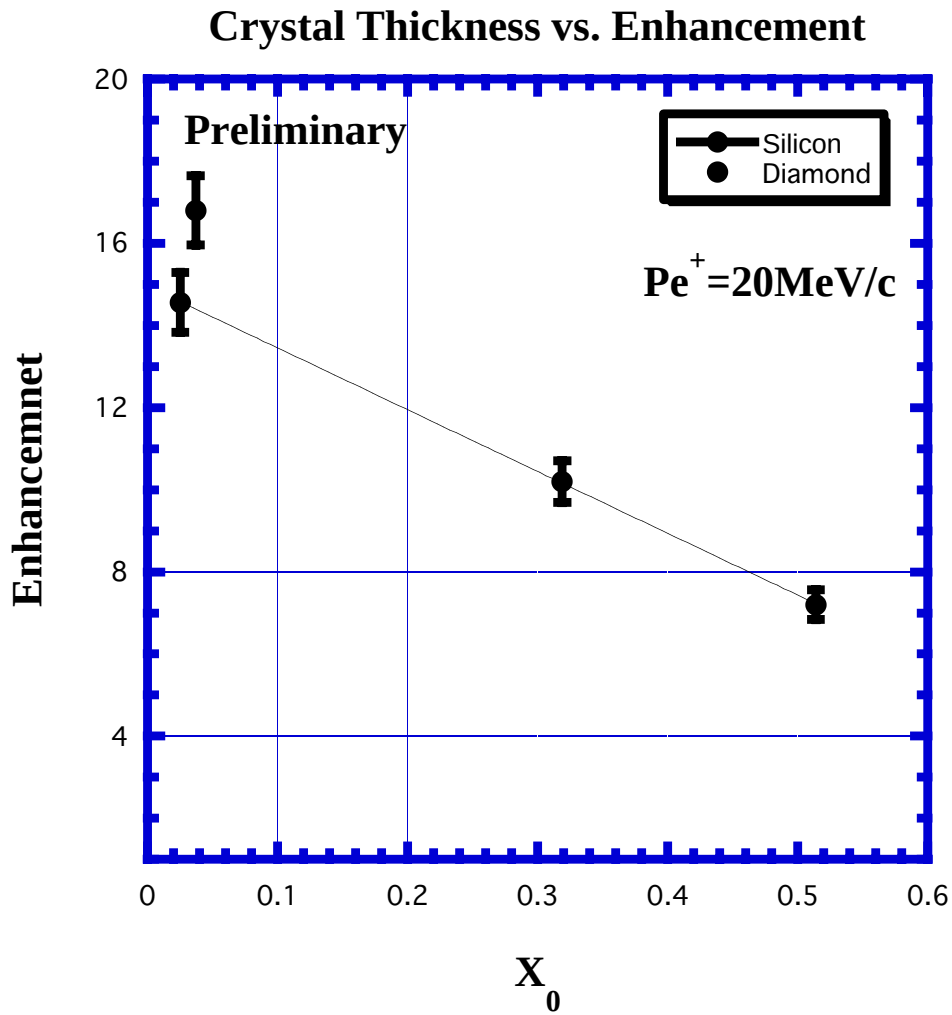

Experimental Results: Positron momentum dependence for the e+ yield enhancement at Ee-=8 GeV

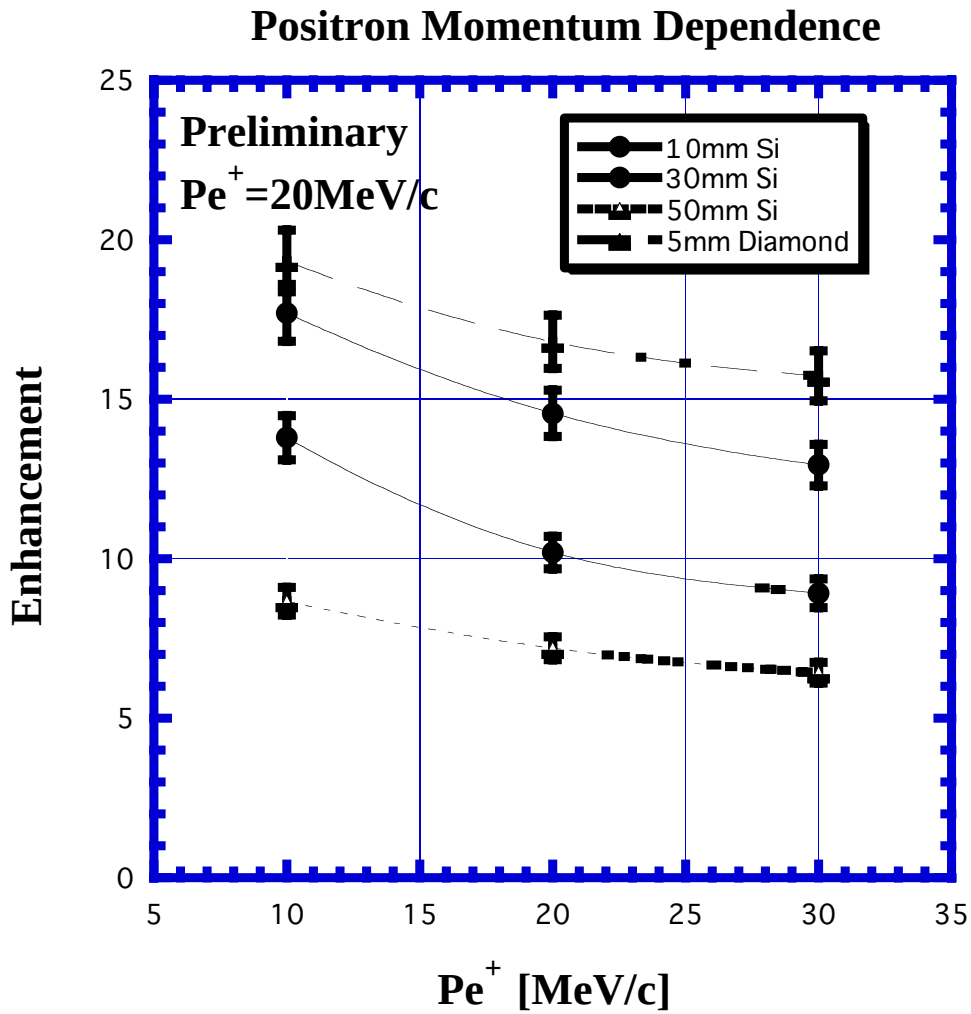

Experimental Results: Variations of the e+ production yield for the amorphous tungstens and off-axis crystal targets at Ee-=8 GeV (Pe+=20MeV/c)

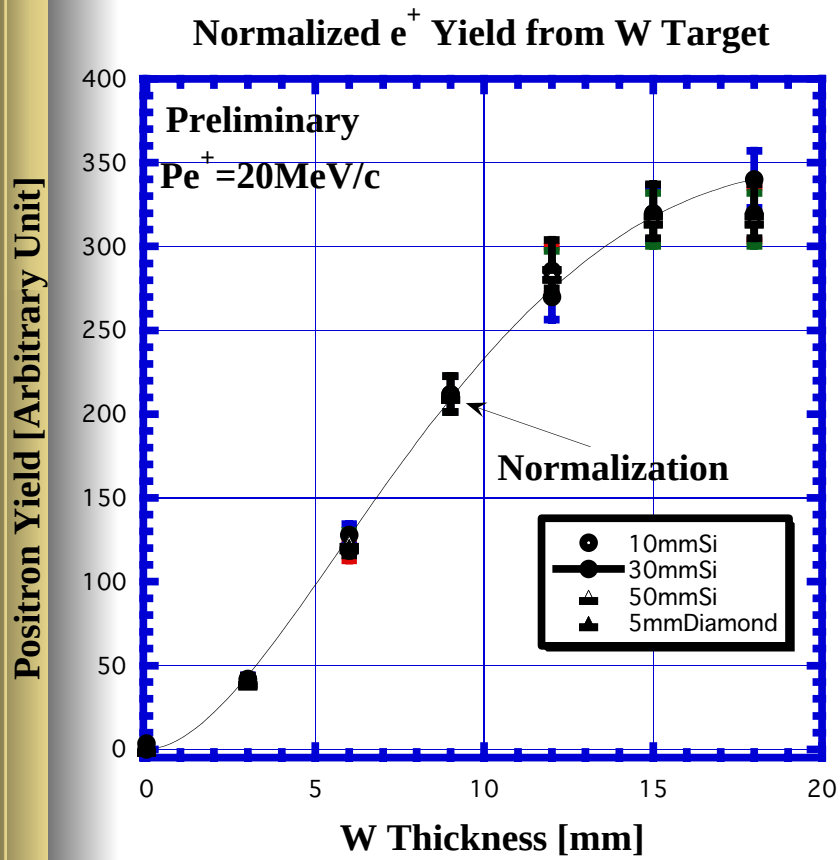

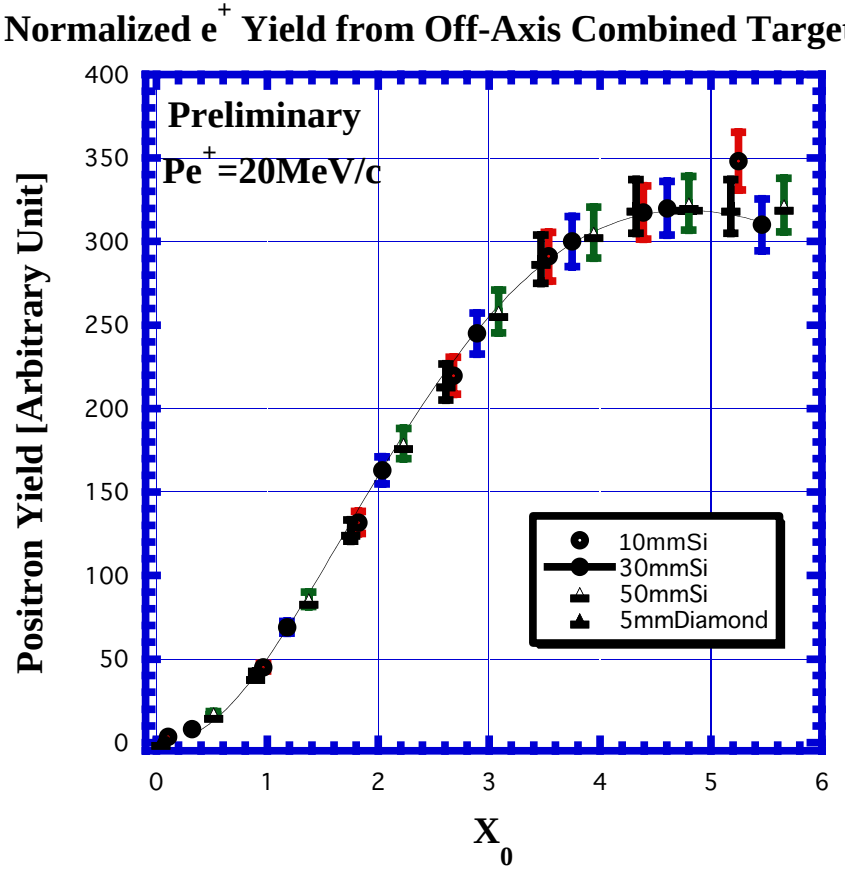

Experimental Results: variations of the e+ production yield for the on-axis crystal targets at Ee-=8 GeV (Pe+=20MeV/c)

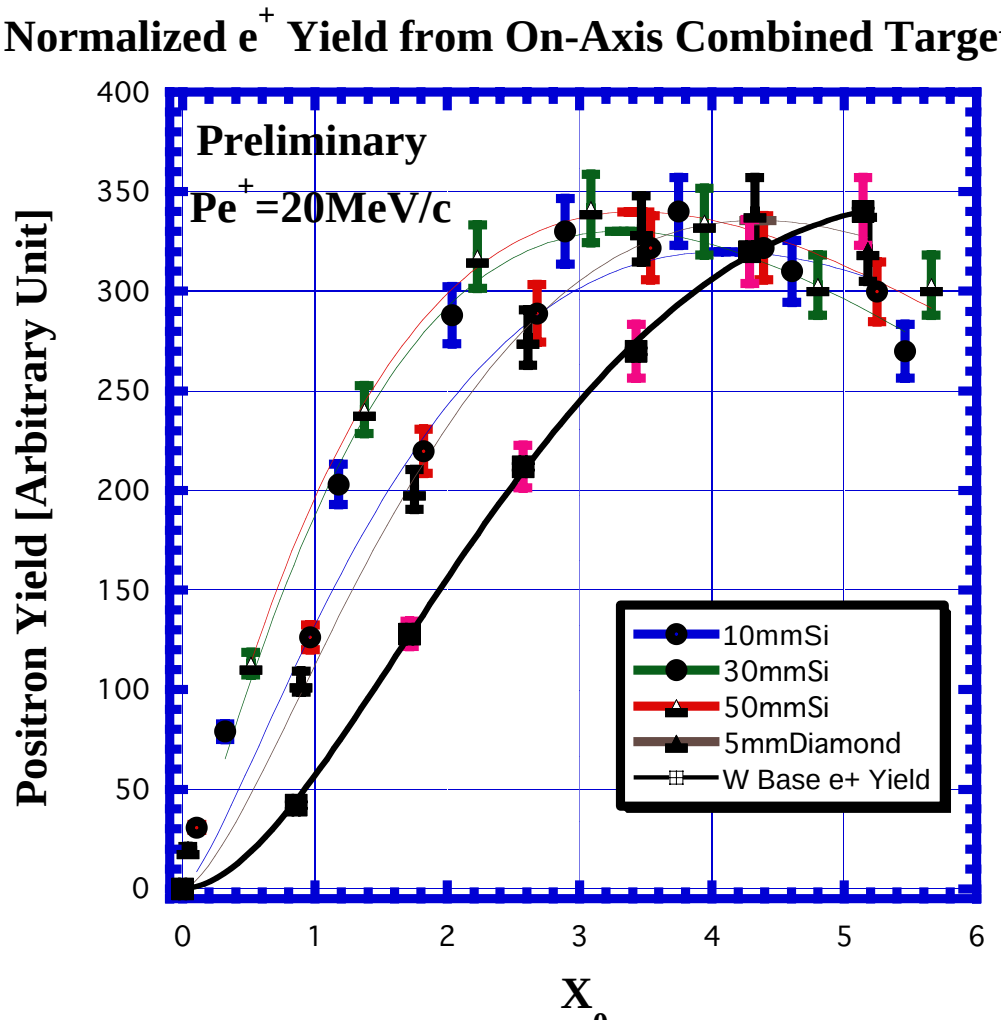

Experimental Results: Variations of the e+ production enhancement for the crystal targets at Ee-=8 GeV (Pe+=20MeV/c)

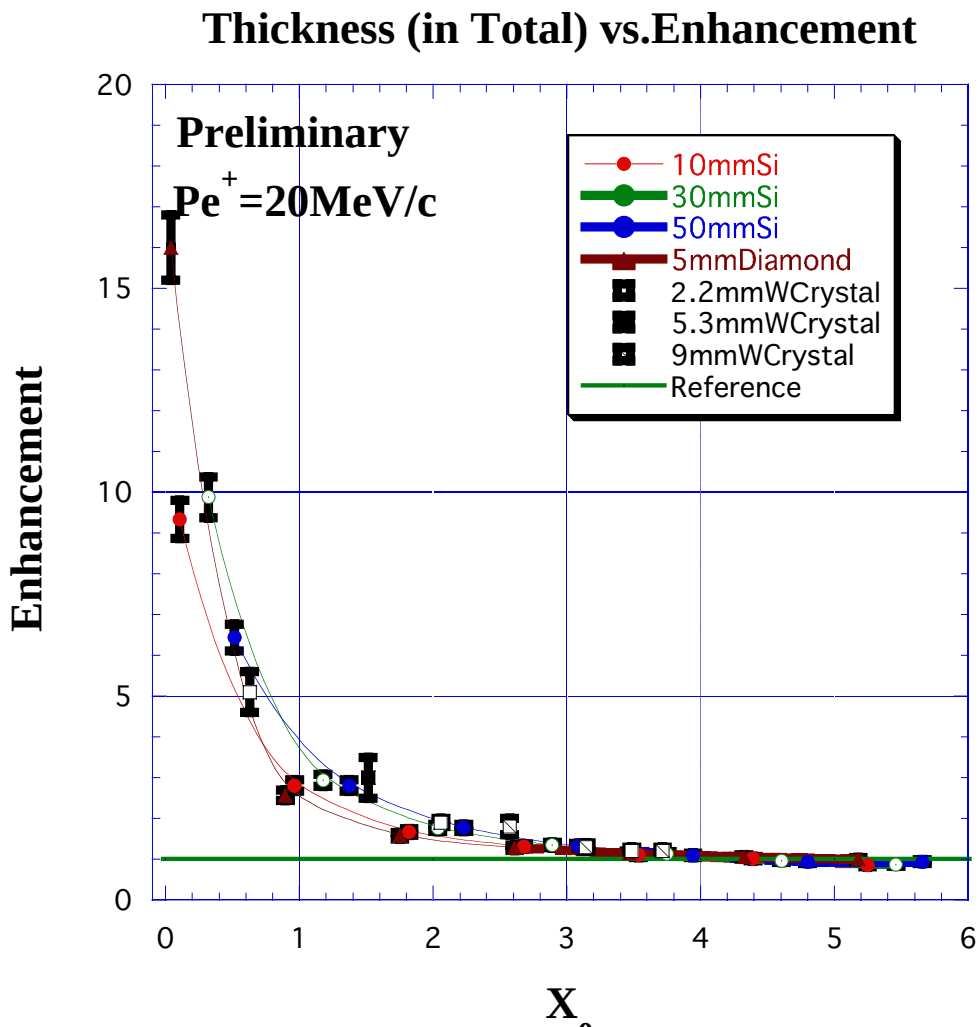

Experimental Results: Crystal effects for the Diamond and Si crystal targets at Ee-=8 GeV (Pe+=20MeV/c)

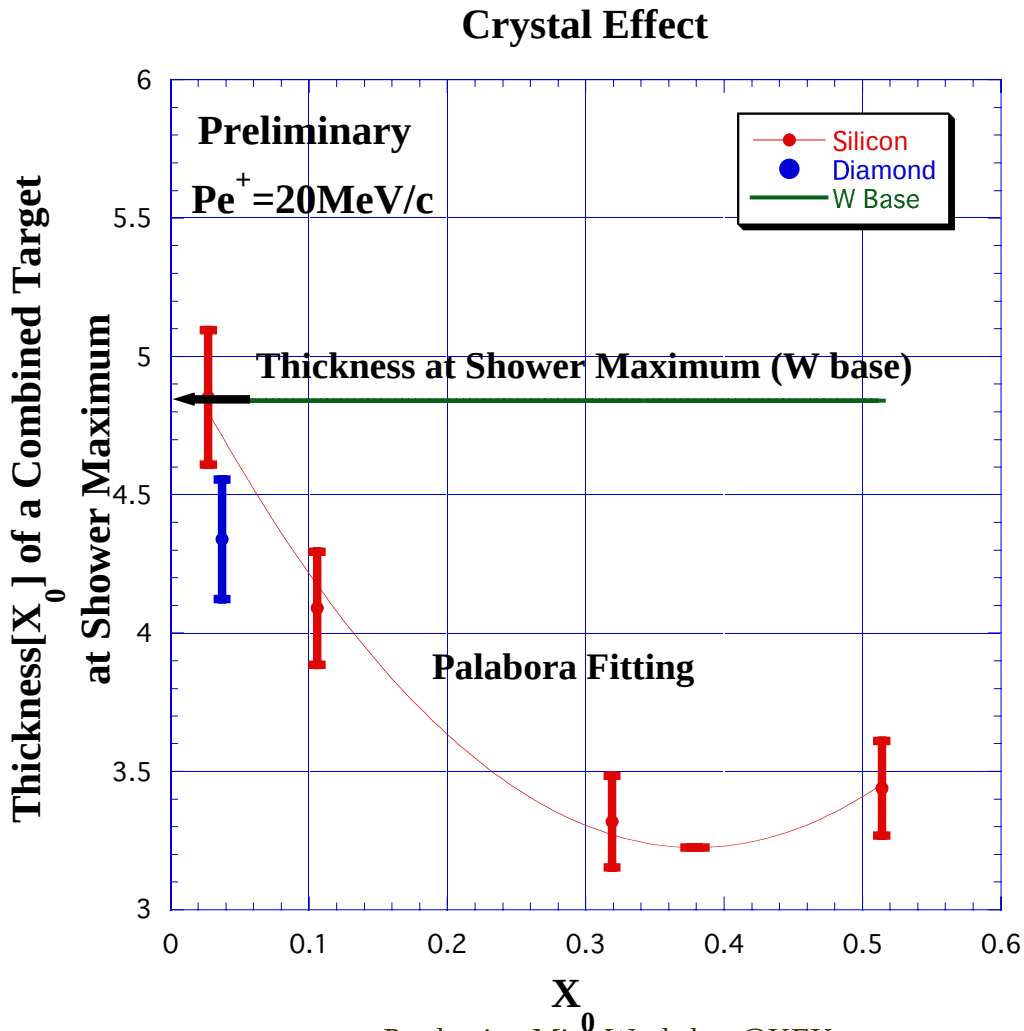

Experimental Results: Multiple Scattering Effect of the Vacuum Windows Using the Diamond crystal at Ee-=8 GeV (Pe+=20MeV/c)

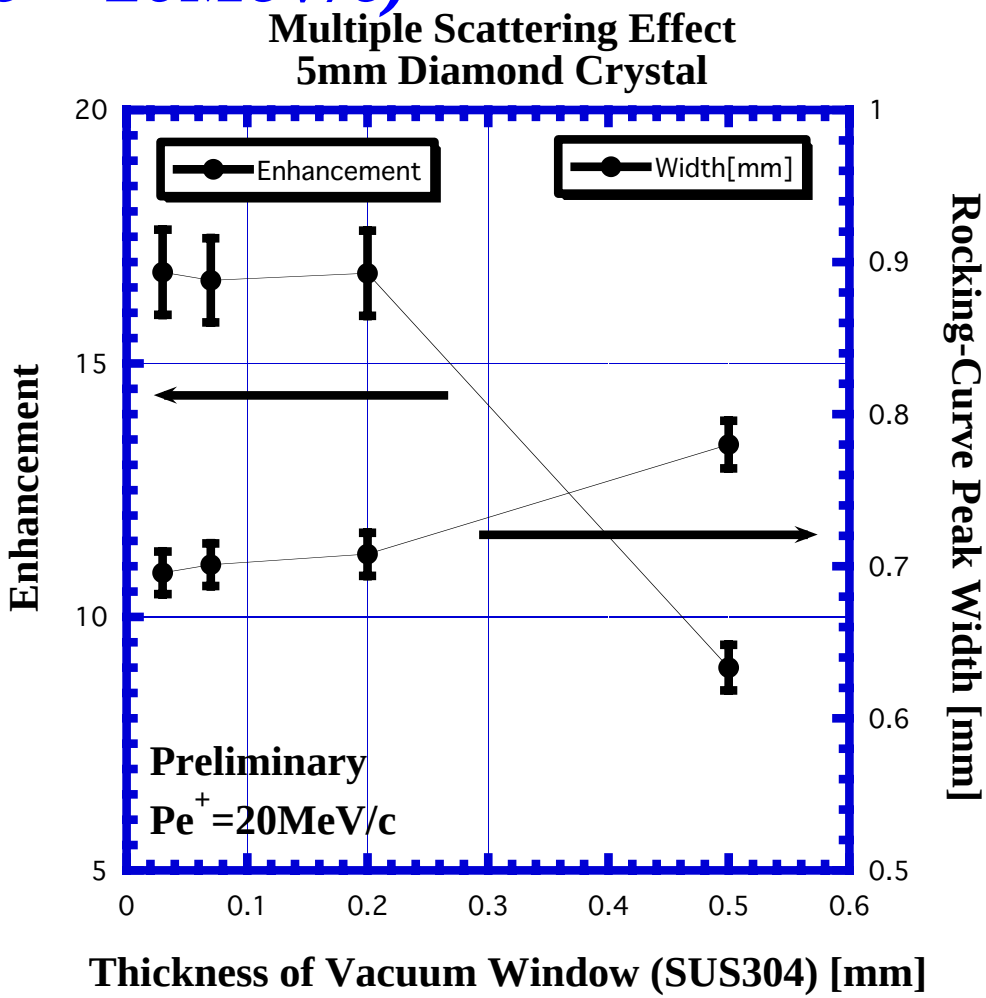

Conclusions

- ***Positron production experiment using Diamond and Silicon crystal targets has been successfully performed at the KEKB 8-GeV electron linac.***
- *Rocking curves*

⇒ ***The obtained widths of the rocking-curve peak is larger than the critical angle,***

⇒ ***and broaden with the thickness of the crystal target.***

⇒ ***These broad width of the rocking curves indicate that coherent bremsstrahlung is the predominant process over the channeling radiation process in this energy region.***

⇒ ***The increase of the peak width depending on the target thickness may come from the multiple scattering of the incident electrons in the target.***

Conclusions (cont'd)

♠*Enhancement (En) and momentum dependence of the e^+ yield for the crystal target alone from 8-GeV channeling electrons at a e^+ momentum of 20MeV/c*

⇒ ***En*= 9.3 ±0.5 (9.9-mmSi), 9.9 ±0.5 (29.9-mmSi),**

⇒ ***En*= 6.4 ±0.3 (48.15-mmSi), 16 ±0.8 (4.57-mmDiamond)**

- *The enhancement is much reduced with an increase of the total target thickness.*
- *No crystal effect enhances the e+ yield at the target thickness larger than ~4.2 X_0 in total.*
- *The e+ yields with Pe+=20MeV/c at Ee-=8GeV were almost the same level as the maximum e+ yield obtained for the amorphous tungsten target.*

♠*New scheme using the combined crystal target indicates that heat load in the amorphous tungsten part of the target could be considerably reduced due to a small amount of the energy loss in total.*

⇒ *It is of great benefit to apply such a crystal target to a high-intensity e+ source required for high-luminosity e+e- colliders and B-fatories.*

Review of experiments on positron production from crystal targets at KEK

R. Hamatsu, J. Hara, K. Sasahara
Department of Physics, Tokyo Metropolitan University

S. Anami, A. Enomoto, K. Furukawa, K. Kakihara, T. Kamitani,
Y. Ogawa, S. Ohsawa, T. Oogoe, M. Satoh, T. Sugimura, T. Suwada
Accelerator Laboratory, KEK

H. Okuno
Institute of Particle and Nuclear Studies, KEK

K. Umemori
Institute of Materials Structure Science, KEK

K. Yoshida
School of Allied Health Science, Kitasato University

R. Chehab
LAL, IN2P3-CNRS, Orsay, France

V. Ababiy, A.P. Potylitsyn, I.E. Vnukov
Nuclear Physisce Institute, Tomsk Polytechnic University, Russia

Introduction

- Intense positron sources are required for
  - e^+- e^- Linear colliders
  - high luminosiy B-factory
- Linear collider projects require more positron

Project	Flux(e^+)	Q(J/g)	P(kW)
CLIC	1.0×10^{14}	65	22
NLC	1.8×10^{14}	40	16
JLC	2.2×10^{14}	140	49
Tesla	2.8×10^{14}	222	5

Quoted numbers are taken from the T4-report/Snowmass 2001

Introduction (continued)

- Proposed design
  - NLC

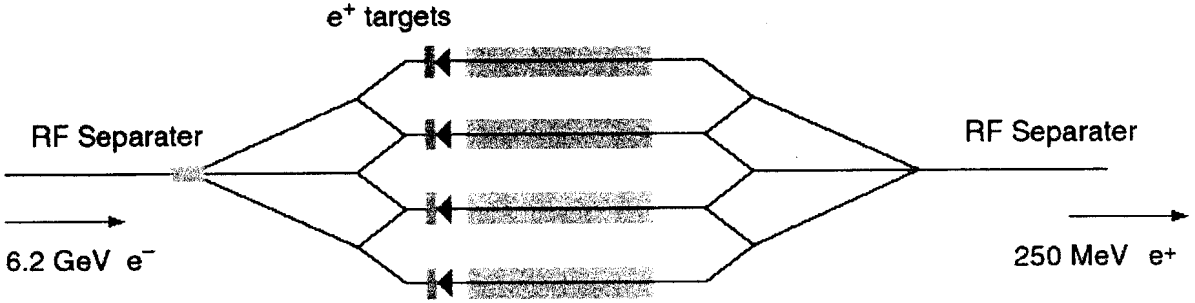

3 out of 4 target system scheme

  - Tesla

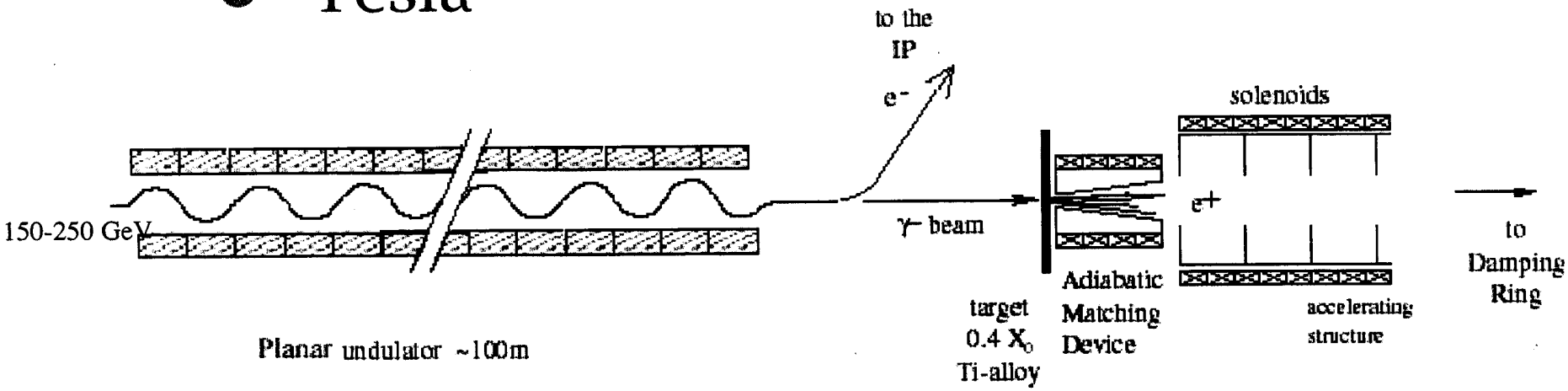

Figures from the T4-report/Snowmass 2001

Positron source using oriented crystals

- Oriented crystal plays an atomic undulator
- Coherent generation of photons yields more positrons than amorphous with the same thickness
- Need to study: optimum thickness crystal/amorphous combination

Channeling and Coherent Bremsstrahlung

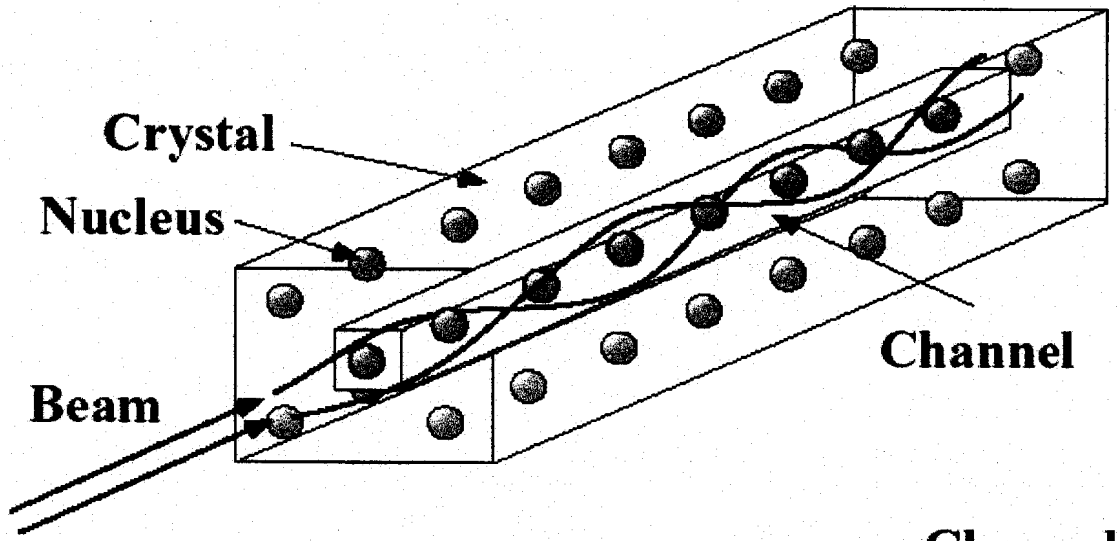

- In single crystal
  these two phenomena
  enhance e.m. shower
  (photon) and positron yields

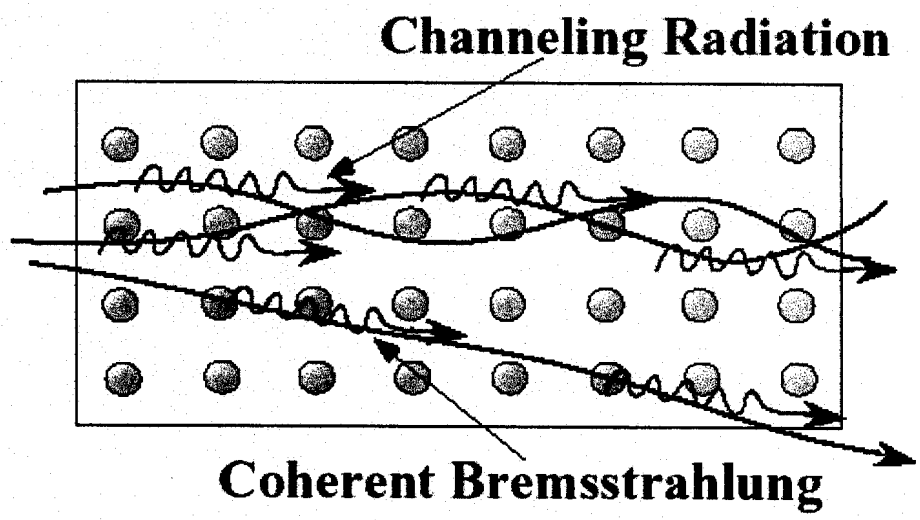

Experimental investigations

- Proof-of-principle experiments
  - Orsay in 1992-93
  - INS-Tokyo at 1.2 GeV in 1996
    - ✓ 3 times more positrons from 1.2 mm thick W-crystal in 10-20 MeV/c momentum range
- More detailed experiments at ~1 GeV in INS-Tokyo (~1999)
- Experiments at higher electron energies using KEK-B injector linac (2000~)

Experiments at INS-Tokyo

- Proof-of-principle experiment
  - Rocking curve: e+ yield as a function of crystal angle
  - ~3times more positrons from W crystal (1.2mm) at 1.2GeV
- More detailed experiments at INS-Tokyo in ≦1 GeV region

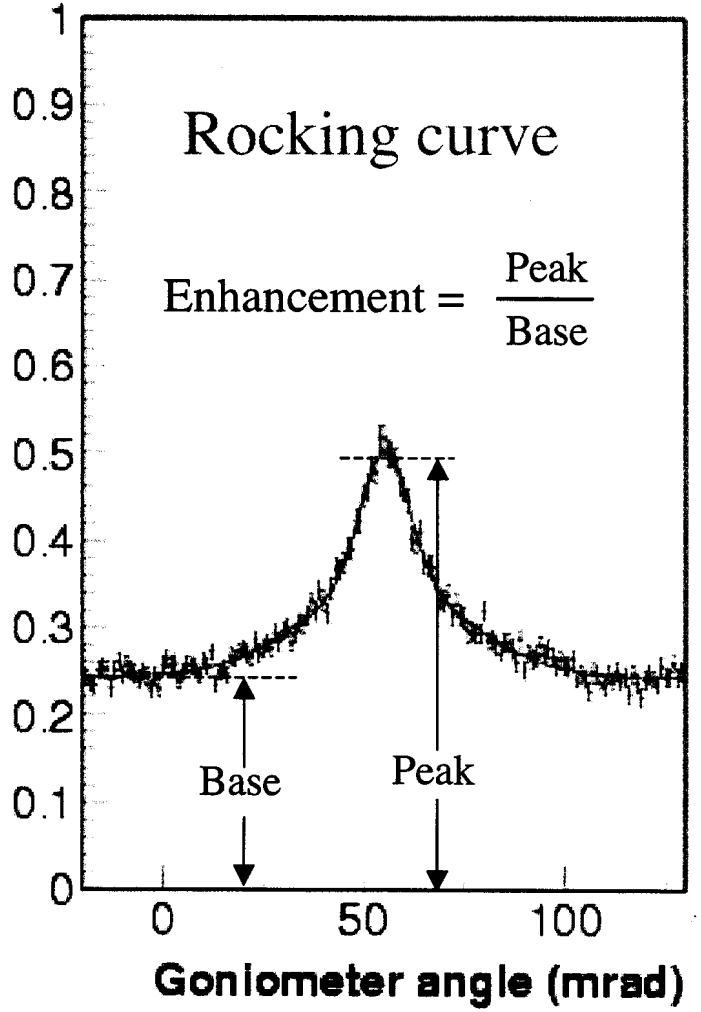

Experiments at INS-Tokyo (cont.)

- Enhancement factor of 2.3 for 1.2mm thick W crystal with <111> axis at 1 GeV
- More enhancement at higher energies
- Angular widths of the rocking curves are much wider than the Lindhard angle
- Rocking curves are explained well by the coherent Bremsstrahlung (CB)
- Angular and momentum distributions of positrons are about the same for on- and off-axis conditions

Experiments at KEK

- Beam energy 4 and 8GeV @KEK-Linac
- Positrons with p = 5~20 MeV/c
  - Rocking curves/Crystal orientation
  - Crystal thickness
    Tungsten W (2.2, 5.3, 9.0 mm)
  - Other crystals
    Diamond (5mm), Silicon(10, 30, 50mm)
  - And combination with amorphous
    Tungsten (3, 6, 9, 12, 15, 18 mm)

Experimental Setup

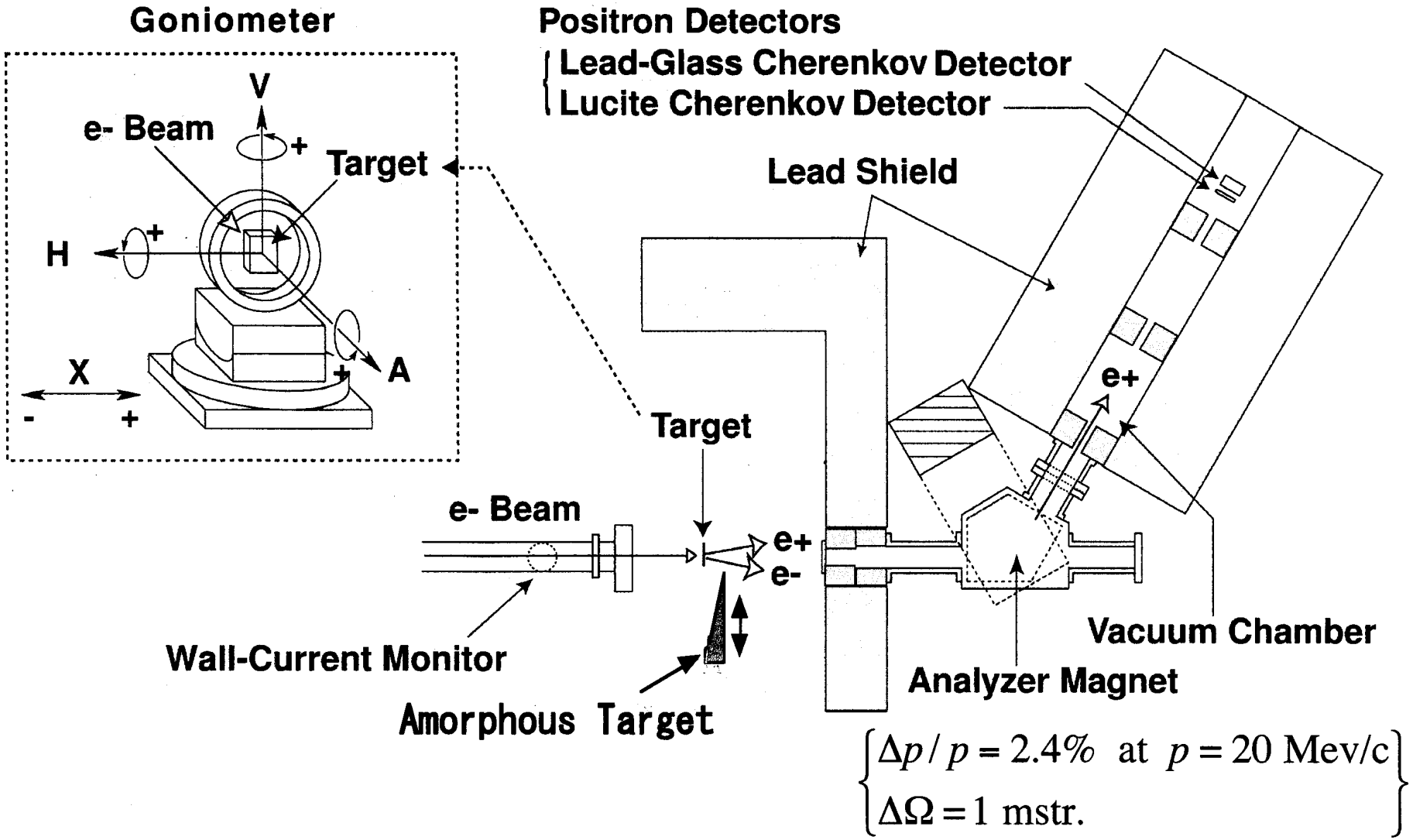

$$\begin{cases} \Delta p/p = 2.4\% \ \text{ at } \ p = 20 \text{ Mev/c} \\ \Delta\Omega = 1 \text{ mstr.} \end{cases}$$

Experimental conditions

■Beam

- Energy: 4 and 8 GeV
- S-band single bunch, pulse width 10ps
- Repetition: 2 ⇨ 25 Hz
- Beam intensity: 1.3×10^{9} e^{-}/bunch (0.2nC)
- Transverse beam size: 1-1.5 mm dia.
- Angular spread: 0.2 and 0.1 mrad for 4 and 8 GeV due to the multiple scattering in the beam window (100 μm thick stainless steel ⇨ 30 μm)

Experimental conditions (cont.)

- Crystal targets

Material Orientation	Thickness mm (rad. lengths)	Mosaicity mrad
Tungsten <111>	2.2 (0.63) 5.3 (1.51) 9.0 (2.57)	1.5 0.5 0.5
Diamond <110>	4.6 (0.037)	0.04
Silicon <110>	10 (0.025) 30 (0.32) 50 (0.51)	not measured

- Amorphous W-targets
  0, 3, 6, 9, 12, 15, 18 mm on the target stage

Rocking curves at 4 GeV

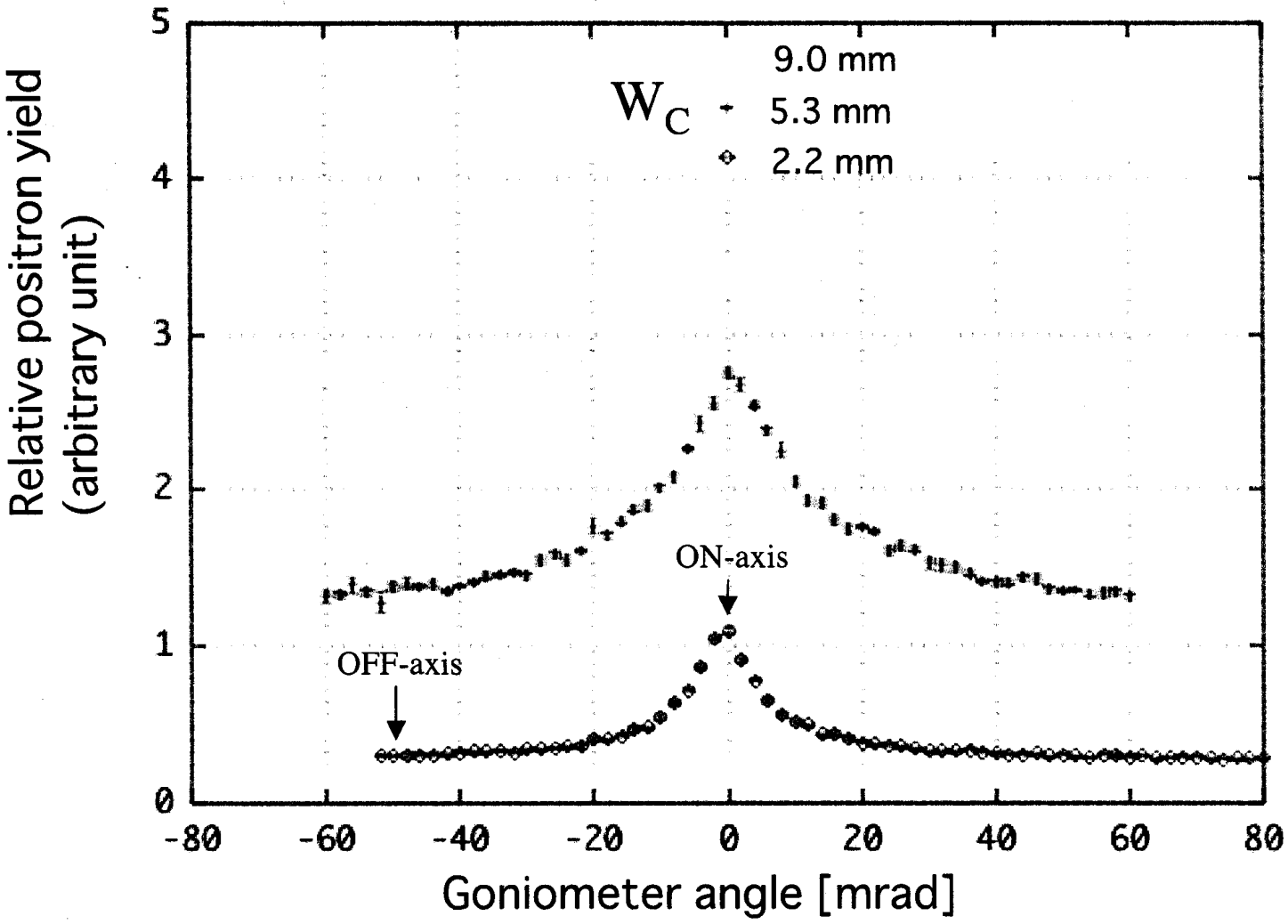

Rocking curves at 8 GeV

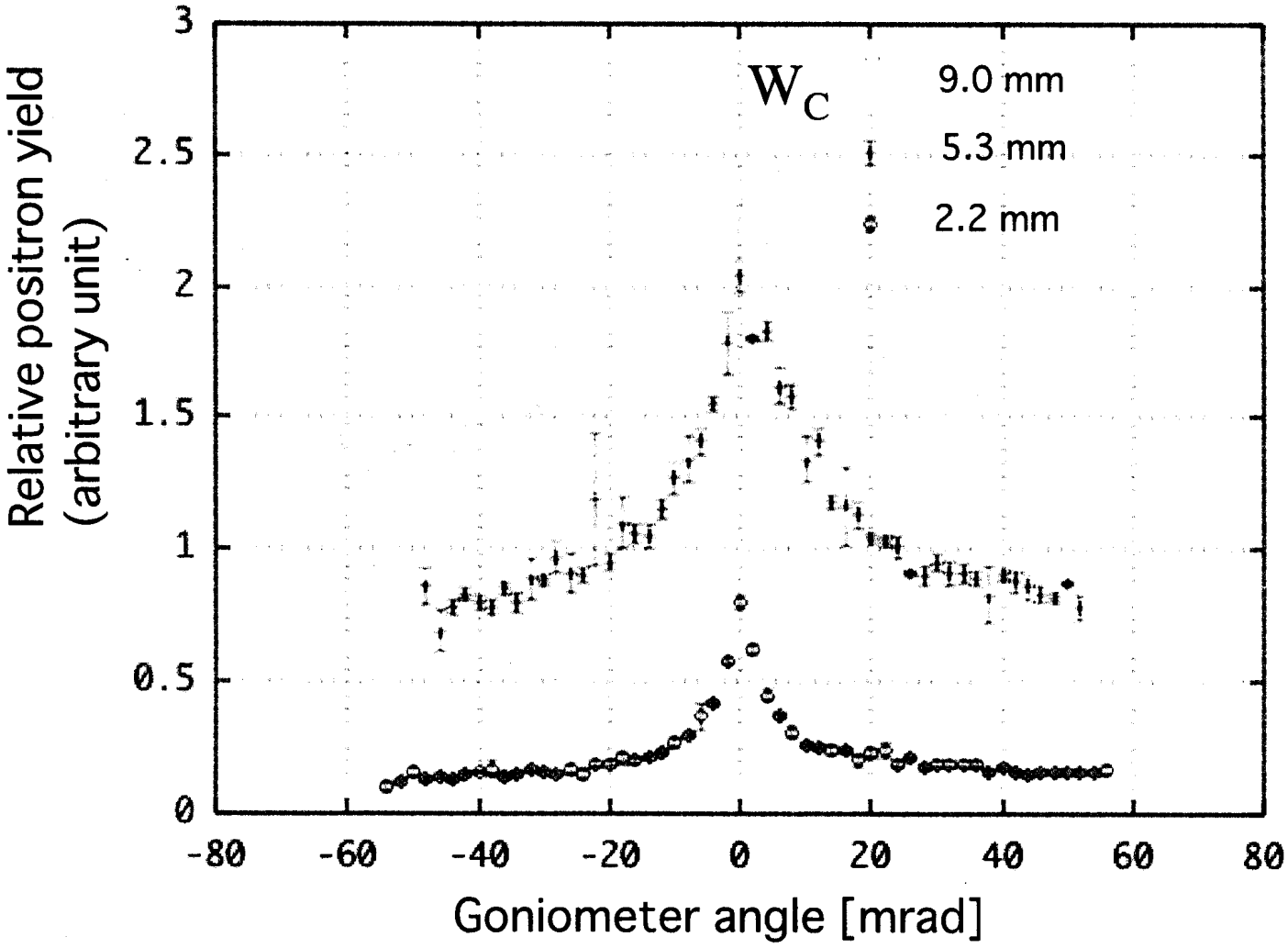

Simulation of CBS with EGS4

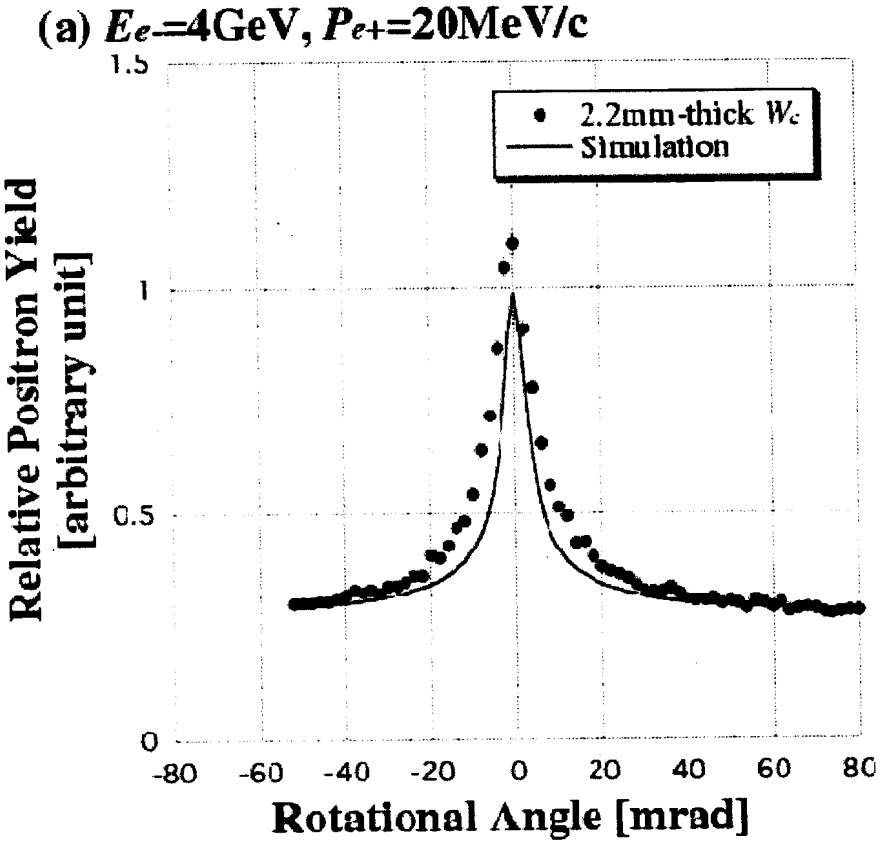

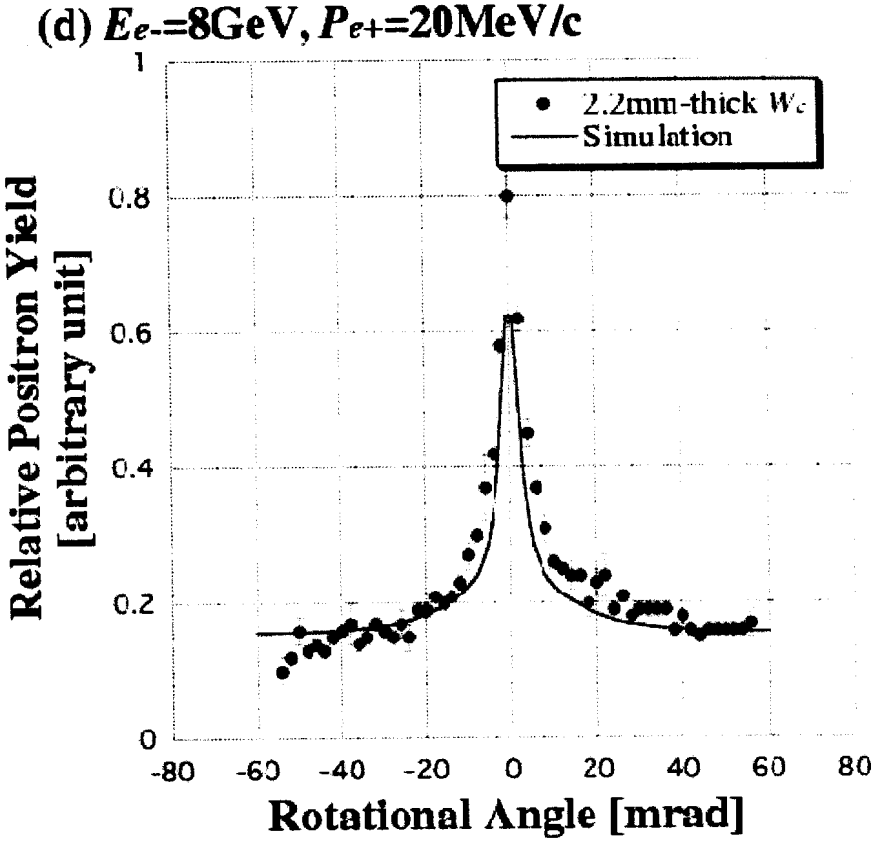

Enhancement v.s. electron energy

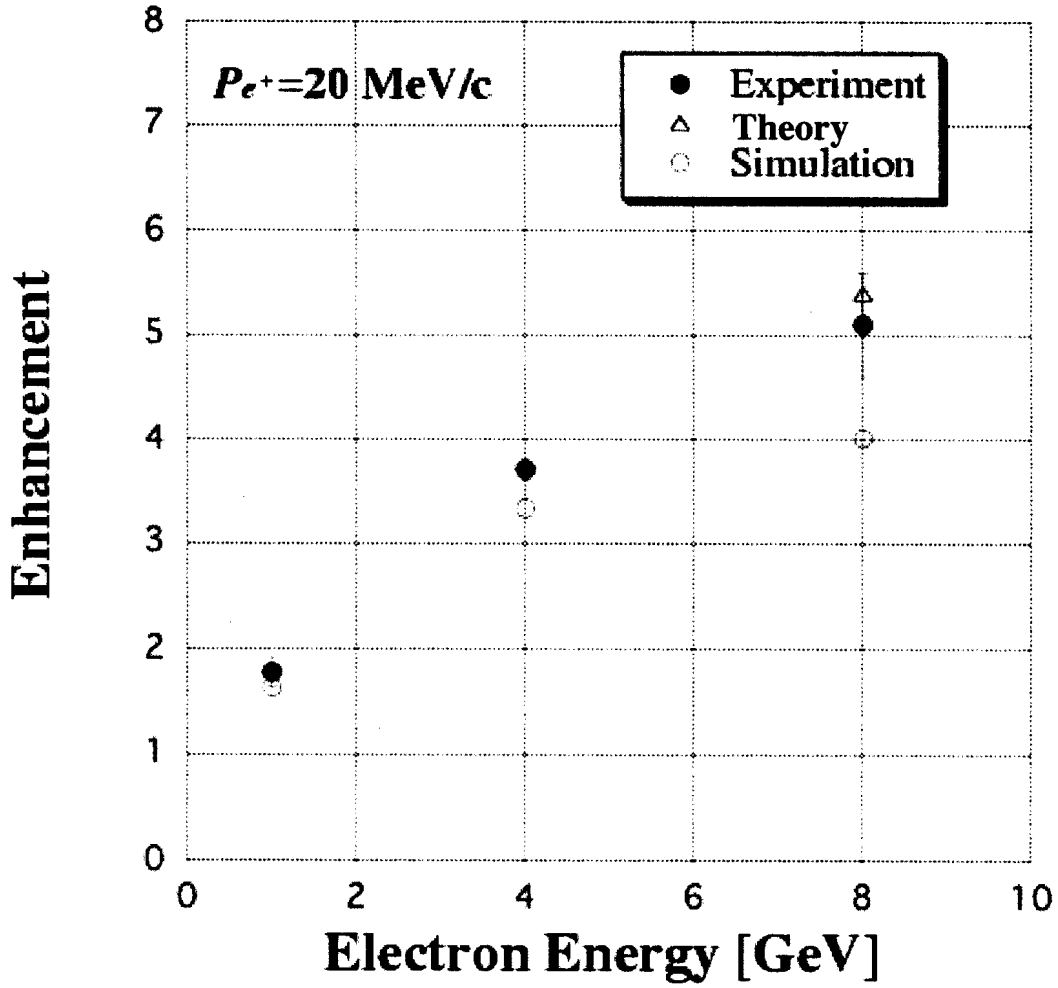

2.2 mm Wc

△ Baier and Strakhovenko

Peak width v.s. crystal thickness

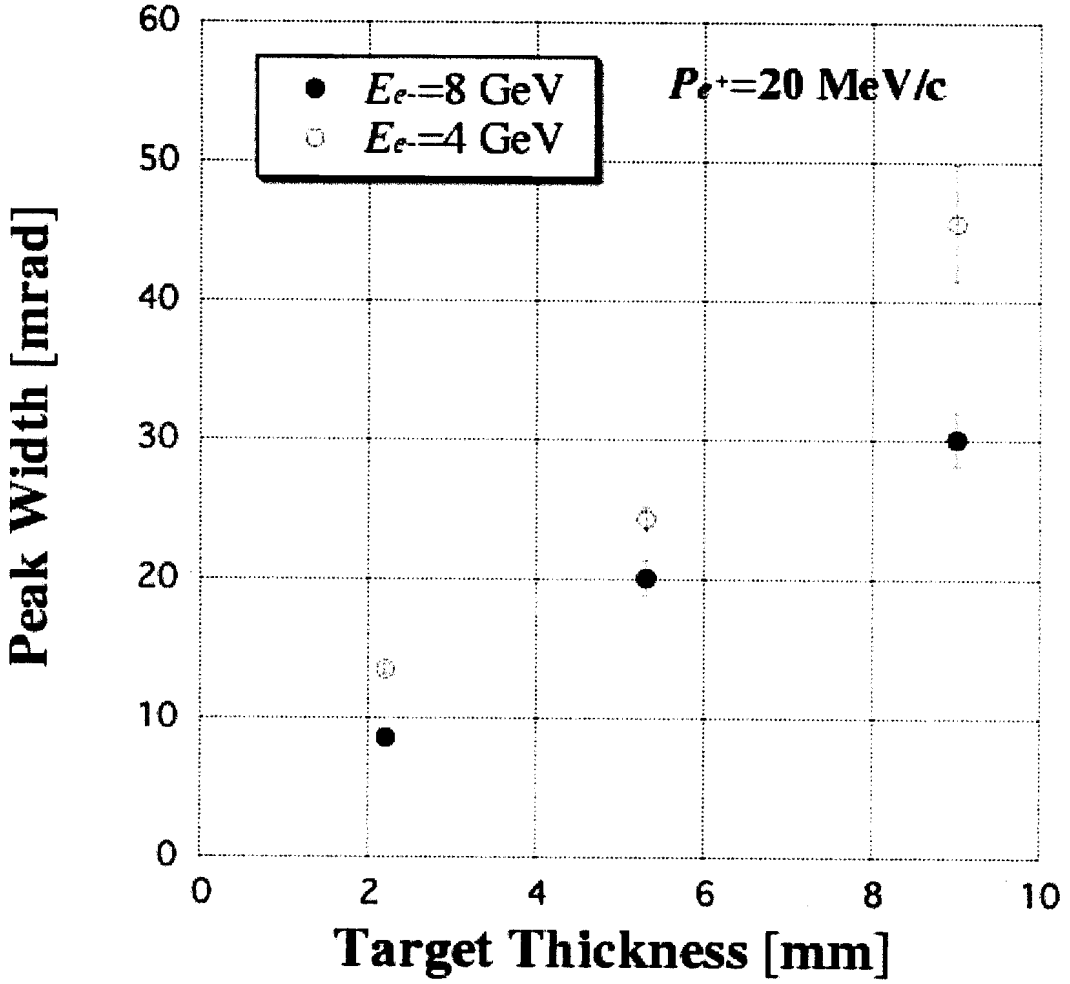

Combination of crystal + amorphous

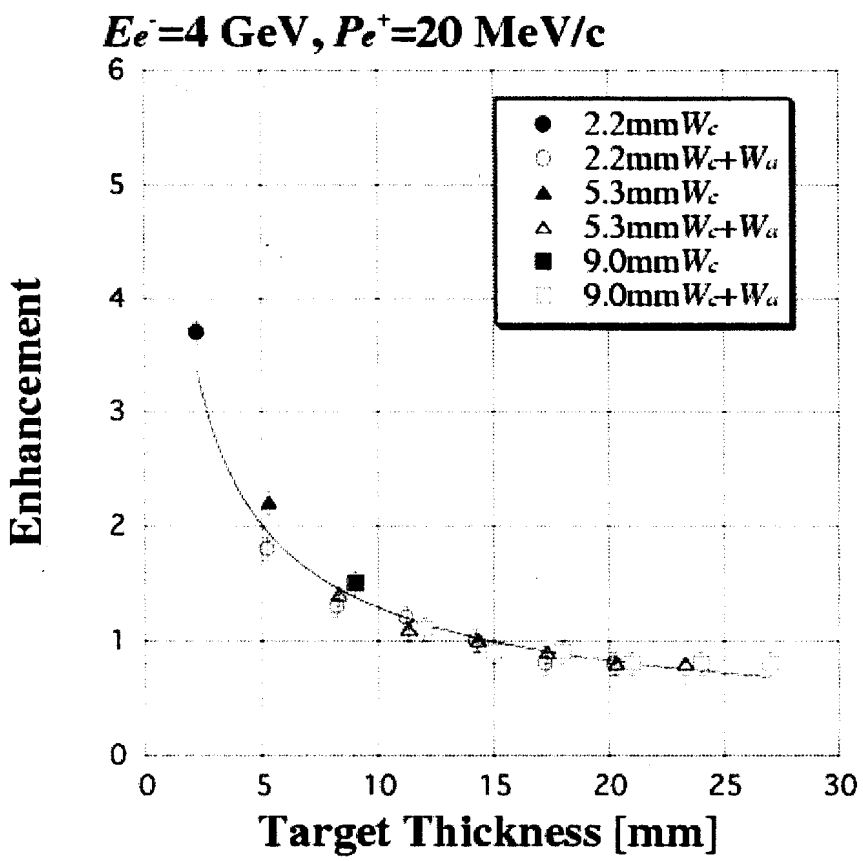

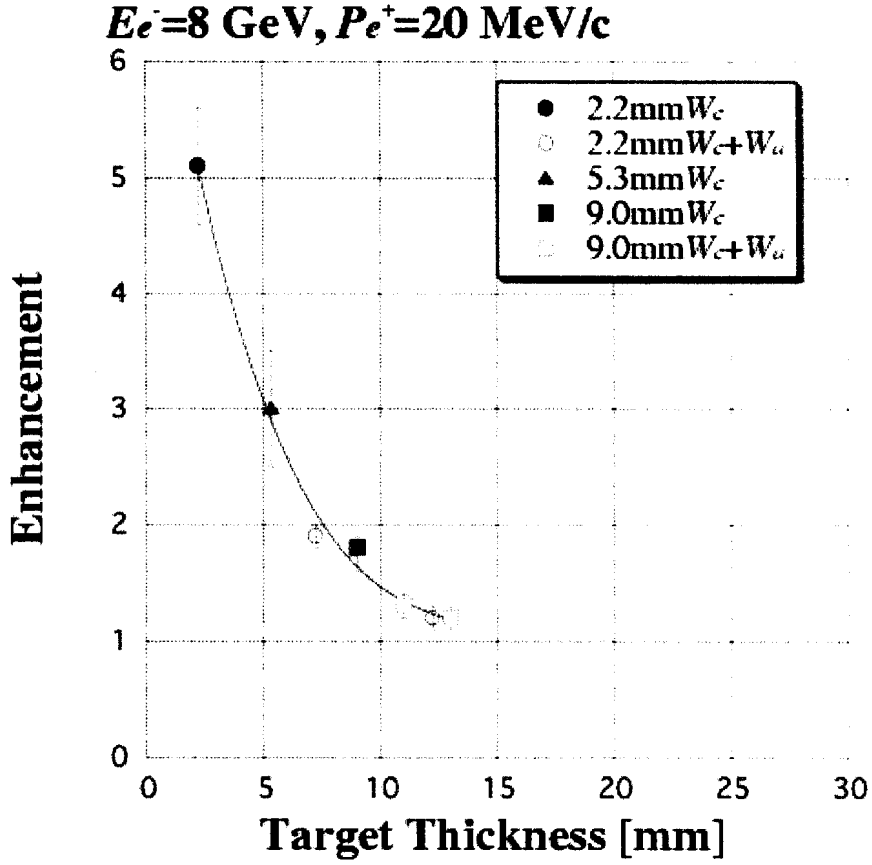

Crystal v.s. Amorphous at 8GeV

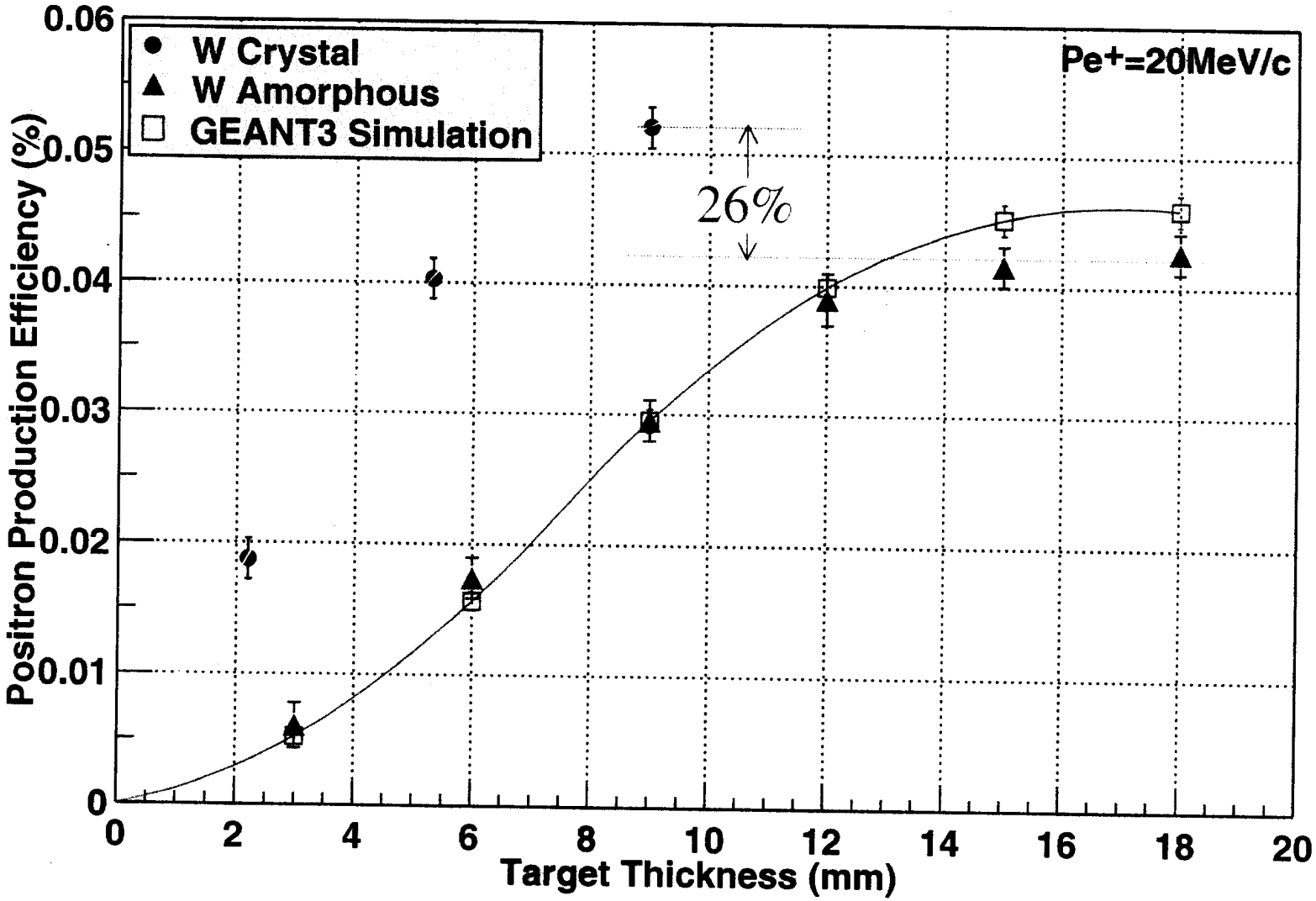

Diamond target

- Diamond is known to be the best crystal for producing intense CB photons
- Thermal conductivity is very high;
  660 W/m/K >> 170 W/m/K for tungsten
  Good for heat dissipation
- Seems high tolerance against the radiation damage; there is an estimate up to 10^{20} e^-/cm^2

◆Need to check

Summary

■ W crystals

1. Angular widths of rocking curves; much larger than the channeling critical angles
2. Enhancement factor increases with the electron beam energies 1-8 GeV
3. Positron yield from 9mm thick crystal is 26% greater than 18mm amorphous at 8 GeV
4. Effective radiation lengths for crystal is compressed;

   $L_{eff} = 0.55 \times L_{rad}$ at 8 GeV, 0.62 at 4 GeV
5. Enhancement factors; Good agreement with Baier and Strakhovenko
   - For a given number of accepted positrons, the energy deposited in a crystal is less than in an amorphous; ~40% smaller at 5 GeV

Summary (cont.)

- Need better simulation codes; Our data for W_c will become a set of inputs for improving calculations and simulations
- Diamond 5mm and Si 10,30,50 mm

1. Preliminary data showed large enhancement for diamond; ~20
2. Combinations with amorphous W; wait for analysis
3. More experiments for thicker diamond; ~10 mm will be available

LC e+ sources

By Takuya Kamitani

At Channeling e+ source Workshop

2003.Jan.17 at KEK

Comparison of the LC e+ sources

	JLC	NLC	CLIC	TESLA
Collision Energy [TeV]	0.5~1.0	0.5~1.0	1.0~3.0	0.5~0.8
Luminosity [10^{34}]	2.5	2.0	10.0	3.4
Ne+/pulse [10^{11}]	14.4	17.1	6.2	560.0
e+ (γ) generation	EM shower	EM shower	EM shower	Undulator
primary e- energy	10.0 GeV	6.2 GeV	2.0 GeV	250 GeV
Ne-/pulse [10^{11}]	19.2	28.5	20.8	560.0
Repetition rate	150 Hz	120 Hz	200 Hz	5 Hz
e- beam power	461 kW	340 kW	133 kW	11200 kW
e- radius on target	2.5 mm	1.6 mm	2.0 mm	(γ) 0.7 mm
# of target system	3	3 out of 4	1	1
Peak energy density	35 J/g	35 J/g	35 J/g	?
Target material	W75Re25	W75Re25	W75Re25	Ti
Target thickness	6.0 X0	4.0 X0	4.0 X0	0.4 X0
Matching system	AMD	AMD	AMD	AMD

Target Destruction Issue

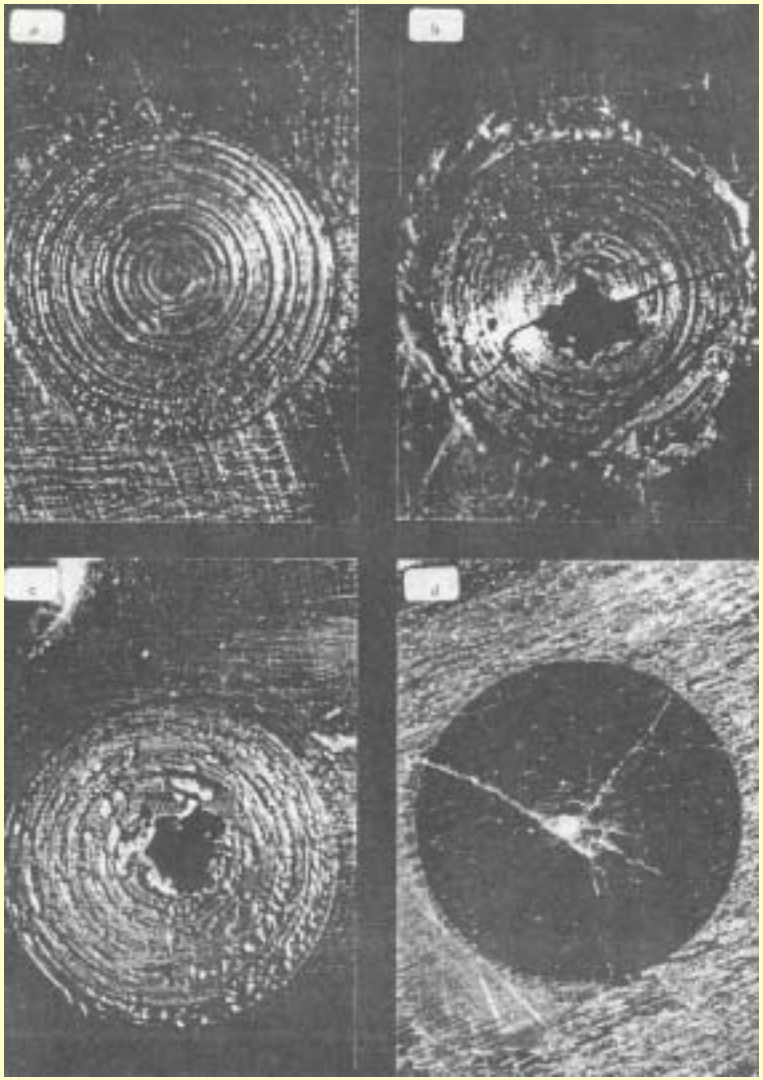

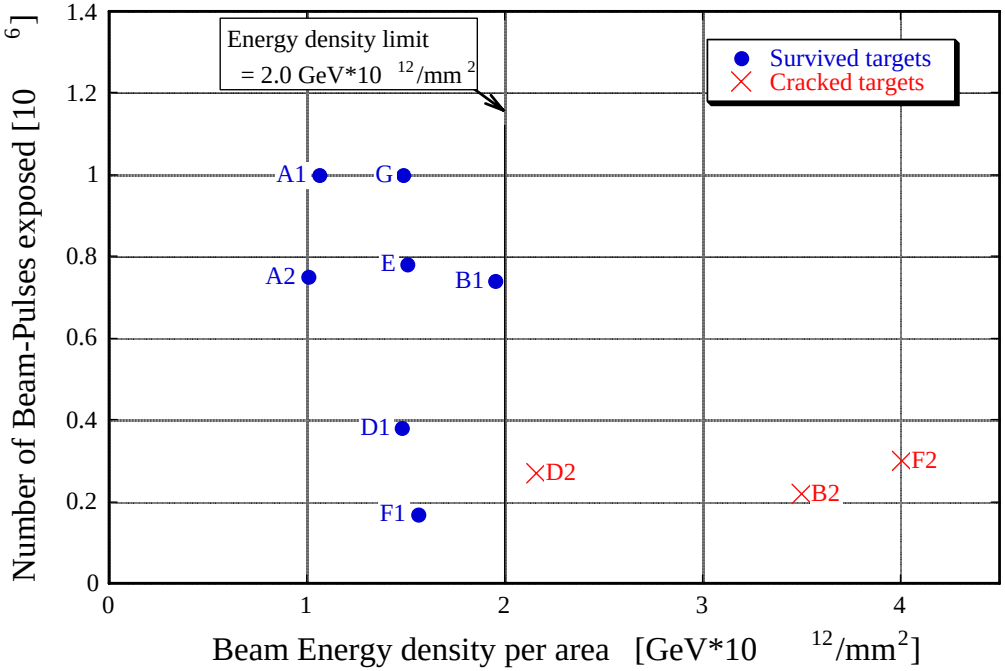

W75Re25 targets were irradiated by 20-GeV, 16-nC e- beam at SLAC. By changing the beam spot size, the energy density threshold for the destruction was studied.

(S. Ecklund, SLAC-CN-128, 1981)

Local volume Energy Density

SLAC Limit condition

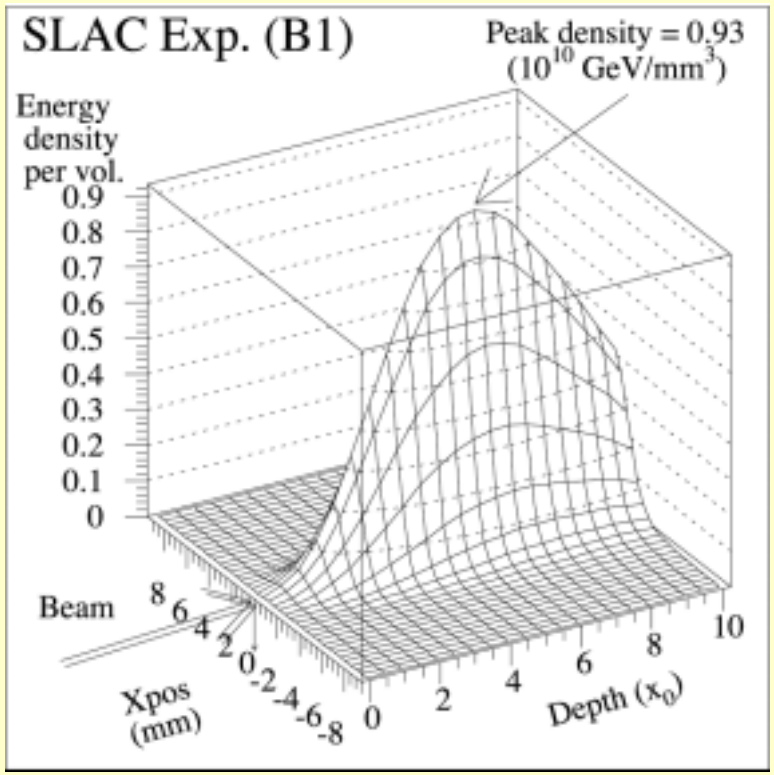

CLIC Design

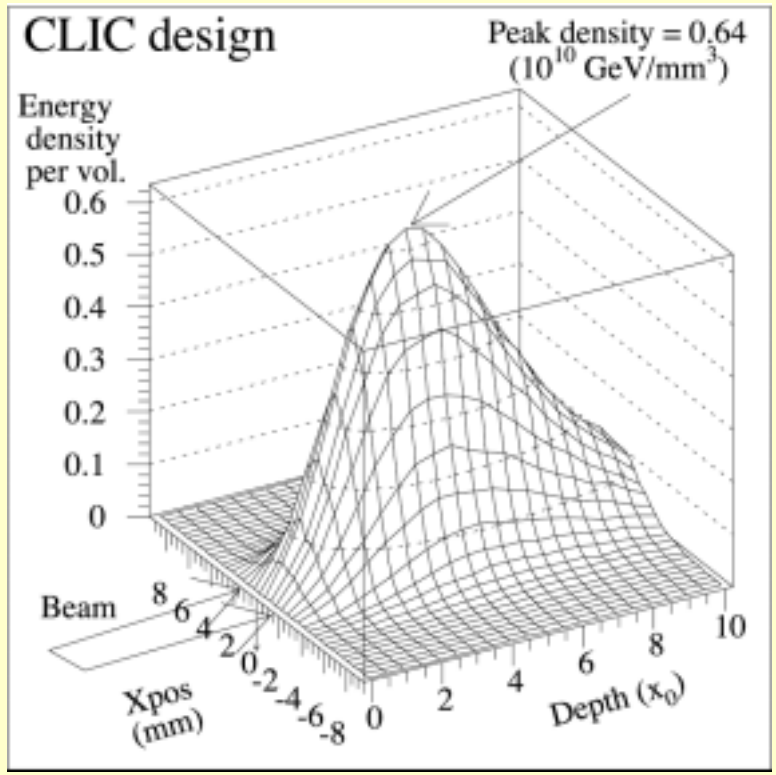

Local volume density is more essential for the destruction.

Redection of energy density by enlarging the beam spot size

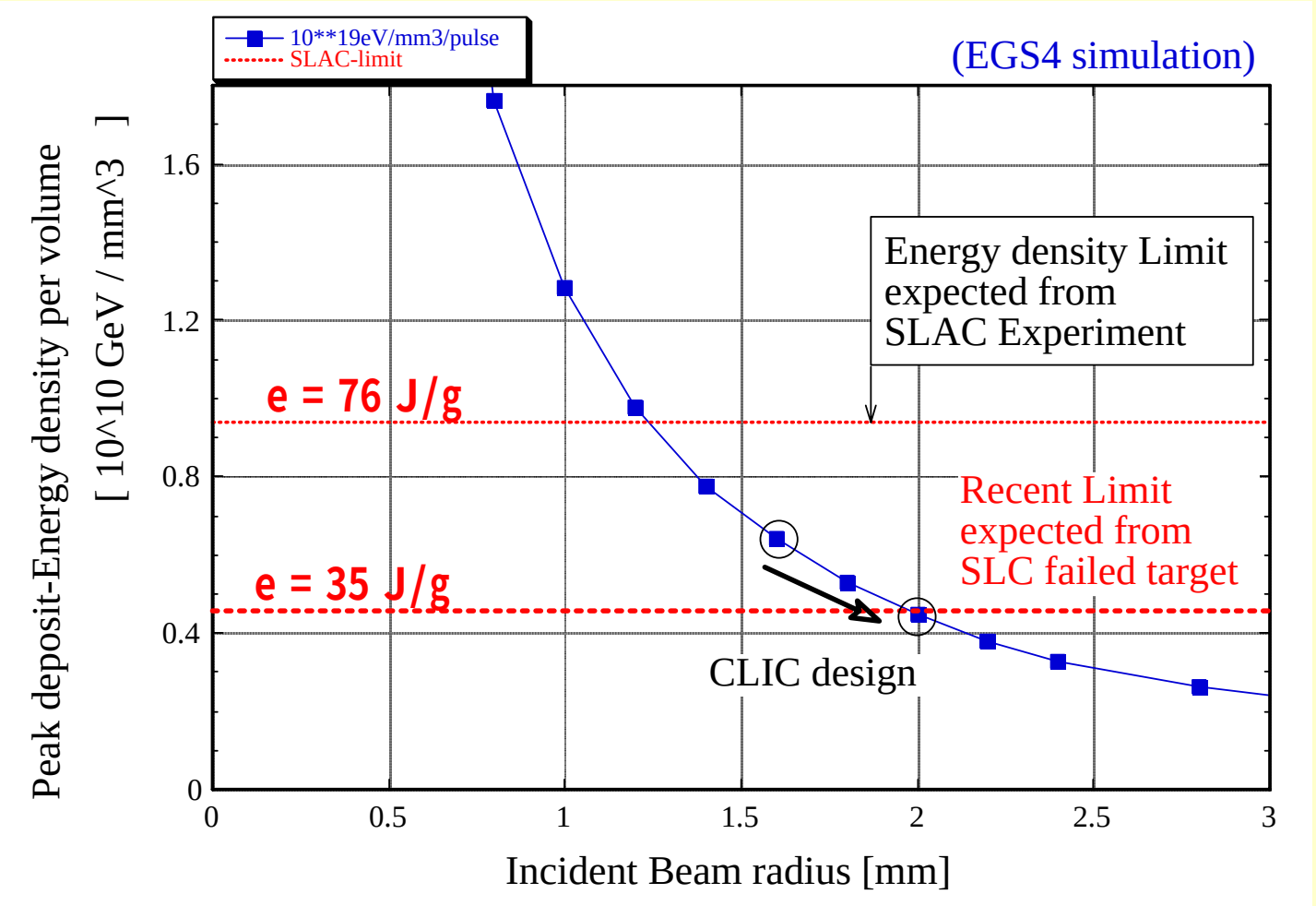

Multiple Target system

From http://www-project.slac.stanford.edu/lc/wkshp/snowmass2001/

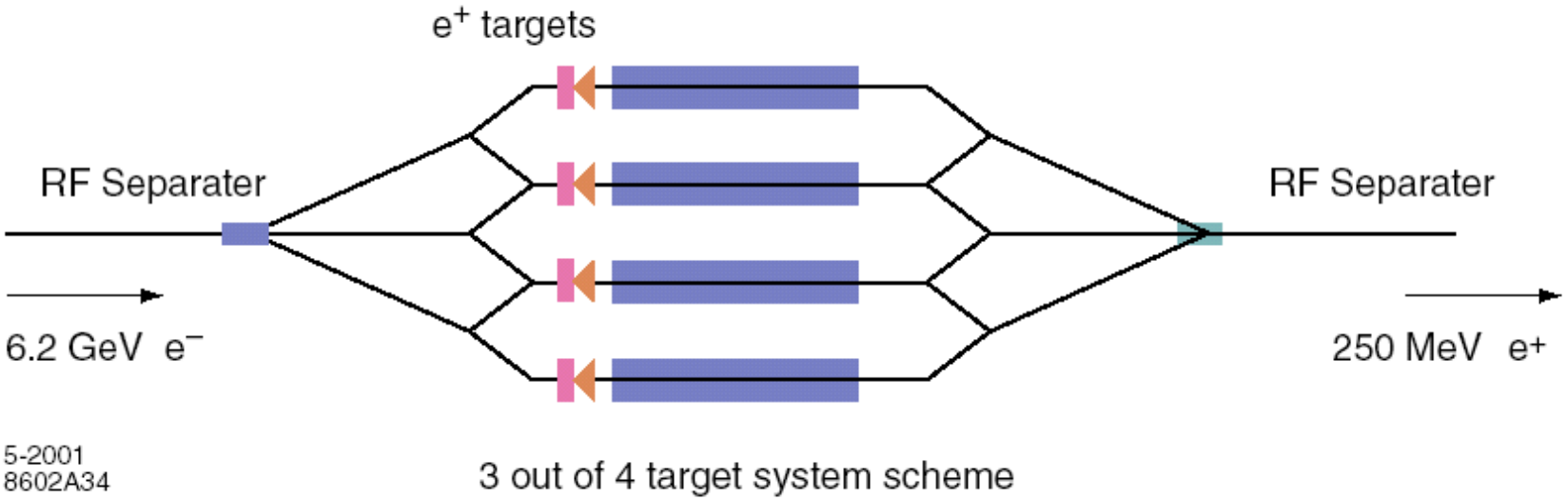

Figure 5.3: Schematic of the 3x4 NLC positron target system

- A bunch train is separated into 3 sparse trains by the RF separator
- Each trains hit one of the three target - capture section system
- They are merged by another RF deflector

TESLA e+ source

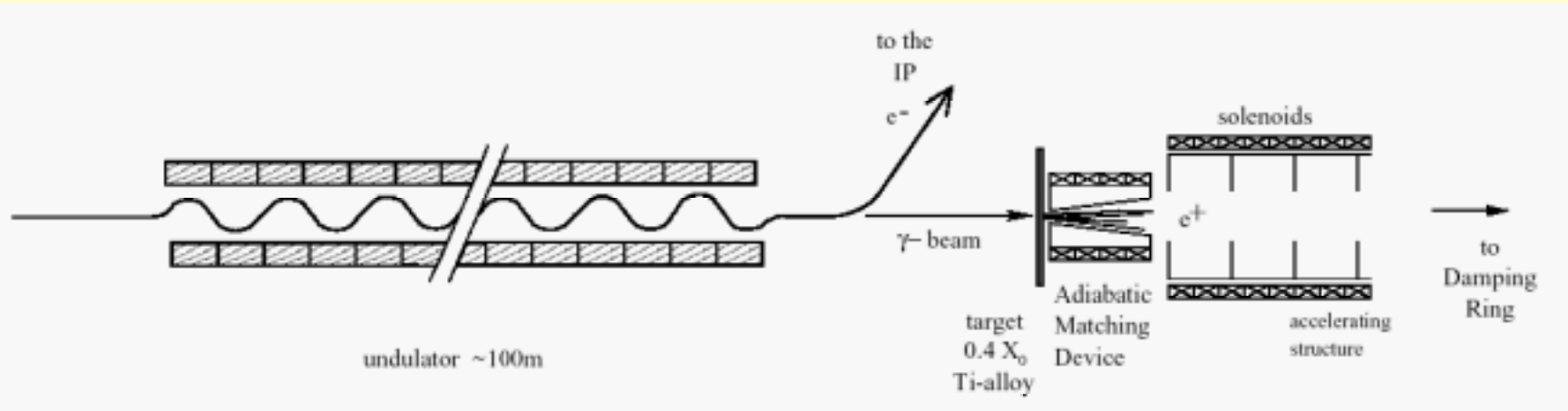

Beam intensity in a pulse is too large to irradiate directly the target material. Instead, very high energy e- beam and undulator are used to generate 20 MeV photons.

Target material is very thin (0.4 X0) to reduce the energy deposition, however, sufficient for the low energy photons.

JLC Positron Source

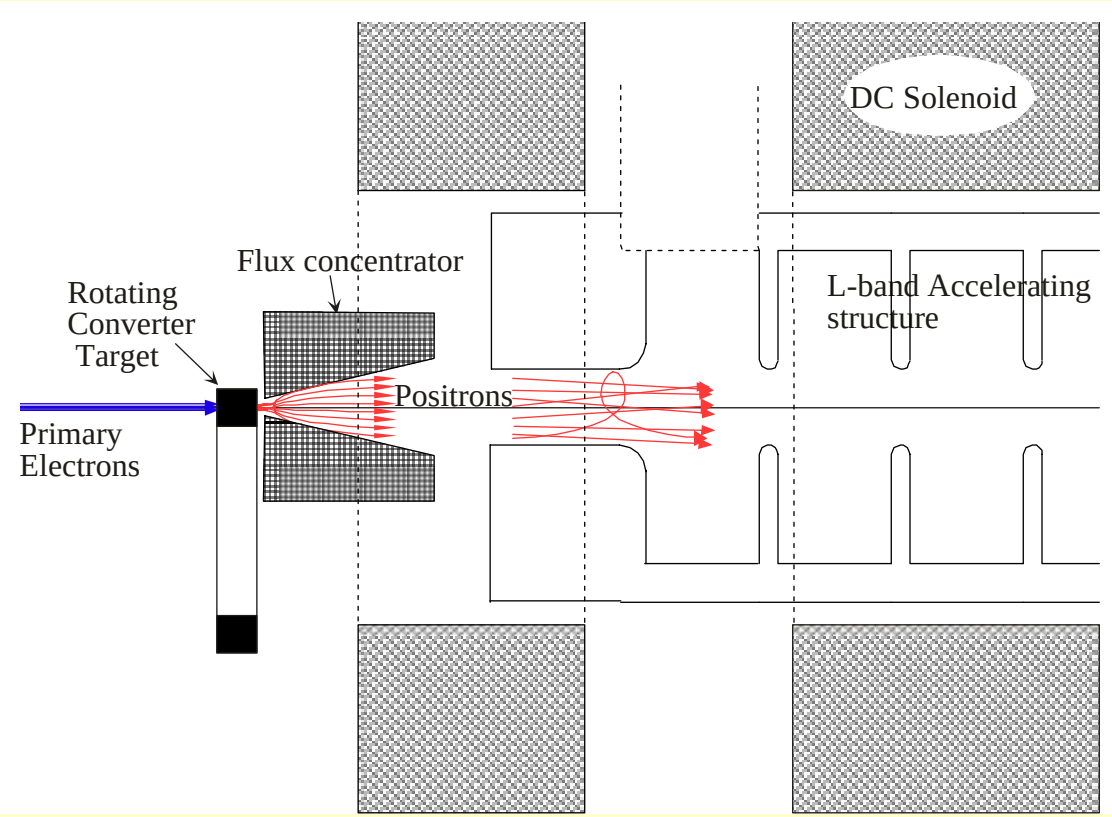

- W75Re25 target
- Thickness 6.0 X0
  (=21mm)
- Adibatic matching system
  Bi = 7.0 T, Bf = 0.5 T
- L-band capture section
  up to 180 MeV
- S-band Linac
  up to 1.98 GeV
- Pre-damping ring and
  Main damping ring
  at 1.98 GeV

E(e-) = 10 GeV
N(e-) = 192x10^10
150 Hz Rep. Rate

Target Thickness Optimization

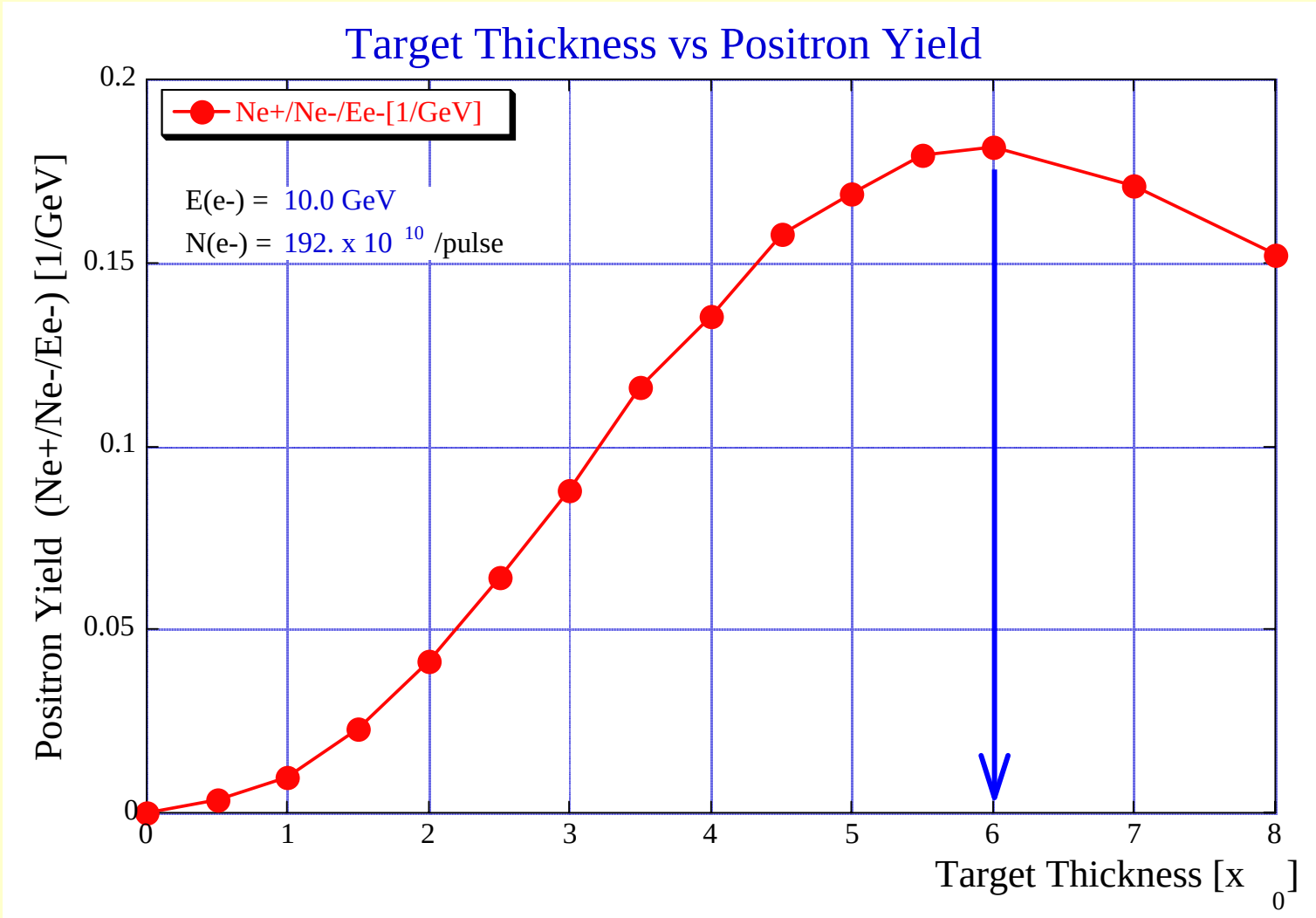

Total Energy Deposition

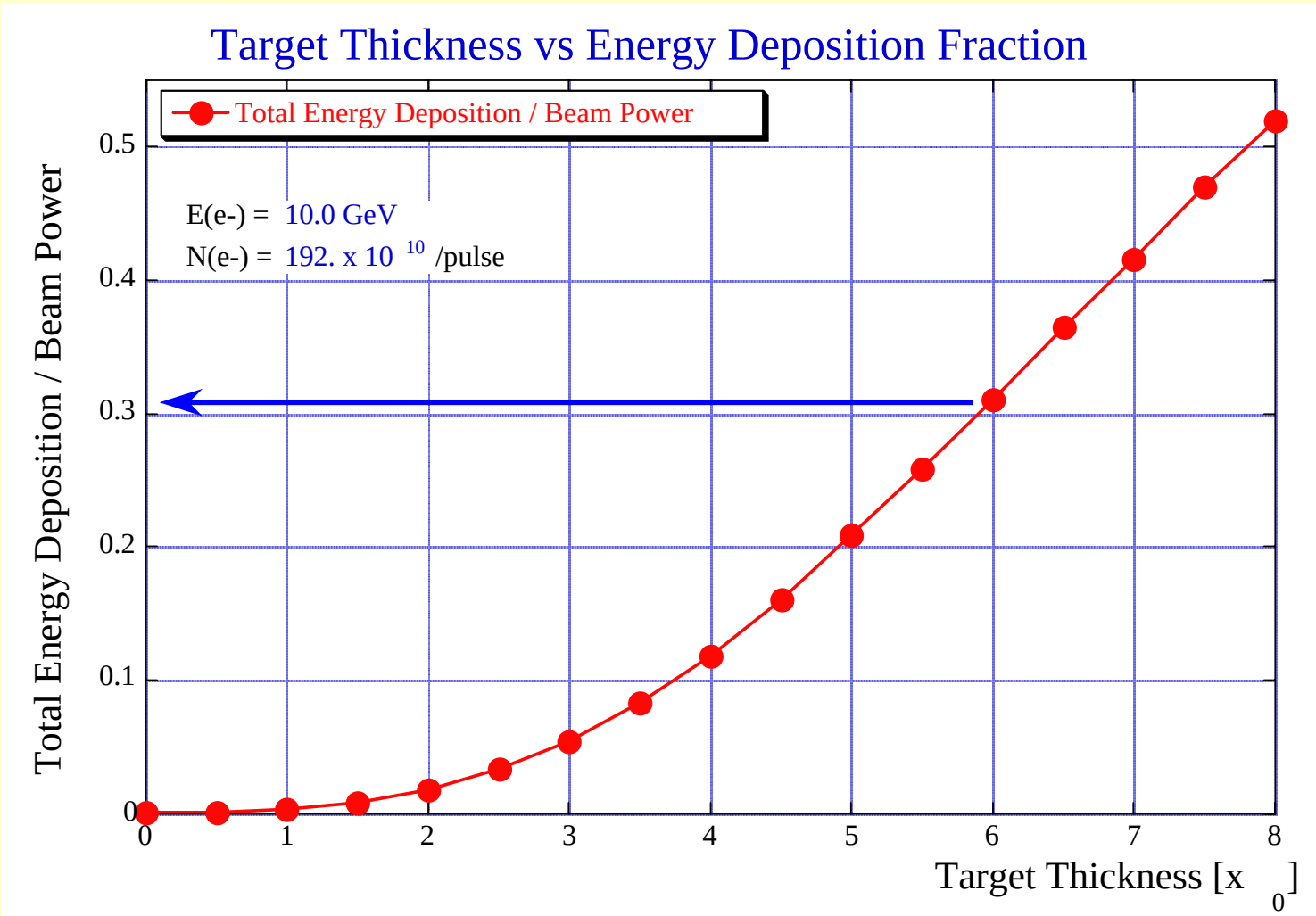

30% of Beam Power is deposited on the target

Local volume Energy density

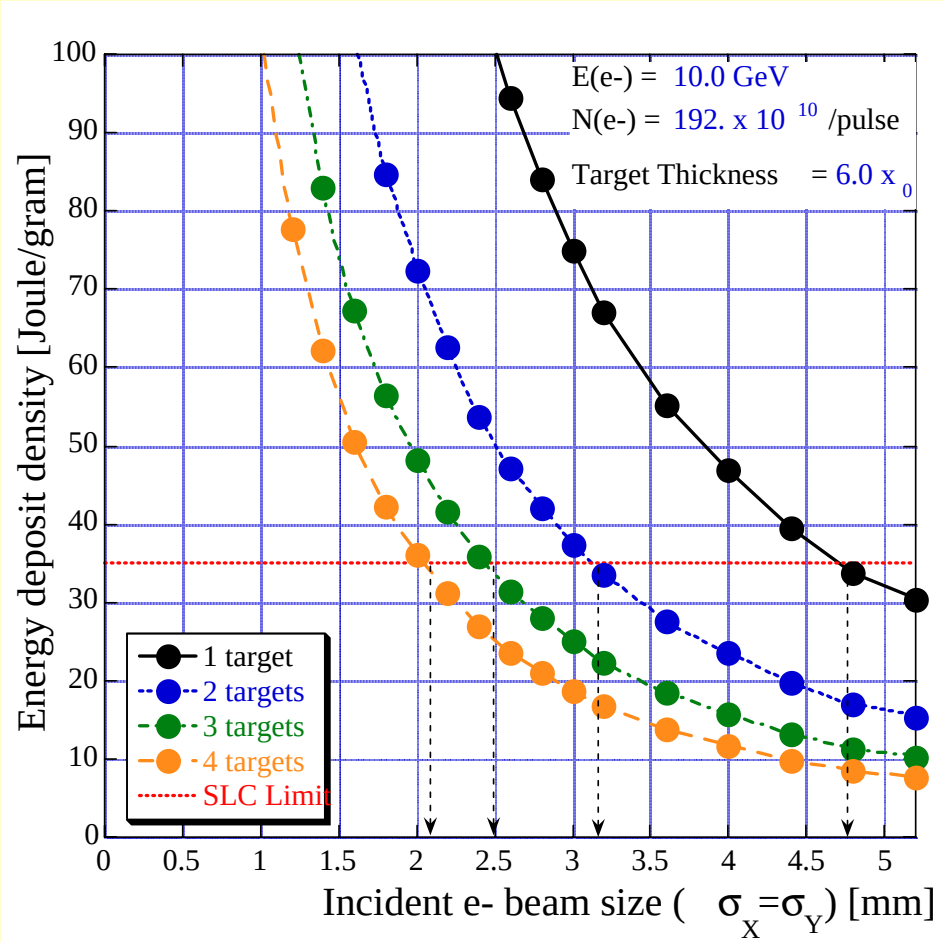

To make the peak energy denisty below the destruction limit, very large spot size or multiple target system is necessary.

Positron Yield vs Beam spot size

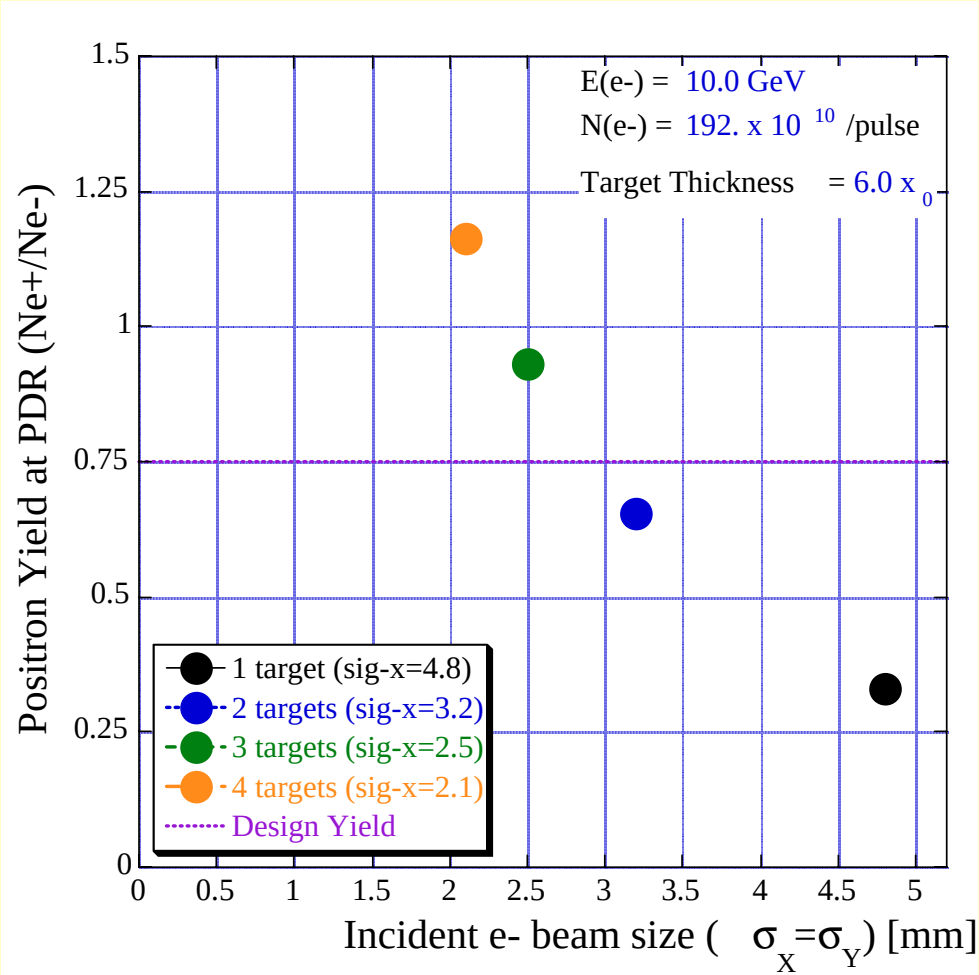

With large spot size, the positron yield is lower. Single or 2 target system is not acceptable. At least, 3 target system is necesarry.

Positron Yield Estimation

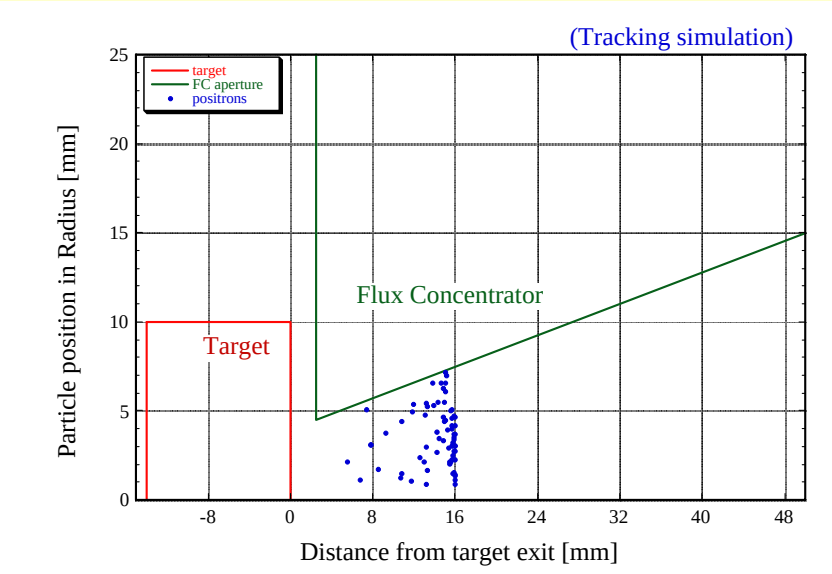

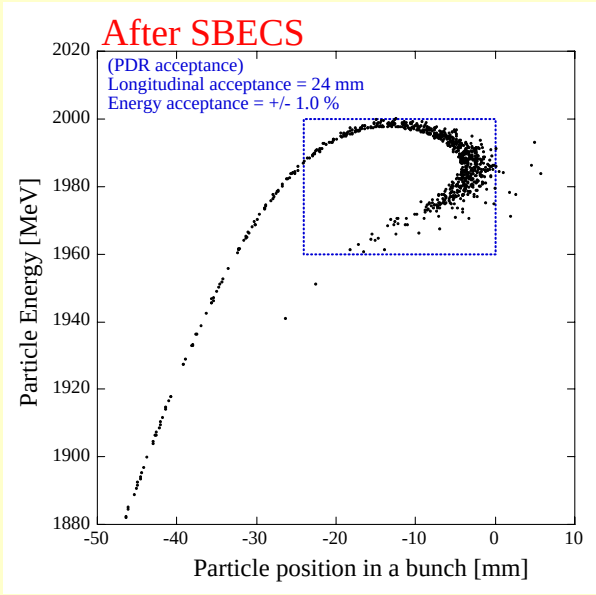

- **Positron Generation at target (EGS4)**
- **Positron Tracking in the capture section (SOLEIL)**
- **Positron Tracking in the e+ 1.98-GeV linac (SAD)**
- **Elimination with Pre-damping Ring acceptance (both in transverse and longitudinal phase space)**

Proposals to Channeling Experts

- Design Goal of Channeling target for JLC
  to replace W75Re25 to crystal
  Comparable positron yield with
  1/3 of Peak energy density

- Search for the target material (crystal or hybrid) which generates sufficient positrons and comfirm it experimentally
- Establish the channeling simulation code which is consistent with the experiments
  - To generate sample particles for realstic yield estimation
  - To estimate the energy density distribution in the target

Comparison of undulator-based and crystal-based positron sources

A. Potylitsyn

Tomsk Polytechnic University

1. Conventional positron sources are based on a cascade shower process initiated by an electron with energy E_0 in the amorphous converter.

The number of positrons in the maximum of the shower curve:

$$N_{e+} \sim \frac{1}{3}(N_{e+} + N_{e-} + N_{ph}) = \frac{1}{3} N_{tot} = \frac{1}{3} \frac{E_0}{2E_{cr}}$$

$$E_{cr} = \frac{610\ \text{MeV}}{Z + 1.24}$$

For $E_0 = 30$ GeV in an iron ($E_{cr} \approx 22$ MeV) in the shower maximum ($t \approx 6 X_0$)

$N_{e+} \sim 90$ (EGS4), $N_{e+} \sim 220$ (rough estimation)

Positron source at SLC — $E_0 = 30$ GeV, $t = 6 X_0$

Energy efficiency $f = \frac{N_{e+}\ \text{accept.}}{N_{e-} \cdot E_{e-}}$

(see L. Rinolfi, T. Kamitani LC2002)

SLC $f = 0.05$; CLIC (project) $f = 0.30$

It means the „energy cost" for each positron

$E_c = 20$ GeV (SLC), $E_c = 3.3$ GeV (CLIC)

The main problem is connected with huge energy deposition in a thick

2. TESLA e^+ source

Positrons are generated by undulator radiation in a thin rotatable convertor ($t = 0.4 X_0$)

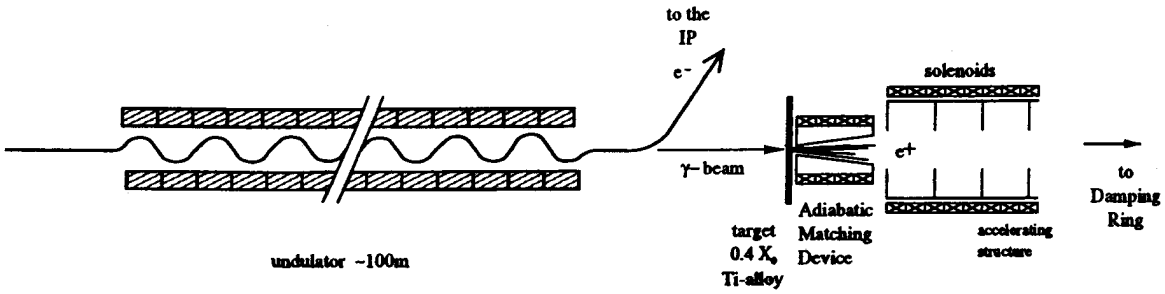

Figure 4.3.1: *Sketch of the positron source layout.*

parameter	SLC	TESLA
No. of positrons per pulse	$(3\text{–}5) \times 10^{10}$	5.6×10^{13}
No. of bunches per pulse	1	2820
pulse duration	3 ps	0.95 ms
bunch spacing	8.3 ms	337 ns
repetition frequency	120 Hz	5 Hz

Table 4.3.1: *Comparison of TESLA and SLC positron source parameters.*

gap [mm]	λ_u [cm]	B_{max} [T]	E_1 [MeV]
4.0	1.25	0.85	31.6
4.5	1.34	0.8	29.5
5.0	1.42	0.75	27.8

Table 4.3.2: *Parameters of the planar undulator.*

$$K = 0.934 \cdot B[T] \cdot \lambda_u [cm] = 1$$

$$L_u = 100\ m \qquad N_u = \frac{L_u}{\lambda_u} \approx 7000$$

Undulator	
peak field	0.75 T
period length	14.2 mm
gap height	5 mm
γ-spot size on target	0.7 mm
photon beam power	135 kW
Target	
material	Ti-alloy
thickness	1.42 cm ($0.4X_0$)
pulse temperature rise	420 K
av. power deposition	5 kW
Adiabatic Matching Device	
initial field	6 T
taper parameter	$30\,\mathrm{m}^{-1}$
end field	0.16 T
capture cavity iris radius	23 mm
General	
capture efficiency	16%
No. of positrons per electron	2
norm. e^+-beam emittance	0.01 m
total energy width	$\pm$30 MeV
required D.R. acceptance	0.048 m

Table 4.3.3: *Overview of the positron source main parameters.*

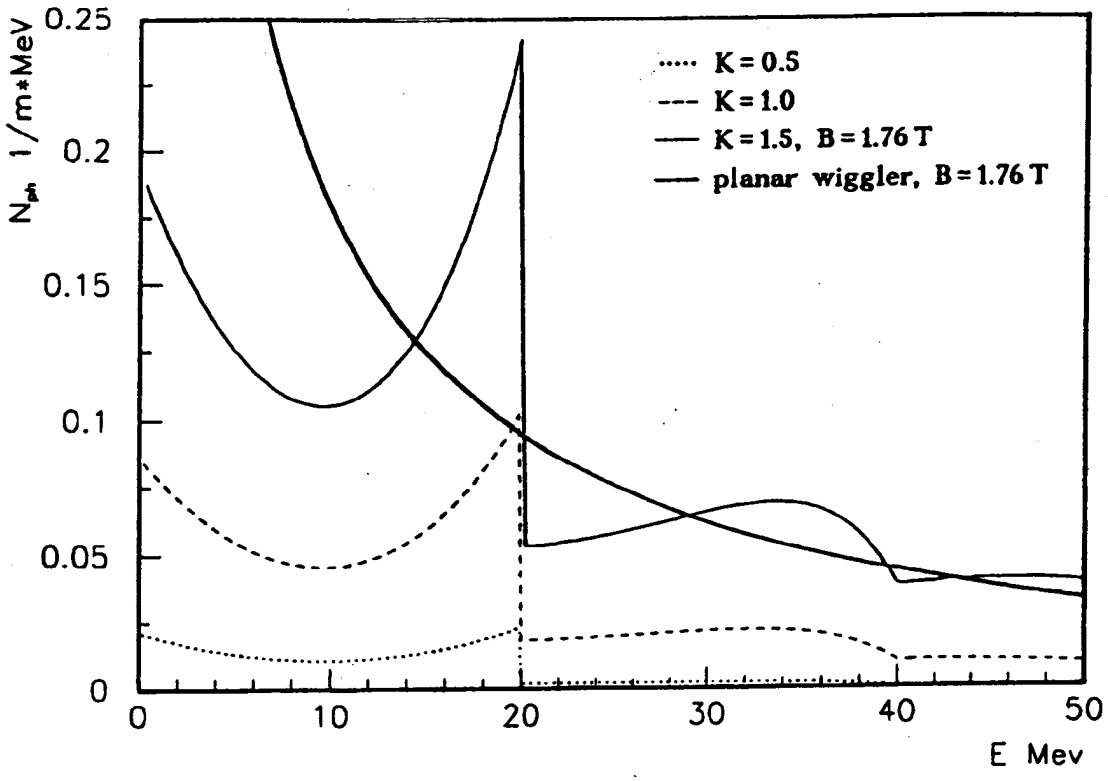

Fig. 1.5 Photon number spectrum for helical undulators and a planar wiggler, E = 250 GeV. We will discuss the spectrum of a helical undulator in more detail in ch. 2.6.0.

Radiation losses $\Delta E_{rad} = 3\ GeV$

The proposed scheme may provide 2 accepted positrons per initial electron.

The „energy cost" is 1.5 GeV only

due to large number of the emitted „soft" photons.

$$N_{ph} \sim 2\pi\alpha N_u \frac{K^2}{1+K^2} \approx 160\ ph/e^-$$

The exact calculations (K. Flottmann, DESY-93-161)

$$N_{ph} = [3.56 - 0.69K]\, K^2 \cdot N = 200\ ph/e^-$$

The average photon energy

$$\langle E_{ph} \rangle = \frac{\Delta E_{rad}}{N_{ph}} = 15\ MeV$$

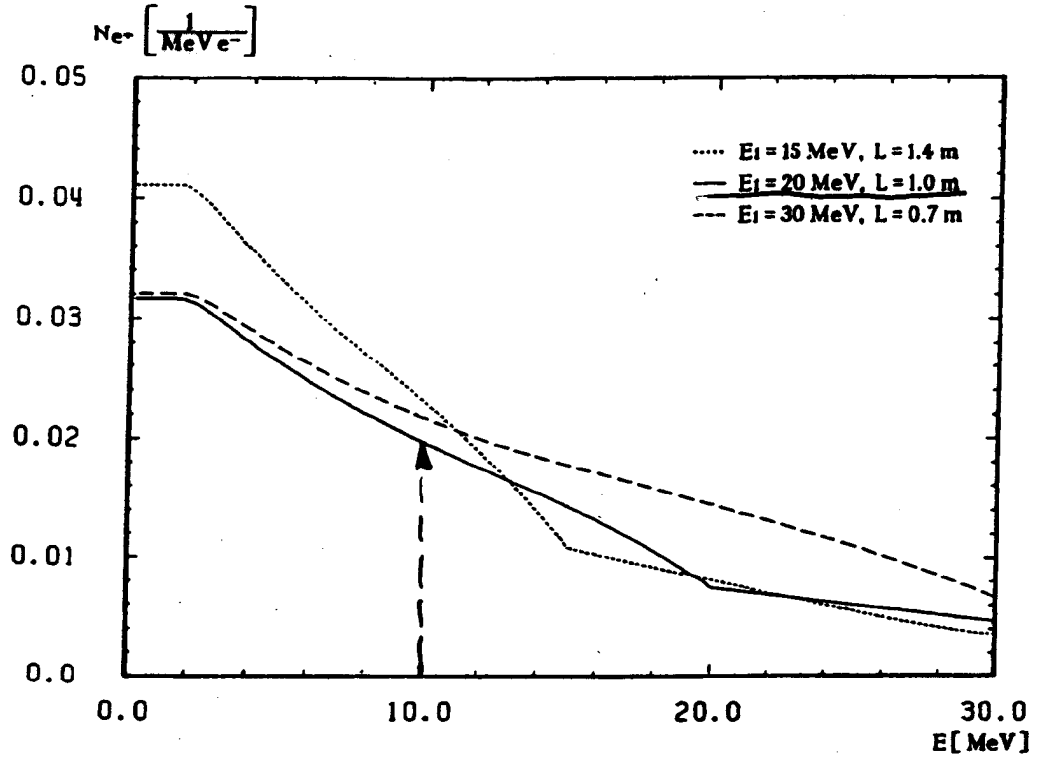

Fig. 1.9 Positron spectra for various E_1; K = 1, E = 250 GeV

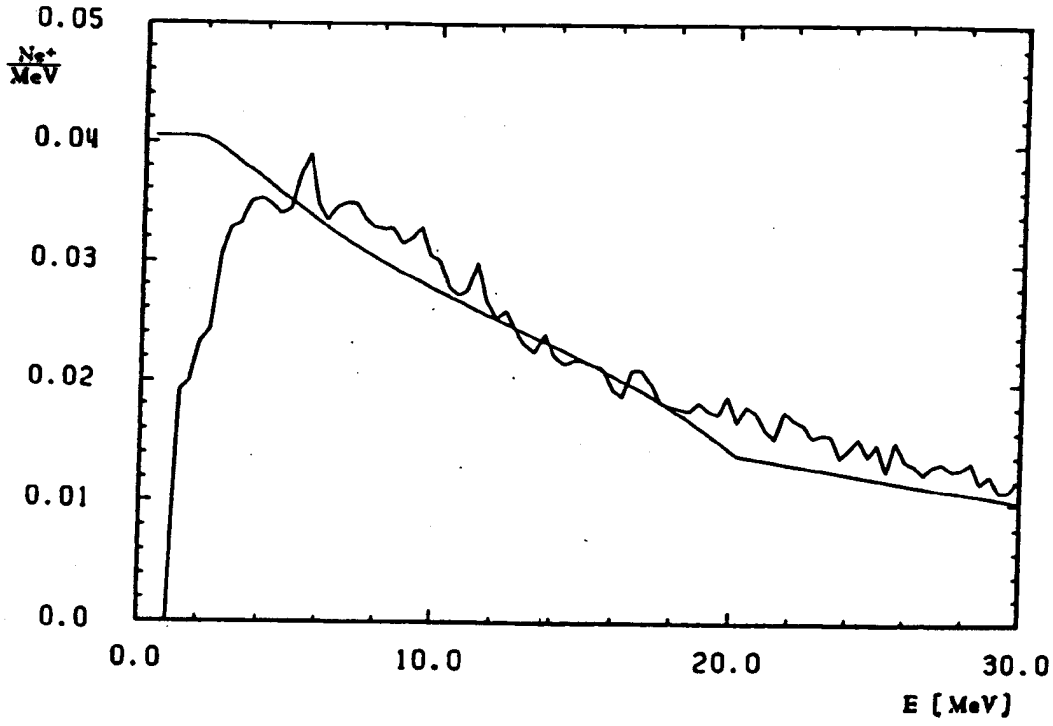

Fig. 1.10 Comparison of positron spectra calculated by means of the approximative method and by means of the shower code EGS 4

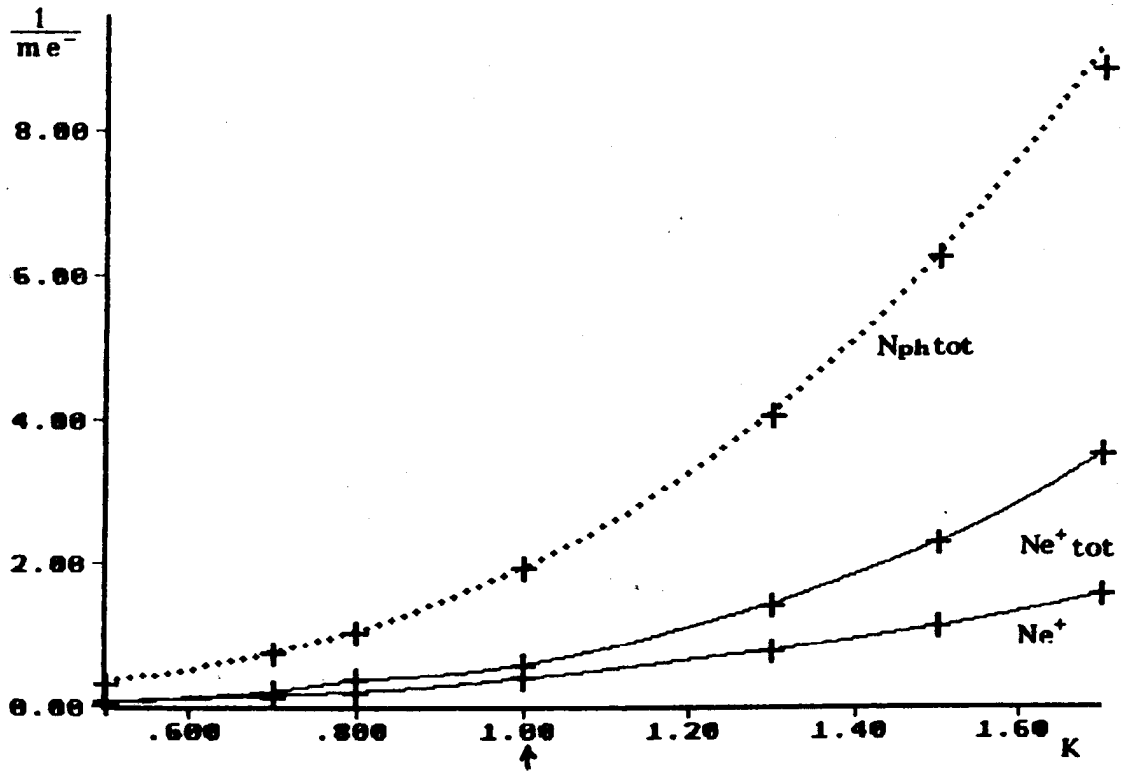

Fig 1.7 Dependence of the photon production and the positron production per radiation length on the parameter K, $E_1 = 20$ MeV, $E = 250$ GeV; dotted line: approximation according to eq. 1.9

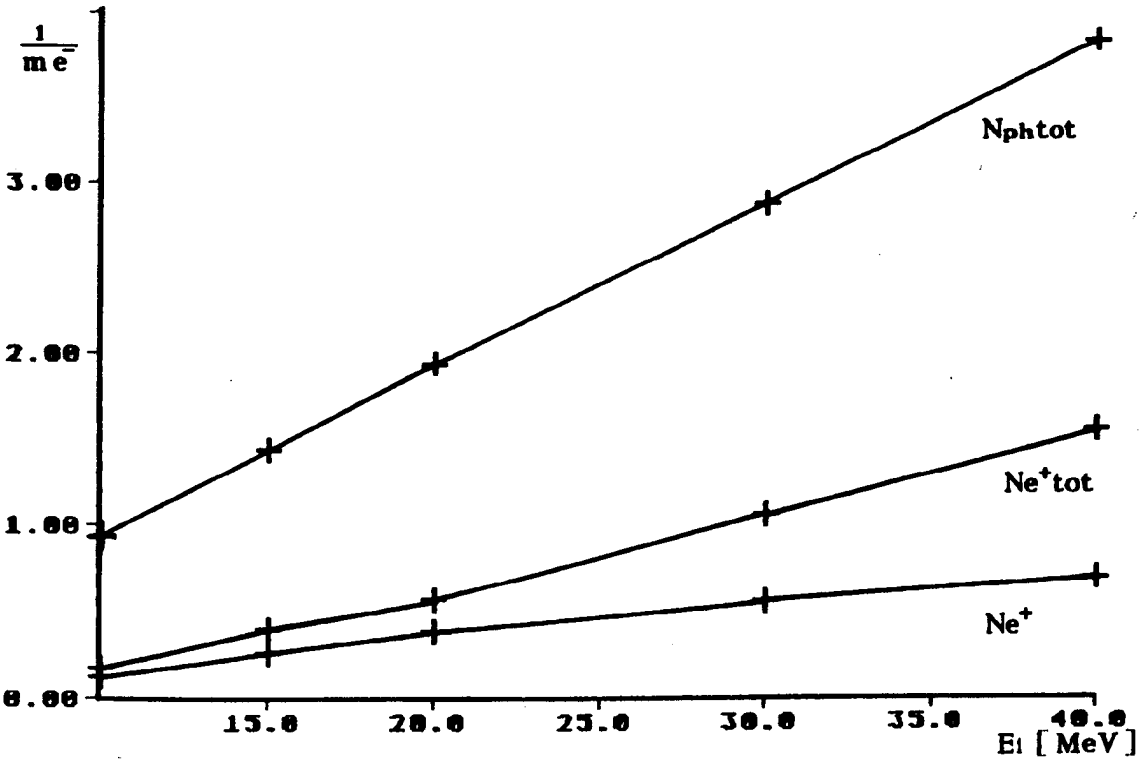

Fig. 1.8 Dependence of the positron production per radiation length on E1; K = 1, E = 250 GeV

3. A crystal may be considered as some kind of a solid-state undulator.

Is it possible to use one as a photon emitter ?

In principle, yes.

Low energy experiments (Tomsk, Kharkov, INS) demonstrated the possibility to use crystal targets with thickness $t >> L_{dechanneling}$ to produce a radiation enriched by „soft" photons.

For usual bremsstrahlung

$$\langle \omega_{BS} \rangle = \frac{\Delta E_{rad}}{\langle N_{ph} \rangle}$$

$$\Delta E_{rad} \approx \frac{t}{X_0} \int_{\gamma\omega_p}^{E_0} d\omega = \frac{t}{X_0} E_0 , \quad t \lesssim X_0$$

ω_p is plasmon energy ($\omega_p = 30 eV$ for Si)

$$\langle N_{ph} \rangle = \frac{t}{X_0} \int_{\gamma\omega_p}^{E_0} \frac{1}{\omega} d\omega = \frac{t}{X_0} \ln \frac{mc^2}{\omega_p} \sim 10 \frac{t}{X_0}$$

$$\langle \omega_{BS} \rangle \approx 0.1 E_0$$

For channeling radiation

$$u = \frac{\omega_{ch}}{E_0 - \omega_{ch}} \approx \frac{2\gamma\theta_c \frac{\lambda\!\!\!^{-}e}{a_s}}{1 + \rho/2} = \frac{2\gamma^{1/2}\sqrt{\frac{V_0}{mc^2}} \frac{\lambda\!\!\!^{-}e}{a_s}}{1 + \frac{\gamma V_0}{2mc^2}}$$

(see V. Baier et al. NIM B 103 (1995) 147)

For Si, $E_0 \sim 1 GeV$, (111)

$\omega_{ch} \sim 0.015 E_0 \sim 15 MeV$

For coherent bremsstrahlung

$$u = \frac{\omega_{cBS}}{E_0 - \omega_{cBS}} \sim \frac{\pi \gamma \theta}{a}$$

If $\langle \theta_{ms} \rangle > \theta_c$ then one may consider $\langle \theta_{ms} \rangle$ as an orientation angle

For 10 mm Si, $E_0 = 1$ GeV

$\omega_{cBS} \sim 0.05 E_0 \sim 50$ MeV

4. For axial orientation radiation losses consist of two parts:

$$\Delta E_{ax} = \Delta E_{BS} + \Delta E_{cr}$$

For $E_0 = 0.9$ GeV (Tomsk's data)

	diamond 10 mm	Si 10 mm	Tungsten 1.2 mm
$\frac{\Delta E_{cr}}{\Delta E_{BS}}$	~ 2.5	~ 1.8	~ 1.5

$$\langle N_{ph}^{cr} \rangle \approx \frac{\Delta E_{cr}}{\langle \omega_{cr} \rangle}$$

Even for $E_0 \sim 1$ GeV

$$\langle N_{ph}^{cr} \rangle > \langle N_{ph}^{BS} \rangle$$

SPECTR (747x1044x2 pcx)

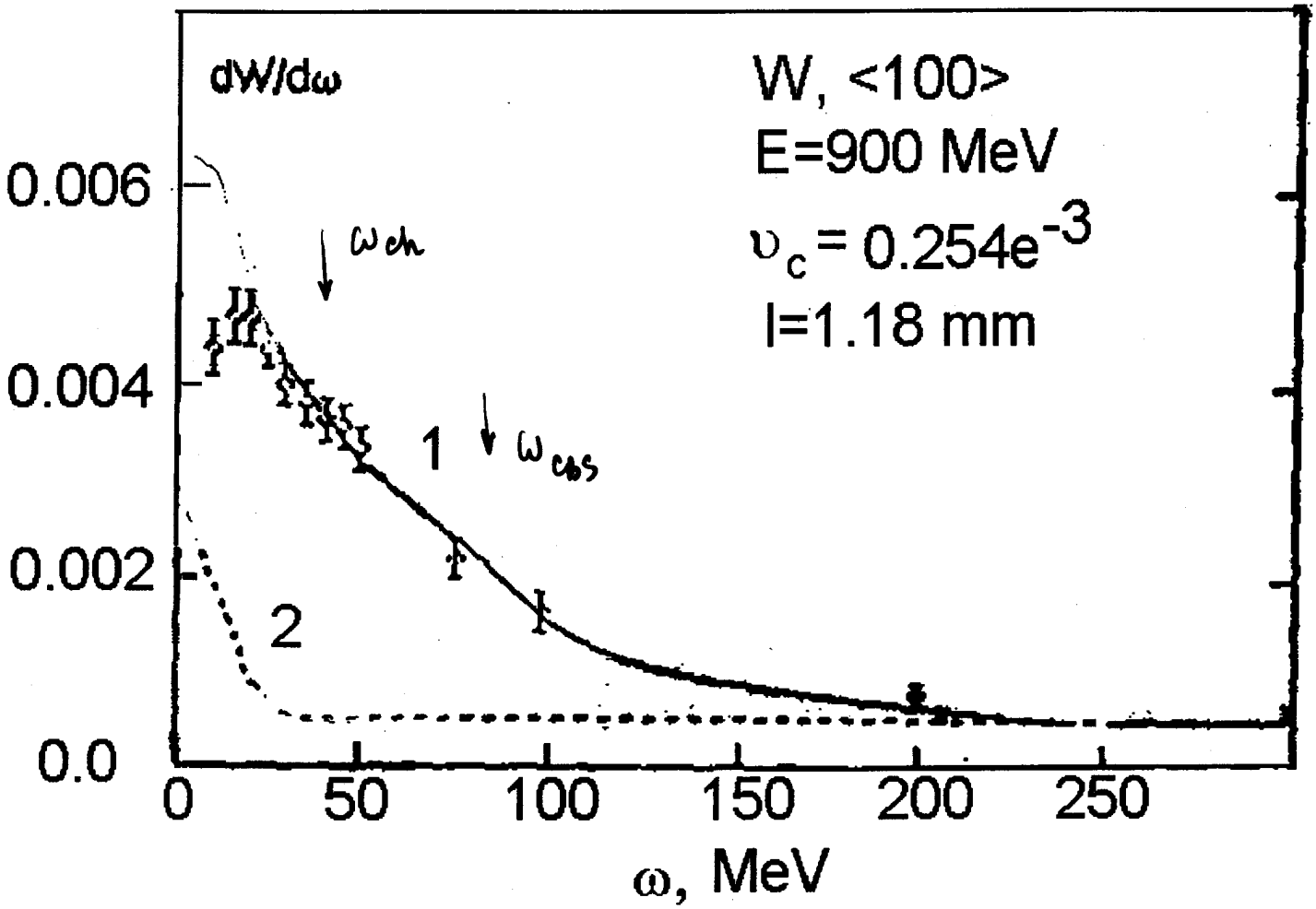

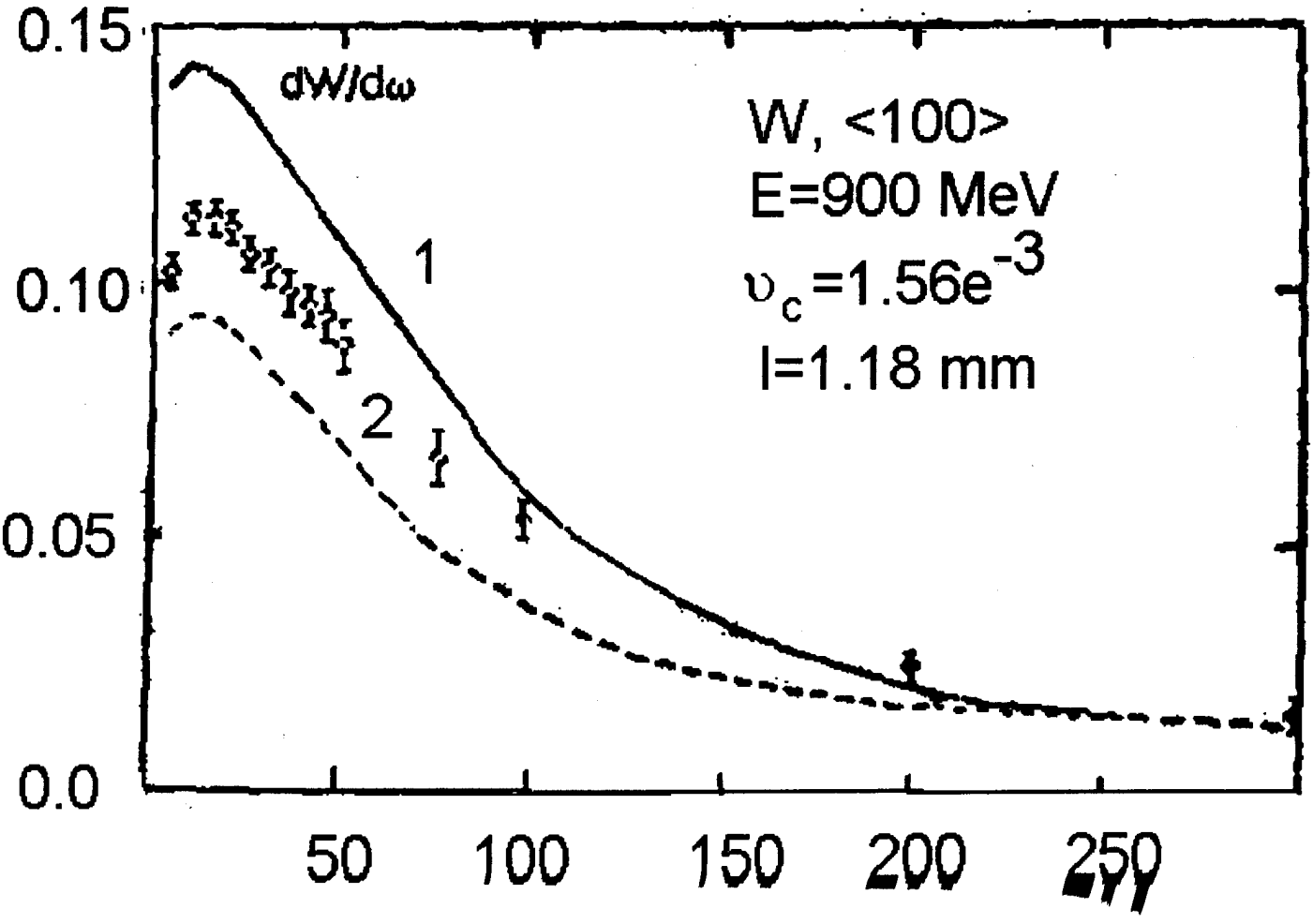

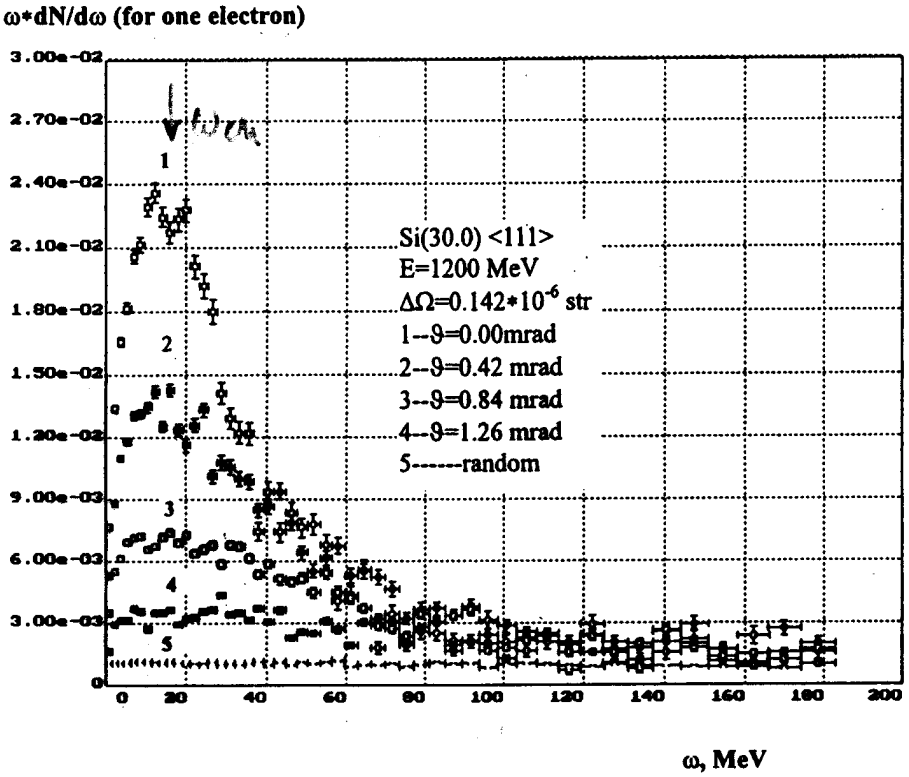

Fig. 3. Spectral-angular distribution of gamma-radiation for the silicon single crystals ⟨1 1 1⟩ with thickness 30 mm for electrons with energy $E = 1200$ MeV in solid angle $\Delta\Omega = 0.142 \times 10^{-6}$ sr.

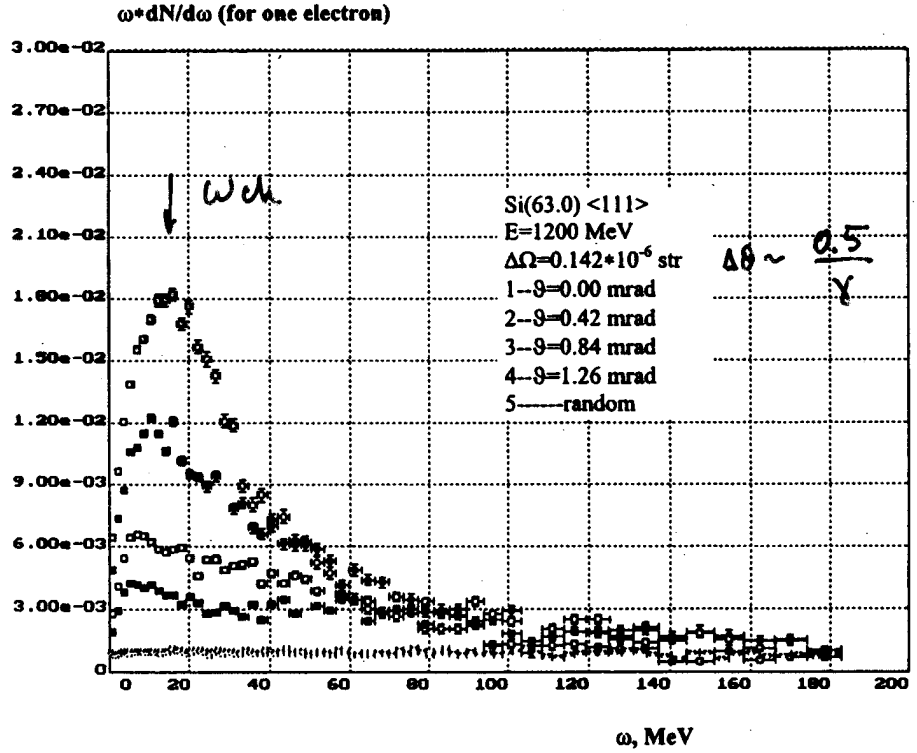

Fig. 4. Spectral-angular distribution of gamma-radiation for the silicon single crystals ⟨1 1 1⟩ with thickness 63 mm for electrons with energy $E = 1200$ MeV in solid angle $\Delta\Omega = 0.142 \times 10^{-6}$ sr.

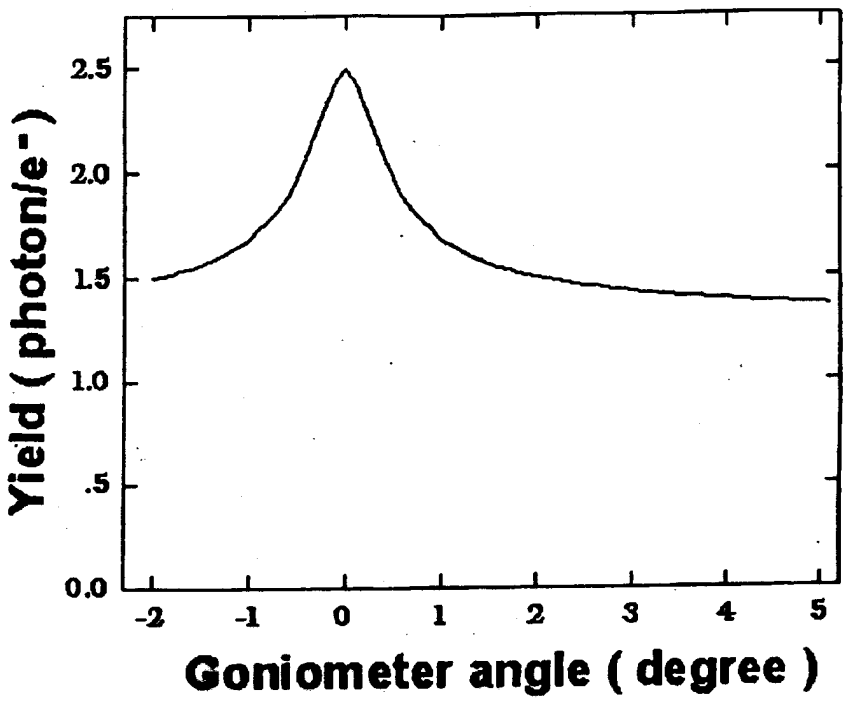

$E_e = 1.2$ GeV

$t = 1.2$ mm W

CBS only

Fig. 9. Calculated orientation dependence of photon yield with the energy greater than 21 MeV.

Positron yield (p = 20 MeV/c)

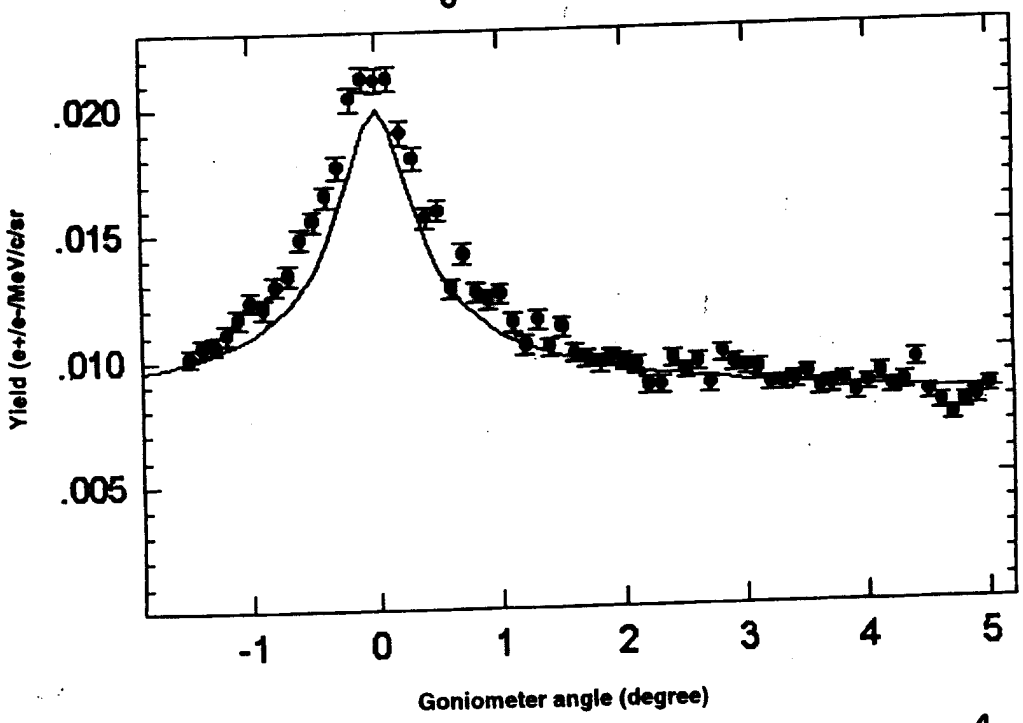

Contribution from coherent bremsstrahlung only

E = 1.0 GeV

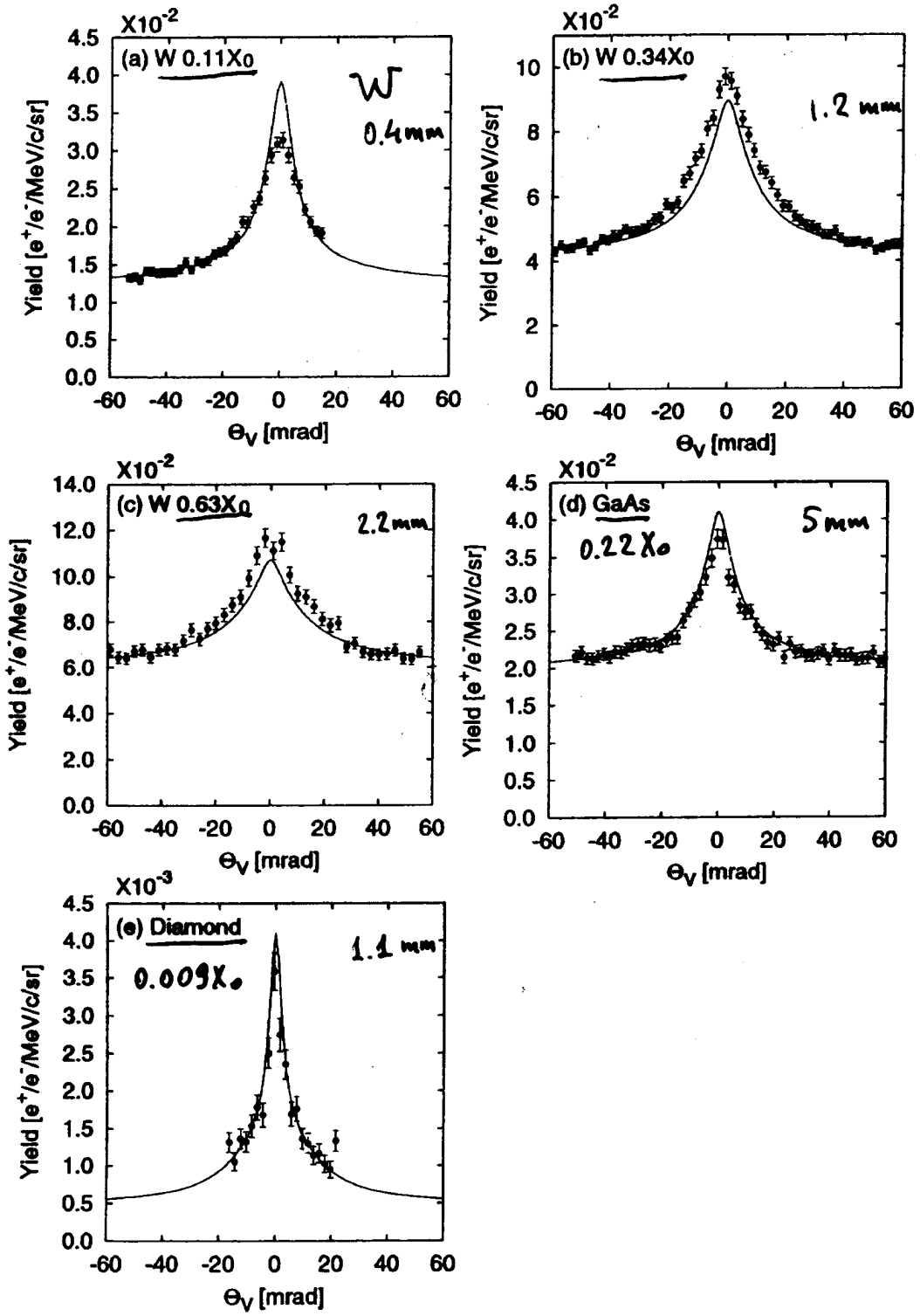

Fig. 12. Rocking curves of positron yields at $E_{e^-} = 1.0$ GeV, $\theta_{e^+} = 0°$ and $P_{e^+} = 20$ MeV/c. Target: (a) W with t = 0.4 mm (0.11 X_0), (b) W with $t = 1.2$ mm (0.34 X_0), (c) W with $t = 2.2$ mm (0.63 X_0), (d) GaAs with $t = 5.0$ mm (0.22 X_0) and (e) diamond with $t = 1.1$ mm (0.009 X_0). The curves shown in the figures are the results of simulations based on the coherent bremsstrahlung process.

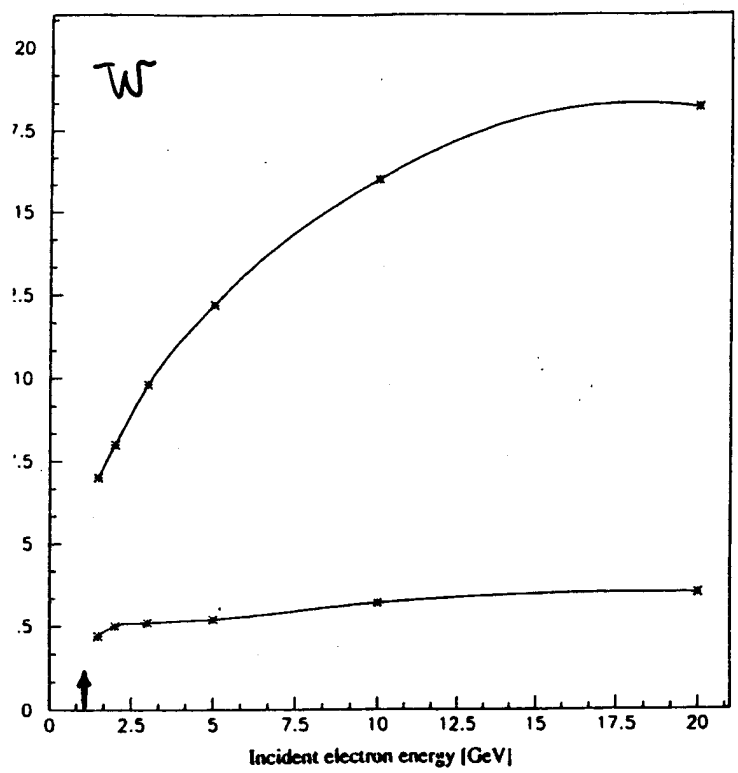

. 2. Photon yield versus incident electron energy for 1 mm
:kness; cut-off energy = 1 MeV. Upper figure: crystal, lower figure: amorphous.

Simulation
(X. Artru et al.)

$\frac{I_0}{I_{rand}} \approx 3$

$\langle N_{\gamma} \rangle \sim 10$
for $E = 4$ GeV

1.2 mm
W

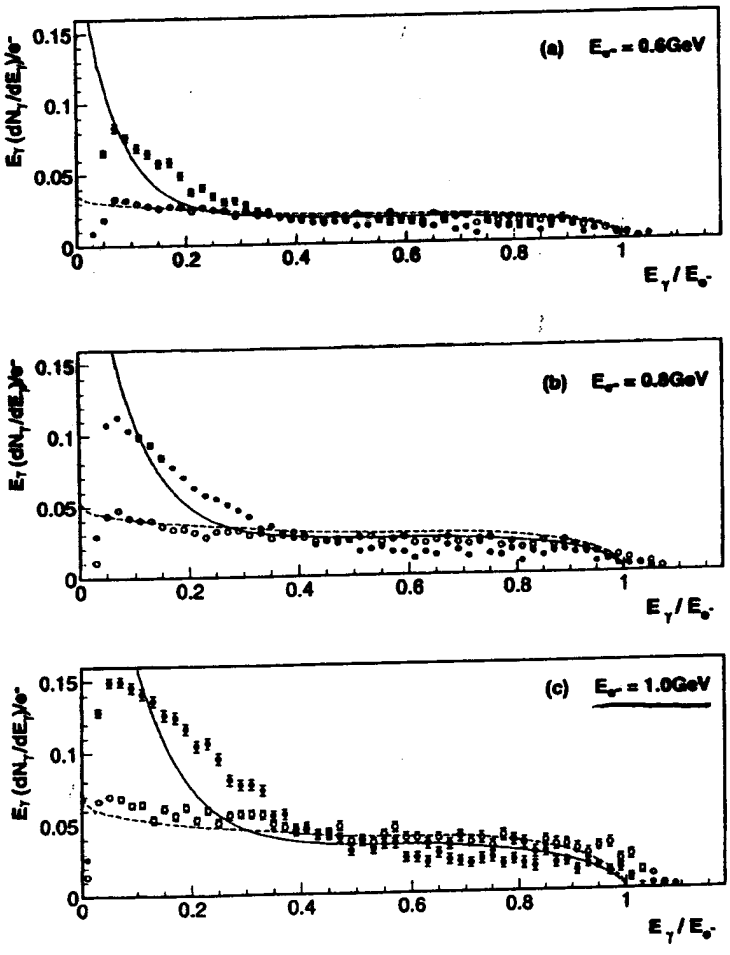

Experiment

$\frac{I_0}{I_{random}} \approx 2.3 \pm 0.14$

E = 10 GeV (A. Vodopianov et al., JINR, Russia)

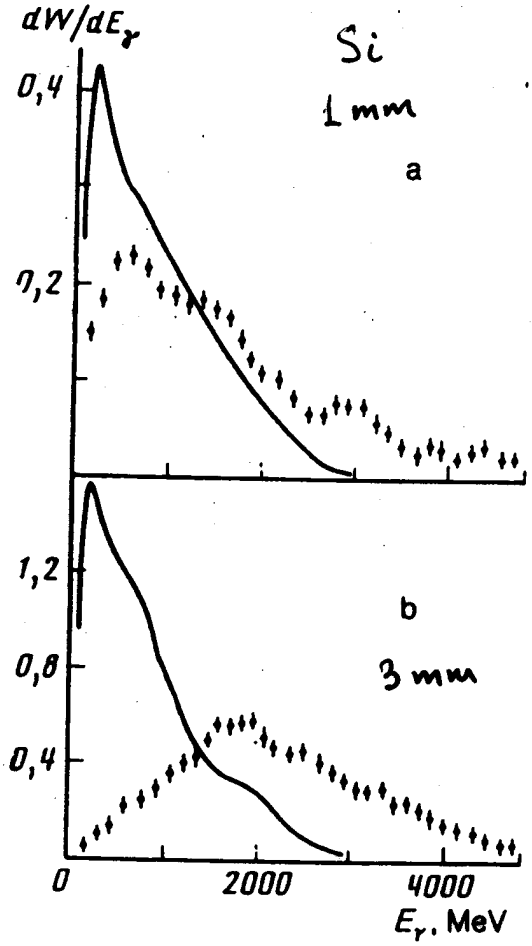

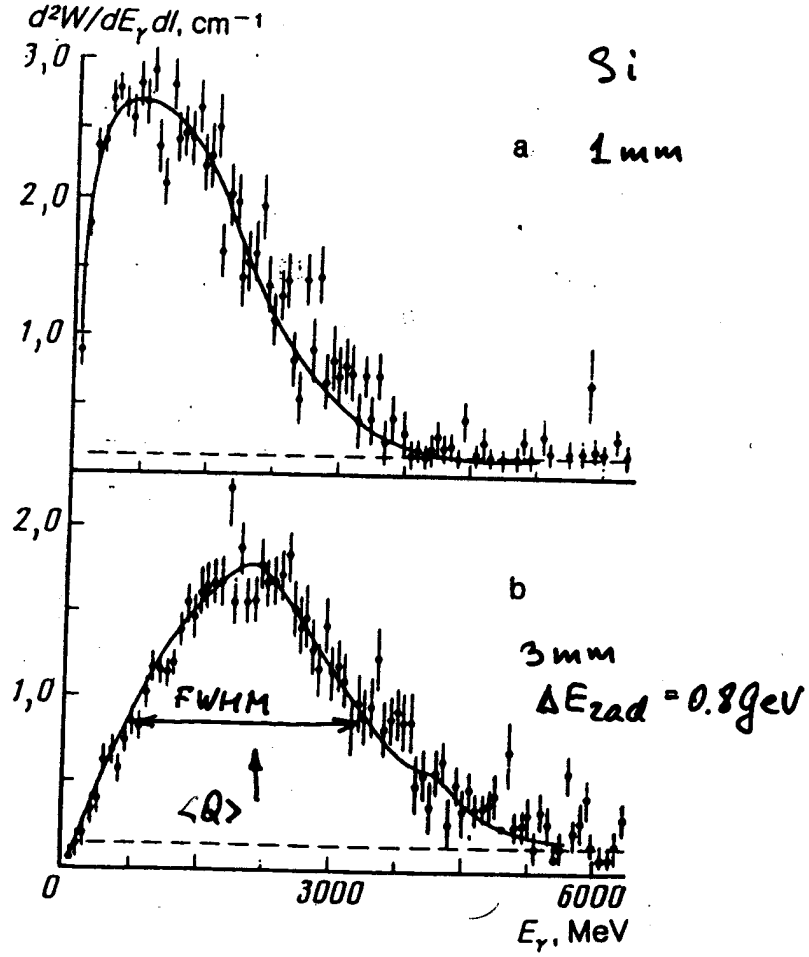

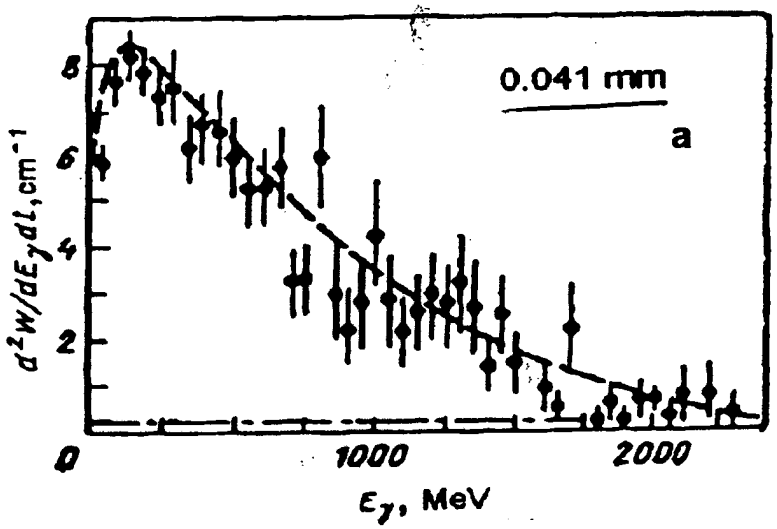

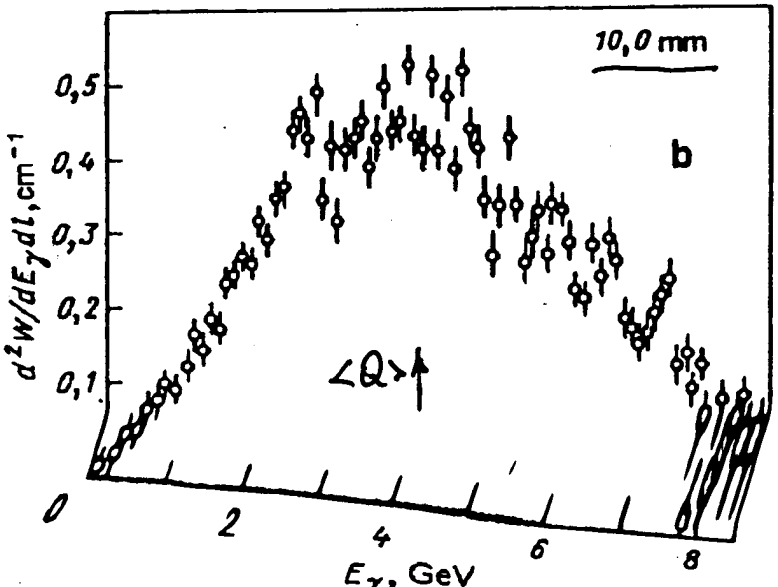

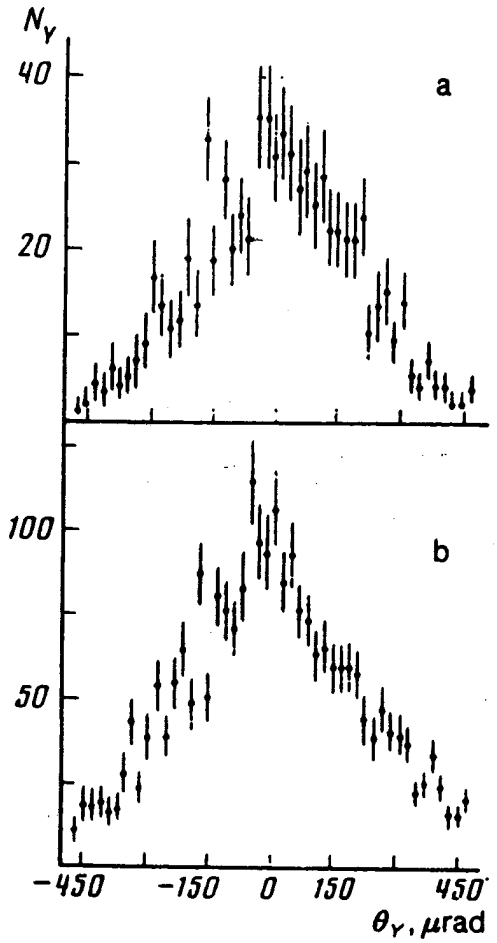

Channeling electrons

$\theta_e \leq \theta_c$

$\theta_e \leq 3\theta_c$

FIG. 4. Distribution of the exit angles of gamma photons from a silicon crystal 3.0 mm thick for events characterized by the following entry angles relative to the axis: a) from 0 to 130 μrad; b) from 0 to 400 μrad.

No significant difference

Estimation of a photon multiplicity from the energy loss distribution (energy straggling) – see A. Kolchuzhkin, A. Potylitsyn, NIMB 173 (2001) 126

If $\langle Q \rangle$ is the mean energy losses, σ is a variance of the energy distribution, then

$$\langle N_{ph} \rangle \sim \frac{\langle Q \rangle^2}{\sigma^2}$$

For Dubna's experiment, $E_0 = 10$ GeV

$t = 3$ mm, $\langle Q \rangle \approx 2.3$ GeV, $\sigma \approx \frac{FWHM}{2.36} = 1.1$ GeV

$$\langle N_{ph} \rangle \approx 4 \text{ ph/e}^-$$

$$\langle \omega \rangle \approx \frac{\Delta E_{rad}}{\langle N_{ph} \rangle} \approx \frac{0.8 \text{ GeV}}{4} = 200 \text{ MeV}$$

MC simulations (M.D. Bavizhev et al. Sov. Phys. JETP, v. 68, (1989) 803)

BLE I.

ystal ckness,	Multiplicity of emission (ω_{thr} = 20 MeV)		
	Experiments		
	θ_{in} = 0–800 μrad	θ_{in} = 0–130 μrad	Monte Carlo calculations
0.8	1.2	1.7	1.8
3.0	3,9	5,2	5,4

$t = 3$ mm

$t = 10$ mm, $\langle Q \rangle \approx 4$ GeV, $\sigma \approx 1.8$ GeV

$$\langle N_{ph} \rangle \approx 5 \text{ ph/e}^-$$

$$\langle \omega \rangle \approx \frac{1.2 \text{ GeV}}{5} \approx 240 \text{ MeV}$$

V. Baier, V. Katkov, V. Strakhovenko
Sov. Phys. Usp. 32 (1989) 972

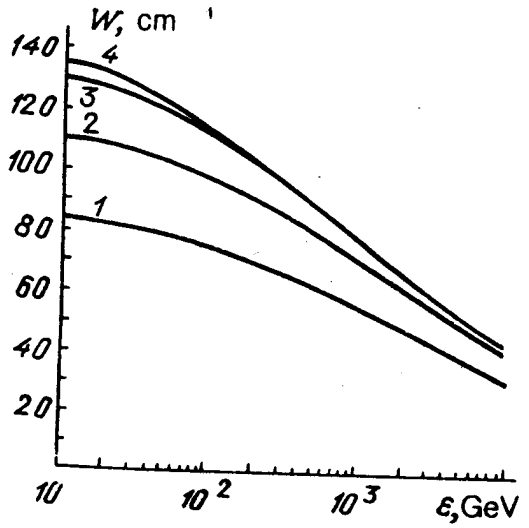

FIG. 2. Energy dependence of the total probability of radiation in Si ⟨110⟩ ($T = 293$ K, curve 1), in diamond ⟨111⟩ ($T = 293$ K, curve 2), in Ge ⟨110⟩ ($T = 280$ K, curve 3), and in Ge ⟨110⟩ ($T = 100$ K, curve 4).

For 3 mm Si the total photon number

$N_{tot} \approx 24$ ph/e⁻

Many photons with $\omega < 1.02$ MeV

E = 4.5 GeV R. Avakian et al.

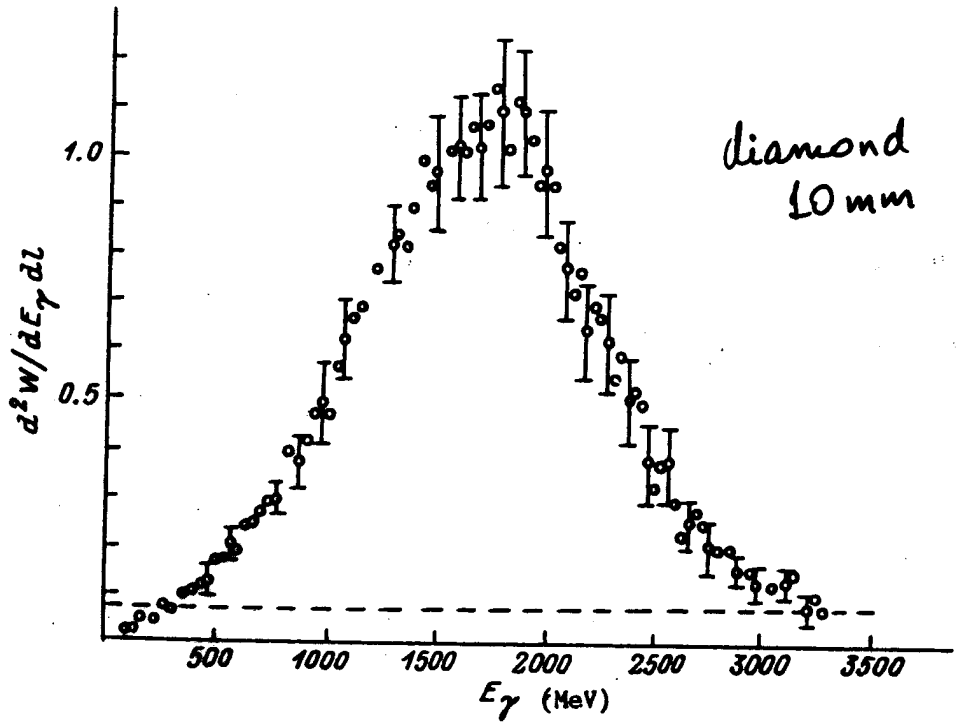

FIG. 1. Energy spectrum radiated by electrons during axial channeling.

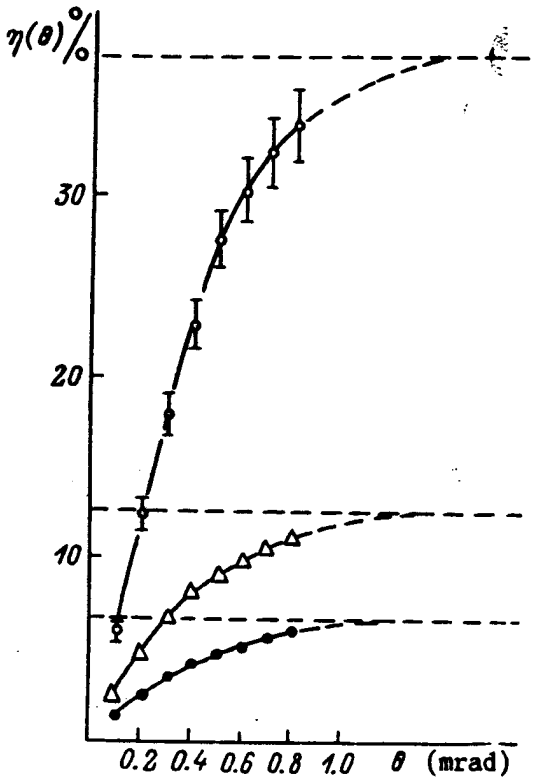

FIG. 3. Integrated radiation yield as a function of the photon emission angle. The horizontal dashed line shows the level of the radiation yield over all photon emission angles.

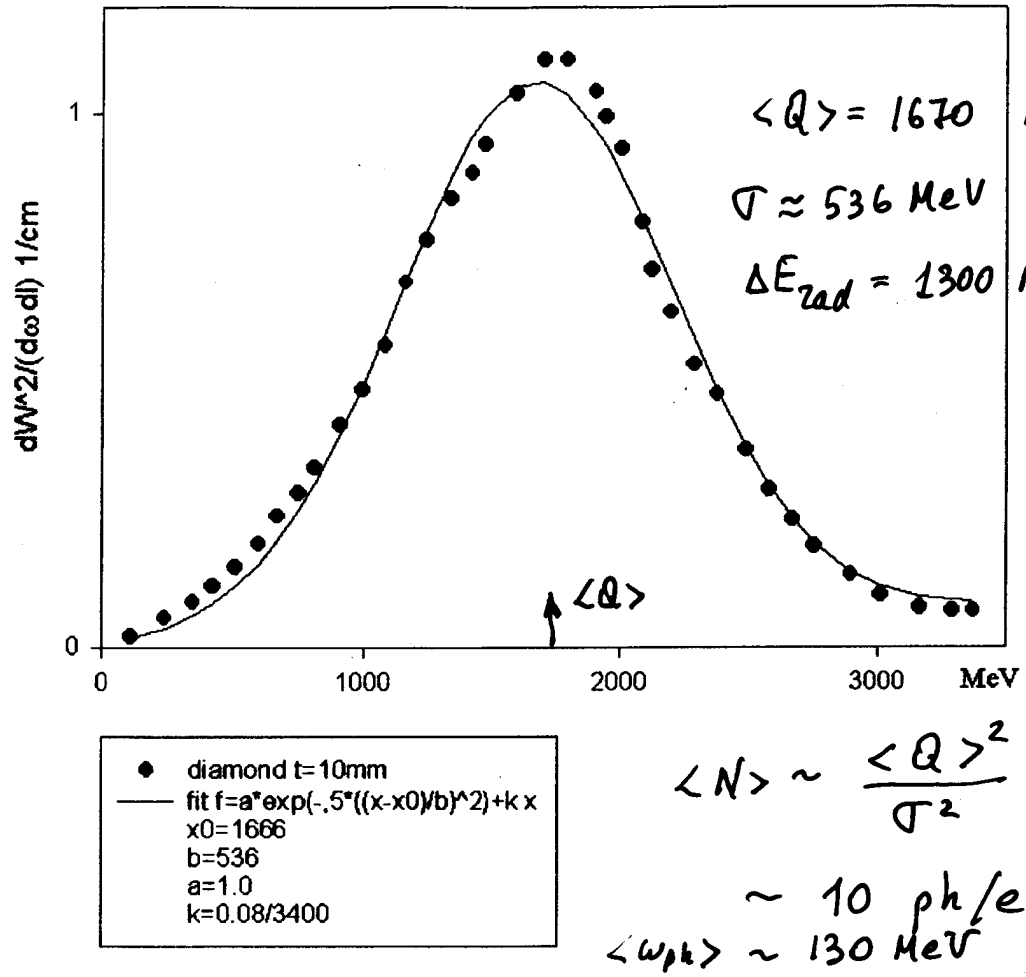

Fig.3 ***Radiation energy losses distribution for 4.5 GeV electrons channeled along <111> axis in 10mm diamond crystal.***

- Diamond is the best crystal for generation of intense CBS beams.
- Thermal conductivity of diamond is very high
  660 W/m/K against 170 W/m/K (for tungsten)
- SLAC test for diamond target
  (τ_B ~ 1psec, S_B ~ 0.06 μm², N_e ~ $2\cdot10^{10}$ e⁻/bunch)
  No visible damage

4. Last experimental results (R. Hamatsu, QABP report) allow to think that scheme with light Z crystal photon emitter is more effective for electron energy $E_0 < 10$ GeV.

Let's estimate positron yield for combined target

diamond <111>, 15 ÷ 20 mm thickness
+ amorphous converter $t_{am} = 1\ X_0$

and electrons with $E_0 = 5$ GeV.

For this diamond thickness one may expect

$$\Delta E_{rad} \approx 0.5\ E_0 = 2.5\ \text{GeV}$$

$$\underline{\langle \omega \rangle \sim 150\ \text{MeV}}, \quad \underline{\langle N_{ph} \rangle \sim 17\ \text{ph/e}^-}$$

After passing through crystal the initial electron will have energy $E_- = E_0 - \Delta E_{rad} = 2.5$ GeV

In amorphous converter e^+ will be produced by this electron and a number of „soft" photons.

Positron spectrum for first case and thin target ($t_{am} \lesssim X_0$) may be calculated analytically (see A. Potylitsyn, NIMA, v. 398 (1999) 395)

$$\frac{dN_+}{dE_+} \approx 0.07\ \frac{t^2}{X_0^2} \left[\ln\left(\frac{1}{\lambda}\right) - 0.5\right] \left(\frac{1}{E_+} - \frac{1}{E_-}\right), \quad \left[\frac{1}{\text{MeV}}\right]$$

$$\lambda = \frac{Z^{1/3}}{111}$$

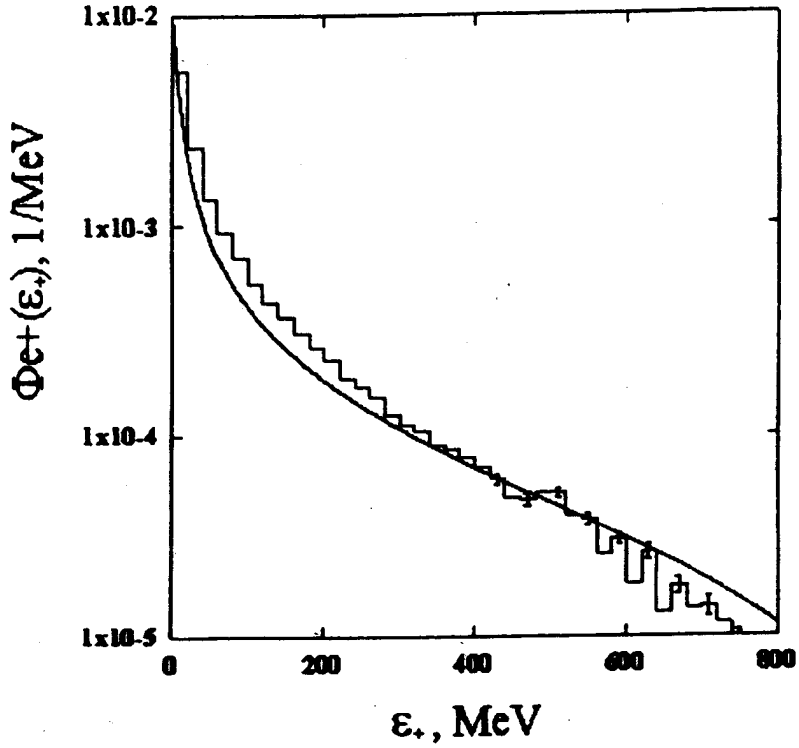

Fig. 2. Positron spectrum generated by electron with energy $E = 1$ GeV in amorphous target of the thickness $t = 0.5$ rad. length. (Histogram) Monte Carlo simulations [7], (curve) calculations from Eq. (5).

The similar approach may be developed for initial photons.

Let's consider model „flat" photon spectrum (closed to UR one):

$$\frac{dN_{ph}}{d\omega} = \begin{cases} \frac{N_{ph}}{\omega_{max}}, & \omega \leq \omega_{max} \\ 0 & \omega > \omega_{max} \end{cases}$$

In this case

$$\Delta E_{zad} = \int_0^{\omega_{max}} \omega \frac{dN}{d\omega} d\omega = N_{ph} \frac{\omega_{max}}{2} = N_{ph} < \omega >$$

From here $\omega_{max} = 2 < \omega >$

After convolution with this spectrum it is possible to obtain analytycal expression for positron spectrum:

$$(*) \quad \frac{dN_+}{dE_+} \approx 0.14 \frac{t}{X_0} \frac{N_{ph}}{\omega_{max}} \ln\left(\frac{\omega_{max}}{E_+}\right) \left\{ \frac{1}{2} \ln\left[\frac{\omega_{max} E_+}{(mc^2)^2}\right] - 1.2 \right\}$$

Flottmann's calculations for UR with

$\omega_{max} = E_1 = 21$ MeV, $N_{ph} = 2 ph/e^-$ ($L_u = 1$ m)

gives result $\frac{dN_+}{dE_+} = 0.18$ for $E_+ = 10$ MeV

From (*) one may obtain (for the same parameters):

$$\frac{dN}{dE_+} = 0.20$$

Positron spectra

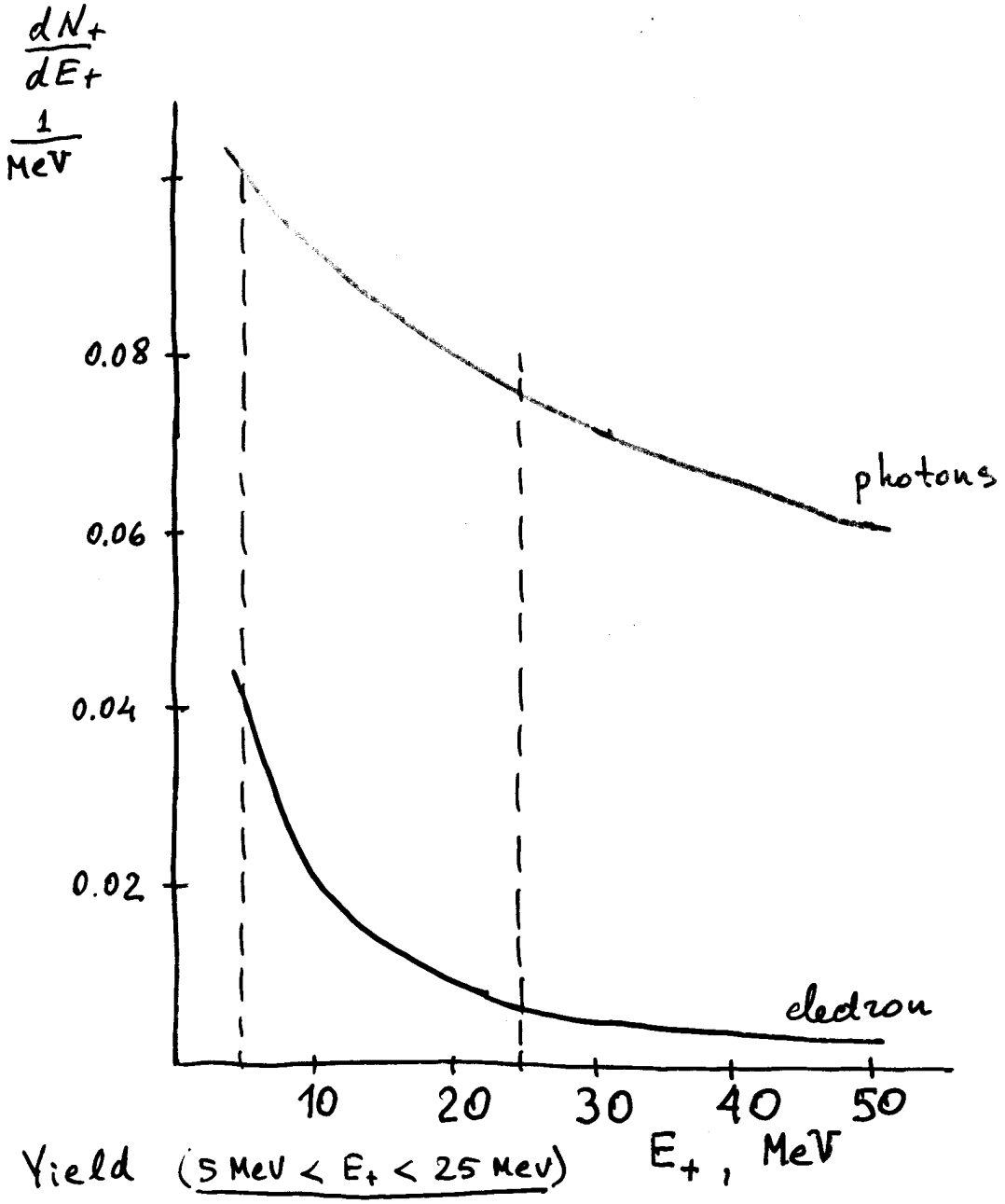

Yield ($5\ MeV < E_+ < 25\ MeV$)

e^-: $\Delta N_+ = 0.32\ e^+/e^-$

photons: $\Delta N_+ = 1.74\ e^+/e^-$

$\Sigma \approx 2\ e^+/e^-$

Summary

- Scheme for positron generation with combined target looks more preferrable
- Thick diamond crystal is the best candidate for a photon emitter
- Problem of an artificial diamond producing with thickness $10 \div 20$ mm may be resolved in the nearest future
- Measurements of radiation losses (energy distribution of electron beam passed through light Z crystal target) may be very important for comparison with theory
- Detailed 6-D simulation of crystal-based e^+ source is needful to choose configuration of source (E_0, Z, t_{cr}, t_{am}) for highest efficiency

KEK Workshop
Jan/17/2003

Semiclassical Theory of Crystal-Assisted Pair Production: Beyond the Uniform Field Approximation

H.Nitta, Y.Nagata, and S.Onuki
Tokyo Gakugei University
M.Kh.Khokonov
Kabardino-Balkarian State University

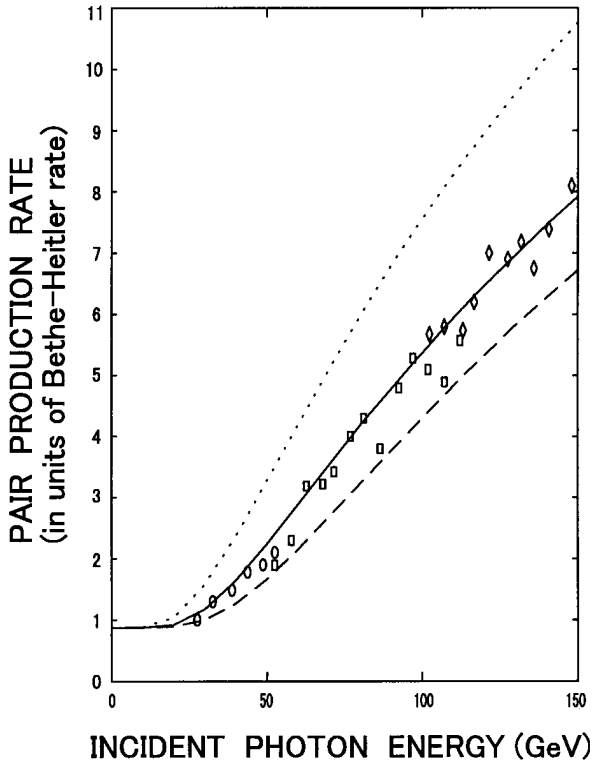

【Classical Radiation 】

Schwinger(Phys.Rev.**75** 1912(1949))

$$\frac{dN}{d\omega}(t) = \frac{2\alpha}{\pi\gamma^2}\, J(t,\omega)$$

$$J = \int_0^\infty \gamma^2(1-\boldsymbol{\beta}_+\cdot\boldsymbol{\beta}_-)\sin\Delta_s\frac{d\tau}{\tau} - \frac{\pi}{2} \qquad (1)$$

$$\Delta_s = \omega(\tau - |\boldsymbol{r}_+ - \boldsymbol{r}_-|/c)$$

where α is the fine structure factor, γ the Lorentz factor, $\boldsymbol{r}_\pm$,$\boldsymbol{\beta}_\pm$ the position and velocity at time $t\pm\tau/2$, respectively:

$$\begin{cases} t_+ = t+\tau/2 \\ t_- = t-\tau/2 \end{cases} \quad \begin{cases} \boldsymbol{\beta}_+ = \boldsymbol{\beta}(t_+) \\ \boldsymbol{\beta}_- = \boldsymbol{\beta}(t_-) \end{cases} \quad \begin{cases} \boldsymbol{r}_+ = \boldsymbol{r}(t_+) \\ \boldsymbol{r}_- = \boldsymbol{r}(t_-) \end{cases}$$

Decomposing the motion of the electron as longitudinal and transverse ones.

$$\begin{cases} \boldsymbol{r}(t) = \boldsymbol{\rho}(t) + \boldsymbol{z}(t) \\ \boldsymbol{\beta}(t) = \boldsymbol{\beta}_\perp(t) + \boldsymbol{\beta}_z(t) \end{cases}$$

Eq.(1) may be rewritten in the form that includes only the transverse motion:

$$J = \int_0^\infty \left[1 + \frac{\gamma^2}{2}(\delta\boldsymbol{\beta}_\perp)^2\right] \sin\Delta_s \frac{d\tau}{\tau} - \frac{\pi}{2}$$

$$\Delta_s = \frac{\omega\tau}{2\gamma} - \frac{\omega}{2c^2\tau}(\delta\boldsymbol{\rho})^2 + \frac{\omega}{2}\int_{t_-}^{t_+} \beta_\perp^2(\tau')d\tau' \qquad (2)$$

$$\begin{cases} \delta\boldsymbol{\beta}_\perp = \boldsymbol{\beta}_\perp(t_+) - \boldsymbol{\beta}_\perp(t_-) \\ \delta\boldsymbol{\rho} = \boldsymbol{\rho}(t_+) - \boldsymbol{\rho}(t_-) \end{cases}$$

By expanding factors in terms of τ, we obtain,

$$\Delta_s = \frac{3}{2}\xi(x + x^3/3 + a_5x^5 + a_7x^7 + ...)$$

$$1 + \frac{\gamma^2}{2}(\delta\boldsymbol{\beta}_\perp)^2 = (1 + 2x^2 + b_4x^4 + b_6x^6 + ...)$$

where x and ξ are Schwinger's dimensionless time and frequency parameters, respectively:

$$x = \frac{g\gamma\tau}{2} \quad , \quad \xi = \frac{2\omega}{3g\gamma^3}.$$

g the acceleration divided by c. $a_5, a_7, ..., b_4, b_6, ...$ may be represented by the time derivatives of $\boldsymbol{g}$ and γ.

【Synchrotron Approximation】

If we approximate the instantaneous trajectory about $t = 0$ by a circular path, then we have $a_5, b_4 \sim 1/\gamma^2$, $a_7, b_6 \sim 1/\gamma^3 \cdots$. So, by neglecting the higher order terms under the condition $\gamma \gg 1$, we obtain the synchrotron formula:

$$J_{\mathrm{syn}} = \frac{1}{\sqrt{3}} \left[2\mathrm{K}_{\frac{2}{3}}(\xi) - \int_{\xi}^{\infty} \mathrm{K}_{\frac{1}{3}}(\lambda) d\lambda \right] \tag{3}$$

where $\mathrm{K}_n(x)$ is the modified Bessel functions.

If the trajectory of the electron is sufficiently a circular path at the radiation point, then the formula holds. However, if the trajectory becomes like a straight path, the circular path approximation does not hold because the neglected terms become larger.

【Standard th-trajectory】

A model trajectory for an arbitraly motion where at $t \to \pm\infty$ the velocity becomes constant while at $t = 0$ the acceleration is maximum (Khokonov and Nitta, Phys.Rev.Lett. **89** 094801 (2002)):

$$\boldsymbol{\beta}_\perp(t) = \boldsymbol{b}_0 + \boldsymbol{b}\tanh\left(\frac{t}{T}\right)$$

$$\boldsymbol{b}_0 = \frac{\boldsymbol{\beta}_{\perp 1} + \boldsymbol{\beta}_{\perp 2}}{2} \quad , \quad \boldsymbol{b} = \frac{\boldsymbol{\beta}_{\perp 2} - \boldsymbol{\beta}_{\perp 1}}{2} \tag{4}$$

$$\begin{cases} \boldsymbol{\beta}_{\perp -} \equiv \boldsymbol{\beta}_\perp(t \to -\infty) \\ \boldsymbol{\beta}_{\perp +} \equiv \boldsymbol{\beta}_\perp(t \to +\infty) \end{cases}$$

where T is the interaction time.
With this "th-trajectory" we obtain an analytic expression of radiation spectrum which has two parameters. From (2) and (4), we obtain,

$$J_{\rm th} = \int_0^\infty (1 + 2\nu^2 \tanh^2 z) \sin\Delta_{\rm s} \frac{dz}{z} - \frac{\pi}{2}$$

$$\Delta_{\rm s} = \frac{3}{2}\xi\nu[(1+\nu^2)z - \nu^2 \tanh z] \tag{5}$$

$\nu \equiv \gamma b$ (non-dipole parameter)

【Quantum Correction】

The well known Baier-Katokov formula has been used for quantum correction. We have

$$\frac{dN}{d\eta} = \frac{\alpha c}{\pi \lambda_C} \frac{1}{\gamma} J \tag{6}$$

where λ_C is the Compton wavelength, $\eta = \hbar\omega/E$. J is given as

Synchrotron approximation

$$J_{syn} = \frac{1}{\sqrt{3}} \left[\left(1 - \eta + \frac{1}{1-\eta} \right) K_{\frac{2}{3}}(\xi^*) - \int_{\xi^*}^{\infty} K_{\frac{1}{3}}(\lambda) d\lambda \right] \tag{7}$$

th-trajectory approximation

$$J_{th} = \int_0^{\infty} \left[1 - \nu^2 \left(1 - \eta + \frac{1}{1-\eta} \right) \tanh^2 z \right] \sin \Delta_s \frac{dz}{z} - \frac{\pi}{2}$$

$$\Delta_s = \frac{3}{2} \xi^* \nu \left[\left(1 + \nu^2 \right) z - \nu^2 \tanh z \right] \tag{8}$$

$$\begin{cases} \xi^* = 2\eta/3(1-\eta)\chi \\ \chi = \gamma \lambda_C F / mc^2 \end{cases} \tag{9}$$

where F is the transverse force from the field. We call χ invariant field parameter.

【Crossing Symmetry】

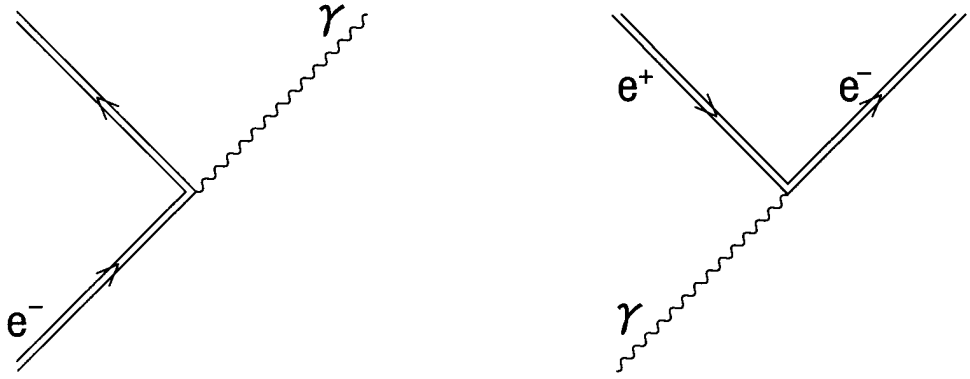

Once an expression of radiation is established, the pair production can be calculated by using the *crossing symmetry* of the matrix element.

By changing the variables as

$$\begin{cases} E & \text{(initial energy)} & \to & -E_{\mathrm{p}} & \text{(produced positron)} \\ E' & \text{(final energy)} & \to & E_{\mathrm{e}} & \text{(produced electron)} \\ \omega & \text{(emitted photon)} & \to & -\omega & \text{(absorbed photon)} \end{cases}$$

and multipling the rate of the density of final states to dN

$$\frac{E_{\mathrm{p}}^2 dE_{\mathrm{p}}}{(\hbar\omega)^2 d(\hbar\omega)}$$

we obtain the pair production probability for the th-trajectory approximation as well as the synchrotron approximation.

【Pair Production】

The pair production probability per unit time is given as

$$\frac{dN}{d\eta} = \frac{\alpha c}{\pi \lambda_{\mathrm{C}}} \frac{mc^2}{\hbar\omega} J^{\mathrm{pp}} \tag{10}$$

where $\eta = E^{(+)}/\hbar\omega$ (the energy ratio of the produced positron and the incident photon).

Uniform Field (Synchrotron) Approximation

$$J^{\mathrm{pp}}_{\mathrm{syn}} = \frac{1}{\sqrt{3}} \left[\left(\frac{1-\eta}{\eta} + \frac{\eta}{1-\eta} \right) \mathrm{K}_{\frac{2}{3}}(\xi^*) + \int_0^\infty \mathrm{K}_{\frac{1}{3}}(\lambda) d\lambda \right] \tag{11}$$

Th-trajectory Approximation

$$J^{\mathrm{pp}}_{\mathrm{th}} = \int_0^\infty \left[\nu^2 \left(\frac{1-\eta}{\eta} + \frac{\eta}{1-\eta} \right) \tanh^2 z - 1 \right] \sin \Delta_{\mathrm{s}} \frac{dz}{z} + \frac{\pi}{2}$$

$$\Delta_{\mathrm{s}} = \frac{3}{2} \xi^* \nu \left[\left(1 + \nu^2\right) z - \nu^2 \tanh z \right] \tag{12}$$

$$\xi^* = \frac{2}{3\eta(1-\eta)\chi}$$

non-dipole parameter

$\nu = \gamma_{\mathrm{p}} b$ $\quad$ γ_{p} : (positron's Lorentz factor)

invariant field parameter

$$\chi = \frac{\hbar\omega\lambda_{\mathrm{C}} F}{m^2 c^4}$$

Pair production probability for $\chi = 1$. dotted line:UFA.

A: J_c. B: J_{spin} (spin-flip contribution)

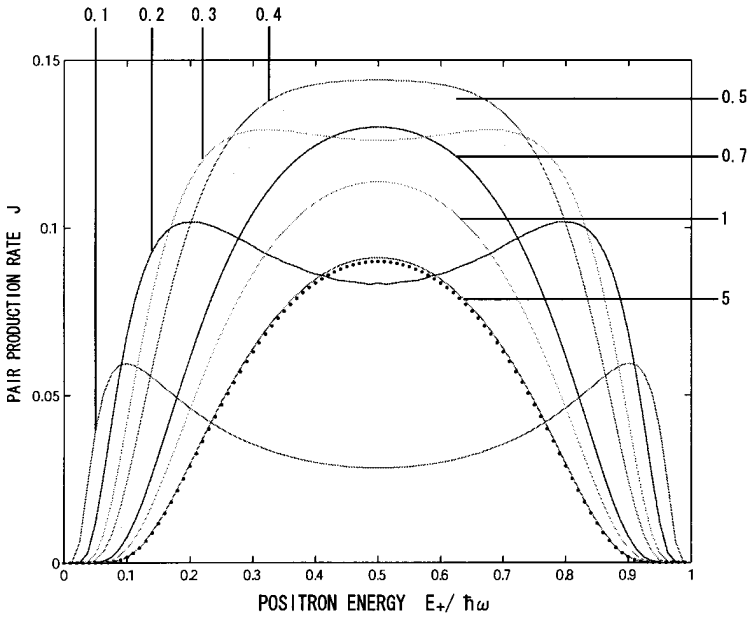

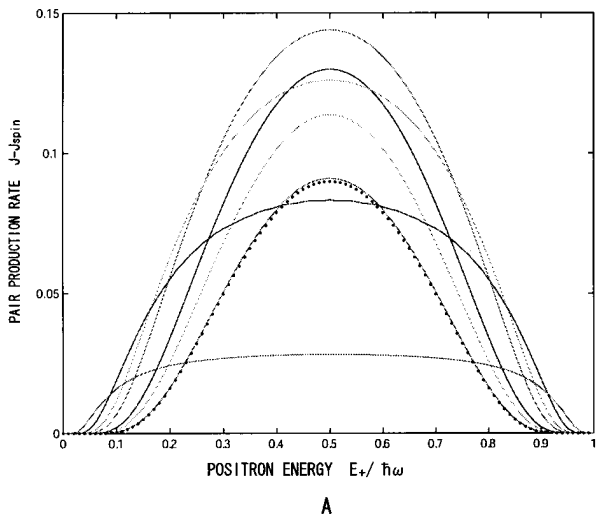

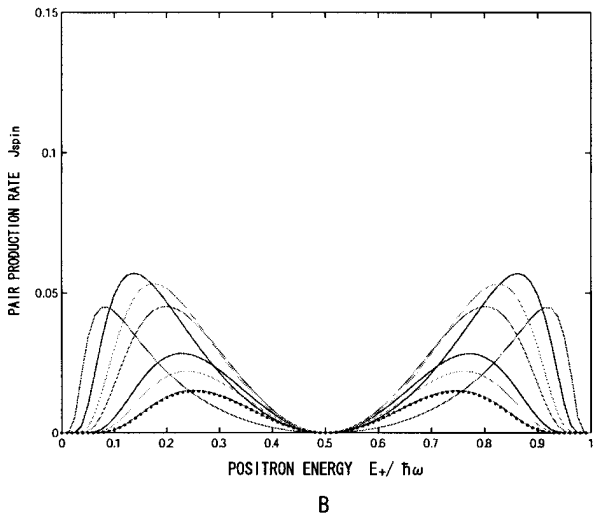

$\chi = 5$:

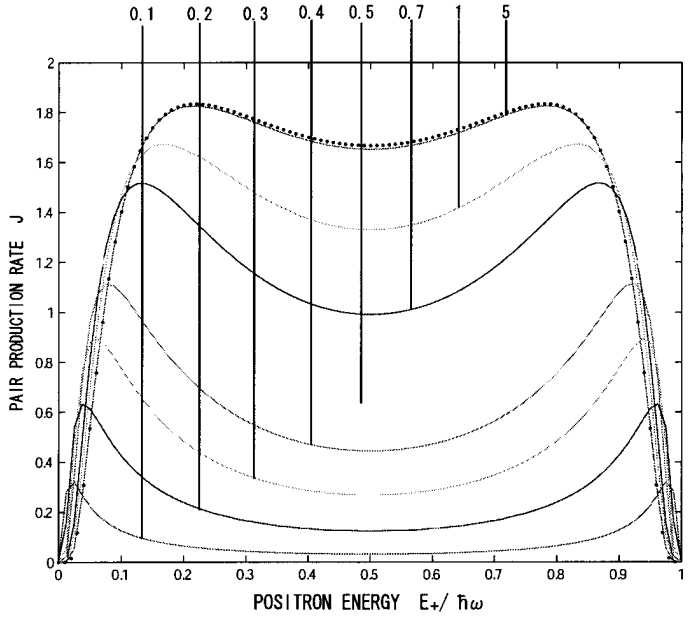
0.1
0.2
0.3
0.4
0.5
0.7
1
5
PAIR PRODUCTION RATE J
POSITRON ENERGY E+/ ħω

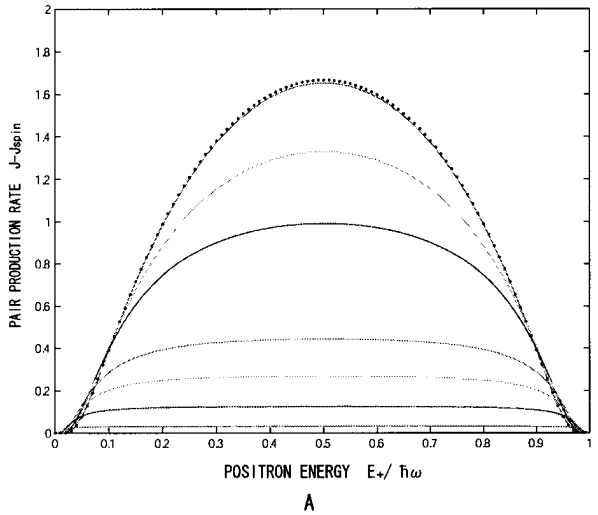
PAIR PRODUCTION RATE J-Jspin
POSITRON ENERGY E+/ ħω

A

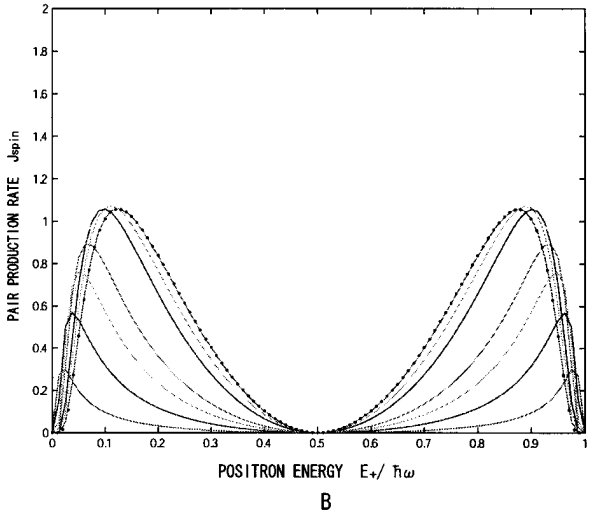
PAIR PRODUCTION RATE Jspin
POSITRON ENERGY E+/ ħω

B

【Impact Approximation】

non-dipole parameter ν is determined by the scattering angle.

$$\nu = \gamma_p \left| \frac{\vec{\beta}_{\perp+\infty} - \vec{\beta}_{\perp-\infty}}{2} \right| \tag{13}$$

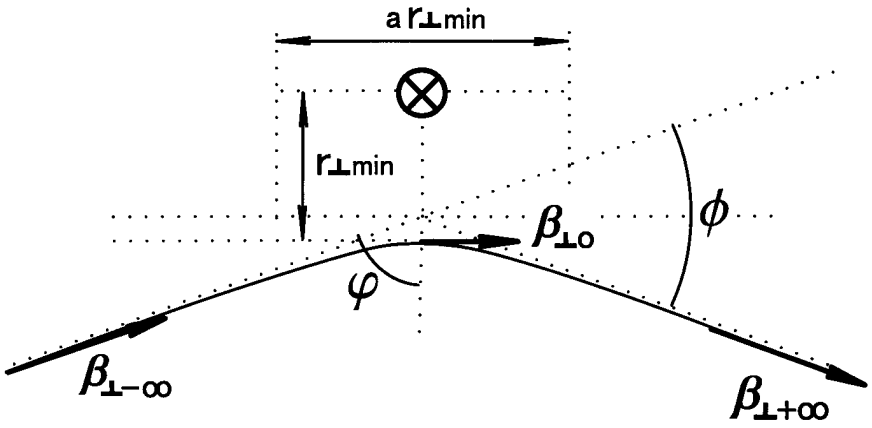

For simplicity, we employ the impact approximation:

$$\gamma_p mc\boldsymbol{\beta}_{\perp+\infty} - \gamma_p mc\boldsymbol{\beta}_{\perp-\infty} = \boldsymbol{F}(\rho_0)\Delta t$$

where we have taken Δt as

$$\Delta t = \frac{a\rho_0}{c\beta_{\perp 0}}$$

a is the fitting parameter: $a \sim 1$. By taking $\rho_0 = r_{\perp min}$, the non-dipole parameter becomes

$$\nu = \frac{a}{2}\frac{F(r_{\perp min})\, r_{\perp min}}{mc^2\theta_\gamma} \tag{14}$$

where θ_γ is the incident angle of the photon to the crystal axis.

Pair production spectra. The numbers represent the incident angle [mrad]. The dotted line shows UFA.
50[GeV] photon $\rightarrow$ Si$<110>$:

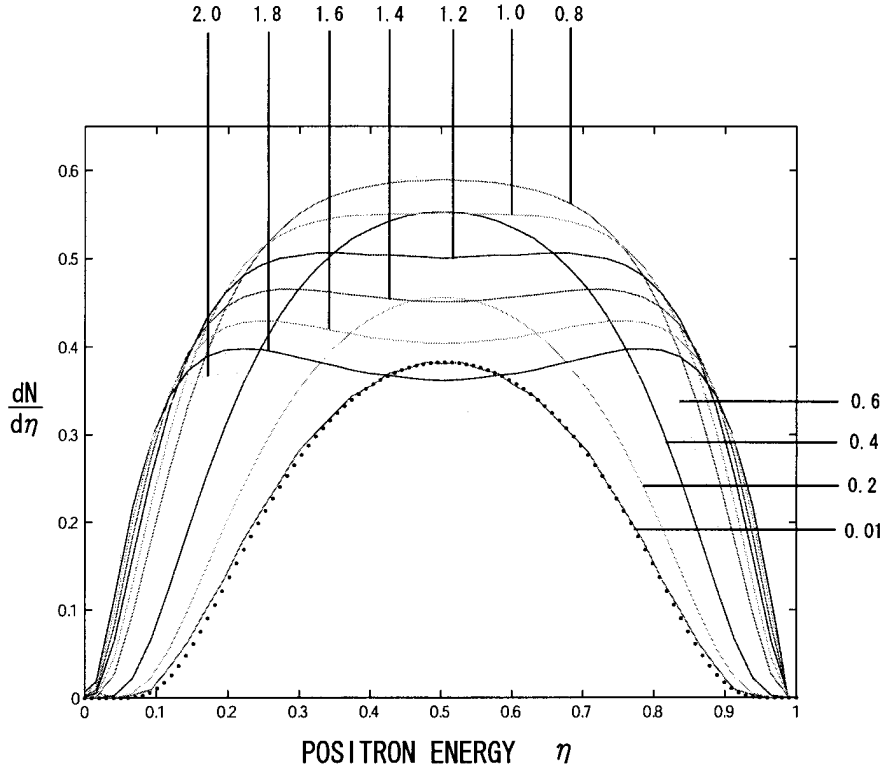

:

150[GeV]:

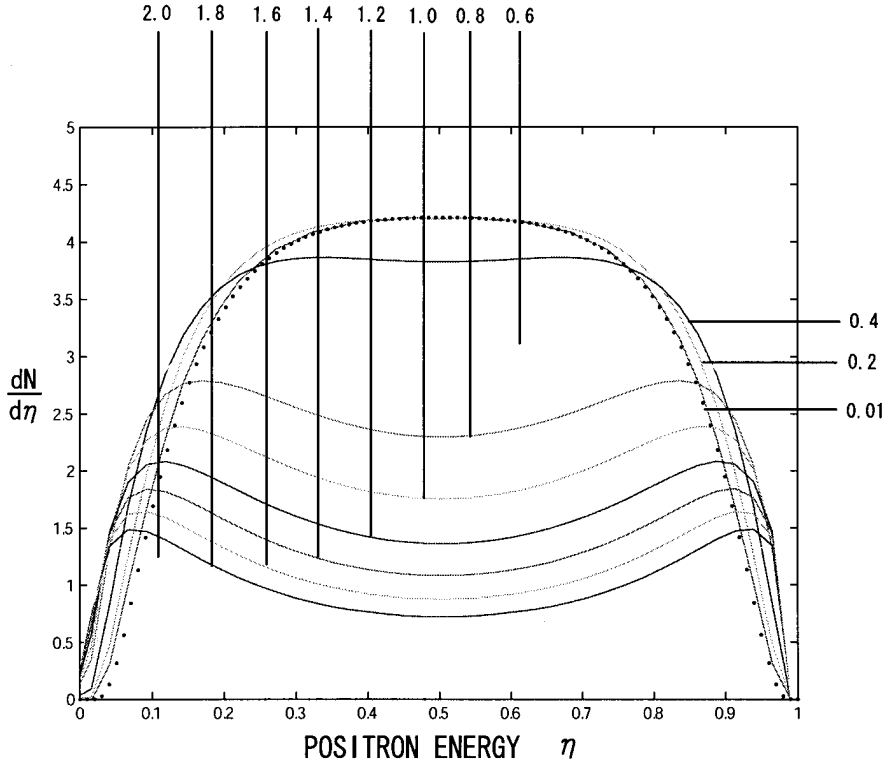

Impulse approximation:

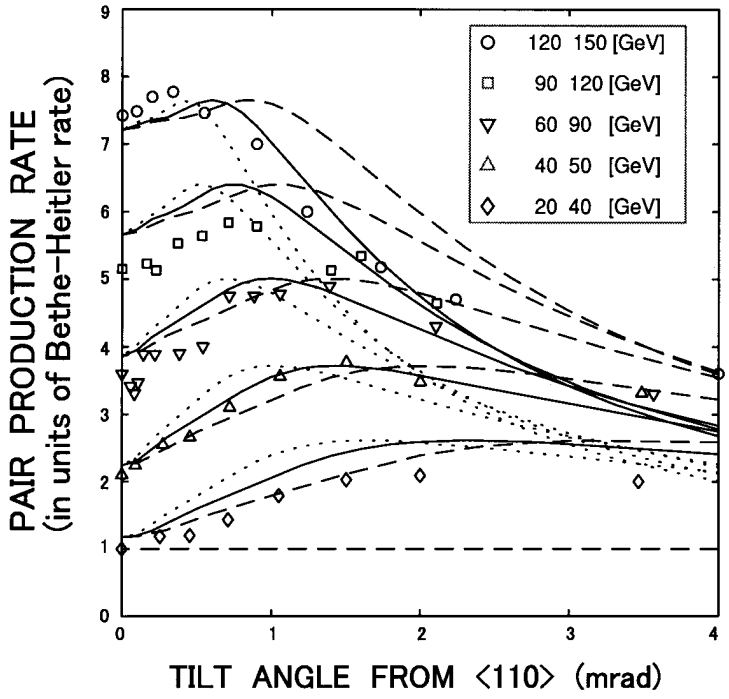

One-string Molière potential ($T = 100$K):

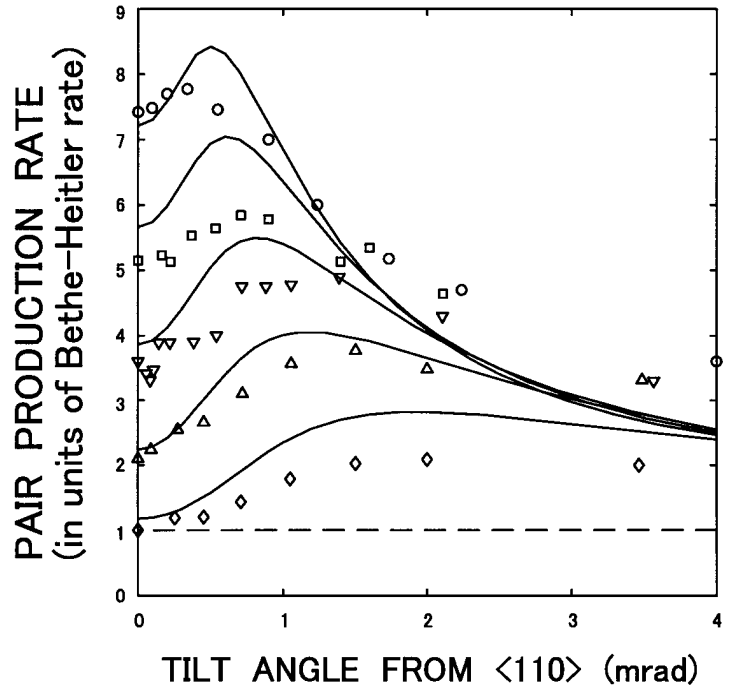

Impulse approximation:

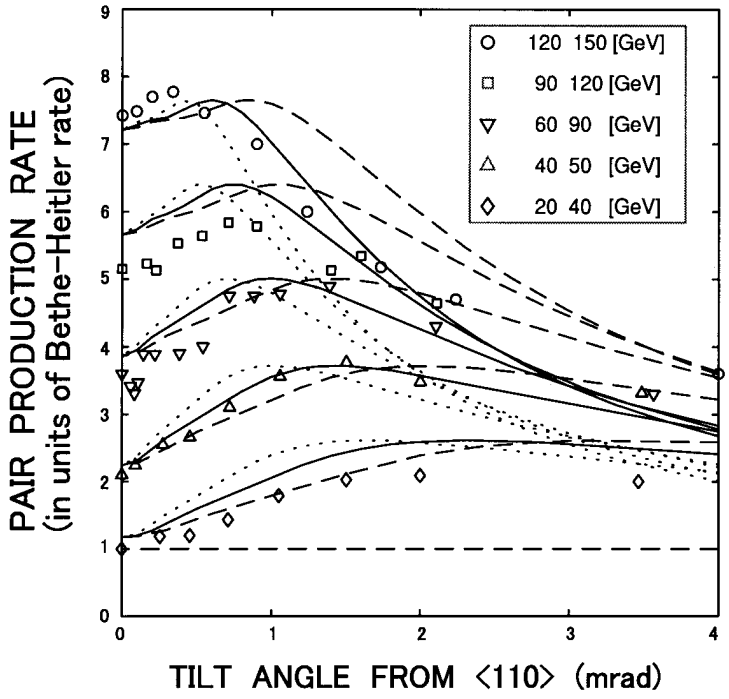

One-string Molière potential ($T = 100$K):

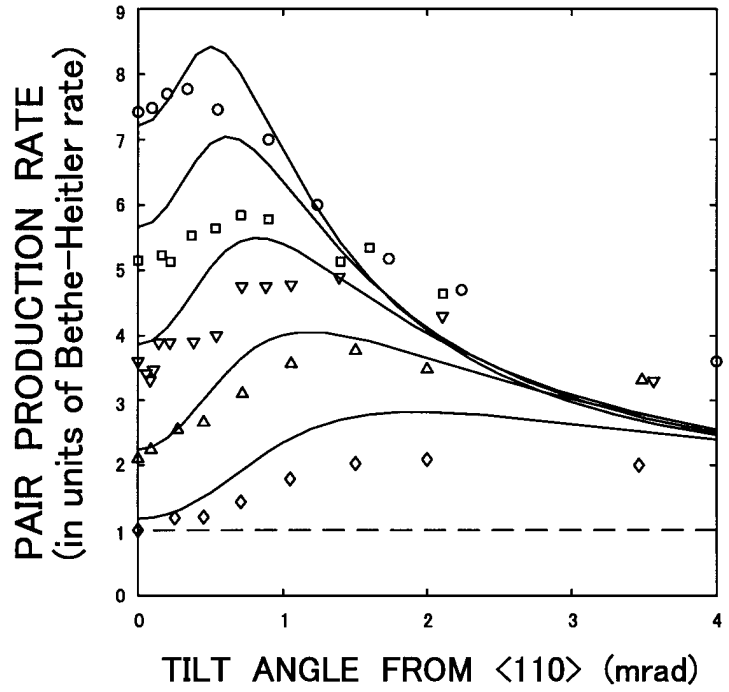

Summary paper

Positron production in axially oriented single crystals: comparison of theory with experiment

V. N. Baier and V.M. Strakhovenko
Budker Institute of Nuclear Physics,
Novosibirsk, 630090, Russia

February 19, 2003

Abstract

The theory of radiation from high energy electrons moving near a crystalline axis is outlined. The intensity of radiation in thick crystal is discussed. Starting from the energy $\varepsilon \sim 1$ GeV the contribution of channeling radiation dominates. For energies a few GeV the development of the electron - photon showers in axially aligned single crystals is described including the formula for the intensity spectrum. Both channeling radiation and bremsstrahlung are taken into account. Some characteristics of the positron yield measured in recent experiments are calculated. Theoretical estimations display a rather good agreement with experimental results obtained using 3 to 10 GeV electrons aligned to the $< 111 >$ - axis of the tungsten crystals. Such comparison verified that the accuracy of our approach is quite sufficient to make a reliable choice for optimal parameters of the positron source using axially aligned crystals for future linear colliders.

1 Introduction

An efficient positron source is one of the important components of future electron - positron colliders. Positrons are generated from electrons in the course of the $e^-e^+\gamma$ - shower developing in a medium. In high-energy region, the basic processes involved in the shower development are typically considerably enhanced in oriented crystals as compared with corresponding amorphous media . The most pronounced effects take place at axial alignment when initial electrons are moving along the main axes of a crystal. This alignment alone will be considered below.

1.1 Radiation in axially oriented crystals

A theoretical description of the specific radiation which occurs when high-energy particles are moving near the crystalline axes in single crystals depends essentially on whether a crystal is thin or thick. In thin crystal, by definition, the distribution

function (DF) in a transverse (to the direction of the axes) phase space doesn't vary when a particle passes through a crystal and is defined by the initial conditions. In thick crystals, a dependence of the DF on the depth of penetration of particles into a crystal should be taken into account. A multiple scattering and radiation energy losses are the basic processes which govern the kinetics of the DF.

The effect under discussion can be used as a source of hard and directed radiation concentrated within a comparatively narrow frequency range [1]. Thick crystals are of greatest interest for applications of the mentioned specific radiation in the range of not too high energies. One of the most important characteristics is the total radiation intensity into a given solid angle. Different properties of radiation in thick axially oriented crystals were analyzed in [1], [2], [3], [4].

According to the analysis performed in [4] where the kinetics was due to multiple scattering, the DF for large depth l is of the form

$$dF(\mathbf{v}_\perp, \boldsymbol{\varrho}, l) = \frac{d^2\varrho}{S}\frac{d^2v_\perp}{\pi g(l)}\exp\left(-\frac{v_\perp^2}{g(l)}\right), \tag{1.1}$$

where $\boldsymbol{\varrho} = \boldsymbol{\varrho}(x, y)$ are the transverse coordinates, $|\boldsymbol{\varrho}| \leq r_0$, $S = \pi r_0^2$ is the area of a cell in the transverse plane which contains the projection of one atomic chain, and $n_\perp = 1/S$ is the density of chains of atoms (axes). The function $g(l)$ has the form

$$g(l) = \Delta^2 + \int_0^l \dot{\vartheta}_s^2(t)dt, \tag{1.2}$$

where $\dot{\vartheta}_s^2$ is the rate of variation of the squared angle of multiple scattering in an appropriate amorphous medium. The time (depth) dependence of $\dot{\vartheta}_s^2$ is connected with the variation of the particle energy because of radiation losses.The first term in $g(l)$ reflects the character of the angular (over the transverse velocity) distribution established at the initial stage of electron motion in a crystal which depends on the angular (over the angle of incidence ϑ_0) distribution in an incident beam. Even in the case $\vartheta_0 = 0$, the angular spread of particles in the crystal proves to be roughly equal to the Lindhard angle, $\vartheta_c = \sqrt{2U_0/\varepsilon}$ (U_0 is the depth of the potential well of the axis, ε is the energy of a particle). Therefore, assuming the incident beam to be rather narrow, $\vartheta_0 \leq \vartheta_c$, we put in [1] $\Delta^2 = \vartheta_c^2$.

In thick crystals some processes, mainly, multiple scattering and radiation energy losses change the DF. The multiple scattering, on the average, increases particle transverse energy. As a result, particles can leave a channel(dechanneling). We introduce the critical dechanneling length owing to multiple scattering l_d over which the root mean square angle of scattering becomes equal to the Lindhard angle ϑ_c:

$$l_d = \frac{\alpha}{4\pi}\left(\frac{\varepsilon\vartheta_c}{m}\right)^2 L_{rad}, \tag{1.3}$$

where m is the electron mass, and L_{rad} is the radiation length in an appropriate amorphous medium.

For energies from several hundreds of MeV to several GeV and crystal thickness $L \gg l_d$ we have for the multiple scattering angle $\vartheta_s \gg 1/\gamma$ and $\vartheta_s \gg \vartheta_c$, then

the factor $\exp\left(-\frac{v_\perp^2}{g(l)}\right)$ can be substituted for unity and the distribution proves to be uniform in a transverse phase space. As a consequence, for the intensity of the radiation under consideration (labeled by ch) at the depth l we have

$$\frac{dI_{ch}}{d\Omega} = \frac{\bar{I}}{\pi g(l)}, \tag{1.4}$$

where $\bar{I} = \int I(\varrho) d^2\varrho / S$. It is worth to note that $\bar{I}$ coincides with I_{as}, the asymptotic value achieved by the radiation intensity at the angle of incidence $\vartheta_0 \geq \vartheta_c$. One should emphasize that Eq.(1.4) incorporates the radiation from channeled particles as well as from the above-barrier ones. Appearance of I_{as} in Eq.(1.4) is due to the uniformity of the distribution in the transverse phase space under indicated assumptions, while the uniformity of the distribution with respect to $v_\perp$ resulted in Eq.(1.4) in a uniform distribution with respect to the solid angle of emitted photons for angles $\vartheta_{ph} \ll \vartheta_s$.

The values of $\bar{I} = I_{as}$ can be readily calculated for any potential of the axes. We use the axial potential in the form (see [2], [3])

$$U(x) = V_0 \left[\ln\left(1 + \frac{1}{x+\eta}\right) - \ln\left(1 + \frac{1}{x_0+\eta}\right) \right]. \tag{1.5}$$

Neglecting recoil effects (or, in other words, using the classical theory) we obtain for this potential

$$\bar{I} = I_{as} = I_0 \varphi(\eta), \tag{1.6}$$

where

$$I_0 = \frac{8\pi e^2 V_0^2 \varepsilon^2}{3m^4} n_\perp, \quad \varphi(\eta) = (1+2\eta)\ln\left(1+\frac{1}{\eta}\right) - 2. \tag{1.7}$$

In Eq.(1.5) $x = \varrho^2/a_s^2$, a_s is the screening radius, $x_0 = r_0^2/a_s^2$, and the parameter η is proportional to the squared amplitude of thermal vibrations u_1. The fitting parameters V_0, a_s, η are given in Table 1 for the $< 111 >$ axis.

A simple estimation of the range of typical photon energies being radiated is evidently useful. The characteristic radius of the region giving the main contribution to the radiation is the screening radius a_s (see also [2], [3]). The transverse velocity of the electron in the channel is $v_\perp \leq \vartheta_c$. Therefore, the corresponding frequency of motion is ϑ_c/a_s and the corresponding radiation frequency, with the Doppler effect taken into account, is equal to

$$\omega_{ch} \simeq 2\gamma^2 \frac{\vartheta_c}{a_s} \tag{1.8}$$

This estimate is valid in the dipole case, when the corresponding parameter

$$\rho = 2\gamma^2 \mathbf{v}_\perp^2, \tag{1.9}$$

where $\mathbf{v}_\perp$ is the transverse velocity of particle, is small ($\rho \ll 1$) and quantum recoil is neglected. In the case $\rho \gg 1$ the radiation is of magnetic bremsstrahlung type (that is higher harmonics dominate in the spectrum). So the parameter ρ characterizes the structure of radiation spectrum, it can be called the multipolar parameter.

For particle in the channel ($\vartheta_0 \leq \vartheta_c$) we have

$$\rho \simeq \rho_c = \frac{2V_0\varepsilon}{m^2}. \tag{1.10}$$

and at above-barrier motion ($\vartheta_0 \geq \vartheta_c$)

$$\rho \simeq \left(\frac{2V_0}{m\vartheta_0}\right)^2 \tag{1.11}$$

The values of $a_s\,, V_0$ and other parameters for different crystals are given above in Table 1.

At high energies the quantum recoil becomes significant. The quantum character of radiation is determined by the parameter

$$\chi_s = \frac{eE_s\varepsilon}{m^3} = \frac{V_0\varepsilon}{a_s m^3}, \tag{1.12}$$

Where E_s is the typical value of the electric field of axis, $eE_s = V_0/a_s$. At $\chi_s \ll 1$ the classical theory is valid. Because of $\rho_c/\chi_s = 2a_s m \sim 10^2$ for crystals under consideration, at $\chi_s \sim 1$ where the radiation is essentially quantum, one has $\rho \sim 10^2$ so that radiation in this case is of the magnetic bremsstrahlung nature. However, one should take into account that the quantum effects in the magnetic bremsstrahlung are "turn on" rather early. For example, already at $\chi = 0.1$ the classical value of the total intensity of radiation is around 1.5 times larger than the correct value. Using quantum approach one finds [5] that quantum corrections exceed 10% at the energy near 5 GeV in Si and diamond and at the energy near 3 GeV in Ge. So, at the energy $\varepsilon = 1$ GeV the corrections to the numbers R given in Table 1 for mentioned crystals are small. The situation is different for tungsten where already at the energy of 1 GeV the correction to the radiation intensity is 23% at room temperature and 33% for T=77 K. This means that actually we have $R(1\text{ GeV}) = 1.14$ for tungsten at room temperature and $R(1\text{ GeV}) = 1.59$ at T=77 K.

Besides the radiation under study, the bremsstrahlung (below with the subscript "*br*") also contributes to the intensity. Actually, the bremsstrahlung process changes in comparison with an amorphous medium under channeling conditions [6]. Typical scale of this effect is of the order 10%. Therefore, for crude estimates one can use the bremsstrahlung intensity in a corresponding amorphous medium. Under assumptions used above, we have for the bremsstrahlung intensity at depth l

$$\frac{dI_{br}}{d\Omega} = \frac{I_{br}}{\pi g(l)} \equiv \frac{1}{\pi g(l)}\frac{\varepsilon}{L_{rad}}, \tag{1.13}$$

It follows from above analysis that radiation intensity in a crystal Si or Ge is of the order that of the conventional bremsstrahlung at electron energies $\varepsilon \simeq 1$ GeV. While in diamond and tungsten the radiation intensity exceeds that of the conventional bremsstrahlung at this energy. It is seen also that the spectrum of radiation is relatively soft. Basing on these properties of the photon emission process, the use of this phenomenon in positron source for future accelerators was proposed

Table 1: Parameters of the potential Eq.(1.5) for $< 111 >$ axis and some characteristics of the radiation

Crystal	u_1 (10^{-8}cm) T=293 K	V_0 (eV)	U_0 (eV)	η	a_s (10^{-8}cm)	R	ω_{ch} (MeV)	ρ_c
$C_{(d)}$	0.040	29	103	0.025	0.326	1.87	21.1	0.22
Si	0.075	54	106	0.150	0.30	0.80	23.3	0.41
Ge	0.085	91	191	0.13	0.30	0.53	31.1	0.7
W	0.050	417	937	0.115	0.215	1.48	31	3.2
W (77 K)	0.030	348	1255	0.027	0. 228	2.38	35	2.7

In the table u_1 is the amplitude of thermal vibrations, V_0, β, a_s are the parameters of the potential, U_0 is the depth of potential well, R=I_{as}/I_{br} ratio at $\varepsilon = 1$ GeV, ω_{ch} is the characteristic photon energy calculated by means Eq.(1.8), the parameter ρ_c Eq.(1.10) is calculated at $\varepsilon = 1$ Gev. For position of spectrum maximum in tungsten it is taken into account that at energy $\varepsilon = 1$ Gev radiation is nondipole ($\rho_c \simeq 3.2$)

[7]. The pair production rate which is due to the coherent (crystal) effects exceeds that of the standard (Bethe-Heitler) mechanism starting with photon energies $\omega \simeq \omega_{th}$. The value of ω_{th} is about 22 GeV for the $< 111 >$ - axis of tungsten being several times larger for another crystals. (See review [8] and recent book [9] for further details concerning QED - processes in crystals.) For energies well above ω_{th}, the crystal effects become really strong and may be used to create effective and compact electromagnetic calorimeters [10]. For very high energies ($\varepsilon \gg \omega_{th}$) of initial and created particles, kinetic equations describing the shower development were solved analytically [11]. Though the initial electron energies were high enough in the first experimental investigation [12] of shower formation in crystals, energies of detected particles were too low to allow us the direct comparison with [11]. To explain the results of [12], Monte-Carlo simulations were performed in [13]. The probabilities of basic processes used in [13] were obtained within so-called constant field approximation (CFA). A good agreement was demonstrated in [13] with the results of [12] for Ge crystals.

1.2 Electromagnetic showers in crystal at GeV energies [14]

When the initial electron energy is below ω_{th}, photons are mainly emitted with energies $\omega \ll \omega_{th}$ and so, up to minor modifications (see [17], [18]), the pair production process proceeds in a crystal as in an amorphous medium. The enhancement of radiation from initial electrons is thereby the main crystal effect in this energy region.

Here we consider the case when the angle of incidence ϑ_0 with respect to the chosen axis is not too large as compared to the Lindhard angle $\vartheta_c = (2U_0/\varepsilon)^{1/2}$, since in this case the most pronounced effects take place.

Let us start with the coherent contribution to the radiation. As already mentioned, at sufficiently high energies corresponding expressions valid at any ϑ_0 were obtained in [16]. For $\vartheta_0 \ll V_0/m$ they reproduce CFA-limit. But even if the initial electron energy is high enough to apply mentioned description, charged particles arising in the course of a shower development may not satisfy this condition. In the case of a soft cascade we have to describe the radiation from these "soft" particles as well. Let us remind that within semi-classical theory of the QED- processes in any external field there are only two parameters: ρ and χ. The parameter ρ is a measure of the particle velocity deviation from a straight line in units of the natural emission angle $\gamma^{-1} = m/\varepsilon$, while the parameter χ being the ratio of the external field strength in the particle rest system to the critical QED-value $E_c = 1.32 \cdot 10^{16}\, eV/cm$ is responsible for the magnitude of quantum recoil effects. Let us remind also that at $\rho \ll 1$ the dipole approximation for a description of the radiation is valid and a typical formation time is $\sim \omega_0^{-1}$, where ω_0 is the characteristic frequency of motion. At $\rho \gg 1$ CFA is valid, the radiation formation time is $\sim \omega_0^{-1}\rho^{-1/2}$, i.e. much less than a period of motion. In this case the description of the emission process becomes local and we do not need to know what the particle trajectory is like contrary to the case of small $\rho \leq 1$ when we have to know it . If we now recollect that generally the two-dimensional problem of particle motion has not been solved yet in an analytical form, then evidently the same is true for the much more complicated problem of obtaining a radiation spectrum at such motion. We emphasize that for the coherent contribution to the total intensity of radiation $I_{ch}(\varepsilon)$ CFA gives a correct result up to very small energies when semi-classical approximation is still valid (see corresponding discussion in [16]).

The known (see Eq.(1.4) in [16]) estimate for the characteristic frequency of emitted photons ω at given frequency of motion ω_0 reads

$$u \equiv \frac{\omega}{\varepsilon - \omega} \simeq \frac{2N\omega_0\varepsilon}{m^2\,(1 + \rho/2)}, \tag{1.14}$$

where N is the characteristic number of emitted harmonics. Note that N = 1 for $\rho \leq 1$ and N $\propto \rho^{3/2}$ for $\rho \gg 1$. Using also that $\omega_0 \sim \theta_0/a_s$, (see Eq.(1.8)) we suggest to describe the radiation from channeled and moving not very high above the potential barrier particles the following heuristic intensity spectrum:

$$\frac{dI_{ch}}{d\omega} = \frac{r(\varepsilon)\varepsilon}{u_0(\varepsilon)}\left[1 + \frac{1}{(1+u)^2}\right]\left(\frac{u}{u_0}\right)^{1/3} \ln\left(\frac{u_0}{u}\right)\vartheta(u_0 - u), \tag{1.15}$$

where $\vartheta(z) = 1$ for $z > 0$ and $\vartheta(z) = 0$ for $z < 0$,

$$u_0 = \frac{25}{6}\chi_s + 80\,\frac{1}{ma_s}\,\frac{\sqrt{\rho_c}}{(2 + \rho_c)}. \tag{1.16}$$

The function $r(\varepsilon)$ in Eq.(1.15) is determined by the condition of the coincidence of the total intensity

$$I_{ch}(\varepsilon) = \int_0^{\varepsilon} d\omega \left(\frac{dI_{ch}}{d\omega}\right) \tag{1.17}$$

given by Eq.(1.15) with a corresponding expression obtained in CFA (see Eq.(3.1) in [16] without corrections to CFA) for the uniform distribution over transverse coordinates. So Eq.(1.15) reproduces the energy dependence of coherent contribution to the radiation length, $L_{ch} = \varepsilon / I_{ch}(\varepsilon)$ inherent to CFA which as mentioned above is valid in a wide energy range. For the sake of possible use, we have fitted our results for the function $r(\varepsilon)$ in the energy interval $\varepsilon < 5GeV$ by a polynomial

$$r(\varepsilon) = \sum_{n=0}^{9} a_n \varepsilon^n ,$$

where ε is measured in GeV and coefficients a_n for $< 110 >$-axis of Si and Ge crystals and for $< 111 >$-axis of W crystal are given in Table in [14]. This fitting provides the accuracy better than 1 percent for Si and Ge and better than 3 percent for W.

The position of a maximum in the spectrum given by Eq.(1.15) is always consistent with the estimate Eq.(1.14). For relatively small energies when $\rho_c \ll 1$ and correspondingly $u_0 \ll 1$, we can neglect the first term in the right-hand side of Eq.(1.16) since $\rho_c / \chi_s = 2ma_s \gg 1$. In this case the spectrum Eq.(1.15) has a maximum at $\omega = \omega_{max} \simeq 0.05 \varepsilon u_0 \simeq 2\varepsilon \sqrt{\rho_c}/(ma_s)$ which evidently coincides in this (dipole) approximation with Eq.(1.14). When $\rho_c \gg 1$ and CFA is valid the spectrum Eq.(1.15) reproduces not only the position of a maximum but also the shape of spectral distributions like those shown in Fig.2 of [16] obtained within the approximation mentioned . We have compared the shape of the spectrum Eq.(1.15) with available experimental data, but this procedure is somewhat indirect for several reasons. Sometimes very thin samples were used where the distribution of electrons over transverse coordinates was far from being uniform, sometimes energy loss spectra were measured which are noticeably different from true intensity spectra, sometimes emitted photons were collimated that also results in a change of the observed shape of spectra. Nevertheless, a qualitative agreement of the spectrum Eq.(1.15) with known experimental data holds for all energies beginning with $900\, MeV$. Of course, Eq.(1.15) can not give a correct description of the coherent contribution to the radiation from particles with energies less than $100\, MeV$. Furthermore, multiple scattering is very intensified in this energy region so that particles may acquire an angle with respect to the axis noticeably exceeding θ_c. At the same time, for such energies the intensity $I_{ch}(\varepsilon)$ is already small as compared to that caused by the incoherent contribution $I_{br}(\varepsilon)$ which is always present in crystals in slightly modified form comparatively to the amorphous case. For instance, at $\varepsilon = 70\, MeV$ near $< 111 >$ axis of tungsten we have $I_{ch}/I_{br} \simeq 0.1$ and the coherent contribution can be simply neglected. Nevertheless, for the sake of consistency we shall use Eq.(1.15) at any energy up to ε_f to describe the coherent contribution to the radiation. But for the particles acquiring an angle $\theta \geq \theta_c$ owing to multiple scattering, the quantity u_0 in Eq.(1.16) will be multiplied by the factor $0.5\sqrt{1 + (\theta/\theta_c)^2}$ according to Eq.(1.14) , since $\omega_0 \propto \theta$ at $\theta \geq \theta_c$.

Analysis of incoherent contribution to the radiation and pair-production probabilities is given in detail in [14].

The contribution to any process going on in a crystal is a sum $Y = Y_{coh} + Y_{inc}$ where, generally speaking, the incoherent contribution Y_{inc} differs from the amorphous value Y_{am}. The scale of this modification depends on the process under consideration. For the total intensity of the incoherent radiation and the quantity $\tilde{L}_{rad} = \varepsilon / I_{br}$ connected to it, the typical scale of diminishing of I_{br} as compared to I_{am} at room temperature is depending on media 9 to 13 per cent. The diminishing of the total probability of pair-production is of the same order of magnitude. In particular, for tungsten in the case of a full screening $\tilde{L}_{rad} = 1.1\, L_{rad}$. As far as the coherent contribution to the pair-production probability is negligible in the considered energy region and modifications of incoherent contributions are small, distinctions in the soft cascade development in crystal and amorphous media are mainly due to the coherent contribution to the radiation. This contribution changes the shape of photon spectra, enriching their soft part and noticeably diminishing the effective radiation length L_{ef} determined by the relation

$$L_{ef}^{-1} = \tilde{L}_{rad}^{-1} + L_{ch}^{-1}. \tag{1.18}$$

So, for the $< 111 >$ axis of tungsten, we find $L_{ef} \simeq 0.13\, cm$ at $\varepsilon = 2GeV$ and $L_{ef} \simeq 0.08\, cm$ at $\varepsilon = 5GeV$, which are several times less than the amorphous value $L_{rad} \simeq 0.35\, cm$. Thus in a crystal the initial electron is converted into photons along appreciably shorter length than in a corresponding amorphous medium, while further development of the soft shower in both media is more or less the same. Hence the most pronounced distinctions of shower characteristics in the amorphous and crystal case appear for small thicknesses. It is clear that for the valuable use of crystal properties one can utilize a hybrid target composed of crystal and amorphous layers, the former must be of a few L_{ef} thick.

In the hybrid target which consists of the crystal part followed by the amorphous one, the thickness of the crystal constituent of several L_{ef} is obviously quite enough. Indeed, at the depth $L_0 \approx (3 \div 4) L_{ef}$ most of the particles, including the initial electrons, are sufficiently soft to reduce the coherent contribution to the radiation to the level of the incoherent one. Thereby, the further development of the shower proceeds more or less in the same way for the crystal or amorphous type of the remaining part of the target. We emphasize that the crystal part $L \leq L_0$ of the target serves as the radiator, and secondary charged particles are still not so numerous at this stage of the shower development. Therefore only a small portion of the total energy loss is deposited in the crystal part of the target which considerably reduces a danger of its overheating. The softness of photon spectra is another important feature of the crystal radiator giving additional advantages for the positron production in comparison with the entirely amorphous target. To get more definite idea concerning the shape of the power spectrum one can use its explicit form given by Eq.(1.15). To present the scale, let us list some values ω_{max} where this spectrum is maximum: $\omega_{max}(1\ GeV) \simeq 31$ MeV, $\omega_{max}(4\ GeV) \simeq 170$ MeV, and $\omega_{max}(8\ GeV) \simeq 490$ MeV. Note that the width of the spectrum is typically several times larger than ω_{max}. The increase in the number of relatively soft photons turns out to be much more pronounced than that in the total radiation intensity. In the end, just this fact leads to the substantial enhancement of the positron yield from crystal targets.

To estimate the possibility of utilization of crystal targets in a positron source it is important to know not the total number of created positrons but the number of positrons in a definite phase space which can be accepted by the corresponding matching optical system. We shall use typical parameters of such system mentioned in [15], assuming that the energies of accepted positrons and their transverse (with respect to the incident beam direction) momenta must satisfy the following relation

$$5MeV \leq \varepsilon \leq 25MeV \ , \ p_{\perp} \leq 4MeV/c \, .$$

The number of accepted positrons N_{+}^{A} depending on the initial electron energy, the thickness and type of crystals are presented in Figs. 1-3. It is seen that the maximal yield is achieved at $L \sim 4L_{rad}$ and the maximal value increases with the atomic number, Z . The latter property is connected with the fact that with increasing Z the number of additional photons emitted by the coherent mechanism increases as well. An enlargement of the transverse momentum boundary value leads naturally to an increase of the accepted positron number and vice versa, what is illustrated by Fig.4.

The energy deposited in a target by the initial electron and created charged particles is one of the fundamental characteristics of the positron source. Because we use simplified formula for ionization energy losses, our results for the dissipated energy must be considered as the upper bound. In Fig.5 both the accepted positron yield and the deposited energy per one incident electron are presented for amorphous and crystal tungsten depending on the target thickness. It is seen that the relative gain for a crystal increases with increasing energy of initial electrons. For given number of accepted positrons N_{+}^{A} , the energy deposited ε_{dep} in a crystal sample is less than in an amorphous one.

Recently the positron production in axially aligned single crystals was studied in two series of experiments performed at CERN [19], [20] and KEK [21], [22]. The initial energy of electrons was 3 GeV [21], 6 and 10 GeV [20], 8 GeV [22], and 10 GeV [19]. In all cases the initial electron beam was aligned with the $< 111 >$ - axis of the tungsten crystal that sometimes served as the crystal part of the hybrid target which contained an additional amorphous tungsten target. A noticeable enhancement of the low-energy positron yield was observed in all experiments cited above when the yield from the crystal target was compared with that from the amorphous target of the same thickness. The experimental results and our theoretical estimations presented in the next Section display a rather good agreement with each other.

2 Comparison of theory with experiment

Theoretical results for the conditions of the experiments cited above were obtained using the approach developed in [14] and [18] where various positron and photon distributions as well as deposited energies in different crystals were calculated for the energy range of initial electrons from 2 to 300 GeV. In these papers, all the formulas used in Monte-Carlo simulations of the specific $e^{-}e^{+}\gamma$ - shower characteristics are given in the explicit form. Remember that our simplified description of the

shower development takes into account coherent (induced by the regular motion of particles in the field of crystal axes) and incoherent (like that in an amorphous medium) mechanisms of photon emission and pair production processes. The multiple scattering and the ionization energy loss of electrons and positrons are taken into account neglecting crystal effects. The coherent radiation from channeling and moving not very high above the axis potential barrier particles is described using the semi - phenomenological spectrum suggested in [14]. The corresponding computer code was developed. This allows one to calculate energy, angular, and coordinate distributions of positrons emergent from the crystal or hybrid target and to find an amount of the energy deposition. We think that the investigation of such distributions should be the main object of the experiments having the creation of the crystal assisted positron source as their ultimate aim.

2.1 Experiment (CERN) at $\varepsilon_0 = 10$ GeV

Among experiments cited above, spectral - angular distributions of created positrons were measured only in WA103 experiment at CERN (see [19], [20]) where our code was used in simulations as the event generator. This simulation allowed for the acceptance conditions and the efficiency of the detectors used. Shown in Fig.6 taken from [20] is one example of the measured and simulated distributions of positrons from 10 - GeV electrons aligned with the $< 111 >$- axis of the 8 - mm - thick crystal tungsten.

The angular acceptance conditions in WA103 experiment were approximately $|\vartheta_V^{out}| \leq 1.5^\circ$ for the vertical and $0 \leq \vartheta_H^{out} \leq 25^\circ$ for the horizontal angle of outgoing positron with respect to the initial electron beam direction. We shell see below that the shape of the positron spectrum depends on the degree of collimation. The one-dimensional (over ϑ_H^{out}) angular distribution is presented for positrons having energies in the $5 \div 45$ MeV range. We emphasize that the relative difference between measured and simulated results typically does not exceed 20 % in both spectral and angular distributions as seen in Fig.6. We are aware that preliminary results for another settings used in the same experiment do not contradict with the estimated scale of the difference between the data and theoretical predictions. We hope that this interrelation will not become worse after performing the complete analysis of the data which now is underway. This analysis will also give more detailed information concerning spectral - angular distributions of positrons depending on initial electron energies and target thicknesses.

2.2 Experiment (KEK) at $\varepsilon_0 = 3$ GeV

The main goal of the experiment [21] was an attempt to apply the crystal target to the working electron/positron linac, the injector for the electron - positron collider B - Factory at KEK. Thus, the acceptance conditions for created positrons were determined by the momentum acceptance of the positron linac with the matching section which is 8.2 MeV/c $< p <$ 11.6 MeV/c and $p_\perp <$ 2.4 MeV/c. The hybrid target used consists of 1.7 - mm - thick tungsten crystal followed by 7 - mm - thick

amorphous tungsten. The observed positron yield was enhanced by the factor 1.40 when the $< 111 >$ crystal axis was aligned with 3 GeV incident electron beam as compared to the case of the disoriented crystal. Our number for this enhancement is 1.47 being only 5 % larger than the experimental one. Note that in the experiment [21] the crystal and amorphous parts of the hybrid target were separated by the distance of 70 mm. This circumstance, which, in principle, may slightly change the enhancement value, was not taken into account in our calculation. Recollect that the amount of the energy deposited in the crystal part (ε_{dep}^{cr}) of the hybrid target may be much smaller than that (ε_{dep}^{am}) in the amorphous one. Such interrelation of ε_{dep}^{cr} and ε_{dep}^{am} should take place in the case of [21], where the crystal thickness is about 1.8 L_{ef} (see discussion in the Introduction). This is confirmed by our calculations which give $\varepsilon_{dep}^{cr} \simeq 11$ MeV and $\varepsilon_{dep}^{am} \simeq 277$ MeV per one incident electron.

2.3 Qualitative features of positron distributions and experiment (KEK) at $\varepsilon_0 = 8$ GeV

In [22] the positron production efficiency from 2.2 - mm, 5.3 - mm and 9.0 - mm - thick tungsten crystals was measured using an 8 - GeV electron beam. Positrons produced in the forward direction with momenta 10, 15 and 20 MeV/c were detected by the magnetic spectrometer. Thus, only several points in the energy distribution were determined under hard collimation conditions. Therefore, before going on to the comparison of the experimental results with our, let us remind some important qualitative features of spectral - angular distributions using 8 GeV electrons and the $< 111 >$ - axis of the tungsten crystals as an example. For the sake of comparison, the corresponding distributions for amorphous tungsten will be presented as well. Below all the quantities characterizing the positron yield are normalized per one incident electron.

The use of matching systems implies some collimation (typically $\vartheta_{out} \leq 25°$) of outgoing positrons. Shown in Fig.7 is the energy dependence (energy step is equal to 10 MeV) of the positron yield from crystal (a) and amorphous (b) targets of the same thickness $L = 2.2$ mm. In the case of the hard collimation, when $\vartheta_{out} \leq 1°$ (open circles), the yield is multiplied by 10 to make it visible. The larger the positron energy, the smaller is the typical value of ϑ_{out} since both production and multiple scattering processes are characterized by smaller angles for higher energies. This is seen in Fig.7 (a) where the spectral curves for $\vartheta_{out} < 180°$ and that for $\vartheta_{out} \leq 24°$ are overlapping within precision better than 1 % starting from $\varepsilon_{cr}^{(1)} \simeq 55$ MeV. In turn, from $\varepsilon_{cr}^{(2)} \simeq 110$ MeV the same happens with curves corresponding to $\vartheta_{out} \leq 24°$ and $\vartheta_{out} \leq 12°$. Such behavior is also seen in Fig.7 (b) for the amorphous target where $\varepsilon_{am}^{(1)} \simeq 50$ MeV and $\varepsilon_{am}^{(2)} \simeq 105$ MeV. In other words, positrons with energies $\varepsilon > \varepsilon^{(1)}$ are practically concentrated within the cone $\vartheta_{out} \leq 24°$ and those with $\varepsilon > \varepsilon^{(2)}$ have $\vartheta_{out} \leq 12°$. In accordance with this picture, the spectral maximum is shifted to the right while the width of the distribution increases when the collimation angle decreases. The enhancement μ, being bin-by-bin ratio of the positron yield from the crystal target to that from the amorphous one at the same collimation, is almost constant for $\varepsilon < 45$ MeV and monotonically

decreases with growing positron energy. This means that positron spectra from the crystal target are softer. Somewhat lower values of $\varepsilon^{(1)}, \varepsilon^{(2)}$ in the amorphous case point at the same feature. For given collimation, the variation of the enhancement is about 20 % over the whole energy interval presented in Fig.7. The maximum values of the enhancement at different collimation are $\mu_{max}(\vartheta_{out} \leq 180°) \simeq 6.09$, $\mu_{max}(\vartheta_{out} \leq 24°) \simeq 5.92$, $\mu_{max}(\vartheta_{out} \leq 12°) \simeq 5.67$, and $\mu_{max}(\vartheta_{out} \leq 1°) \simeq 5.29$. Apparently, they diminish as the collimation angle does so. Shown in Fig.8 is the same as in Fig.7 but for the target thickness $L = 9.0$ mm. The yield at $\vartheta_{out} \leq 1°$ (open circles) is multiplied now by 30. The qualitative behavior of spectra depending on the collimation angle at $L = 9.0$ mm is the same as at $L = 2.2$ mm. However, all the spectra become softer for the larger target thickness. This is indicated already by the increase in $\varepsilon^{(1)}$, $\varepsilon^{(2)}$ values which are now $\varepsilon^{(1)}_{cr} \simeq 85$ MeV, $\varepsilon^{(2)}_{cr} \simeq 185$ MeV, $\varepsilon^{(1)}_{am} \simeq 75$ MeV, $\varepsilon^{(2)}_{am} \simeq 165$ MeV. It is clear that the magnitude of the yield from the thicker target is essentially larger but this increase is different in the crystal and amorphous cases. For example, in the energy range $\varepsilon < 45$ MeV the yield is increased by $6 \div 7$ times for a crystal and by $17 \div 20$ times for amorphous samples. As a result, the enhancement at $L = 9.0$ mm is almost 3 times less than at $L = 2.2$ mm in this energy range. At $L = 9.0$ mm the enhancement is peaked in the first bin ($\varepsilon \in (5 \div 15)$ MeV) for every collimation. Its maximum values are $\mu_{max}(\vartheta_{out} \leq 180°) \simeq 2.25$, $\mu_{max}(\vartheta_{out} \leq 24°) \simeq 2.15$, $\mu_{max}(\vartheta_{out} \leq 12°) \simeq 2.08$, and $\mu_{max}(\vartheta_{out} \leq 1°) \simeq 2.06$. The enhancement monotonically decreases with growing positron energy and approximately halves at $\varepsilon \approx 250$ MeV. Thus, positron spectra from the crystal target are softer at $L = 9.0$ mm as well, and this property is much more pronounced in comparison with $L = 2.2$ mm.

Matching systems can be characterized also by the maximum transverse momentum $p_\perp^{max}$ of accepted positrons. In this connection, spectra of positrons having $p_\perp < p_\perp^{max}$ are of definite interest. Such spectra at $L = 2.2$ mm (a) and at $L = 9.0$ mm (b) from crystal and amorphous targets are shown in Fig.9. In contrast to the case of the pure angular selection (cf. Figs.7,8 the position of spectral maxima at limited $p_\perp$ values is always in the first bin ($\varepsilon \in (7.5 \div 12.5)$ MeV). Corresponding maximum values are $\mu_{max}(5\ MeV/c) \simeq 5.82$, $\mu_{max}(2.5\ MeV/c) \simeq 5.62$ at $L = 2.2$ mm and $\mu_{max}(5\ MeV/c) \simeq 2.17$, $\mu_{max}(2.5\ MeV/c) \simeq 2.11$ at $L = 9.0$ mm. The enhancement monotonically decreases with growing positron energy. Its variation over the whole energy interval presented in Fig.9 is about 15 % at $L = 2.2$ mm and 40 % at $L = 9.0$ mm. So, for this selection too, positron spectra from crystal targets are softer than those from amorphous targets of the same thickness. The interesting feature of spectral curves in Fig.9 is the similarity of those obtained for two different values of $p_\perp^{max}$ from the same target. The scaling factors η are $\eta_{cr} \simeq 2.6$, $\eta_{am} \simeq 2.5$ at $L = 2.2$ mm and $\eta_{cr} \simeq 3.1$, $\eta_{am} \simeq 3.0$ at $L = 9.0$ mm. These factors turn out to be practically (within an accuracy of a few percent) independent of the total positron momentum p. This fact can be easily understood if we assume that the width of the angular distribution of positrons is completely due to multiple scattering being, thereby, proportional to p^{-1}. Such assumption is confirmed by results of the calculation shown in Fig.10 for two groups of positrons. One of them contains positrons having momentum in the interval $p \in (8.5 \div 11.5)$ Mev/c , for

another group $p \in (17 \div 23)$ Mev/c.

For the given target, the width of the angular distribution of positrons with $p \approx$ 10 Mev/c is approximately twice as much that for $p \approx 20$ Mev/c as expected. The width of every distribution evidently increases when we go on to the thicker target of the same kind. Comparing angular distributions from crystal and amorphous targets of the same thickness, we find that at $L = 9.0$ mm the distributions are somewhat (about 1.5°) wider in the crystal case for both groups. In units of FWHM of the distribution from the crystal target these differences are about 6.5 % at $p \approx 10$ Mev/c and 14 % at $p \approx 20$ Mev/c. At $L = 2.2$ mm the distribution from the crystal target is wider by 15.5 % at $p \approx 20$ Mev/c whereas this is narrower by 10 % at $p \approx 10$ Mev/c.

Going on to the comparison of our results with those obtained in [22], let us remind that to perform an accurate comparison of such kind, exact information is needed concerning the acceptance conditions and registration efficiency of detectors in the experiment. As noted in [22], at $p = 20$ Mev/c, the momentum acceptance ($\Delta p/p$) was 3 % (FWHM) and the polar angle acceptance was less than 20 mrad (FWHM). Since the shape of the acceptance curves was unavailable to us, we have tried to simulate experimental conditions using the same angular collimation $\vartheta_{out} \leq \vartheta_{out}^{max}$ and the same value of $\Delta p/p$ for all momenta and targets. So, at the calculation of the magnitude of positron production efficiency (PPE), we simply put ϑ_{out}^{max} to 20 mrad. The value of $\Delta p/p$ was chosen to reproduce at applied collimation the experimental magnitude of PPE for the 9.0 - mm - thick amorphous target. Acting in this way, we have got $\Delta p/p = 3.2$ %. We realize that our regard for the acceptance conditions is rather rough. An additional inaccuracy was introduced when we determined the PPE numbers from Fig.10 of [22]. Note that the experimental numbers obtained in a such way, which are presented by filled symbols in Fig.11, do not reproduce exactly the whole set of mean experimental values for the enhancement given in Table 1 of [22]. Moreover, in Fig.10 of [22] there are no experimental points for 2.2 and 5.3 - mm - thick amorphous targets. For these two cases, we present in Fig.11 the values of PPE given by smooth - curve fits corresponding to simulation fitting in Fig.10 of [22]. Bearing all this in mind, we, nevertheless, can assert that a rather good agreement is seen in Fig.11 of the experimental results and our estimations. Relative difference of them is better than 13 % everywhere except the values of PPE at $p = 10$ and 15 Mev/c from both thinnest ($L = 2.2$ mm) targets, where the experimental yield is underestimated by 19 % to 42 %. Note that just for this thickness the largest inaccuracy was introduced while determining the PPE numbers from Fig.10 of [22] at $p = 10$ and 15 Mev/c, as the magnitude of the yield is especially small in this case.

In contrast to the magnitude of the positron yield, the enhancement is not very sensitive to the acceptance conditions. The calculated values of the enhancement(theory) are presented in Table 2 along with those taken from Table 1 of [22] (experiment). Purely statistical errors are figured in Table 2 as theoretical ones. The relative error in PPE was estimated as $N_{ef}^{-1/2}$, where N_{ef} is the mean number of events in the phase space corresponding to the acceptance conditions used in calculations. The total statistics was chosen so that approximately to equalize values

Table 2: Enhancement of the positron yield from crystal targets

Momentum (MeV/c)	Enhancement (2.2-mm-thick)		Enhancement (5.3-mm-thick)		Enhancement (9.0-mm-thick)	
	theory	experiment	theory	experiment	theory	experiment
10	6.0 ± 0.5	6.5 ± 0.6	3.2 ± 0.3	3.4 ± 0.7	2.1 ± 0.2	2.3 ± 0.4
15	5.5 ± 0.3	6.2 ± 0.8	3.2 ± 0.2	3.2 ± 0.5	2.0 ± 0.1	2.0 ± 0.2
20	5.4 ± 0.2	5.1 ± 0.5	2.9 ± 0.1	3.0 ± 0.5	1.8 ± 0.1	1.8 ± 0.2

of N_{ef} for amorphous and crystal targets of the same thickness. At given total statistics, the quantity N_{ef} increases with growing positron momentum in accord with a shape of the positron spectra at hard collimation shown in Figs. 2,3. This fact leads to a better statistical accuracy for larger momentum. We emphasize that the differences of the estimated and experimental enhancement values are smaller than corresponding experimental errors for all momenta and samples figured in Table 2.

3 Conclusion

Using the simple computer code suggested in [14] and [18], we have compared the theoretical predictions for some characteristics of the electromagnetic shower developing in axially aligned crystals with experimental results reported in [19],[20] and [21],[22]. On the whole, theory and experiment are consistent within the experimental accuracy. From this comparison we also conclude that the accuracy provided by the existing simplified code is at least better than 20%. This accuracy may be slightly improved if we include into consideration some processes like annihilation of positrons or Compton scattering of photons which were ignored as corresponding cross sections are small in the energy region of interest. However, the approximate character of the radiation spectra at axial alignment used in our calculations still provides the main theoretical uncertainty. Nevertheless, we believe that the level of the accuracy already achieved in the theoretical description is quite sufficient to make a reliable choice for optimal parameters of the positron source using axially aligned single crystals.

Acknowledgments We are grateful to Prof. H.Okuno for providing us with details of the experiment [22] and to the authors of [20] for numerous fruitful discussions. Support of this work by the Russian Fund of Basic Research under Grants 00-02-18007, 01-02-16926, and 00-02-22003 is also gratefully acknowledged.

References

[1] V.N.Baier, V.M.Katkov and V.M.Strakhovenko, phys.stat.sol.(b)**133** (1986) 583.

[2] V.N.Baier, V.M.Katkov and V.M.Strakhovenko, Phys. Lett. A, **95** (1983) 403.

[3] V.N.Baier, V.M.Katkov and V.M.Strakhovenko, Nucl. Instr. and Meth. B **4** (1984) 346.

[4] V.N.Baier, V.M.Katkov and V.M.Strakhovenko, Sov.Phys.Dokl. **29** (1984) 306.

[5] V.N.Baier, V.M.Katkov and V.M.Strakhovenko, Phys. Lett. A, **162** (1992) 429.

[6] V.N.Baier, V.M.Katkov and V.M.Strakhovenko, phys.stat.sol.(b)**149** (1988) 403.

[7] V.N.Baier and R.Chehab, Positron Source based on Channeling Radiation, Proposal for an Experiment at Orsay, LAL, Orsay, France (May 1990).

[8] V.N.Baier, V.M.Katkov and V.M.Strakhovenko, Sov. Phys. Usp. **32** (1989) 972.

[9] V.N.Baier, V.M.Katkov and V.M.Strakhovenko, *Electromagnetic Processes at High Energies in Oriented Single Crystals*, World Scientific Publishing Co, Singapore, 1998.

[10] V.N.Baier, V.M.Katkov and V.M.Strakhovenko, Nucl. Instr. and Meth. A **250** (1986) 514.

[11] V.N.Baier, V.M.Katkov and V.M.Strakhovenko, Nucl. Instr. and Meth. B **27** (1987) 360.

[12] R.Medenwaldt et al.,Phys. Lett. B **227** (1989) 483.

[13] V.N.Baier, V.M.Katkov and V.M.Strakhovenko, Nucl. Instr. and Meth. B **119** (1996) 131.

[14] V.N.Baier, V.M.Katkov and V.M.Strakhovenko, Nucl. Instr. and Meth. B **103** (1995) 147.

[15] X.Artru, V.N.Baier, R.Chehab, and A.Jejcic, Nucl. Instr. and Meth. A **344** (1994) 443.

[16] V.N.Baier, V.M.Katkov and V.M.Strakhovenko, Sov.Phys.JETP, **65** (1987) 686.

[17] V.N.Baier, V.M.Katkov and V.M.Strakhovenko, phys.stat.sol.(b)**149** (1988) 403.

[18] V.N.Baier and V.M.Strakhovenko, Nucl. Instr. and Meth. B **155** (1999) 403.

[19] R.Chehab et al. Proceedings of LINAC2000, Monterey, CA, USA, August 2000, p.143

[20] R.Chehab et al. Phys. Lett. B, **525** (2002) 41.

[21] M.Inoue, S.Takenaka, K.Yoshida et al, Nucl. Instr. and Meth. B **173** (2001) 104.

[22] H.Okuno et al. Report on RREPS-01 Conference, Lake Aya, Russia, September 2001; KEK Preprint 2001-146.

Figure captions.

Fig.1. Number of accepted positrons N_+^A versus crystal thickness L in Si near $< 110 >$-axis . The initial electron energy (in GeV) is indicated near corresponding curves.

Fig.2. The same as in Fig.1 but for Ge near $< 110 >$-axis .

Fig.3. The same as in Fig.1 but for W near $< 111 >$-axis .

Fig.4. Number of positrons having energies in the interval $5 \div 25 MeV$ versus thickness of tungsten crystal for different values of boundary transverse momentum $p_\perp$ indicated (in MeV/c) near corresponding curves.

Fig.5. Number of accepted positrons N_+^A (curves 3,4) and deposited energy ε_{dep} (curves 1,2) for $\varepsilon_i = 5GeV$ in amorphous (curves 1,3) and crystal (curves 2,4) tungsten depending on the thickness L .

Fig.6. Spectral (left) and angular (right) distributions of positrons from 10 GeV electrons traversing 8 - mm - thick crystal tungsten target along the $< 111 >$- axis. Open circles: simulation, filled circles: experiment.

Fig.7. Positron yield depending on energy from 2.2 - mm - thick crystal (a) and amorphous (b) targets at different collimation. Filled triangles - no collimation ($\vartheta_{out} \leq 180°$), open triangles - $\vartheta_{out} \leq 24°$, filled circles - $\vartheta_{out} \leq 12°$, and open circles - $\vartheta_{out} \leq 1°$ (multiplied by 10).

Fig.8. Positron yield depending on energy from 9.0 - mm - thick crystal (a) and amorphous (b) targets at different collimation. Filled triangles - no collimation ($\vartheta_{out} \leq 180°$), open triangles - $\vartheta_{out} \leq 24°$, filled circles - $\vartheta_{out} \leq 12°$, and open circles - $\vartheta_{out} \leq 1°$ (multiplied by 30).

Fig.9. Positron yield depending on energy at $L = 2.2$ mm (a) and $L = 9.0$ mm (b) for $p_\perp^{max} = 2.5$ MeV/c (curves 1 and 3) and for $p_\perp^{max} = 5$ MeV/c (curves 2 and 4). Solid curves represent the yield from crystal and dotted from amorphous targets.

Fig.10. Angular distribution $dN^{(+)}/d\Omega$ depending on outgoing positron angle at $L = 2.2$ mm (a) and at $L = 9.0$ mm (b) for $p \in (8.5 \div 11.5)$ Mev/c (curves 1 and 3) and for $p \in (17 \div 23)$ Mev/c (curves 2 and 4). Solid curves represent the yield from crystal and dotted from amorphous targets.

Fig.11. Positron production efficiency from crystal (a) and amorphous (b) targets depending on thickness. Open symbols - our calculation, filled symbols - results from Fig.5 of [22]; open triangles are for $p = 20$ Mev/c, open circles are for $p = 15$ Mev/c, and open squares are for $p = 10$ Mev/c.

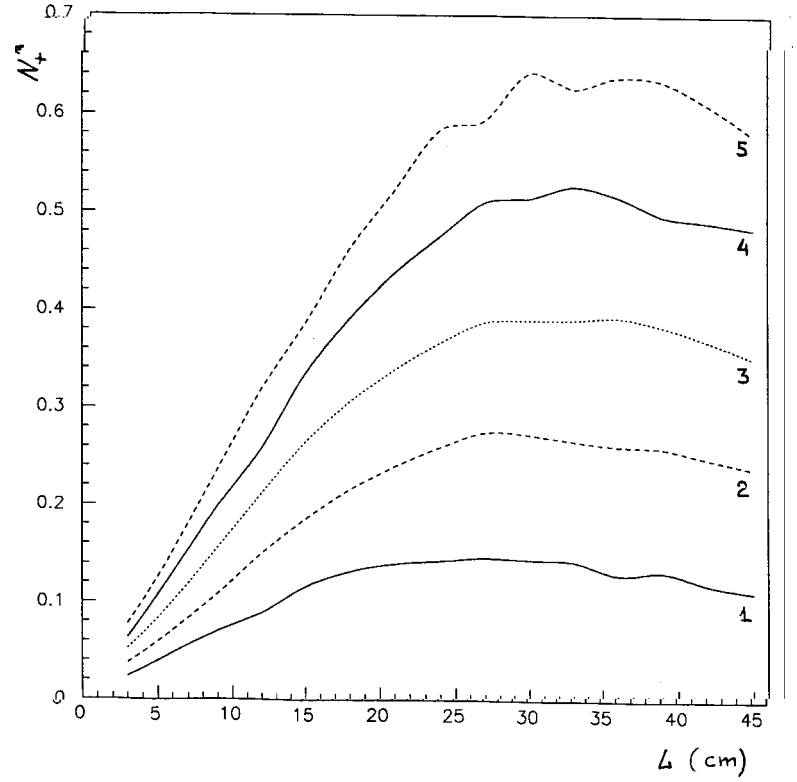
0.7
0.6
0.5
0.4
0.3
0.2
0.1
0
0
5
10
15
20
25
30
35
40
45
L (cm)
1
2
3
4
5

Fig. 1

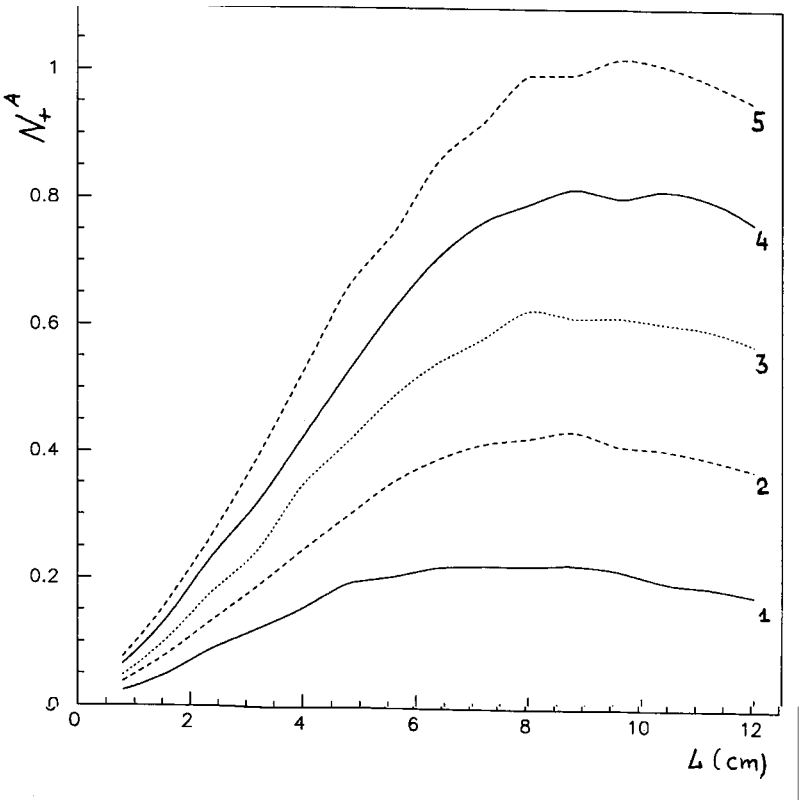
1
0.8
0.6
0.4
0.2
0
0
2
4
6
8
10
12
L (cm)
1
2
3
4
5

Fig. 2

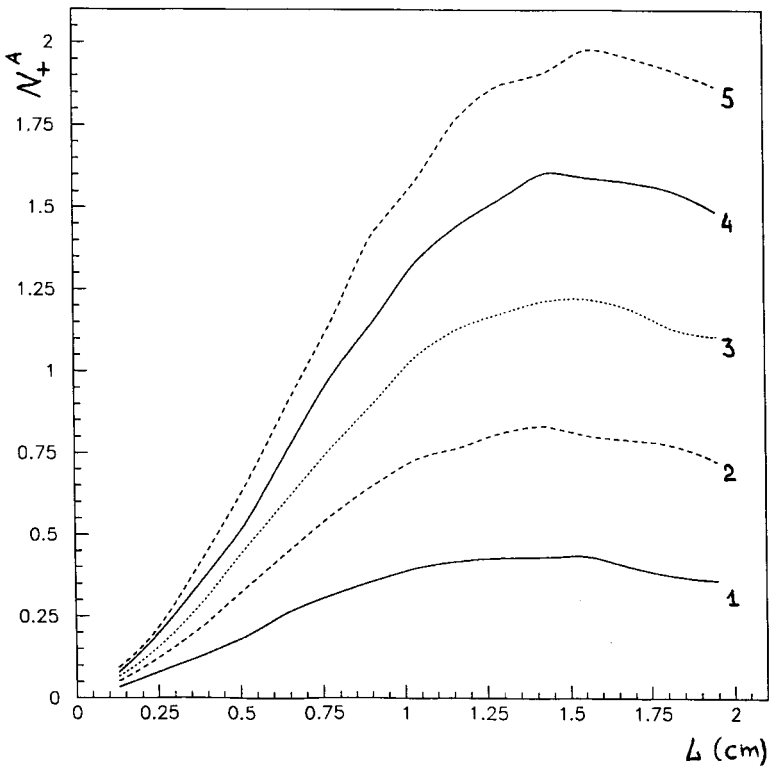
N_+^A
2
1.75
1.5
1.25
1
0.75
0.5
0.25
0
0
0.25
0.5
0.75
1
1.25
1.5
1.75
2
L (cm)
5
4
3
2
1

Fig. 3

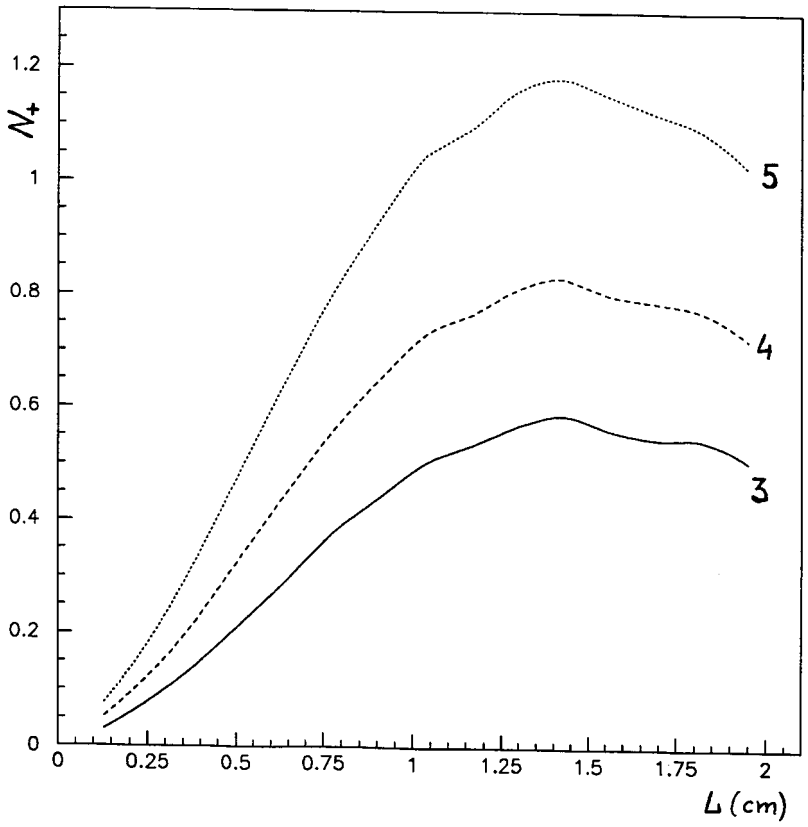
N_+
1.2
1
0.8
0.6
0.4
0.2
0
0
0.25
0.5
0.75
1
1.25
1.5
1.75
2
L (cm)
5
4
3

Fig. 4

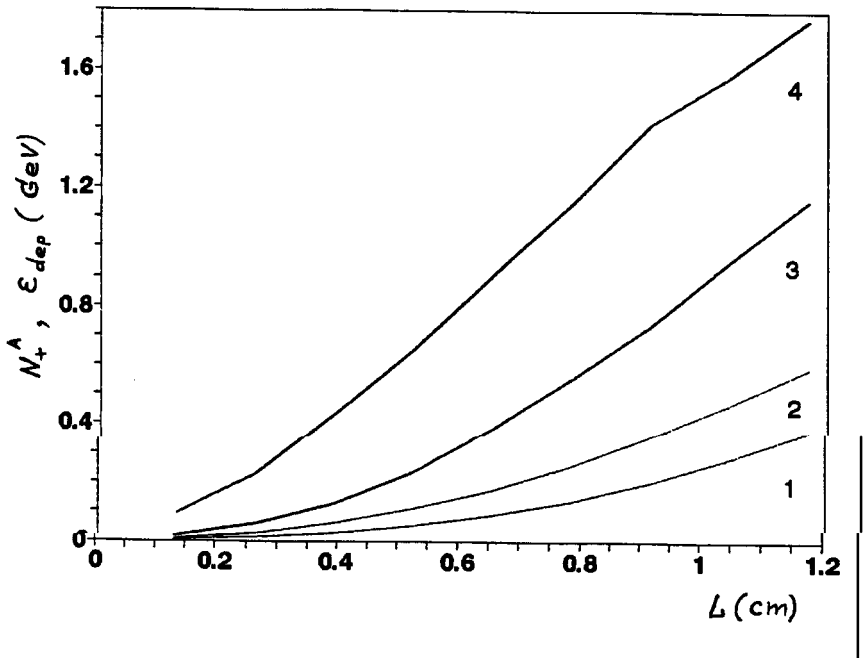

Fig. 5

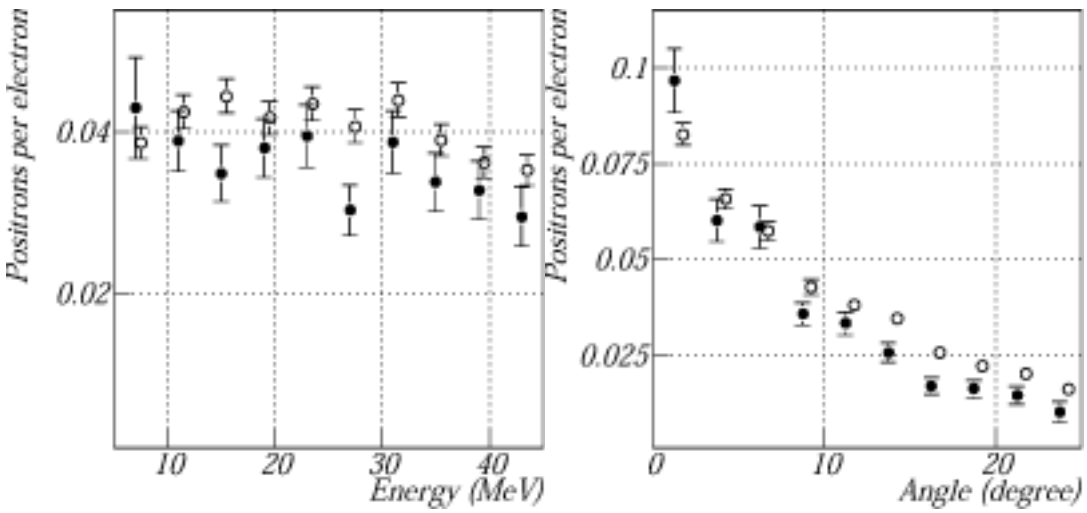

(a) (b)

Fig. 6

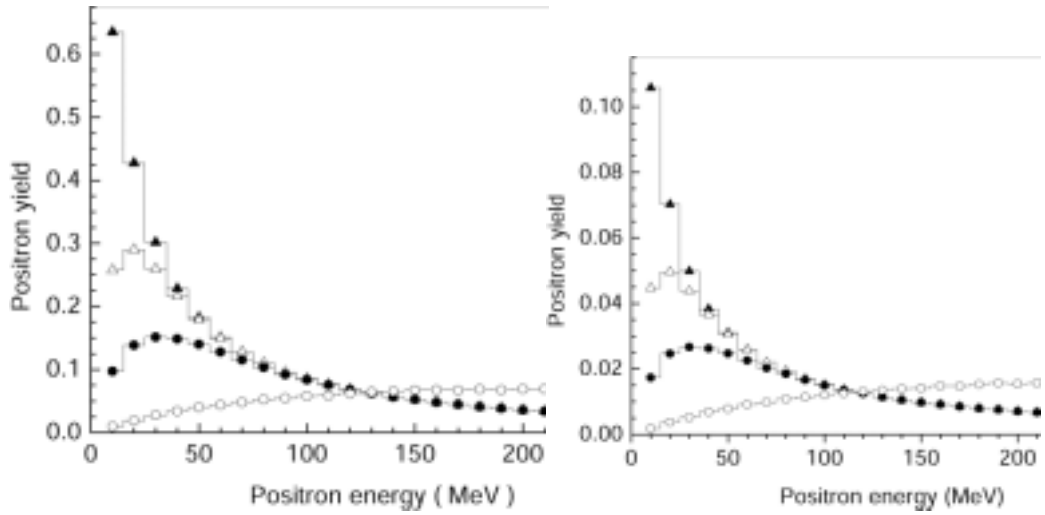

(a) (b)

Fig. 7

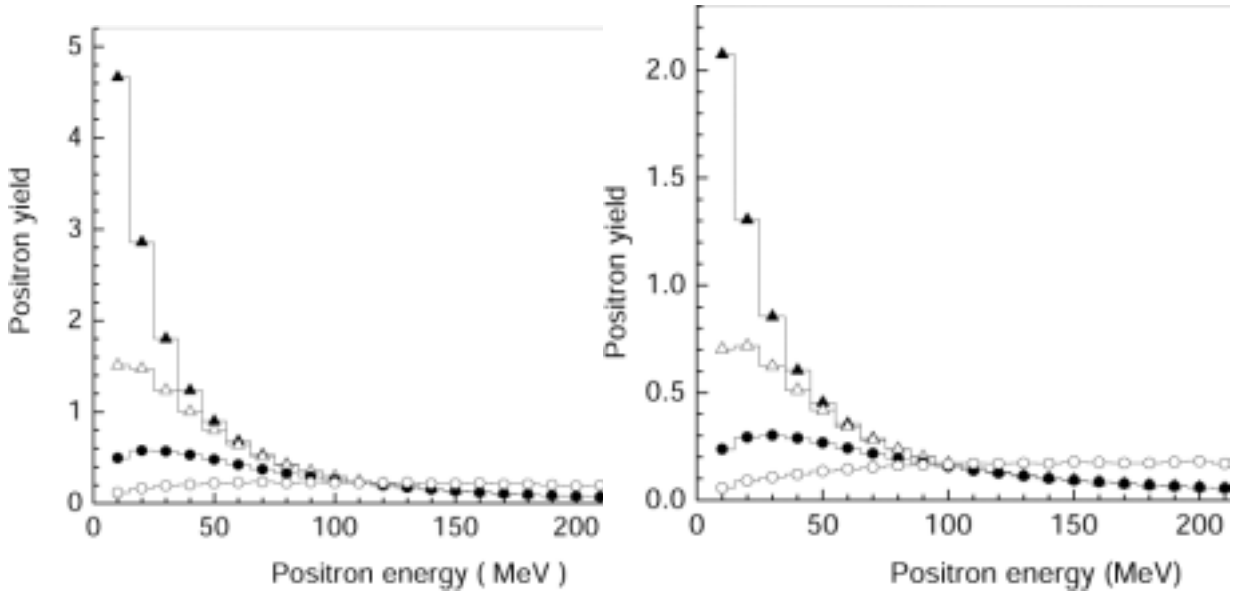

(a) (b)

Fig. 8

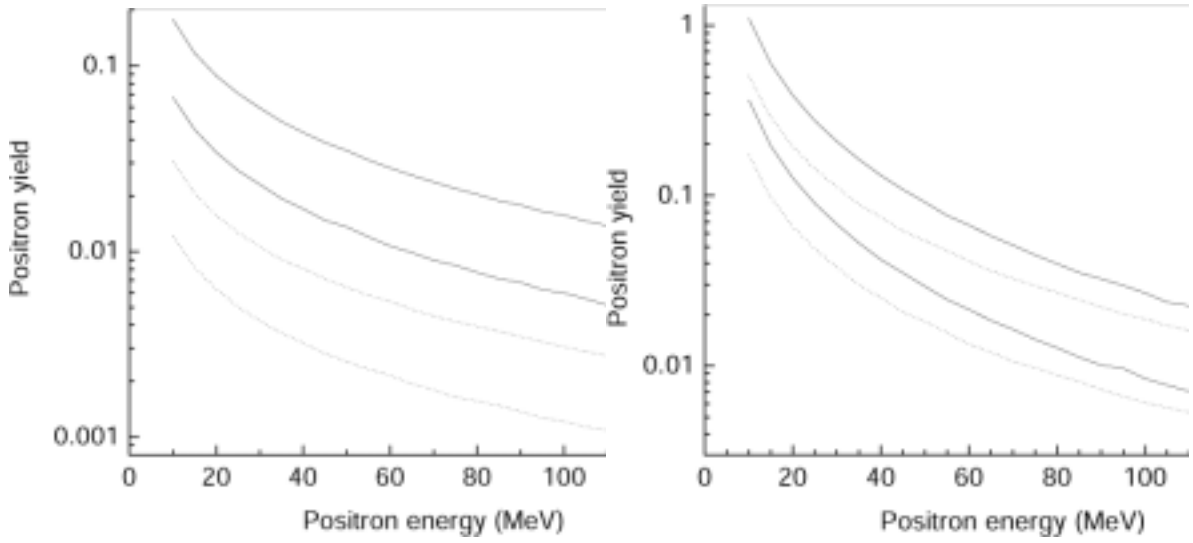

(a) (b)

Fig. 9

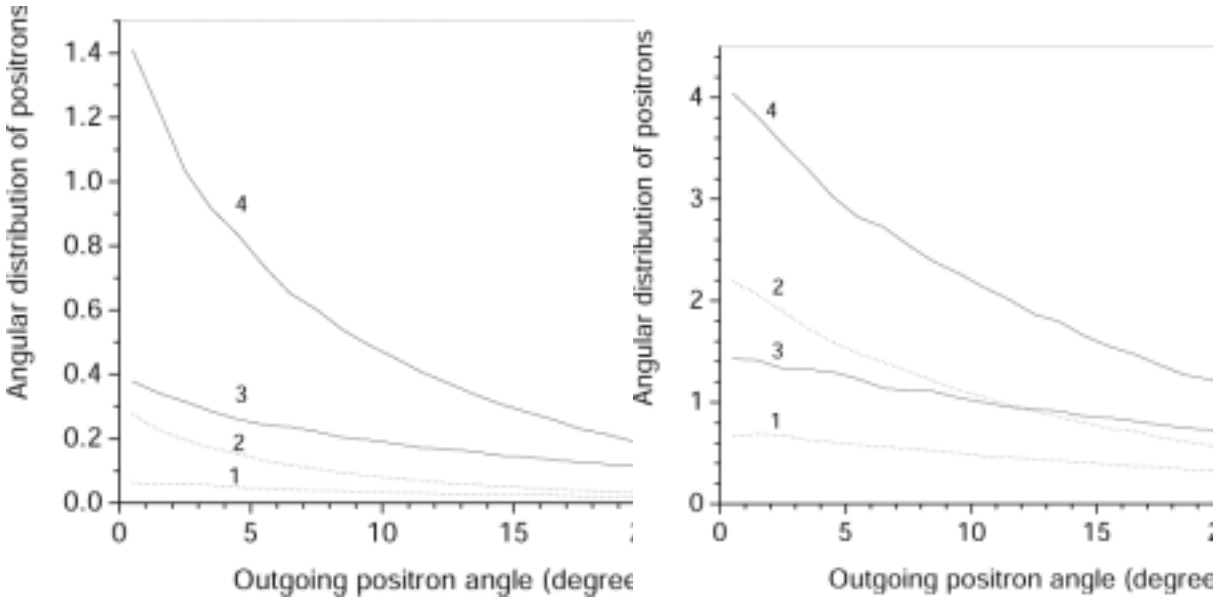

(a) (b)

Fig. 10

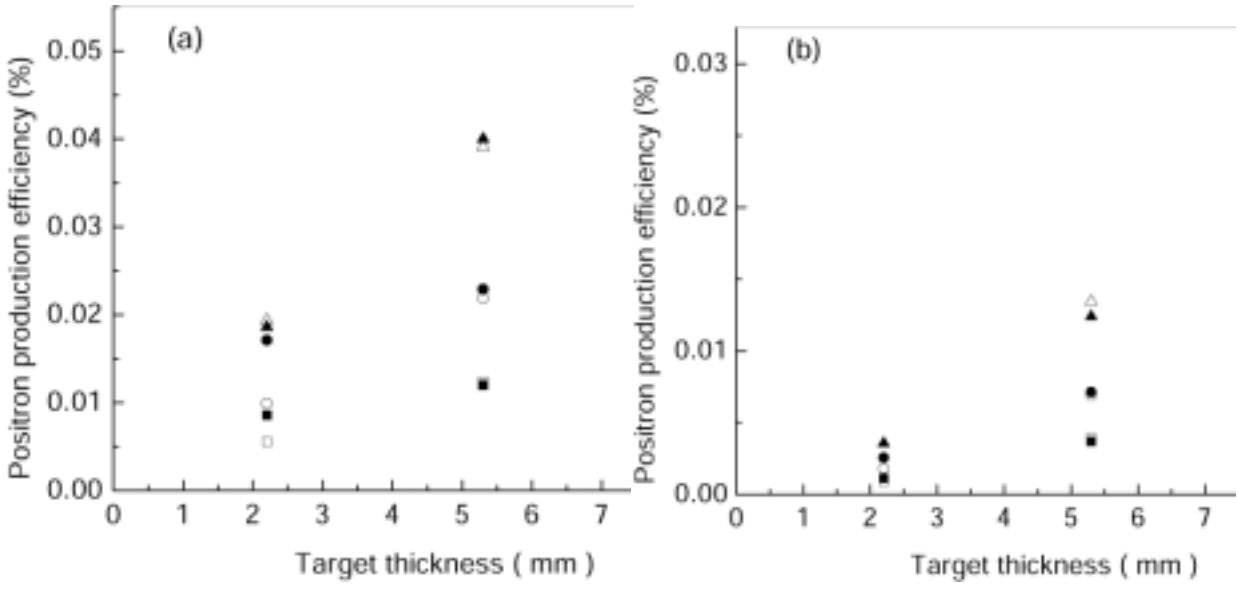

(a) (b)

Fig. 11

Comparison of theory with experiment for positron production from high-energy electrons moving along crystal axes

V. N. Baier and V. M. Strakhovenko
Budker Institute of Nuclear Physics, 630090 Novosibirsk, Russia
(Received 25 September 2002; published 5 December 2002)

Using the approach developed earlier for the description of the electron-photon showers in axially aligned single crystals, some characteristics of the positron yield measured in recent experiments are calculated. Theoretical estimations display a rather good agreement with experimental results obtained using 3 to 10 GeV electrons aligned to the $\langle 111 \rangle$ axis of the tungsten crystals. Such comparison verified that the accuracy of our approach is quite sufficient to make a reliable choice for optimal parameters of the positron source using axially aligned crystals for future linear colliders.

DOI: 10.1103/PhysRevSTAB.5.121001 PACS numbers: 12.20.Ds, 03.65.Sq

I. INTRODUCTION

An efficient positron source is one of the important components of future electron-positron colliders. Positrons are generated from electrons in the course of the $e^- e^+ \gamma$ shower developing in a medium. In a high-energy region, the basic processes involved in the shower development are typically considerably enhanced in oriented crystals as compared with corresponding amorphous media. The most pronounced effects take place at axial alignment when initial electrons are moving along the main axes of a crystal. This alignment alone will be considered below. According to [1], the radiation intensity in a crystal exceeds that of the conventional bremsstrahlung starting with electron energies $\varepsilon \sim 1$ GeV. Simple estimations of the width of the power spectrum indicated a soft character of this spectrum. So the use of high-energy electrons impinging on the axially oriented crystals "... as a source of hard and directed radiation concentrated within a comparatively narrow frequency range ..." was proposed in [1]. Based on mentioned properties of the photon emission process, the use of this phenomenon in the positron source for future accelerators was proposed [2,3]. The pair production rate which is due to the coherent (crystal) effects exceeds that of the standard (Bethe-Heitler) mechanism starting with photon energies $\omega \simeq \omega_{th}$. The value of ω_{th} is about 22 GeV for the $\langle 111 \rangle$ axis of tungsten being several times larger for other crystals. (See the review [4] and the recent book [5] for further details concerning QED processes in crystals.) For energies well above ω_{th}, the crystal effects become really strong and may be used to create effective and compact electromagnetic calorimeters [6]. For very high energies ($\varepsilon \gg \omega_{th}$) of initial and created particles, kinetic equations describing the shower development were solved analytically [7]. Though the initial electron energies were high enough in the first experimental investigation [8] of shower formation in crystals, energies of detected particles were too low to allow us the direct comparison with [7]. To explain the results of [8], Monte Carlo simulations were performed in [9]. The probabilities of basic processes used in [9] were obtained within so-called constant field approximation. A good agreement was demonstrated in [9] with the results of [8] for Ge crystals.

When the initial electron energy is below ω_{th}, photons are mainly emitted with energies $\omega \ll \omega_{th}$ and so, up to minor modifications (see [10,11]), the pair production process proceeds in a crystal as in an amorphous medium. The enhancement of radiation from initial electrons is thereby the main crystal effect in this energy region. The substantial advance in the description of shower formation at axial alignment was caused by the invention of the semiphenomenological radiation spectrum [12]. This allows one to consider the relatively low (of a few GeV) energy range of the initial electrons which is presumed for the efficient positron source. The radiation intensity increases with the initial electron energy. As a result, at some energy the effective radiation length $L_{\rm ef}$ in the crystal becomes smaller than the conventional radiation length $L_{\rm rad}$ and continues its decrease at further increase of the energy. All numerical examples will be given below for the electron beam aligned with the $\langle 111 \rangle$ axis of the tungsten crystals. Then we have for the quantity $L_{\rm ef}$ defined as in Sec. 3 of [12]: $L_{\rm ef}(1\ \text{Gev}) \simeq 0.166$ cm, $L_{\rm ef}(4\ \text{Gev}) \simeq 0.084$ cm, and $L_{\rm ef}(8\ \text{Gev}) \simeq 0.061$ cm. In the hybrid target which consists of the crystal part followed by the amorphous one, the thickness of the crystal constituent of several $L_{\rm ef}$ is obviously quite enough. Indeed, at the depth $L_0 \approx (3\text{–}4)L_{\rm ef}$ most of the particles, including the initial electrons, are sufficiently soft to reduce the coherent contribution to the radiation to the level of the incoherent one. Thereby, the further development of the shower proceeds more or less in the same way for the crystal or amorphous type of the remaining part of the target. We emphasize that the crystal part $L \leq L_0$ of the target serves as the radiator, and secondary charged particles are still not so numerous at this stage of the shower development. Therefore only a small portion of the total energy loss is deposited in the crystal part of the target which considerably reduces a danger of its

overheating. The softness of the photon spectra is another important feature of the crystal radiator giving additional advantages for the positron production in comparison with the entirely amorphous target. To get a more definite idea concerning the shape of the power spectrum one can use its explicit form given by Eq. (2) in [12]. To present the scale, let us list some values $\omega_{\max}$ where this spectrum is maximum: $\omega_{\max}(1\ \mathrm{GeV}) \simeq 31$ MeV, $\omega_{\max}(4\ \mathrm{GeV}) \simeq 170$ MeV, and $\omega_{\max}(8\ \mathrm{GeV}) \simeq 490$ MeV. Note that the width of the spectrum is typically several times larger than $\omega_{\max}$. The increase in the number of relatively soft photons turns out to be much more pronounced than that in the total radiation intensity. In the end, just this fact leads to the substantial enhancement of the positron yield from crystal targets.

Recently the positron production in axially aligned single crystals was studied in two series of experiments performed at CERN [13,14] and KEK [15,16]. The initial energy of electrons was 3 GeV [15], 6 and 10 GeV [14], 8 GeV [16], and 10 GeV [13]. In all cases the initial electron beam was aligned with the $\langle 111 \rangle$ axis of the tungsten crystal that sometimes served as the crystal part of the hybrid target which contained an additional amorphous tungsten target. A noticeable enhancement of the low-energy positron yield was observed in all experiments cited above when the yield from the crystal target was compared with that from the amorphous target of the same thickness. The experimental results and our theoretical estimations presented in the next section display a rather good agreement with each other.

II. COMPARISON OF THEORY WITH EXPERIMENT

Theoretical results for the conditions of the experiments cited above were obtained using the approach developed in [11,12] where various positron and photon distributions as well as deposited energies in different crystals were calculated for the energy range of initial electrons from 2 to 300 GeV. In these papers, all the formulas used in Monte Carlo simulations of the specific $e^- e^+ \gamma$-shower characteristics are given in the explicit form. Remember that our simplified description of the shower development takes into account coherent induced by the regular motion of particles in the field of crystal axes) and incoherent like that in an amorphous medium) mechanisms of photon emission and pair production processes. The multiple scattering and the ionization energy loss of electrons and positrons are taken into account neglecting crystal effects. The coherent radiation from channeling and moving not very high above the axis potential barrier particles is described using the semiphenomenological spectrum suggested in [12]. The corresponding computer code was developed. This allows one to calculate energy, angular, and coordinate distributions of positrons emergent from the crystal or hybrid target and to find an amount of the energy deposition. We think that the investigation of such distributions should be the main object of the experiments having the creation of the crystal assisted positron source as their ultimate aim.

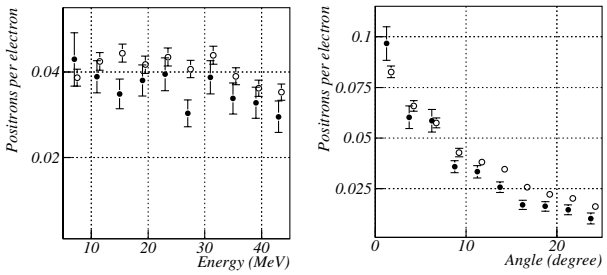

FIG. 1. Spectral (top) and angular (bottom) distributions of positrons from 10 GeV electrons traversing a 8-mm-thick crystal tungsten target along the $\langle 111 \rangle$ axis. Open circles: simulation; filled circles: experiment.

A. Experiment (CERN) at $\varepsilon_0 = 10$ GeV

Among experiments cited above, spectral-angular distributions of created positrons were measured only in the WA103 experiment at CERN (see [13,14]), where our code was used in simulations as the event generator. This simulation allowed for the acceptance conditions and the efficiency of the detectors used. Shown in Fig. 1 taken from [14] is one example of the measured and simulated distributions of positrons from 10 GeV electrons aligned with the $\langle 111 \rangle$ axis of the 8 mm-thick crystal tungsten.

The angular acceptance conditions in the WA103 experiment were approximately $|\vartheta_V^{\mathrm{out}}| \leq 1.5°$ for the vertical and $0 \leq \vartheta_H^{\mathrm{out}} \leq 25°$ for the horizontal angle of the outgoing positron with respect to the initial electron beam direction. We shall see below that the shape of the positron spectrum depends on the degree of collimation. The one-dimensional (over $\vartheta_H^{\mathrm{out}}$) angular distribution is presented for positrons having energies in the 5–45 MeV range. We emphasize that the relative difference between measured and simulated results typically does not exceed 20% in both spectral and angular distributions as seen in Fig. 1. We are aware that preliminary results for other settings used in the same experiment do not contradict with the estimated scale of the difference between the data and theoretical predictions. We hope that this interrelation will not become worse after performing the complete analysis of the data which now is underway. This analysis will also give more detailed information concerning spectral-angular distributions of positrons depending on initial electron energies and target thicknesses.

B. Experiment (KEK) at $\varepsilon_0 = 3$ GeV

The main goal of the experiment [15] was an attempt to apply the crystal target to the working electron/positron

linac, the injector for the electron-positron collider B-Factory at KEK. Thus, the acceptance conditions for created positrons were determined by the momentum acceptance of the positron linac with the matching section which is $8.2 < p < 11.6$ MeV/c and $p_\perp < 2.4$ MeV/c. The hybrid target used consists of 1.7-mm-thick tungsten crystal followed by 7-mm-thick amorphous tungsten. The observed positron yield was enhanced by the factor 1.40 when the $\langle 111 \rangle$ crystal axis was aligned with 3 GeV incident electron beam as compared to the case of the disoriented crystal. Our number for this enhancement is 1.47 being only 5% larger than the experimental one. Note that in the experiment [15] the crystal and amorphous parts of the hybrid target were separated by the distance of 70 mm. This circumstance, which, in principle, may slightly change the enhancement value, was not taken into account in our calculation. Recollect that the amount of the energy deposited in the crystal part ($\varepsilon_{\rm dep}^{\rm cr}$) of the hybrid target may be much smaller than that ($\varepsilon_{\rm dep}^{\rm am}$) in the amorphous one. Such interrelation of $\varepsilon_{\rm dep}^{\rm cr}$ and $\varepsilon_{\rm dep}^{\rm am}$ should take place in the case of [15], where the crystal thickness is about 1.8 $L_{\rm ef}$ (see the discussion in the Introduction). This is confirmed by our calculations which give $\varepsilon_{\rm dep}^{\rm cr} \simeq 11$ MeV and $\varepsilon_{\rm dep}^{\rm am} \simeq 277$ MeV per one incident electron.

C. Qualitative features of positron distributions and experiment (KEK) at $\varepsilon_0 = 8$ GeV

In [16] the positron production efficiency from 2.2, 5.3, and 9.0-mm-thick tungsten crystals was measured using an 8-GeV electron beam. Positrons produced in the forward direction with momenta 10, 15, and 20 MeV/c were detected by the magnetic spectrometer. Thus, several points in the energy distribution were determined under hard collimation conditions. To give an idea of spectral-angular distributions on the whole, let us remind their important qualitative features using 8 GeV electrons and the $\langle 111 \rangle$ axis of the tungsten crystals as an example. For the sake of comparison, the corresponding distributions for amorphous tungsten will be presented as well. Below all the quantities characterizing the positron yield are normalized per one incident electron.

The use of matching systems implies some collimation (typically $\vartheta_{\rm out} \leq 25°$) of outgoing positrons. Shown in Fig. 2 is the energy dependence (energy step is equal to 10 MeV) of the positron yield from crystal (a) and amorphous (b) targets of the same thickness $L = 2.2$ mm. In the case of the hard collimation, when $\vartheta_{\rm out} \leq 1°$ (open circles), the yield is multiplied by 10 to make it visible. The larger the positron energy, the smaller the typical value of $\vartheta_{\rm out}$ since both production and multiple scattering processes are characterized by smaller angles for higher energies. This is seen in Fig. 2(a) where the spectral curves for $\vartheta_{\rm out} < 180°$ and that for $\vartheta_{\rm out} \leq 24°$ are overlapping within precision better than 1% starting from $\varepsilon_{\rm cr}^{(1)} \simeq 55$ MeV. In turn, from $\varepsilon_{\rm cr}^{(2)} \simeq 110$ MeV the same happens with curves corresponding to $\vartheta_{\rm out} \leq 24°$ and $\vartheta_{\rm out} \leq 12°$. Such behavior is also seen in Fig. 2(b) for the amorphous target where $\varepsilon_{\rm am}^{(1)} \simeq 50$ MeV and $\varepsilon_{\rm am}^{(2)} \simeq 105$ MeV.

In other words, positrons with energies $\varepsilon > \varepsilon^{(1)}$ are practically concentrated within the cone $\vartheta_{\rm out} \leq 24°$ and those with $\varepsilon > \varepsilon^{(2)}$ have $\vartheta_{\rm out} \leq 12°$. In accordance with this picture, the spectral maximum is shifted to the right while the width of the distribution increases when the collimation angle decreases. The enhancement μ, being a bin-by-bin ratio of the positron yield from the crystal target to that from the amorphous one at the same collimation, is almost constant for $\varepsilon < 45$ MeV and monotonically decreases with growing positron energy. This means that positron spectra from the crystal target are softer. Somewhat lower values of $\varepsilon^{(1)}$, $\varepsilon^{(2)}$ in the amorphous case point at the same feature. For given collimation, the variation of the enhancement is about 20% over the whole energy interval presented in Fig. 2. The maximum values of the enhancement at different collimation are $\mu_{\rm max}(\vartheta_{\rm out} \leq 180°) \simeq 6.09$, $\mu_{\rm max}(\vartheta_{\rm out} \leq 24°) \simeq 5.92$,

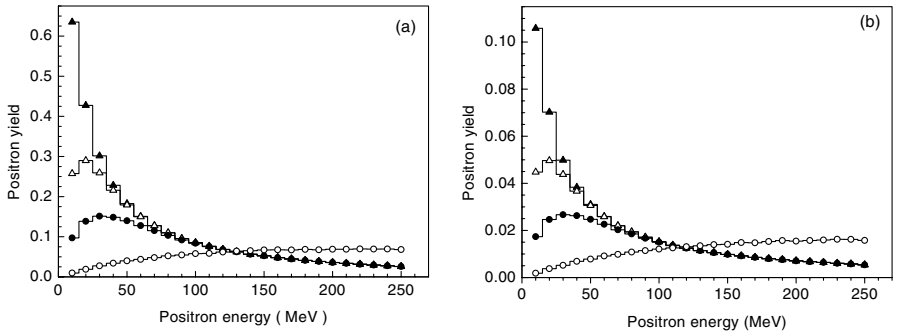

FIG. 2. Positron yield depending on energy from 2.2-mm-thick crystal (a) and amorphous (b) targets at different collimation. Filled triangles: no collimation ($\vartheta_{\rm out} \leq 180°$); open triangles: $\vartheta_{\rm out} \leq 24°$; filled circles: $\vartheta_{\rm out} \leq 12°$; and open circles: $\vartheta_{\rm out} \leq 1°$ (multiplied by 10).

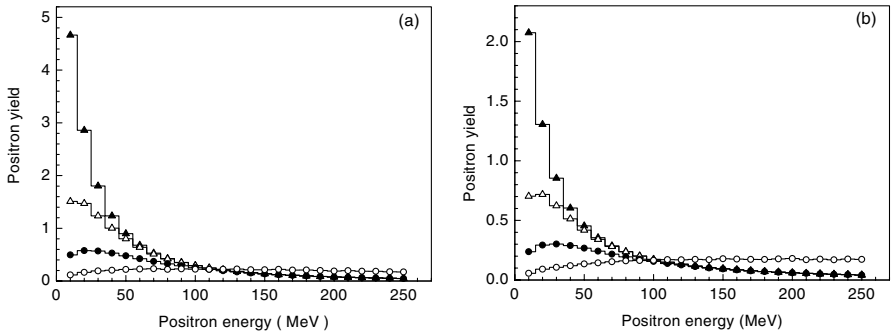

FIG. 3. Positron yield depending on energy from 9.0-mm-thick crystal (a) and amorphous (b) targets at different collimation. Filled triangles: no collimation ($\vartheta_{\text{out}} \leq 180°$); open triangles: $\vartheta_{\text{out}} \leq 24°$; filled circles: $\vartheta_{\text{out}} \leq 12°$; and open circles: $\vartheta_{\text{out}} \leq 1°$ (multiplied by 30).

$\mu_{\max}(\vartheta_{\text{out}} \leq 12°) \simeq 5.67$, and $\mu_{\max}(\vartheta_{\text{out}} \leq 1°) \simeq 5.29$. Apparently, they diminish as the collimation angle does so.

Figure 3 is the same as Fig. 2 but for the target thickness $L = 9.0$ mm. The yield at $\vartheta_{\text{out}} \leq 1°$ (open circles) is multiplied now by 30. The qualitative behavior of spectra depending on the collimation angle at $L = 9.0$ mm is the same as at $L = 2.2$ mm. However, all the spectra become softer for the larger target thickness. This is indicated already by the increase in $\varepsilon^{(1)}$, $\varepsilon^{(2)}$ values which are now $\varepsilon_{\text{cr}}^{(1)} \simeq 85$ MeV, $\varepsilon_{\text{cr}}^{(2)} \simeq 185$ MeV, $\varepsilon_{\text{am}}^{(1)} \simeq 75$ MeV, and $\varepsilon_{\text{am}}^{(2)} \simeq 165$ MeV. It is clear that the magnitude of the yield from the thicker target is essentially larger but this increase is different in the crystal and amorphous cases. For example, in the energy range $\varepsilon < 45$ MeV, the yield is increased by 6–7 times for a crystal and by 17–20 times for amorphous samples. As a result, the enhancement at $L = 9.0$ mm is almost 3 times less than at $L = 2.2$ mm in this energy range. At $L = 9.0$ mm the enhancement is peaked in the first bin [$\varepsilon \in$ (5–15) MeV] for every collimation. Its maximum values are $\mu_{\max}(\vartheta_{\text{out}} \leq 180°) \simeq 2.25$, $\mu_{\max}(\vartheta_{\text{out}} \leq 24°) \simeq 2.15$, $\mu_{\max}(\vartheta_{\text{out}} \leq 12°) \simeq 2.08$, and $\mu_{\max}(\vartheta_{\text{out}} \leq 1°) \simeq 2.06$. The enhancement monotonically decreases with growing positron energy and approximately halves at $\varepsilon \approx 250$ MeV. Thus, positron spectra from the crystal target are softer at $L = 9.0$ mm as well, and this property is much more pronounced in comparison with $L = 2.2$ mm.

Matching systems can be characterized also by the maximum transverse momentum $p_{\perp}^{\max}$ of accepted positrons. In this connection, spectra of positrons having $p_{\perp} < p_{\perp}^{\max}$ are of undoubted interest. Such spectra at $L = 2.2$ mm (a) and at $L = 9.0$ mm (b) from crystal and amorphous targets are shown in Fig. 4.

In contrast to the case of the pure angular selection (cf. Figs. 2 and 3), the position of spectral maxima at limited $p_{\perp}$ values is always in the first bin [$\varepsilon \in$ (7.5–12.5) MeV]. Corresponding maximum values are $\mu_{\max}(5\ \text{MeV}/c) \simeq 5.82$, $\mu_{\max}(2.5\ \text{MeV}/c) \simeq 5.62$ at $L = 2.2$ mm, and $\mu_{\max}(5\ \text{MeV}/c) \simeq 2.17$, $\mu_{\max}(2.5\ \text{MeV}/c) \simeq 2.11$ at $L = 9.0$ mm. The enhancement monotonically decreases with growing positron energy. Its variation over the whole energy interval presented in Fig. 4 is about 15% at $L = 2.2$ mm and 40% at $L = 9.0$ mm. So, for this selection too, positron spectra from crystal targets are softer than those from amorphous targets of the same thickness. The interesting feature of spectral curves in Fig. 4 is the similarity of those obtained for two different values of

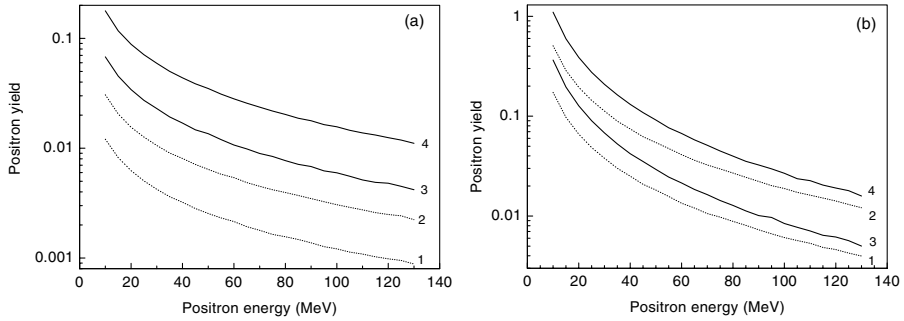

FIG. 4. Positron yield depending on energy at $L = 2.2$ mm (a) and $L = 9.0$ mm (b) for $p_{\perp}^{\max} = 2.5\ \text{MeV}/c$ (curves 1 and 3) and for $p_{\perp}^{\max} = 5\ \text{MeV}/c$ (curves 2 and 4). Solid curves represent the yield from crystal and dotted curves from amorphous targets.

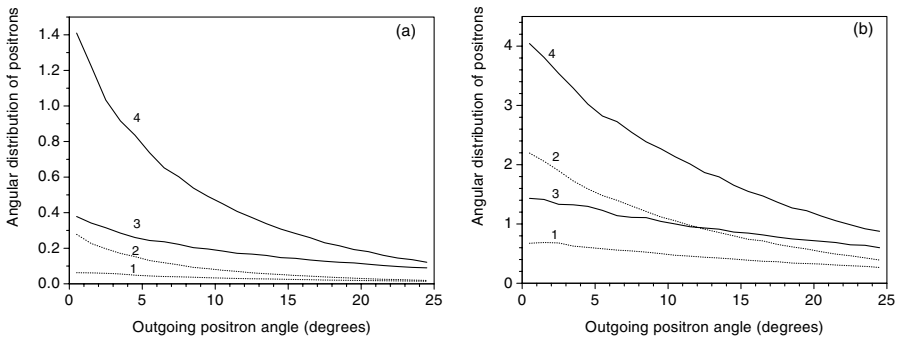

FIG. 5. Angular distribution $dN^{(+)}/d\Omega$ depending on outgoing positron angle at $L = 2.2$ mm (a) and at $L = 9.0$ mm (b) for $p \in (8.5\text{–}11.5)$ Mev/c (curves 1 and 3) and for $p \in (17\text{–}23)$ Mev/c (curves 2 and 4). Solid curves represent the yield from crystal and dotted curves from amorphous targets.

$p_{\perp}^{\max}$ from the same target. The scaling factors η are $\eta_{\rm cr} \simeq 2.6$, $\eta_{\rm am} \simeq 2.5$ at $L = 2.2$ mm and $\eta_{\rm cr} \simeq 3.1$, $\eta_{\rm am} \simeq 3.0$ at $L = 9.0$ mm. These factors turn out to be practically (within an accuracy of a few percent) independent of the total positron momentum p. This fact can be easily understood if we assume that the width of the angular distribution of positrons is completely due to multiple scattering being, thereby, proportional to p^{-1}. Such an assumption is confirmed by results of the calculation shown in Fig. 5 for two groups of positrons. One of them contains positrons having momentum in the interval $p \in (8.5\text{–}11.5)$ Mev/c, for another group $p \in (17\text{–}23)$ Mev/c.

For the given target, the width of the angular distribution of positrons with $p \approx 10$ Mev/c is approximately twice as much that for $p \approx 20$ Mev/c as expected. The width of every distribution evidently increases when we go on to the thicker target of the same kind. Comparing angular distributions from crystal and amorphous targets of the same thickness, we find that at $L = 9.0$ mm the distributions are somewhat (about 1.5°) wider in the crystal case for both groups. In units of FWHM of the distribution from the crystal target these differences are about 6.5% at $p \approx 10$ Mev/c and 14% at $p \approx 20$ Mev/c. At $L = 2.2$ mm the distribution from the crystal target is wider by 15.5% at $p \approx 20$ Mev/c whereas this is narrower by 10% at $p \approx 10$ Mev/c.

Going on to the comparison of our results with those obtained in [16], let us remember that to perform an accurate comparison of such kind, exact information is needed concerning the acceptance conditions and registration efficiency of detectors in the experiment. As noted in [16], at $p = 20$ Mev/c, the momentum acceptance ($\Delta p/p$) was 3% (FWHM) and the polar angle acceptance was less than 20 mrad (FWHM). Since the shape of the acceptance curves was unavailable to us, we have tried to simulate experimental conditions using the same angular collimation $\vartheta_{\rm out} \leq \vartheta_{\rm out}^{\max}$ and the same value of $\Delta p/p$ for all momenta and targets. So, at the calculation of the magnitudes of positron production efficiency (PPE), we simply put $\vartheta_{\rm out}^{\max}$ to 20 mrad. The value of $\Delta p/p$ was chosen to reproduce at applied collimation the experimental magnitude of PPE for the 9.0-mm-thick amorphous target. Acting in this way, we have $\Delta p/p = 3.2\%$. We realize that our regard for the acceptance conditions is rather rough. An additional inaccuracy was introduced

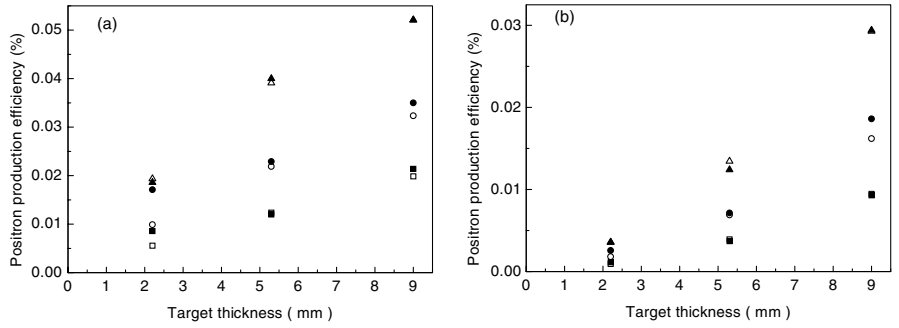

FIG. 6. Positron production efficiency from crystal (a) and amorphous (b) targets depending on thickness. Open symbols: our calculation; filled symbols: results from Fig. 5 of [16]; open triangles are for $p = 20$ Mev/c, open circles are for $p = 15$ Mev/c, and open squares are for $p = 10$ Mev/c.

TABLE I. Enhancement of the positron yield from crystal targets.

Momentum (MeV/c)	Enhancement (2.2 mm thick) Theory	Enhancement (2.2 mm thick) Experiment	Enhancement (5.3 mm thick) Theory	Enhancement (5.3 mm thick) Experiment	Enhancement (9.0 mm thick) Theory	Enhancement (9.0 mm thick) Experiment
10	6.0 ± 0.5	6.5 ± 0.6	3.2 ± 0.3	3.4 ± 0.7	2.1 ± 0.2	2.3 ± 0.4
15	5.5 ± 0.3	6.2 ± 0.8	3.2 ± 0.2	3.2 ± 0.5	2.0 ± 0.1	2.0 ± 0.2
20	5.4 ± 0.2	5.1 ± 0.5	2.9 ± 0.1	3.0 ± 0.5	1.8 ± 0.1	1.8 ± 0.2

when we determined the PPE numbers from Fig. 5 of [16]. Note that the experimental numbers obtained in such a way, which are presented by filled symbols in Fig. 6, do not reproduce exactly the whole set of mean experimental values for the enhancement given in Table I of [16]. Moreover, in Fig. 5 of [16] there are no experimental points for 2.2 and 5.3-mm-thick amorphous targets. For these two cases, we present in Fig. 6 the values of PPE given by smooth-curve fits corresponding to simulation fitting in Fig. 5 of [16]. Bearing all this in mind, we, nevertheless, can assert that a rather good agreement is seen in Fig. 6 of the experimental results and our estimations. A relative difference of them is better than 13% everywhere except the values of PPE at $p = 10$ and 15 Mev/c from both thinnest ($L = 2.2$ mm) targets, where the experimental yield is underestimated by 19% to 42%. Note that just for this thickness the largest inaccuracy was introduced while determining the PPE numbers from Fig. 5 of [16] at $p = 10$ and 15 Mev/c, as the magnitude of the yield is especially small in this case.

In contrast to the magnitude of the positron yield, the enhancement is not very sensitive to the acceptance conditions. The calculated values of the enhancement (theory) are presented in Table I along with those taken from Table I of [16] (experiment). Purely statistical errors are figured in Table I as theoretical ones. The relative error in PPE was estimated as $N_{\mathrm{ef}}^{-1/2}$, where N_{ef} is the mean number of events in the phase space corresponding to the acceptance conditions used in calculations. The total statistics was chosen so that approximately to equalize values of N_{ef} for amorphous and crystal targets of the same thickness. At given total statistics, the quantity N_{ef} increases with growing positron momentum in accord with a shape of the positron spectra at hard collimation shown in Figs. 2 and 3. This fact leads to a better statistical accuracy for larger momentum. We emphasize that the differences of the estimated and experimental enhancement values are smaller than corresponding experimental errors for all momenta and samples figured in Table I.

III. CONCLUSION

Using the simple computer code suggested in [11,12], we have compared the theoretical predictions for some characteristics of the electromagnetic shower developing in axially aligned crystals with experimental results reported in [13,14,15,16]. On the whole, theory and experiment are consistent within the experimental accuracy. From this comparison we also conclude that the accuracy provided by the existing simplified code is at least better than 20%. This accuracy may be slightly improved if we include into consideration some processes like annihilation of positrons or Compton scattering of photons which were ignored as corresponding cross sections are small in the energy region of interest. However, the approximate character of the radiation spectra at axial alignment used in our calculations still provides the main theoretical uncertainty. Nevertheless, we believe that the level of the accuracy already achieved in the theoretical description is quite sufficient to make a reliable choice for optimal parameters of the positron source using axially aligned single crystals.

ACKNOWLEDGMENTS

We are grateful to Professor H. Okuno for providing us with details of the experiment [16] and to the authors of [14] for numerous fruitful discussions. Support of this work by the Russian Fund of Basic Research under Grants No. 00-02-18007, No. 01-02-16926, and No. 01-02-22003 is also gratefully acknowledged.

[1] V. N. Baier, V. M. Katkov, and V. M. Strakhovenko, Phys. Status Solidi (b) **133**, 583 (1986).
[2] R. Chehab *et al.*, in *Proceedings of the IEEE Particle Accelerator Conference, Chicago, 1989* (IEEE, Piscataway, NJ, 1989), pp. 283–285.
[3] V. N. Baier and R. Chehab, Positron Source based on Channeling Radiation, Proposal for an Experiment at Orsay, LAL, Orsay, France, 1990 (unpublished).
[4] V. N. Baier, V. M. Katkov, and V. M. Strakhovenko, Sov. Phys. Usp. **32**, 972 (1989).
[5] V. N. Baier, V. M. Katkov, and V. M. Strakhovenko, *Electromagnetic Processes at High Energies in Oriented Single Crystals* (World Scientific, Singapore, 1998).
[6] V. N. Baier, V. M. Katkov, and V. M. Strakhovenko, Nucl. Instrum. Methods Phys. Res., Sect. A **250**, 514 (1986).
[7] V. N. Baier, V. M. Katkov, and V. M. Strakhovenko, Nucl. Instrum. Methods Phys. Res., Sect. B **27**, 360 (1987).
[8] R. Medenwaldt *et al.*, Phys. Lett. B **227**, 483 (1989).
[9] V. N. Baier, V. M. Katkov, and V. M. Strakhovenko, Nucl. Instrum. Methods Phys. Res., Sect. B **119**, 131 (1996).

[10] V. N. Baier, V. M. Katkov, and V. M. Strakhovenko, Phys. Status Solidi (b) **149**, 403 (1988).
[11] V. N. Baier and V. M. Strakhovenko, Nucl. Instrum. Methods Phys. Res., Sect. B **155**, 403 (1999).
[12] V. N. Baier, V. M. Katkov, and V. M. Strakhovenko, Nucl. Instrum. Methods Phys. Res., Sect. B **103**, 147 (1995).
[13] R. Chehab *et al.*, in *Proceedings of the LINAC2000, Monterey, CA, 2000* (Stanford Linear Accelerator Center, Stanford, CA, 2000), p. 143.
[14] R.Chehab *et al.*, in Proceedings of the RREPS-01 Conference, Lake Aya, Russia, 2001 [Nucl. Instrum. Methods Phys. Res., Sect. B (to be published)].
[15] M. Inoue *et al.*, Nucl. Instrum. Methods Phys. Res., Sect. B **173**, 104 (2001).
[16] H.Okuno *et al.*, in Proceedings of the RREPS-01 Conference, Lake Aya, Russia, 2001 (Ref. [14]); KEK Report No. 2001-146, 2001.

POSITRON-PRODUCTION EXPERIMENT USING SILICON AND DIAMOND CRYSTALS IN THE KEKB 8-GEV INJECTOR LINAC

Tsuyoshi Suwada†, KEK, Tsukuba, Ibaraki, 305-0801 Japan.

Abstract

Intense positron sources are widely investigated for the next-generation of linear colliders and B-factories. A new method utilizing an axially-oriented crystal as a positron-production target is one of the bright schemes since it provides a powerful photon source through channeling and coherent bremsstrahlung processes when high-energy electrons penetrate the target. A series of positron-production experiments with heavy and light crystals hit by 4 and 8-GeV single-bunch electron beams have been carried out at the KEKB 8-GeV injector linac. This report gives the brief summary on the positron-production experiment using silicon and diamond crystals carried out in December 2002 at KEK. Later the report based on the more precise analysis will be published elsewhere.

1 INTRODUCTION

For future e^+e^- linear colliders and high-luminosity B-factories, it is critically important to develop a high-intensity positron source. In a conventional method using an amorphous heavy-metal target, the target thickness is optimized by taking into account the electromagnetic shower process and the positron capture efficiency in the succeeding acceleration section. The optimum thickness is 4-5 X_0 (radiation length) for a 4-8 GeV electron beam. In this case, the only possibility to increase the positron intensity is to increase the incident electron intensity. However, the electron intensity is limited due to a heat load on the target. One promising method utilizing a crystal target was proposed by Chehab *et al*. in 1994[1]. The benefit of this method is on its high positron-production efficiency due to channeling radiation (CR)[2] and coherent bremsstrahlung (CB), since CR and CB increase low-energy photons in the radiation process. This results in a thinner target compared with the conventional method. It is also expected that the thin target relaxes its heat load, and that the spatial spread of positrons due to multiple scattering in the target is reduced. Yoshida *et al*. demonstrated a clear enhancement of the positron yield in a tungsten crystal target using a 1.2-GeV electron beam[3]. This new scheme has been tested at the positron-production station and the end station of the KEKB injector linac[4]. Chehab *et al*. also studied the positron yield from a crystal target for 5-40 GeV electrons at CERN-SPS[5].

Although a positron enhancement is observed, there have so far been only a few experimental results over a wide energy range of a primary electron beam.

On the theoretical side, various simulation studies have been carried out by various authors. Among them, Baier, Katkov and Strakhovenko have developed the simulation code of the electromagnetic shower formation at axial alignment of a crystal by using the semi-phenomenological radiation spectrum[6]. This scheme allows one to consider a positron-yield enhancement at the relatively low energy range (a few GeV) of the initial electrons, which is suitable for the B-factory injector. The substantial enhancement of the positron yield from crystal targets is expected due to the increase in the number of relatively soft photons in comparison with that from an amorphous target. Thus, more systematic and precise experimental data could help us to understand the complicated mechanism of these elementary radiation processes and to design a high-intensity positron source. A series of experiments[7,8] to investigate the positron yields using various crystal targets are underway for an incident electron energy lower than 8 GeV. The following table shows a historical view of the positron-production experiments carried out at KEK-Tsukuba and KEK-Tanashi branch.

Table 1: Historical view of the positron-production experiments at KEK.

Month/Year	Accelerator	E [GeV]	Positron Target [mm]
May/1997	Tanashi/ES	1.2	Crystal W (W_c)[1.2]
Apr, Jun /1998	KEK/Linac	3	W_c[1.7] + Amor. W (W_a)[7]
Nov/1998	Tanashi/ES	0.6, 0.8, 1	W_c[0.4, 1.2, 2.2], GaAs[0.36], Diamond[1.1]
Sep, Oct /2000	KEK/Linac	8	W_c[2.2], W_c[2.2]+W_a[5,10,15]
Apr/2001	KEK/Linac	8	W_c[2.2], W_c[9] W_c[9]+W_a[2, 4]
Sep/2001	KEK/Linac	8	W_c[2.2], W_c[5.3], W_c[9] Combined targets
Jan/2002	KEK/Linac	4	W_c[2.2], W_c[5.3], W_c[9] Combined targets
Aug-Sep /2002	KEK/Linac	8	Si [2.6, 30, 48] Diamond[4.57] Combined targets
Dec/2002	KEK/Linac	8	Si [10, 30, 48] Diamond[4.57] Combined targets

†E-mail address: tsuyoshi.suwada@kek.jp.

2 EXPERIMENTAL SETUP

2.1 Beam Line

Our experiment was performed in the beam switchyard of the KEKB 8-GeV injector linac (see Fig.1).

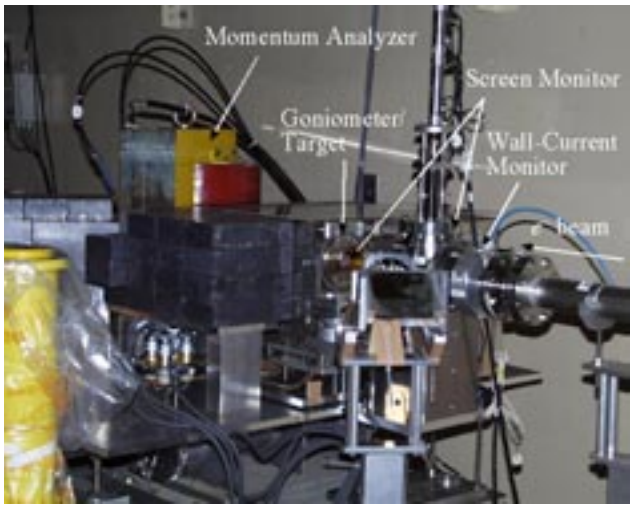

Figure 1: Photograph of the beam line and the experimental setup viewed from the electron beam.

An electron beam with a pulse width of 10 ps (S-band single bunch) and with an energy of 8 GeV impinged on a tungsten target at a repetition rate of 25 Hz. The beam charge (~0.1 nC/bunch) was measured by a wall-current monitor for each pulse. The transverse profile of the electron beam at the target was monitored by a screen monitor during the experiment. The transverse beam size was 0.8 mm (FWHM) in diameter. The angular spreads of the electron beam were expected to be about 22 and 44 μrad in the horizontal (*H*) and vertical (*V*) directions for the 8-GeV electrons, respectively. However, since the electron beam impinged on the target after passing through a vacuum window made of 30μm-thick stainless steel (SUS304), the angular spreads (*H* and *V*) of the electron beam at the target were estimated to be 59 and 70 μrad in total by taking into account the multiple scattering at 8 GeV, respectively. The multiple scattering effect of the vacuum window was investigated by using SUS foils with several thicknesses. These angular spreads were less than the critical angles (170 μrad for Si crystal and 130 μrad for Diamond crystal) of the channeling condition at 8 GeV.

2.2 Experimental Setup

Figure 2 shows a schematic drawing of the experimental setup. This comprises a positron-production target mounted on a precise goniometer, a magnetic spectrometer, collimators, and two kinds of positron detectors (a lead-glass calorimeter and an acrylic Cherenkov counter). All of the collimators and detectors are installed in a vacuum chamber kept at a vacuum pressure of 10^{-1} Pa.

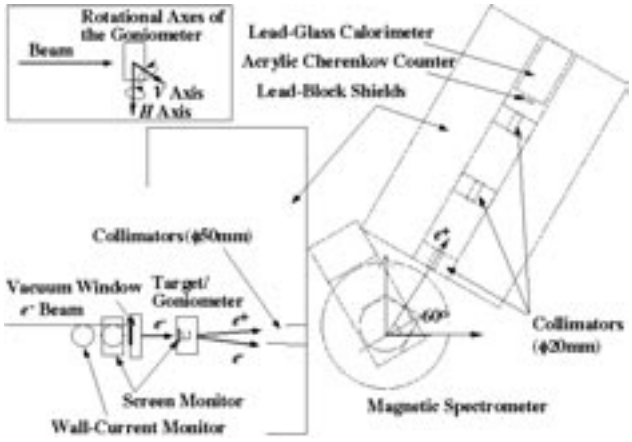

Figure 2: Schematic drawing of the experimental setup.

In this experiment, silicon and diamond crystals of <110> axis with different thicknesses were tested either alone or in combination with an amorphous tungsten plate (W_a). These W_as' with different thicknesses from 3 to 18 mm by 3mm steps are installed on a horizontal movable stage 82.5 mm after the crystal target. These tungsten plates were also used to calibrate the positron yield without the crystal targets. The specification of the crystal targets is summarized in Table 2.

Table 2: Tested crystal specification.

Crystal	Elem.	Denom.	Thickness [mm]	X_0
Diamond	C	5mmDia	4.57	0.0372
Silicon	Si	2.5mmSi	2.55	0.0272
Silicon	Si	10mmSi	9.9	0.1058
Silicon	Si	30mmSi	29.9	0.319
Silicon	Si	50mmSi	48.15	0.514

*$1X_0$=123mm (Diamond), $1X_0$=93.6mm (Silicon). It should be noted that the radiation length of an amorphous carbon (2.3 g/cm^3) is different from that of a diamond crystal (3.5 g/cm^3). This was pointed out by A. Potylitsyn.

The positrons emitted from the target in the forward direction were momentum-analyzed in a momentum range lower than 30 MeV/c by the magnetic field, where the deflection angle was 60^o from the beam axis. The positron trajectory was determined by five collimators installed before and behind the magnetic spectrometer. The geometrical acceptance and momentum acceptance is summarized in Table 3, which were calculated by using the simulation code GEANT3.

The momentum-analyzed positrons were detected with a 3mm-thick acrylic Cherenkov counter and a lead-glass calorimeter shielded by lead blocks. The lead blocks suppressed any background caused by electromagnetic showers generated upstream of the beam line due to the

off-momentum electrons, and caused by electromagnetic showers generated at the collimators. Since the emitted positrons were also shortly bunched, the number of positrons per bunch was measured as a pulse charge from each detector. Signals from the positron detectors and the signal of the electron beam charge were sent to a data-acquisition system using a PC-based CAMAC/ADC system, where all signal charges were simultaneously digitized. The goniometer could rotate the crystal target around two axes (*H* and *V* axes) by a pulse motor. The angular resolutions of the goniometer were 10.5 and 34.9 μrad/pulse in the *H* and *V* axes, respectively. The crystal axis, <110>, was determined by changing the relative rotational angles around the two axes with a step of 2 (or 1) mrad. The positron yields were measured for each target as a function of the rotational angle of the goniometer and as a function of the positron momentum.

Table 3: Acceptance of the positron spectrometer.

Pe^+ (MeV/c)	Acceptance (10^{-4} x (MeV/c•sr))
5	1.08 ± 0.03
10	2.47 ± 0.07
15	3.80 ± 0.10
20	4.81 ± 0.12

3 EXPERIMENTAL RESULTS

3.1 Two-Dimensional Crystal Axis Scan

We developed a computer software which quickly scans a crystal axis in two dimensional plane. The scanning time (10~20 min depending on the step sizes) was much reduced compared with that of the previous one-dimensional scanning. Figures 3(a) and 3(b) show the typical results of the crystal axis scanning measured for the diamond and 30mm-thick silicon crystal, respectively, at the positron momentum of 20 MeV/c.

You can clearly see main sharp peaks for both the crystals generated from the <110> axis orientation together with many weak peaks. The main sharp peak was formed as the intersecting point of the several lines (see the density distribution in the projected plane in Fig.3). These weak peaks or lines may come from plane channeling in the crystal. It is interesting that the number of the weak peaks for the diamond crystal is larger than that of the silicon crystal.

3.2 Rocking Curves

Figures 4(a) (for diamond) and 4(b) (for 30mm-thick silicon) show the measured rocking curves at the positron momentum of 20 MeV/c. You can see very narrow peak widths for both the crystals. The peak widths were obtained to be 0.7 (for diamond) and 1 mrad (for 30mm-thick silicon) in one sigma by the least-squares fitting procedures with two gaussian functions.

Figure 5 shows the variation of the peak width as a function of the crystal thickness in unit of X_0. The peak width increases gradually with the increase of the crystal thickness and its value is about 1 mrad level depending on the crystal thickness.

3.3 Positron-Yield Enhancement

Figure 6 shows the result of the positron-yield enhancement measurement for the crystal alone as a function of the crystal thickness in unit of X_0 at the positron momentum of 20 MeV/c. The enhancement of the silicon crystal changes by a factor of 8-14 depending on the crystal thickness, and for the diamond it is about 17 which is clearly larger than that of the silicon crystals. It means that the crystal effect of the diamond is larger than that of the silicon.

Figure 7 shows the result of the momentum dependence of the positron-production enhancement. The enhancement is slightly dependent on the positron momentum in the measured region.

Figure 8 shows the summarized result of the enhancement measurement together with the tungsten crystal data, which were obtained from the previous experiment. The result shows that although in the region of the thin thickness the enhancement obtained for the light crystals is a little bit high, in the region of the large thickness the enhancement obtained for the tungsten crystals is clearly higher. It is presumed that the channeling photons generated from the light crystal are soft, and thus, the positrons generated in the later amorphous tungsten are absorbed and multiply scattered in the target because they are also soft.

3.4 Positron Yields and Crystal Effect

The detected positron yields were calibrated by using the data from the amorphous tungsten plates with different thicknesses. Figure 9 (a) shows the variations of the positron yield depending on the thickness of the amorphous tungsten plates alone, and they were obtained as the positron-yield calibration data in each crystal measurement. For all the amorphous tungsten data, the positron yield was normalized by using the data of the 9mm-thick amorphous tungsten obtained in the 30mm-thick silicon crystal measurement. Figure 9 (b) shows the variations of the positron yield depending on the total thickness in unit of X_0, where the crystal axis was set in the direction of off axis. These results show that the positron-yield normalization was performed quite well within the experimental accuracy.

Figure 10 shows the summarized result of the normalized positron yield obtained for all the crystal measurements. It is clearly found several following things:

- The maximum positron yield is almost the same level compared with that of the amorphous tungsten except for the data of the 10mm-thick silicon crystal.
- The shower maximum thickness of each crystal is reduced compared with that of the amorphous

tungsten, which means that the radiation thickness is effectively reduced.

- The reduction of the shower maximum thickness of the diamond crystal is relatively large compared with other crystals although the thickness of the diamond is thin.

Figure 11 shows the result of the crystal effect. If we plot the shower maximum peak thickness as a function of the crystal thickness, we can estimate how large the crystal effect is. For the silicon crystal, the effect is saturated around the thickness of 30 mm, and for the diamond crystal, although we have only one data point, the effect is larger than the silicon crystal. This result shows that the maximum positron yield from the 5mm-thick diamond crystal is almost the same level as that of the 30mm-thick silicon crystal, which gives larger crystal effect than that of the diamond even with a 5mm-thcikness. We can expect higher positron-production yield if we use a thicker diamond crystal.

3.5 Effect of the Vacuum Window

Figure 12 shows the result of the positron enhancement measurement depending on the thickness of the vacuum window, where the diamond crystal alone was used in this test. From the result, the enhancement is almost constant up to the window thickness of 200 μm, and the rocking-curve peak width slightly increases with the increase of the window thickness. This may come from the increase of background generated at the window. It is noted that the window thickness of 100 μm has been used in the previous channeling experiment.

4 SUMMARY

The positron-production experiment using diamond and silicon crystal targets has been successfully carried out at the KEKB 8-GeV injector linac. The obtained rocking peak widths are very narrow less than 1 mrad in one sigma for both the crystals. For the crystal target alone, the enhancements of the positron yield are 9.3±0.5 (10mmSi), 9.9±0.5 (30mmSi), 6.4±0.3 (50mmSi), and 16±0.8 (5mmDiamond) at the positron momentum of 20 MeV/c. The enhancement is much reduced with the increase of the total target thickness. The maximum positron yields are the same level as the maximum yield obtained for amorphous tungsten targets.

5 REFERENCES

[1] R.Chehab, Orsay Report No. LAL/RT94-09, 1994.
[2] A.H.Sorensen and E.Uggerhoj, Scientific American June (1989) 70.
[3] K.Yoshida, *et al.*, Phys. Rev. Lett. 80, 1437 (1998).
[4] I. Abe, *et al.*,"The KEKB Injector Linac"; KEK-Preprint-2001-157 (2001); To be published in NIM A.
[5] R. Chehab, *et al.*, RREPS01, Lake Aya, Russia, September 2001, published in NIM **B103** (2003) 243.
[6] V.N. Baier, V.N. Katkov and V.M. Strakhovenko, NIM **B103** (1995) 147.
[7] H. Okuno, *et al.*, RREPS01, Lake Aya, Russia, September 2001, published in NIM **B103** (2003) 259.
[8] T.Suwada, *et al.*, Phys. Rev. **E67**, 016502 (2003).

(a)

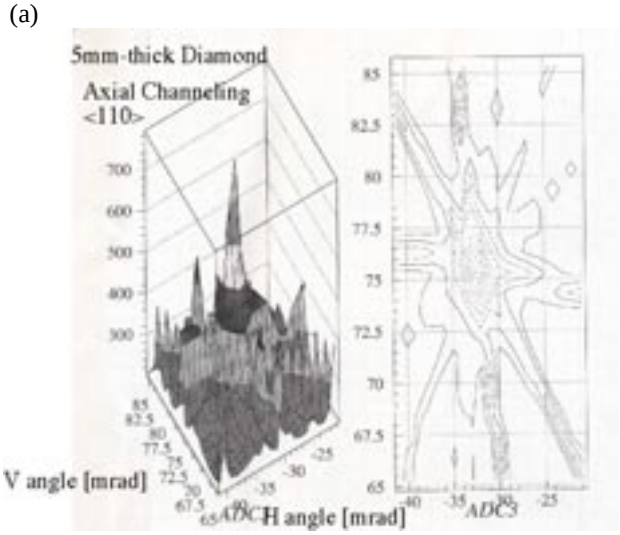

(b)

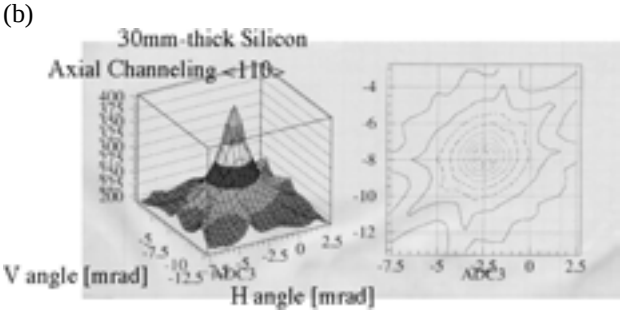

Figure 3: Results of the two-dimensional axis scan for (a) the diamond and (b) silicon crystal. The software of the axis scan was developed by Tokyo Metropolitan Univ.

(a)

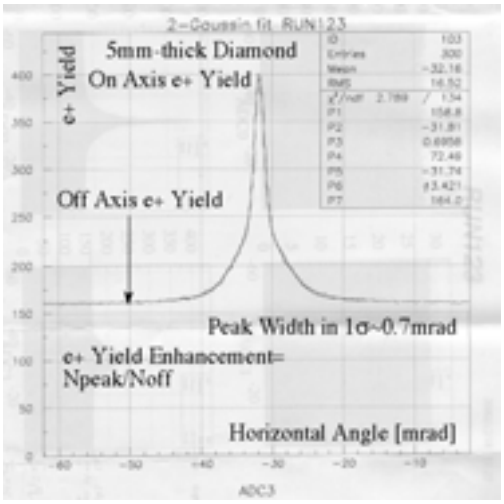

(b)

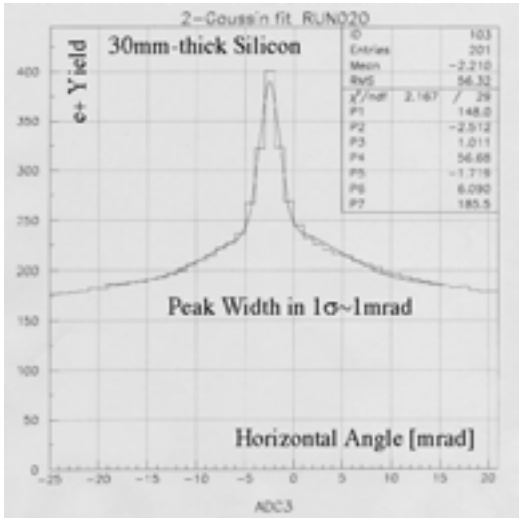

Figure 4: Rocking curves measured for (a) the 5mm-thick diamond and (b) 30mm-thick silicon crystal at the positron momentum of 20 MeV/c.

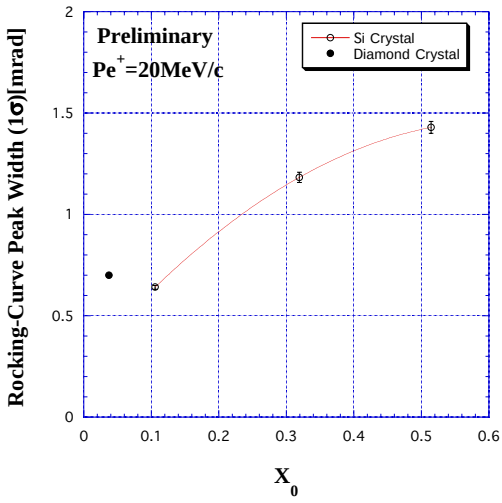

Figure 5: Variations of the rocking-curve peak width measured for (a) the diamond and (b) silicon crystal as a function of the crystal thickness at the positron momentum of 20 MeV/c.

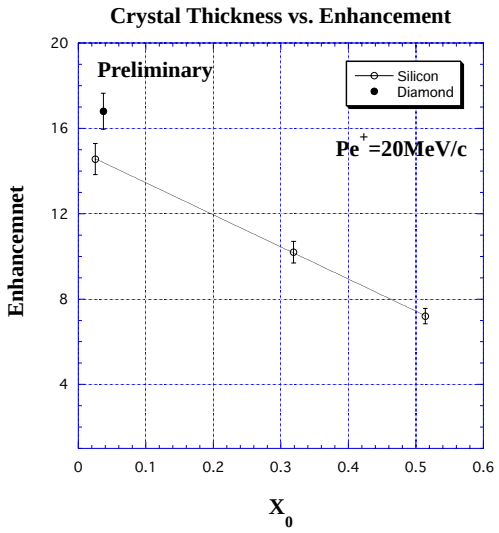

Figure 6: Variations of the positron yield enhancement depending on the crystal alone thickness in unit of X_0 at the positron momentum of 20 MeV/c.

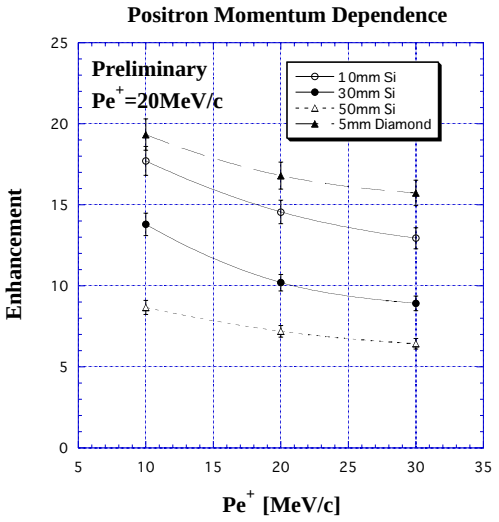

Figure 7: Variations of the enhancement depending on the positron momentum.

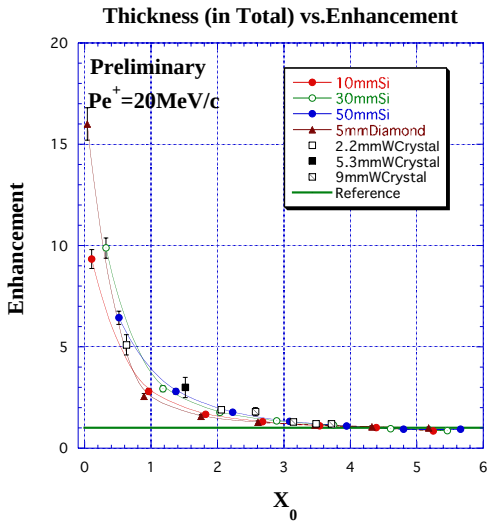

Figure 8: Variations of the positron-yield enhancement depending on the target thickness in total in unit of X_0 at the positron momentum of 20 MeV/c. The crystal tungsten data with three different thicknesses are also added.

(a)

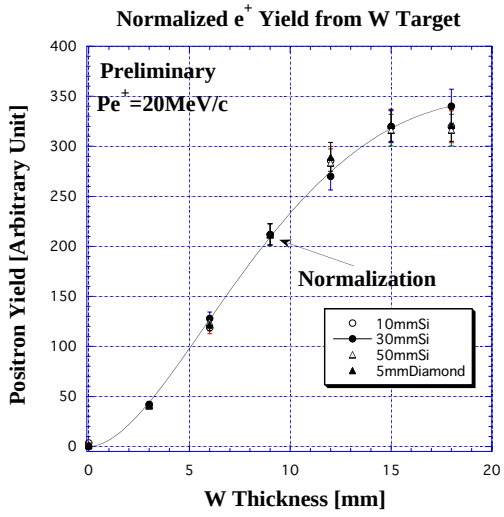

(b)

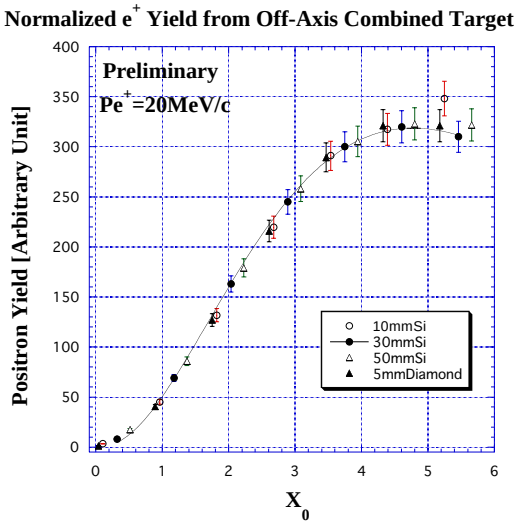

Figure 9: Variations of the shower development curve (positron yield) for (a) the amorphous tungsten plate alone and (b) off-axis combined target depending on the thickness of the combined target at the positron momentum of 20 MeV/c.

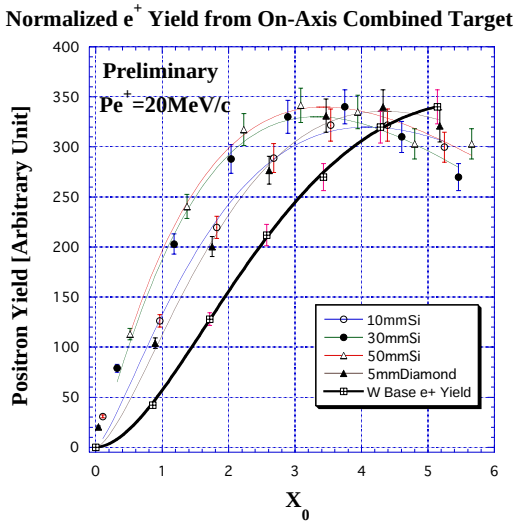

Figure 10: Shower development curves (positron yields) measured for the diamond and silicon crystal as a function of the combined target thickness in total at the positron momentum of 20 MeV/c.

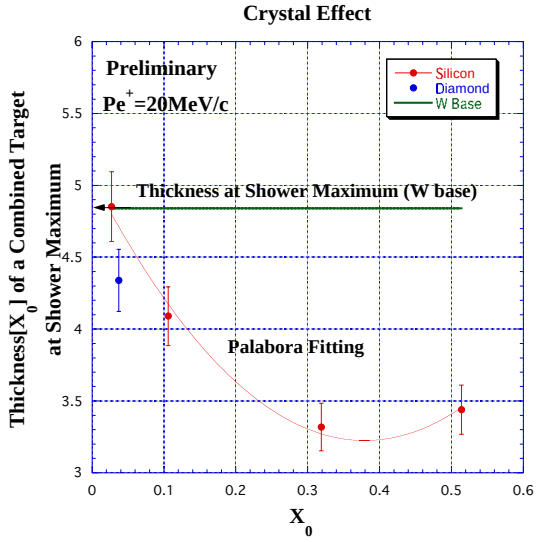

Figure 11: Variations of the crystal effect for the diamond and silicon crystal depending on the crystal thickness.

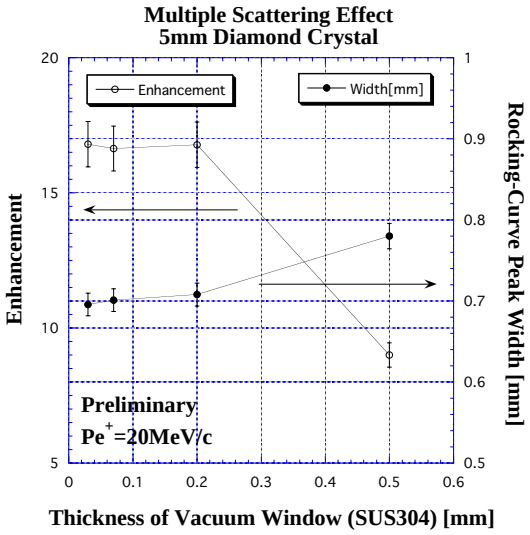

Figure 12: Vacuum-window thickness effect. The effect was estimated by using two parameters “Enhancement” and “Peak width” of the diamond crystal data as a function of the thickness of the vacuum window.

COMPARISON OF UNDULATOR-BASED AND CRYSTAL-BASED POSITRON SOURCES.

A. Potylitsyn

Tomsk Polytechnic University,
Lenin ave., 2A, 634050, Tomsk, Russia

1. A positron source for linear collider has to provide the positron beam intensity close to the electron beam one. Currently there are two approaches to construct a positron source with the required parameters. First one is the conventional source based on an electromagnetic cascade-shower process whereby a heavy-metal target irradiated by high energy electrons from the linear accelerator [1,2]. Among the positrons, only those which have transverse momentum and energy within a certain range are accepted for the consequent acceleration. The target thickness is determined to maximize the number of accelerated positrons, which depends on the incident electron energy. The positron yield is naturally proportional to the incident electron intensity, but when the intensity exceeds a certain limit, the target may be destroyed due to the excessive heat load.

Second one is the rather new and based on the long undulator (~100 m) where electron beam with energy E_0>100 GeV is generated the undulator radiation beam with mean photon energy ω~ 20 MeV. The photon flux is enough to create a few positrons per each initial electron in the thin amorphous target (~$0.4X_0$, X_0 is radiation length) [3,4]. In this case the heat power deposited in the target and, consequently, temperature stress remain at the acceptable level.

An oriented crystal may be considered as some kind of a solid-state undulator with extremely low period. In principle, the appropriate crystal may be used as a “photon emitter” instead undulator with huge length.

Experiments with electron energy E_0~ 1 GeV [5-7] demonstrated the possibility to obtain so-called channeling radiation in oriented crystal targets with thickness t~ $0.1\div0.2\ X_0 >> L_d$ (L_d stands dechanneling length [8]) to produce photon beam with spectrum enriched by “soft” photons.

2. Let’s compare the main characteristics of radiation spectra for ordinary bremsstrahlung (BS), coherent bremsstrahlung (CBS), and channeling radiation (CR). Radiation losses for BS may be estimated as

$$\Delta E_{BS} \approx \frac{t}{X_0} E_0, \quad t \le X_0. \qquad (1)$$

The mean photon energy in the BS spectrum is:

$$< \omega_{bs} > \approx \frac{\Delta E_{BS}}{< N_{BS} >}, \qquad (2)$$

where $< N_{BS} >$ is the mean number of photons emitted by electron [9]:

$$< N_{BS} > \approx \frac{t}{X_0} \int_{\gamma\omega_p}^{E_0} \frac{d\omega}{\omega} = \frac{t}{X_0} \ln \frac{mc^2}{\omega_p} \sim 10 \frac{t}{X_0} \qquad (3)$$

Here γ is the Lorentz-factor, ω_p is the plasmon energy of target material ($\omega_p \approx$ 30 eV for Al and Si). From (1), (2), (3) one may obtain

$$< \omega_{BS} > \approx 0.1\, E_0. \qquad (4)$$

The mean energy for CR may be estimated as following (see [8]):

$$u = \frac{< \omega_{CR} >}{E_0 - < \omega_{CR} >} \approx \frac{2\gamma^{1/2} \sqrt{\frac{V_0}{mc^2}} \frac{\lambda_e}{a_s}}{1 + \frac{1}{2}\gamma \frac{V_0}{mc^2}}, \qquad (5)$$

where V_0 is a potential of axis (or plane), a_s is a screening radius, $mc^2 = 0.511$ MeV, $\lambda_e = 3.86 \cdot 10^{-13}$ m. For <111> axis of Si target and $E_0 \sim 1$ GeV $< \omega_{CR} > \sim 15$ MeV $< < \omega_{BS} >$.

For a coherent bremsstrahlung

$$u = \frac{< \omega_{CBS} >}{E_0 - < \omega_{CBS} >} \sim \frac{\pi\gamma\theta}{a}, \qquad (6)$$

θ stands orientation angle, a stands interplanar distance. As was shown in [5] the first Born approximation for a CBS theory may be used if $\theta >> \theta_c = \sqrt{\frac{V_0}{\gamma mc^2}}$. For an axial orientation of a thick monocrystalline target the rough estimation of an angle θ may be obtained as:

$$\theta \sim < \theta_{ms} > = \frac{21}{E_0} \sqrt{\frac{1}{2} \frac{t}{X_0}}, \quad E_0 \text{ in MeV}.$$

For instance, for Si, t=10mm and $E_0 \sim 1$ GeV $< \omega_{CBS} > \sim 0.05\, E_0 \sim 50$ MeV,

$$< \omega_{CR} > < < \omega_{CBS} > < < \omega_{BS} >. \qquad (7)$$

For axial orientation radiation losses may be considered as consisting of two parts

$$\Delta E = \Delta E_{BS} + \Delta E_{cr},$$

where first term is connected with a radiation from amorphous target with the same thickness, but second one is determined by coherent radiation processes (channeling radiation plus coherent bremsstrahlung). Ratio between these parts was measured for electron energy $E_0 = 900$ MeV [10]:

	diamond <100> t=10 mm	Silicon <111> t= 10 mm	tungsten <110> t=1.2 mm
$\frac{\Delta E_{cr}}{\Delta E_{BS}} =$	~ 2.5	~ 1.8	~ 1.5

Having in mind the relation (7) one may obtain:

$$<N_{cr}> \approx \frac{\Delta E_{cr}}{<\omega_{cr}>} >> <N_{cr}> \qquad (8)$$

because of $\Delta E_{cr} > \Delta E_{BS}$, $<\omega_{cr}> < <\omega_{BS}>$.

3. Authors of experiment [11] that was carried out with electron energy $E_0 = 10$ GeV had measured the energy losses for <111> axial orientation of Si crystals with thickness t = 0.8 and 3.0 mm (see Fig. 1). From Monte-Carlo simulation they obtained the mean photon number (photon multiplicity)

$$< N >=< N_{BS} > + < N_{cr} >$$

for each case:

<N (0.8 mm)> = 1.8 ph/e^-,

<N (0.3 mm)> = 5.4 ph/e^-.

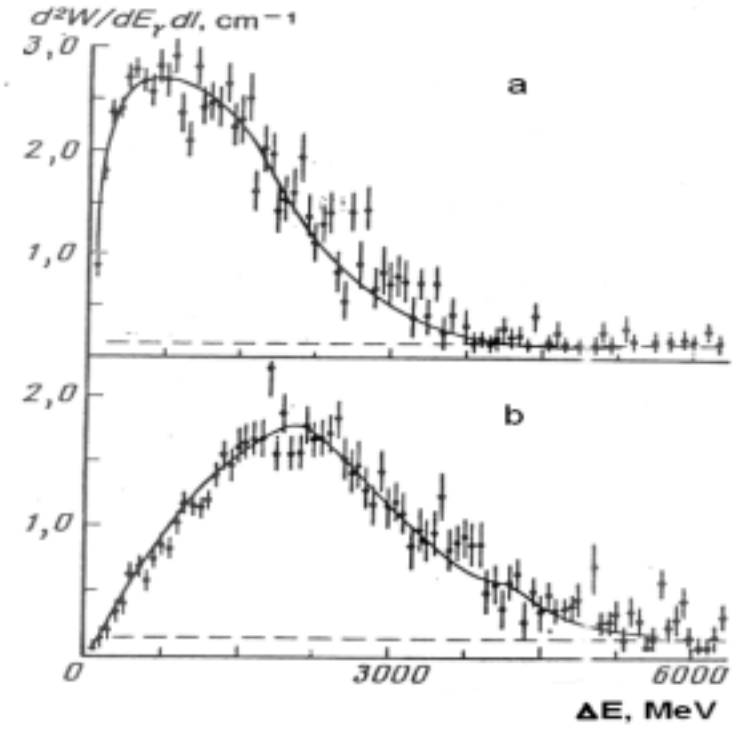

*Fig. 1. Radiation losses spectra for channeled electrons with E_0 = 10 GeV in Si crystal with thickness 0.8 mm (***a***) and 3.0 mm (***b***). Solid lines are the simulation results [11].*

The measurements and simulations were carried out for the threshold photon energy $\omega_t = 20$ MeV. The contribution to the multiplicity from bremsstrahlung is negligible (see eq. (4)):

$$< N_{BS}(0.8) > \approx 0.9 \cdot 10^{-3} \text{ ph/e}^-$$

$$< N_{BS}(3.0) > \approx 3.2 \cdot 10^{-3} \text{ ph/e}^-,$$

In the paper [12] there was proposed an approach to estimate the photon multiplicity from the measured distribution of an energy losses (energy straggling). Disregarding by a bremsstrahlung losses the photon multiplicity and the mean photon energy may be estimated in the following manner [12]:

$$< N_{cr} > \approx \frac{< Q >^2}{\sigma^2} \qquad (9)$$

$$<\omega> \sim \frac{\Delta E_{cr}}{< N_{cr} >},$$

where $< Q >$ is the mean value of the radiation losses calculated from energy losses distribution, σ is the distribution variance, ΔE_{cr} is the total energy losses for axial orientation. Fitting the experimental results [11] by a smooth curve one may obtain for t=3 mm (see Fig. 1).

$<Q> \approx 2.3$ GeV, $\sigma \approx 1.1$ GeV and, consequently:

$<N_{cr}> \approx 4$ ph/e$^-$ and $<\omega_{cr}> = 0.2$ GeV $< <\omega_{BS}> = 1$ GeV.

The multiplicity estimated from this model agrees with Monte-Carlo simulation reasonably. The model of photon multiplicity developed in [7] gives for the considered case (E_0= 10 GeV, t = 3 mm, Si <111>) (see Fig. 17.3 there):

$$< N_{tot} > \approx 24 \text{ ph/e}^-$$

It means there is a large contribution of the soft photons ($\omega \leq 1$ MeV).

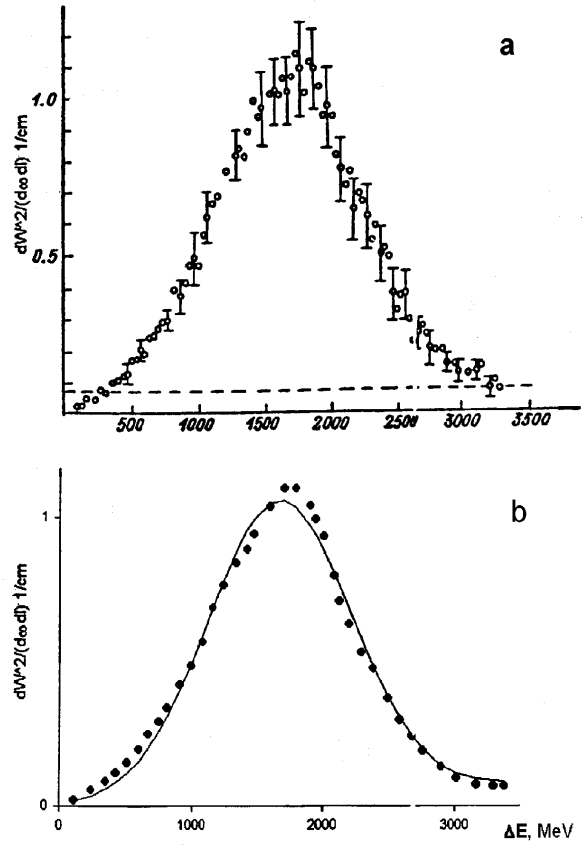

Fig. 2: **a***) Radiation losses spectra for channeled electrons with E_0 = 4.5 GeV in diamond crystal with thickness 10 mm [13],* **b***) Fit by a gaussian with <Q> = 1660 MeV, σ =536 MeV, ΔE=1300 MeV.*

Using the same approach let's estimate the photon multiplicity in the experiment [13]. This experiment was performed at the electron beam with energy E_0 = 4.5 GeV for axial <111> orientation of the natural diamond target with thickness t=10 mm (see Fig. 2a). Fig. 2b shows the fit by a gaussian ($< Q >$ = 1660 MeV, σ = 536 MeV, ΔE_{cr} = 1300 MeV), which gives the following result:

$< N_{cr} > \approx 10$ ph/e$^-$, (10)

$<\omega_{cr}> \approx 130$ MeV.

It allows to think that photon multiplicity may achieve the value $< N_{cr} > \sim 20$ if one shall use the electron beam with energy $E_0 \approx 10$ GeV and diamond target with thickness $t \approx 20$ mm.

Data from Dubna's experiment [14] show that the radiation losses of 10 GeV electron moving along <111> axis in the 10-mm silicon (~ 0.11 rad. length) reach 30%. According to [8] losses from a diamond of the same radiation thickness (~ 13 mm) increases in $\frac{a_{Si}}{a_{di}}$ = 1.5 times.

The usage of diamond with thickness $t \sim 20$ mm leads to radiation increasing also. As a result one may expect that each electron will emit about 50% of the initial energy ($\Delta E \approx 5$ GeV).

The well known dependence of multiple scattering angle on an energy and target thickness makes possible to estimate the mean photon energy for the considered case using formula (6):

$$< \omega_{cr}(E_2, t_2) > \sim \frac{E_2}{E_1} \frac{< \theta_{ms}(E_2, t_2) >}{< \theta_{ms}(E_1, t_1) >} < \omega_{cr}(E_1, t_1) > \approx \sqrt{\frac{t_2}{t_1}} < \omega_{cr}(E_1, t_1) > \qquad (11)$$

For $E_2 = 10$ GeV, $t_2 = 20$ mm, $E_1 = 4.5$ GeV, $t_1 = 10$ mm, $< \omega_{cr}(E_1, t_1) > \approx 130$ MeV one may obtain $< \omega_{cr}(E_2, t_2) > \approx 180$ MeV and $< N_{cr} > \sim 14$ ph/e^-.

This photon flux may be used to produce positrons in a thin amorphous target in a complete analogy with an undulator radiation beam. Moreover there may be some addition to positron yield from an initial electron with remaining part of energy.

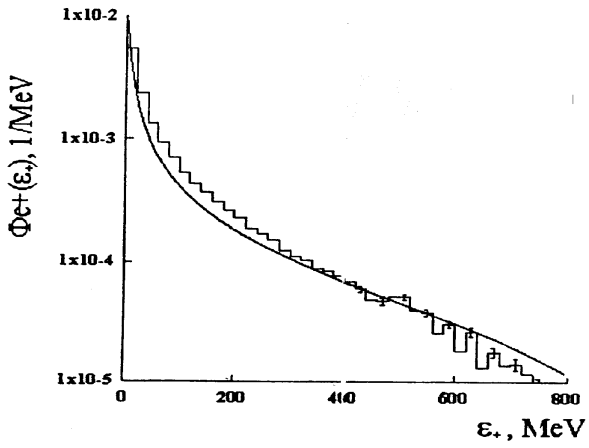

Fig. 3. Comparison of positron spectra from Monte Carlo simulation (histogram) and analytical expression (13). Initial electron energy E_0=1 GeV, converter thickness t= 0.5 rad. length.

4. The positron yield for an initial electron with energy E_0 interacting with a rather thin amorphous target ($t \leq 1$ rad. length) may be calculated using a simple analytical model [15]. In this model an electron passing the layer with thickness $t/3$ emits bremsstrahlung photon which creates e^+e^- pair at the next layer with thickness $t/3$ and, at last, created positron moves through remaining layer ($t/3$) changing outgoing angle due to multiple scattering. The positron spectrum (neglecting ionization and radiation losses) can be written as

$$\frac{dN_+}{d\varepsilon_+} = 0.07 \left(\frac{t}{X_0} \right)^2 \left[\frac{\ln\left(\frac{\varepsilon_+}{mc^2} \right) - 0.19}{\varepsilon_+} - \frac{\ln\left(\frac{E_0}{mc^2} \right) - 0.19}{E_0} \right], \qquad (12)$$

where ε_+ is the positron energy. This formula is valid for the case $E_0 < \frac{2}{\lambda} mc^2$ ($\lambda = \frac{z^{1/3}}{111}$ stands screening parameter). For higher energies of the initial electrons ($E_0 > \frac{2mc^2}{\lambda}$, $\varepsilon_+ > \frac{2mc^2}{\lambda}$) we have

$$\frac{dN_+}{d\varepsilon_+} = 0.07\left(\frac{t}{X_0}\right)^2\left[\ln\left(\frac{1}{\lambda}\right) - 0.5\right]\left[\frac{1}{\varepsilon_+} - \frac{1}{E_0}\right], \quad \left(\frac{1}{MeV}\right). \tag{13}$$

Accuracy of the expressions (12), (13) may be estimated upon comparison with the Monte Carlo simulations [15] (see Fig.3).

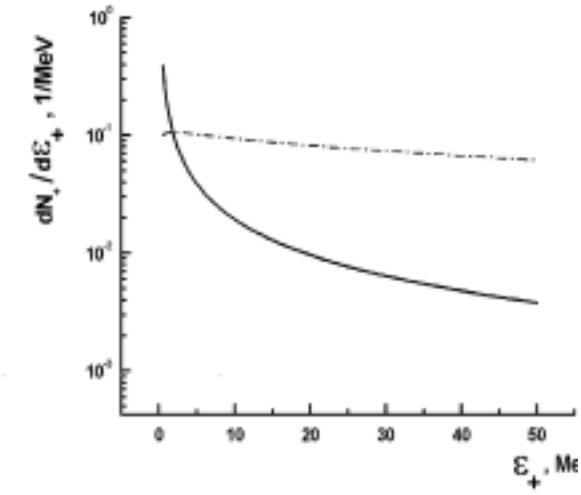

Fig. 4. Positron spectra initiated by an electron with E_0 = 10 GeV in a combined target (20 mm thickness diamond target and 1 rad. length amorphous converter). Upper curve is the spectrum of positrons produced by photon flux from photon emitter, lower curve is the spectrum of positrons produced by an electron passed through photon emitter.

As follows from the figure, for the target thickness $t \le X_0$ one may observe a reasonable agreement, which makes the above approximation applicable to estimations of positron yield.

The similar model may be developed for initial photons. For a simplicity let's consider a "flat" photon spectrum with a photon multiplicity N_{ph} ("triangle" intensity spectrum closed to UR and CBS ones):

$$\frac{dN_{ph}}{\omega} = \begin{cases} \dfrac{N_{ph}}{\omega_{max}}, & \omega \le \omega_{max} \\ 0, & \omega > \omega_{max} \end{cases} \tag{14}$$

Radiation losses may be calculated easily from (14):

$$\Delta E = \int_0^{\omega_{max}} \omega \frac{dN_{ph}}{d\omega} d\omega = N_{ph}\frac{\omega_{max}}{2} = N_{ph} < \omega >,$$

$$\omega_{max} = 2 < \omega > .$$

The positron spectrum produced by photons with the energy ω in the converter with thickness t may be approximated by the expression [15]:

$$\frac{dN_+(\omega)}{d\varepsilon_+} = \begin{cases} 0.14\dfrac{t}{L_{rad}}\dfrac{\ln\left(\dfrac{\omega}{mc^2}\right) - 1.19}{\omega}, & \omega < \dfrac{2}{\lambda}mc^2 \\ 0.14\dfrac{t}{L_{rad}}\dfrac{\ln\dfrac{1}{\lambda} - 0.5}{\omega} & \omega > \dfrac{2}{\lambda}mc^2 \end{cases}.$$

After convolution of this spectrum with photon one (14) it is possible to obtain the analytical expression for output positron spectrum:

$$\frac{dN_+}{d\varepsilon_+} = 0.14\frac{t}{X_0}\frac{N_{ph}}{\omega_{max}}\ln\left(\frac{\omega_{max}}{\varepsilon_+}\right)\left[\frac{1}{2}\ln\left(\frac{E_+\omega_{max}}{m^2c^4}\right) - 1.2\right] \tag{15}$$

Flottmann's calculations [3] for UR with ω_{max} = 21 MeV, $N_{ph} = 2ph/e^-$ give the result $\frac{dN_+}{d\varepsilon_+} = 0.020$ for $\varepsilon_+ = 10$ MeV and $t = 1$ rad. length. Using (15) one obtain the value $\frac{dN_+}{d\varepsilon_+}$ =0.021 for the same parameters.

Fig. 4 shows spectra of positrons generated in the 1 rad. length amorphous converter by a photon flux with N_{ph} = 14 created by an initial electron with energy E_0 = 10 GeV in a thick diamond target (upper curve) and by the same electron with decreased energy $E_f = E_0 - \Delta E$ = 5 GeV (lower curve). The total positron yield for an energy interval 5 MeV $\le \varepsilon_+ \le$ 25 MeV achieves $\Delta N_+ \approx 2$ per each initial electron. From this amount 85% are generated by photons and only 15% by electrons.

5. The proposed scheme of positron source based on using of a combined target (photon emitter from a thick diamond target (t_d = 20 mm) and amorphous converter with thickness t_{am} = $1 X_0$) and electron beam with energy E_0 = 10 GeV looks more preferable in comparison with a homogeneous crystalline target because of the converter thickness in the former case is much less than in latter one and problem of heat loading will be much weaker also.

Such advantages of a diamond as a high thermal conductivity (660 W/m/K against 170 W/m/K for tungsten), high Debye temperature (1860^0 K against 379^0 K for tungsten) and the shortest lattice constant (a =3.56 $\mathring{A}$) allow to consider a thick diamond crystal as the best candidate for a photon emitter.

The problem of growth of an artificial diamond with thickness ~ 20 mm may be resolved in the nearest future (S.A. Terent'ev, private communication).

The measurements of the straggling of an electrons passed through an oriented thick crystal (radiation losses distribution) become very important to verify the proposed model. The detailed 6-D simulation of a crystal-based positron source is also needful to choose the source configuration and to design the new positron source for a linear collider.

In summary it may be noted the considered scheme may provide an efficiency of positron source (the number of accepted and accelerated positrons per initial electron) as high as 1 e^+/e^- at least. The efficiency of an undulator-based positron source [3,4] may achieve the same value also but proposed scheme is much cheaper.

REFERENCES

1. The NLC Collaboration, 2001 Report on the NLC. Preprint SLAC-R-571, 2001.
2. L. Rinolfi, T. Kamitani. *The positron production at CLIC*. CLIC Note 465,

CERN, 2002.

3. K. Flottmann. Investigations toward the development of polarized and unpolarized high intensity positron sources for linear colliders. Preprint DESY 93-161, 1993.
4. K. Flottmann. *Positron source for TESLA and SBLC* in Proceedings of the Workshop on new kinds of positron sources for linear colliders. SLAC-R-502, 1997.
5. R.D. Babadjanov, A.N. Didenko, B.N. Kalinin et al. Rad. Effects, v. 91, No 3-4 (1986) 233.
6. G.L. Bochek, V.I. Kulibaba, N.I. Maslov et al. Nucl. Instrum. and Methods B 145 (1998) 146.
7. S. Anami, M.Yu. Andreyashkin, A. Enomoto et al. Nucl. Instrum. and Methods B 183 (2001) 459.
8. V.N. Baier, V.M. Katkov, V.M. Strakhovenko. *Electromagnetic Processes at H*igh Energies in Oriented Single Crystals. World Scientific, 1998.
9. I.E. Vnukov, B.N. Kalinin, G.A. Naumenko et al. Sov.Phys. Journal, v.34 (1991) 540.
10. K.Yu. Amosov, I.E. Vnukov, B.N. Kalinin et al. Sov. Phys. Journal, v.34 (1991) 472.
11. M.D. Bavizhev, Yu. Nilsen. B.A. Yur'ev. Sov. Phys. JETP, v.68 (1998) 803.
12. A. Kolchuzhkin, A. Potylitsyn., Nucl. Instrum and Methods B 173 (2001) 126.
13. R. Avakian, A.E. Avetisyan, R.A. Asatryan et al., Sov. Tech. Phys. Lett., v.14 (1988) 395.
14. E.I. Tsyganov. Fizika elementarnyx chastits i atomnogo yadra, v. 20 (1989) 5 (in Russian).
15. A.P. Potylitsyn. Nucl. Instrum. and Methods A 398 (1997) 395.

Semiclassical Theory of Crystal-Assisted Pair Production: Beyond the Uniform Field Approximation

H.Nitta, Y.Nagata, and S.Onuki
Department of Physics, Tokyo Gakugei University
M.Kh.Khokonov
Department of Physics, Kabardino-Balkarian State University

Within the semiclassical theory of QED, a simple expression of pair production in strong field is obtained that approaches to the constant field approximation at the strong field limit while it gradually behaves like the Bethe-Heitler type when the field becomes weaker. By using the impact approximation for the calculation of trajectory, a simple expression is obtained. Though simple, it agrees well with the experimental result of crystal-assisted pair production.

1 Introduction

It is widely known that electron-positron pair production is well described by the Bethe-Heitler formula as far as the process can be regarded as the incident photon collides with an isolated atom. However, when photons enter a strong electromagnetic field, the perturbative approach such as the Bethe-Heitlers becomes inappropriate for describing the pair production process. For such strong field QED effect, Baier and Katokov[1] proposed a semiclassical expression for radiation

$$\frac{dN}{d\eta} = \frac{\alpha c}{\pi\lambda_0\gamma}(J_c + J_s), \tag{1}$$

$$J_c = \int_0^\infty \left[1 + \frac{\gamma^2}{2}(\delta\boldsymbol{\beta}_\perp)^2\right] \sin\Delta \ \frac{d\tau}{\tau} - \frac{\pi}{2}, \tag{2}$$

$$J_s = \left(\frac{\gamma - \gamma'}{2\gamma\gamma'}\right) \int_0^\infty \frac{\gamma^2}{2}(\delta\boldsymbol{\beta}_\perp)^2 \sin\Delta \ \frac{d\tau}{\tau}, \tag{3}$$

where $\omega^* = (\gamma/\gamma')\omega$, $\eta = \hbar\omega/E$, $\delta\boldsymbol{\beta}_\perp = \boldsymbol{\beta}_\perp(t_+) - \boldsymbol{\beta}_\perp(t_-)$, $t_\pm = t_0 \pm \tau/2$, $E' = E - \hbar\omega$, $\gamma(\gamma') = E/(m_0c^2)(E'/(m_0c^2))$, E being the initial energy of the particle and m_0 its rest mass. The phase determined by *the trajectory* of a radiating particle is given by

$$\Delta(\tau) = \frac{\omega\tau}{2\gamma^2} - \frac{\omega}{2c^2\tau}(\delta\boldsymbol{\rho})^2 + \frac{\omega}{2}\int_{t_-}^{t_+} \boldsymbol{\beta}_\perp^2(\tau')d\tau', \tag{4}$$

where $\delta\boldsymbol{\rho} = \boldsymbol{\rho}(t_+) - \boldsymbol{\rho}(t_-)$, $\boldsymbol{\rho}(t)$ being the transverse coordinate. Though there are some discussion on the derivation of the Baier-Katokov formula [2, 3], this formula explains very well the radiation as well as pair production in strong fields.

2 "Th-trajectory" and pair production

The pair production probability is obtained by using the crossing symmetry for Eq.(5) [3].

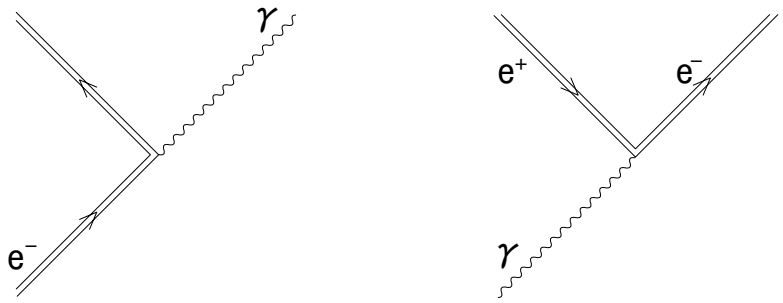

Figure 1: Crossing symmetry. The left-hand figure represents the channeling radiation while the right-hand one represents the pair production.

By changing the variables as

$$\begin{cases} E & \text{(initial energy)} & \rightarrow & -E_+ & \text{(produced positron)} \\ E' & \text{(final energy)} & \rightarrow & E_- & \text{(produced electron)} \\ \omega & \text{(emitted photon)} & \rightarrow & -\omega & \text{(absorbed photon)} \end{cases}$$

and multiplying the ratio of the density of final states,

$$\frac{E_+^2 dE_+}{(\hbar\omega)^2 d(\hbar\omega)},$$

we obtain the pair production probability for the th-trajectory approximation as well as the synchrotron approximation, though one may feel that the idea of particle trajectory is rather "spooky"[3]. We obtain,

$$\frac{dN_+}{d\eta_+} = \left(\frac{\alpha c}{\pi\lambda_0}\right)\left(\frac{m_0c^2}{\hbar\omega}\right) J, \tag{5}$$

where $dN_+/d\eta_+$ represents the number of produced positrons, $\eta_+ = E_+/\hbar\omega$, E_+ being the energy of the produced positrons, α the fine-structure constant, and λ_0 the Compton wavelength.

The factor J for the CFA is given by

$$J_{\rm cf} = \frac{1}{\sqrt{3}}\left[\left(1-\eta_+ + \frac{1}{1-\eta_+}\right)\mathrm{K}_{\frac{2}{3}}(\xi^*) - \int_{\xi^*}^{\infty}\mathrm{K}_{\frac{1}{3}}(\lambda)d\lambda\right], \tag{6}$$

where $\xi^* = 2/[3\eta_+(1-\eta_+)\chi]$ and $\chi = \hbar\omega\lambda_0 F(t_0)/(m_0c^2)^2$ and $F(t_0)$ is the force by the field acting on the positron at time t_0. Eq.(6) is obtained by assuming that the trajectory of produced positrons are circular.

The CFA is applied to evaluate the pair production process when high-energy photons enters a crystal along the major crystal axis. It is reported that when photons are

directed exactly parallel to the crystal axis, CFA agrees very well with the experimental result [5]. However, naturally, CFA does not explain the angular dependence of the pair production rate. For the purpose to calculate the angular dependence, the authors of Ref.[5] calculated the Baier-Katkov formula with some "numerical experiments" [6] and a good agreement of their numerical approach with the experimental result has been demonstrated. However, the process of the "numerical experiments" has not been described in their paper. Therefore, nobody can reproduce the calculations.

Recently, two of the present authors obtained a radiation probability [4] by using a model trajectory called the "th-trajectory"

$$\boldsymbol{\beta}_\perp(t) = \boldsymbol{b}_0 + \boldsymbol{b}\tanh\left(\frac{t}{T}\right), \tag{7}$$

where

$$\boldsymbol{b}_0 = \frac{\boldsymbol{\beta}_{\perp 1}+\boldsymbol{\beta}_{\perp 2}}{2}\ ,\ \boldsymbol{b} = \frac{\boldsymbol{\beta}_{\perp 2}-\boldsymbol{\beta}_{\perp 1}}{2},$$
$$\begin{cases}\boldsymbol{\beta}_{\perp 1} \equiv \boldsymbol{\beta}_\perp(t\to-\infty)\\ \boldsymbol{\beta}_{\perp 2} \equiv \boldsymbol{\beta}_\perp(t\to+\infty).\end{cases}$$

The th-trajectory approaches to the free motion (i.e. straight paths) at $t \to \pm\infty$ while the trajectory is substantially bent at $|t| \lesssim T$ depending on the strength of the field. Since Eq.(7) is integrated analytically, we obtain an analytic expression for J:

$$J_{\rm th} = \int_0^\infty \frac{dz}{z}\left[\nu^2\left(\frac{1-\eta_+}{\eta_+}+\frac{\eta_+}{1-\eta_+}\right)\tanh^2 z - 1\right]\sin\left[\tilde{\xi}(z-\mu\tanh z)\right] + \frac{\pi}{2}, \tag{8}$$

where $\nu = \gamma_+ b$ and $\tilde{\xi} = \nu(1+\nu^2)/[\eta_+(1-\eta_+)\chi]$.

3 Numerical results

A typical ν dependence of Eq.(8) is shown in Fig. 2. When ν becomes larger, the result of $J_{\rm th}$ approaches to $J_{\rm cf}$. From Fig. 2 it is clear that the spectra become CFA-like as the angle decreases while Bethe-Heitler-like as the angle increases.

Based on Eq.(8), we have calculated the crystal-assisted pair production (CAPP) probability as a function of the photon incident angle in comparison with the experimental data by Belckacem et al.[5]. For simplicity, first we calculate the scattering angle by the impact approximation where the momentum change during the collision is proportional to the force multiplied by the "interaction time". The interaction time has been estimated by $a\rho/v_\perp$, where ρ is the impact parameter of the radiation point (for CAPP, we should have called it the "pair production point") and a is the parameter ($a \sim 1$). In Fig. 3 we have shown the results of the impact approximation. Taking account of the simplicity of the impact approximation, the agreement is satisfactory. $J_{\rm th}$ with the impact approximation will be useful for planning experiments.

In Fig. 4, a more involved calculation has been made by using thermally-averaged one-string Molière potential [7] at $T = 100$K. Though in this case we have no free parameter, the agreement is well. The peaks at higher photon energies look like somewhat

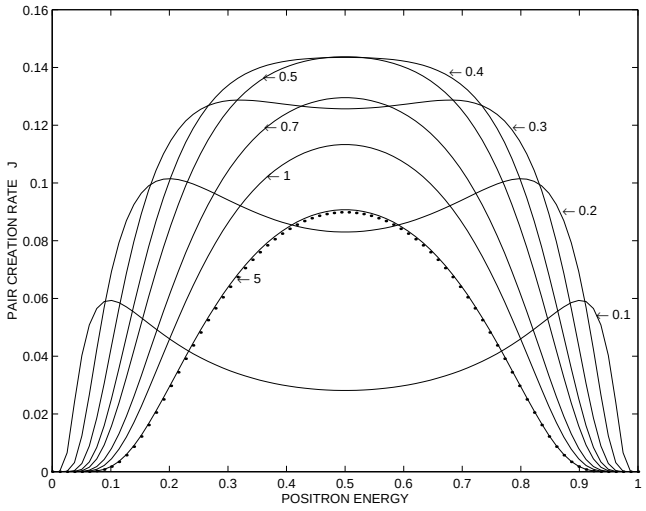

Figure 2: The ν-dependence of pair production probability calculated by using Eq.(8) as a function of the energy of produced positrons $E_+/\hbar\omega$. The dotted line represents the constant field approximation (CFA) of Eq.(6). ($\chi = 1$)

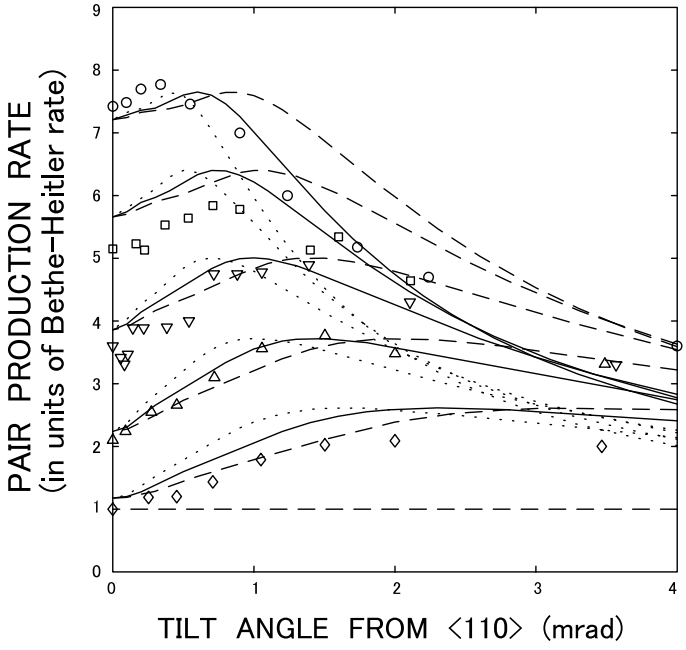

Figure 3: Comparison of the impact approximation results with the experimental data by Belkacem et al. [5]. The symbols mean the experimental results corresponding the energy of photons in the range of: ○: 150-120GeV, □:120-90GeV, ▽:90-60GeV, △:50-40GeV, ◇:40-20GeV. The dotted lines, solid lines, and broken lines correspond to $a = 2$, $a = 2\sqrt{2}$, and $a = 4$, respectively.

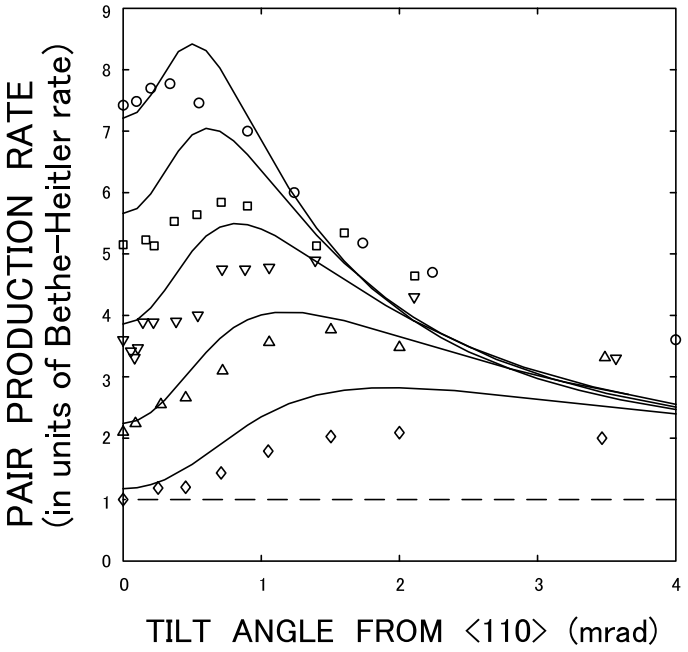

Figure 4: Comparison with experimental data by the rigorous scattering calculation with the use of the Molière one-string potential. No fitting parameter is included.

steeper than the experimental data, which may be due to neglecting of the many-string effect.

More detailed discussion will be published elsewhere.

References

[1] V. N. Baier, and V. M. Katkov, Sov. Phys. JETP,**26**,854 (1968).

[2] J. Lindhard, Phys. Rev. **A43**, 6032 (1991).

[3] J. C. Kimball and N. Cue, Radiat. Eff. Defect in Solids **122-123**, 481 (1991).

[4] M. Kh. Khokonov and H. Nitta, Phys. Rev. Lett. **89**, 094801 (2002).

[5] A. Belkacem et al., Phys. Rev. Lett. **58**, 1196 (1987).

[6] A. Belkacem, N. Cue, and J. C. Kimball, Phys.Lett. **111A**, 86 (1985).

[7] Y.H.Ohtsuki, *Charged Beam Interaction with Solids* (Taylor and Frances, London, 1983).